UC Berkeley
UC Berkeley Electronic Theses and Dissertations

Title

Genome-Wide Screen and Phenotypic Analysis of a Kaposi Sarcoma-Associated Herpesvirus Genome with Insights into Capsid Maturation

Permalink

https://escholarship.org/uc/item/8rz4k580

Author

Smith, Adam Michael

Publication Date

2022

Peer reviewed|Thesis/dissertation

eScholarship.org Powered by the California Digital Library
University of California

Genome-Wide Screen and Phenotypic Analysis of a Kaposi Sarcoma-Associated Herpesvirus Genome with Insights into Capsid Maturation

By

Adam Michael Smith

A dissertation submitted in partial satisfaction of the

requirements for the degree of

Doctor of Philosophy

in

Comparative Biochemistry

in the

Graduate Division

of the

University of California, Berkeley

Committee in charge:

Professor Fenyong Liu, Chair
Professor Lee Riley
Professor Xiaohua Gong
Professor Enrico Moretti

Spring 2022

Abstract

Genome-Wide Screen and Phenotypic Analysis of a Kaposi Sarcoma-Associated Herpesvirus Genome with Insights into Capsid Maturation

By

Adam Michael Smith

Doctor of Philosophy in Comparative Biochemistry

University of California, Berkeley

Professor Fenyong Liu, Chair

Kaposi Sarcoma-associated herpesvirus (KSHV) is a medically important virus that causes two types of human cancer. Infection with KSHV can result in viral persistence for the lifetime of the host. Viral persistence, commonly referred to as latency, is characterized by the absence of gene expression. Reactivation from latency results in entry into the lytic cycle which is characterized by the full repertoire of viral gene expression. A key pathogenic step in KSHV-mediated disease is viral reactivation and viral lytic gene expression. Immunosuppression, regardless of the source (HIV-mediated or iatrogenic), results in log-fold increases in the risk of developing KSHV-mediated diseases.

We adopted a tractable system to study a KSHV genome derived from a clinical isolate. This KSHV genome has been engineered for stable propagation in E. coli. The strain of E. coli harboring the KSHV genome has been engineered for the use of a scarless, site-directed mutagenesis procedure. Parental and mutagenized virus can be introduced into a human cell line via transfection. Transfection of parental virus into this cell line results in stable latency. This cell line has also been engineered to express the major viral-transactivator under an inducible promoter. Expression of the viral-transactivator is sufficient to reactivate KSHV from latency, drive the full repertoire of viral gene expression, and results in significant cell-free progeny.

We implemented this experimental workflow to mutagenize all known canonical Open Reading Frames (ORFs) and several other uncanonical ORFs. Transfection and cell-free progeny analyses resulted in the identification of ORFs essential for completion of the viral lifecycle. Growth analyses of non-essential mutants resulted in the identification of ORFs important for induced and spontaneous viral reactivation. Phenotypic screening of essential mutants using light and electron microscopy resulted in the identification of ORFs playing vital roles in viral lytic gene expression and capsid formation and maturation.

The results of my thesis reveal the identification of novel antiviral targets and live-attenuated vaccine candidates. Moreover, these data suggest a new model for KSHV latency and reactivation. This model proposes that KSHV actively communicates with and responds to the host's immune system in a concerted effort to fine-tune viral latency and reactivation. Supplementary analyses, not provided herein, are underway to elucidate the molecular details for discrete steps in viral egress.

To my family: John, Elizabeth, David and Anna Smith

Table of Contents

Title page

Abstract 1

Dedication i

Table of Contents ii-iii

Acknowledgments iv

Chapter 1: Fundamentals of virology and background on Kaposi Sarcoma-associated herpesvirus 1-17

1.1: Background in general virology and herpesvirus biology 2-8

1.2: Background in Kaposi Sarcoma-associated herpesvirus 8-10

1.3: References 11-17

Chapter 2: Methods for the construction and analyzation of mutant Kaposi Sarcoma-associated herpesviruses 18-41

2.1: BAC16 mutagenesis methods and rationale 19-31

2.2: BAC16-iSLK cell line creation, induction, and phenotypic analyzation methodology 32-39

2.3: References 40-41

Chapter 3: Global phenotypic profiling of a Kaposi Sarcoma-associated herpesvirus 42-153

3.1: Chapter overview and acknowledgements 43

3.2: Part I 44-90

3.2a: Abstract 45

3.2b: Introduction 46

3.2c: Results 47-49

3.2d: Discussion 50-51

3.2e: Main tables and figures 52-58

3.2f: Supporting Information 59-80

3.2f-i: Tables 59-75

3.2f-ii: Figures 76-80

3.2g: References 81-90

3.3: Part II 91-153

3.3a: Overview 92

3.3b: Section I: Creation of BAC16-mutants in E. coli 92-102

3.3c: Section II: Creation of BAC16-iSLK cell lines and general observations 103-117

3.3d: Section III: Light and electron microscopy analyses of BAC16 essential mutant cell lines 118-153
3.3d-i: DNA packaging, capsid maturation, nuclear egress 118-134
3.3d-ii: DNA replication 135-142
3.3d-iii: Core capsid components 143-147
3.3d-iv: Reactivation and late gene expression 148-153
Chapter 4: Kaposi Sarcoma-associated herpesvirus open reading frame 19 is essential for viral capsid maturation during lytic infection 154-201
4.1: Overview 155
4.2: Abstract 155
4.3: Introduction 156-157
4.4: Methods 158-160
4.5: Results 161-164
4.6: Discussion 165-167
4.7: Main figures and tables 168-176
4.8: References 177-181
4.9: Supporting figures and tables 182-184
4.10: Appendix 185-201
4.10a: Creation of stop-ORF19 186-189
4.10b: Creation of res-ORF19 from stop-ORF19 190-196
4.10c: Phenotypic analysis of res-ORF19 and stop-ORF19 cell lines 197-201
Chapter 5: The role of KSHV ORF74 in spontaneous reactivation 202-226
5.1: Overview and acknowledgments 203
5.2: Introduction 203
5.3: Results 204-223
5.4: Discussion 224
5.5: Primer and plasmid tables 225-226
5.6: References 227-228

Acknowledgments

I would like to thank my mentor, Fenyong Liu. Fenyong, you saw something in me that no one else did. You believed in me, and you supported me emotionally and academically throughout my journey. You inspired me to be a become a better person and help as many people as I can. Your patience and empathy have molded me into the person I am today. I would also like to thank Lee Riley for supporting me during my academic journey. Lee, you have been a constant pillar of support from the moment I entered Berkeley. You have witnessed my matriculation twice. You cultivated my curiosity for infectious diseases, augmented my academic scope, and helped me appreciate our responsibility to the public, regardless of who they are. I would also like to thank Xiaohua Gong. Xiaohua, you provided me with intellectual stimulation and insightful feedback on my project proposals that helped see them in a new light.

I would also like to thank Enrico Moretti. Enrico, you provided me with a once in a lifetime opportunity and gave me the room to grow and to make mistakes. Your quote: "……isn't just a science, it's an art" inspired me. The lessons and experiences you gave me will carry me to new heights in my career and in my personal life. Thank you, Martha Olney, for showing me how to approach teaching with care and compassion. I would also like to thank everyone in the UC Berkeley Economics Department. You welcomed me into your home when I had nowhere else to go, and you treated me with respect and compassion. Without your support, I would have failed.

I would also like to thank Rachael Burchfield and Marco-Paliza-Carre for their help and comradery during my journey. Both of you were instrumental in the creation of this work, and much of it is built off the foundations you established. I will be forever indebted to you.

Mom and Dad, you have nourished my curiosity from a young age. From my first book, "*How Things Work*" and my first science experiment using eggs, dough, and a freezer. Though high school, undergraduate, and masters; you always encouraged me to follow my dreams. To never be afraid of failure. To never let anyone take my soul from me. This work is dedicated to you, David, and Anna. Go Ralphie!

Chapter 1

Fundamentals of virology and background on Kaposi Sarcoma-associated herpesvirus

“El lenguaje del amor.” -*redacted*

Overview

The goal of this work is to identify and employ a tractable reverse genetics system to study the role of every Kaposi Sarcoma-associated herpesvirus (KSHV) Open Reading Frame (ORF) in the viral lifecycle. Functional profiling of KSHV ORFs is accomplished using basic molecular biology techniques, and experimentally determined ORF functions are compared to other human herpesviruses. These data are used to form hypotheses about viral latency, reactivation, and lytic replication. These hypotheses are important for understanding the molecular pathogenesis of KSHV-mediated transformation.

The birth of virology

By mid to late 19th century, the view of a diverse microbial world composed of bacteria, protozoa and fungi had become widely accepted in the scientific community. Louis Pasture had soundly disproven spontaneous generation in his experiments using nutrient broth and swan neck flasks. Ignaz Semmelweis's experiments on handwashing and maternal mortality from puerperal fever, and John Snow's essay *On the Mode of Communication of Cholera* had shaken Miasma theory to its core. Robert Koch's work with *Bacillus anthracis* and *Mycobacterium tuberculosis* led to the development of his four postulates, designed to definitively determine the microbial etiology of diseases. These conceptual leaps set the stage for the birth of virology. It was not long after Kock's postulates were developed that Martinus Beijerinck and Adolf Mayer's filtration and dilution experiments using Tobacco Mosaic Virus proved the existence of obligate intracellular parasitic pathogens. These infectious agents, which violate Koch's second postulate, were too small to be observed under the light microscope and able to pass through filters designed to retard all currently known microorganisms. This discovery led to a paradigm shift in humanity's understanding of microorganisms and gave birth to the field of virology.

Viral parasitism and the viral lifecycle

Seminal observations of viral infection led to the understanding of viral redirection of cellular macromolecular synthesis. A major milestone came from work on bacteriophage induced changes on RNA metabolism [1]. These observations led to the partitioning of the viral lifecycle into an eclipse period prior to DNA synthesis, and a late phase after DNA synthesis as well as provided the scientific foundation for discovery of the rapidly turning over species of RNA, mRNA[1]. A year before Watson and Crick elucidated the structure of DNA, phage virologists showed that the component of the phage particle which carries the necessary information for progeny generation was nucleic acid, not protein[2] and a series of elegant in-vitro phage-mutant complementation experiments revealed that self-assembly can be used by living organism to build complex structures[3]. A decade later, bacteriophage capsid morphogenesis was further elucidated as it was observed that capsid maturation occurred in a stepwise fashion and was depended on the proteolytic processing of core capsid elements[4].

Viral transformation

A full appreciation for the transformational capacity of viral infection had to wait until technological advancements in cell culture techniques allowed for the detailed molecular study of animal viruses. The culturing of single cells and the development of an optimal medium were essential for creating experimental systems that allowed for the study of human viruses in the laboratory[5]. Several decades later, our understanding of oncogenes, tumor suppressor genes, and viral transformation began to explode[6-9]. Mechanistic data indicate the existence of a continuum of pathogeneses in microbial-mediated transformation[10]. At one end of the continuum is direct transformation mediated by viral oncogenes that exhibit growth promoting activities, or the ability to modulate host proteins resulting in unnatural cellular proliferation. On the opposite end of the spectrum is the poorly defined mechanism of indirect transformation. This method of transformation is commonly thought of as immunomodulatory, like the chronic inflammation of hepatocytes by Hepatitis B virus or the immunosuppressed state caused by HIV[11].

Viral taxonomy

Human nature implores us to impose order on the world around us using discreate classification systems, and thus it is ironic that evolution has created a continuum of biological systems. The goal of classification is to infer evolutionary relatedness, and the tools to complete this task are as diverse as the continuum they try to divide. Structure, polarity, sequence, method of replication, immunogenicity, tropism, and ecological niche all can be used to infer ancestry. Structuring the continuum into discrete classifications certainly provides additional utility by revealing clues about some of the biological barriers that separate the ability of organisms to exchange genetic material. Viral taxonomy also serves a practical purpose; the identification of common biological characteristics can focus and guide the efforts of clinicians and epidemiologists in the treatment and prevention of viral diseases.

Herpesvirales is an order of viruses that possess the same general structural characteristics. These viruses are double stranded DNA viruses that contain a T=16 icosahedral capsid structure, which is surrounded by a proteinaceous mixture called the tegument enclosed by a protein embedded lipid membrane. This classification is based on morphology, and the order can be split into three distinct families based on ecological niche; *Alloherpesviridae* which infect fish and amphibians, *Herpesviridae* which infect mammals, birds and reptiles, and *Malacoherpesviridae* which infect the invertebrate mollusks[12,13].

Despite a lack of nucleotide homology between these families, their members universally share three functional counterparts, as determined by primary amnio acid sequence; A DNA polymerase, a dUTPase, and an ATPase subunit of the DNA packaging complex called the terminase[14]. While the DNA polymerase and dUTPase are university present in animal cells, and thus could be the result of independent capture events, the ATPase subunit is related to the prokaryotic bacteriophage[15]. Bacteriophages and herpesviruses also share a characteristic fold in their capsid structure that is restricted to these two “organisms”[16]. In support of *Herpesvirales* families’ relatedness is the observation that the *Herpesviridae* species Herpes simplex virus 1 (HSV-1) and the *Alloherpesviridae* species Ictalurid herpesvirus 1 (IcHV-1) (also referred to as

channel catfish virus) package their DNA into capsids in a similar fashion[17]. All families also share an unusually large and unique 3D capsid structure even in the absence of nucleotide sequence relatedness[18-21].

The *Herpesviridae* family can be split into three sub-families based on biological characteristics: *Alphaherpesvirinae*, *Betaherpesvirinae*, and *Gammaherpesvirinae*. All three subfamilies contain human pathogens and there are currently nine herpesviruses that infect humans as their natural host. The subfamilies show a clear evolutionary relationship to one another based on a large set of shared genes called "core genes" that share marginal conservation at the primary amino acid sequence level. Core genes mainly serve roles in herpesvirus DNA replication, genome packaging, and capsid structure. Core genes are found in several distinct blocks of sequence in the central regions of the linear genomes, while the ends are populated by subfamily, genus and species-specific sequences[14,22,23]. Phylogenic analyses indicate that mammalian members of the family co-evolved with their natural hosts millions of years ago[24].

The *Gammaherpesvirinae* subfamily can be split further into four genera, two of which contain human pathogens. The *Lymphocryptovirus* genera contains the human pathogen Epstein-Barr virus (EBV) and the *Rhadinovirus* genera contains the human pathogen Kaposi sarcoma-associated herpesvirus (KSHV). Primary amnio acid sequence analysis reveals that KSHV encodes 27 gene products with no known homology in EBV, and four gene products that contain no known homology in another closely related *Rhadinovirus,* Rhesus monkey rhadinovirus (RRV) [23,25]. Most of the KSHV genes with no known homology in EBV are the result of independent capture or genetic duplication events, and provide KSHV with unique tools to maintain its specialized niche and lifestyle in the host.

The defining feature of the human *Gammaherpesvirinae* is their ability to induce lymphoproliferation and neoplasms. Both EBV and KSHV cause lymphomas and other tissue specific tumors. EBV can cause nasopharyngeal carcinoma which is a head and neck cancer that arises out of the nasopharynx, and leiomyosarcoma which is a cancer of the smooth muscle tissue. KSHV can cause Kaposi Sarcoma (KS) which is vascular neoplasm that arises out of the lymphatic endothelium[26], Primary Effusion Lymphoma (PEL) which is a diffuse large b-cell lymphoma that manifests as a tumorless mass in the pleural, pericardial, or peritoneal cavities[27], and the plasmablastic variant of Multicentric Castleman's Disease (MCD) which is a lymphoproliferative cytokine-mediated disorder[28].

The viral lifecycle

Viruses are some of the smallest and simplest "organisms" in the biosphere. A genome of RNA or DNA and a protein coat are the only two essential components. Some contain a third component, a lipid envelope. This apparent simplicity is deceptive because viruses exhibit a dizzying array of mechanistic diversity to produce progeny. The pathway a cell-free virus must take to produce progeny in a susceptible host can be broken down into discrete steps. Attachment factors aggregate virus on the outside of the cell and facilitate receptor binding. Host cell receptor binding by viral glycoproteins results in intracellular signaling and topological rearrangement of the cell membrane. Membrane rearrangement allows internalization of the

extracellular milieu containing the virus. Some viruses enter the host cell directly at the membrane, while some are engulfed in membrane-enclosed vesicles that allow pseudo-entry of the parasite into the host. This pseudo-entry keeps the virus separate from the internal host surveillance and defense mechanisms while trafficking the viral genome to the appropriate subcellular location; a trojan horse strategy. During trafficking, several protein structural rearrangements occur that result in membrane fusion and/or uncoating of the viral genome. These events lead to the release of the genome from its protective transport vehicles and/or protein shield and into the intercellular environment. Once the genome is released it can begin expression of viral gene products, which eventually leads to replication of viral genomes. The processes of gene expression and genome replication can be quite complex, and these processes depend heavily on the genomic content and polarity of the virus. These steps exemplify the idiosyncrasies of viral life, as certain viruses exploit pathways of information transfer that have not been observed anywhere else in the biosphere. The result of gene expression and genome replication is the assembly of nascent homo and heterooligomeric protein structures into new protein coat structures called capsids. Replicated genomes are packaged into newly formed capsids which then bud into components of the cellular secretory pathway. It is here that enveloped viruses acquire their lipid coat embedded with glycoproteins, and these lipid coats surround the capsids. Glycoproteins and other integral membrane proteins go through complex post-translational maturation processes in the secretory pathway before and after they are incorporated into the viral capsid and envelope. Once they acquire their protein and/or lipid envelope coats, they transverse the interior of the cell using the cellular secretory pathway to reach the plasma membrane where they are released into the extracellular milieu. This completes the lifecycle and allows the process to begin again on an uninfected cell[29-31].

Conserved features of human herpesviruses

All nine human herpesviruses share a set of common biological, structural, maturational, and functional features. Four significant biological properties shared are; 1) the conservation of a large array of enzymes involved in nucleic acid metabolism, DNA synthesis, and processing of proteins, 2) viral gene transcription, genome replication, capsid assembly and capsid loading all occur in the nucleus, and final envelopment occurs in the cytoplasm, 3) lytic infection and production of viral progeny often results in the destruction of the host cell, 4) employment of a cellular latency program defined by the absence of lytic gene expression, which allows the virus to remain undetected by host immune responses and persist throughout the life of the host organism[22].

There are number of conserved structural features among the human herpesviruses. At the core of the mature virion is a single, unit length, linear, naked, double stranded genome packaged into the capsid so tightly that it is in a liquid crystalline state[32]. The 3D architecture of the capsid is an icosahedron with symmetry on the 6-fold, 5-fold, 3-fold and 2-fold axis, for a triangulation number of 16 and an approximately 125nm capsid diameter. The capsids are composed of 161 capsomers of the major capsid protein. 150 homohexameric capsomers make up the faces of the icosahedron, and 11 homopentameric capsomers occupy the vertexes. The 12th vertex is occupied by a ring structure composed of 12 copies of the portal protein[18,33-37]. This

portal is used by the terminase complex to load the genome into the nascent capsid[18,33].Capsomers protrude radially from the base of the capsid forming chimney like structures, and heterotriplexes composed of a monomer and a homodimer rivet the neighboring capsomers together at their base, and help form the capsid floor [34,35,38]. The maturational protease and scaffolding protein(s) are found in the interior of immature capsids and help nucleate the formation and maturation of capsids. Its important to note that secondary, tertiary, and quaternary structure is essential in capsid formation, maturation, and stability[38-41].

Virion maturation involves the sequential and ordered addition of a proteinaceous structure called the tegument on the outside of the capsid; a form of "viral cytoplasm". Inner tegument proteins contact the capsid directly and are mostly acquired in the nucleus and possibly during transition through the perinuclear space[42]. The outer tegument is acquired in the cytoplasm and contains another layer of proteins that bridge the inner tegument and envelope glycoproteins[43]. During egress through the cytoplasm several species of mRNA are also included in the outer tegument [44]. Envelopment of nascent herpesvirus capsids proceeds via complex process that begins with a primary envelopment at the inner nuclear membrane, followed by de-envelopment at the outer nuclear membrane which releases naked capsids into the cytoplasm[45]. Capsids are then transported via microtubule networks and motor proteins to the site of secondary envelopment. Th precises nature of secondary envelopment, and the secretory pathway compartment(s) involved are still poorly understood[43].

Herpesviruses utilize a myriad of mechanisms to achieve astounding functional complexity from a limited genetic space. Techniques ranging from transcription of microRNA and non-coding RNA, alternative splicing, antisense transcription, and cell/tissue specific transcriptional programs lead to a plethora of transcriptional potential[46-48]. Leaky scanning, internal translation start sites, and posttranslational modifications also reinforce a controversial dogma; of one gene, many functions[49,50]. Despite this complexity there are some common functional themes that are conserved among the mammalian herpesviruses. Gene expression happens in a temporally ordered cascade which ultimately results in the synthesis of new viral DNA and virion assembly. This temporal cascade follows a familiar pattern; Immediate early genes require no new cellular or viral protein synthesis for their transcription, early genes display transcription that is independent of viral DNA replication, and late genes display transcription that is restricted until after viral DNA replication begins. All human herpesviruses subfamilies also encode a diverse array of proteins that; 1) drive the expression of each temporal class of genes[22,51,52], 2) disable and subvert the host innate and adaptive immune responses[22,53], 3) augment host metabolism, macromolecular biosynthesis, and transport[22].

Key capsid components

In cell free systems, the major capsid protein, triplex protein 1 and 2, and scaffolding protein are required for capsid formation[39,54]. However, in baculoviral expression systems, five genes are required for complete capsid formation; major capsid protein, triplex protein 1 and 2, scaffolding protein, and the maturational protease[55]. These data indicate that viral capsid proteins

alone contain all the necessary information for capsid formation and that capsid formation can occur in the absence of other host factors.

Capsid species

Herpesvirus capsid assembly results in several morphologically distinct capsid species that represent intermediates in the capsid maturation process. In-vitro capsid assembly systems have determined that the capsid is assembled in stepwise fashion, with partially formed procapsids that appear as wedges and exhibit the same curvature and ratio of shell to scaffolding protein as the complete spherical procapsid[54]. Heterotriplex's are essential in capsid assembly, and they are incorporated into the nascent capsid as it progresses from the partially formed wedges into the spherical procapsid[39,54,55]. The procapsid is fragile and refractory to isolation from centrifugation techniques, however, immuno-precipitation has been used to visualize the procapsid by cryoelectron microscopy. Diameter analyses from these studies confirm the morphological observations from thin section electron microscopy that the procapsid is an almost perfect sphere. Cryoelectron reconstructions of procapsids also indicate that the procapsid undergoes significant tertiary and quaternary structure maturations to become the more angular capsid versions.

In the procapsid there are virtually no major capsid subunit connections in the capsomers (intracapsomeric connections) at the outer face for both hexons and pentons, and the axial channels in capsomers are far more relaxed and porous compared to the angular version. The only major capsid subunit connections observed in the procapsid occur in the floor region of the capsomers. These connections in the floor region result in more defined symmetry compared to the outer face of the procapsid, where the relaxed symmetry results in the procapsids overall spherical nature. Intercapsomere connections in the procapsid are also absent at the outer face, and neighboring capsomers are linked solely at their bases by the triplexes. The floor of the procapsid also appears more porous than the angular capsid because it lacks triplex connections between the center and edge hexons as well triplex connections between the penton and the peripentonal hexon that make up the center of the triangular faces[56].

Procapsids mature into a more angular capsid, and there are three distinct angular capsid species that have been characterized to date. A-capsids contain an empty/hollow core, B-capsids contain in an internal ring structure, and C-capsids contain a single, naked, unit-length copy of the viral genome. Reverse genetics combined with biochemical and biological data has revealed that the B-capsid is a precursor to both A and C-capsids, and that A-capsids result from an abortive genome packaging event[57].

DNA packaging is essential in capsid maturation

Herpesviruses replicate their DNA using a rolling circle mechanism that results in concatemeric genomes, and all genomes contain *cis*-acting sequencings that direct the packaging and cleavage of unit length genomes into the capsid. Studies in HSV-1 have revealed that seven viral genes are responsible for successful DNA packaging into nascent capsids. These proteins are encoded by HSV UL6 (KSHV ORF 43), UL25 (KSHV ORF19), UL15 (KSHV ORF29),

UL28 (KSHV ORF7), UL32 (ORF68), UL33 (67.5/67A), UL17 (KSHV ORF32). All these proteins are required for the formation of fully packaged C-capsids that contain DNA. Mutation of any one of these genes causes the accumulation of either B-capsid species (HSV UL6, UL15, UL28, UL32, UL33, UL17) or A capsid species (UL25)[57].The DNA is packaged so tightly into nascent capsids that it is in a liquid crystalline state[32].

Overview of KSHV

The first known documentation of Kaposi Sarcoma Herpesvirus (KSHV) infection was made by the Hungarian dermatologist Moritz Kaposi. He observed multifocal brownish-red or blueish-red nodules/plaques on the feet and hands of several patients. His observations went largely unnoticed by the scientific community until the molecular discovery of the KSHV genome by representational difference analysis of HIV-positive individuals in 1994 by Moore and Chang[58]. Shortly after its discovery, KSHV was proposed to be the causative agent of Kaposi Sarcoma (KS) and Primary Effusion Lymphoma (PEL) as well as several other lymphoproliferative and cytokine-mediated disorders[27,28,58-60]. These observations led to an explosion of research and an appreciation of the diverse immunomodulatory and cell cycle control mechanisms KSHV employed[61,62]. Studies on reactivation and KSHV-induced oncogenesis have also been fueled by the epidemiological consensus that reactivation from latency is strongly correlated to disease phenotype[63,64].

Structure and organization of the genome

Genomic sequencing of a KSHV clinical isolate revealed the genome is 165-170kb in length with a 140.5kb long unique region (LUR) and 35-45 copies of tandem repeats at the genomic termini. The long unique region contains over 80 traditional open reading frames (ORF's) and 5 internal repeat regions. The LUR is flanked by 803-bp long, 85% GC terminal tandem repeats which are distributed asymmetrically on either end of the genome[65,66]. A recent report details the genomic sequencing of a second Rhadinoviral linage that is distinct from the KSHV lineage. Both Rhadinoviral lineages retain positional and sequence homology for core gene blocks containing DNA synthesis genes, virion structural component genes, as well as the G*ammaherpesvirus*-specific immediate early and latency loci. However, significant sequence divergence is found in the genomic regions that correspond to the 'K' genes in KSHV. These "K" genes are found in the 25-35kb region and the 85-95kb region of the KHSV genome[67].These 'K' genes are putatively responsible for innate and adaptive immune modulation.

Viral latent and lytic cycles

Latency is the default program for KSHV infection. The host cellular and microenvironment play an important role in the decision to enter and maintain viral latency during de-novo infection (chapter 2). After de-novo infection, a limited bust of lytic gene transcription modulates the host cell and microenvironment. These events prepare an ecological niche in the host organism that is amenable for establishment and maintenance of latency, and subversion/modulation of host innate and adaptive immunity. After this initial "lytic burst" of gene expression, most viral gene expression is repressed, leaving only a handful of genes that are

continually expressed; this is the establishment of latency for KSHV[68,69]. While the transcriptional profile of latency can vary for different tissue and cell types, the major polycistronic latency transcript is expressed in some form for virtually all KSHV infected cells[63,70-73]. The observation that PEL cell lines harboring latent KSHV can be reactivated to produce cell free virus by adding histone deacetylase inhibitors to culture medium support the hypothesis that the control of latency, and by extension the decision to reactivate, is an epigenic construct. Recent ChIP-seq data corroborates this hypothesis[74].

KSHV ORF 73 (LANA) and ORF50 (RTA) serve diverse physiological functions that drive the latent and lytic cycles

KSHV ORF50 encodes a transcriptional activator whose expression is necessary and sufficient to drive the entire lytic cascade of gene expression[52,75,76]. Its transcriptional activation potential is broad, and its mechanistic approach is diverse. ORF50 directly induces transcription from many sites in the viral genome[77,78]. It also works cooperatively with host cell factors to induce transcription in a cell-dependent fashion[77,79-81]. ORF50 also recruits host cell transcription factors to induce a positive feedback loop of autoactivation[82]. ORF50 also promotes reactivation by meditating the destruction of host innate antiviral response proteins, facilitating a cellular environment conducive to effective viral replication[83].

KSHV ORF73, Latency Associated Nuclear Antigen (LANA), is a protein coded for from the major latency associated transcript. LANA binds the viral terminal repeat sequences to tether viral episomes to host chromatin and mediates segregation of latent viral DNA to daughter cells during mitosis[84,85]. LANA also is responsible for the recruitment of host factors that replicate the latent genome[86]. LANA can act as a transcriptional activator or repressor on cellular and viral genes, and acts as an autoregulator of itself, and by extension, the KSHV polycistronic major latency locus[87]. LANA binds to Rb and p53 and causes the altered regulation of many genes in these respective pathways[87-89]. Binding of LANA to p53 results in inhibition of p53 mediated apoptosis, and binding of LANA to Rb results in the release of the cells from the G1/S phase checkpoint. LANA is believed by some to be the master regulator of transcription. It can bind to ORF50 and suppress ORF50 autoactivation, which results in a decrease in virion accumulation in the supernatant under inducing conditions[90].

KSHV latency

Epigenetic modifications to “viral chromatin” serve to activate and repress the viral transcriptome. Genome wide studies using ChIP-seq have observed that the vast majority of the KSHV genome is enriched for the transcriptionally repressive H3K27me3 histone modification marker, including the promoter region of ORF50. They also revealed that the major latency locus is enriched in the activating AcH3 marker. These studies also provide insight into the myriad of complex epigenetic patterns unique to the various forms and staging of KSHV-mediated disease both in-vitro and in-vivo[74,91,92]. The theory of epigenetic control over latency is supported by the observation that treatment with Histone Deacetylase inhibitors (HDAC) is sufficient to reactive KSHV from latency by driving ORF50 expression[93]. Viral genome methylation is another strategy that KSHV uses to control latency, and there have been several observations that this

nucleotide modification is also important for maintaining viral latency[92,94]. Also of note is the observation that various host factor interactions (CTCF and cohesion) with the viral genome seem to be important for transcriptional control of viral gene expression[95,96].

KSHV pathogenesis

Several KSHV RNA transcripts and gene products are capable of various levels on transformation in-vitro and in-vivo[97,98]. However, the complex interplay between their direct and indirect effects on host signaling pathways means that infection with KSHV alone is generally regarded as insufficient to transform human cells in-vitro and in-vivo. There are a pair of reports documenting KSHV-mediated transformation and tumorgenicity, one in primary rat cells and another in endothelial cells. However, the field largely considers that these reports are the exception, not the norm[60,98,99]. In support of the theory that KSHV infection alone is insufficient to drive cellular transformation is the observation that when explanted in culture, KS spindle cells lose the viral episome after serial passage but retain their transformed phenotype. These data are peculiar considering that the three main KSHV-mediated diseases are of a proliferative nature, and two of the proliferative diseases are in the B-cell linage. There are no reports of KSHV-mediated transformation in primary B-cells in-vitro, however, this could be due to the fact B-cells are generally refractory to infection with KSHV in-vitro.

While the latency program has been accepted as the cause of EBV-mediated transformation, a clear and causal connection between transformation and latency alone has not been established for KSHV. It is slowly becoming accepted that while the latency program of KSHV certainly contributes to immortalization in-vivo, latency alone is not sufficient to drive tumorigenesis. In all forms of KSHV mediated disease, there is a small percentage of cells that undergo spontaneous reactivation into the lytic cycle. KSHV reactivation from latency and lytic replication is a defining characteristic of KS and MCD. Patients with detectable levels of KSHV viremia have a 10-fold greater risk of developing KS than those who do not display KSHV viremia, and the level of KSHV DNA in PBMCs is strongly correlated with disease severity and staging of KS[100,101]. Increased levels of viral genome copy number in PMBC cells are also correlated with symptomatic episodes of MCD[102]. Treatment of KS patients with the herpesvirus DNA replication inhibitors foscarnet and ganciclovir has also been shown to increase the time frame of clinical progression of KS[103]. These data support the hypothesis that reactivation from latency is a key pathogenic step for KSHV-mediated disease, and that reactivation results in inheritable changes to the host cell that synergistically drive proliferation.

Referecnes:

1 Astrachan, L. & Volkin, E. Properties of ribonucleic acid turnover in T2-infected Escherichia coli. *Biochim Biophys Acta* **29**, 536-544, doi:10.1016/0006-3002(58)90010-6 (1958).

2 Hershey, A. D. & Chase, M. Independent functions of viral protein and nucleic acid in growth of bacteriophage. *J Gen Physiol* **36**, 39-56, doi:10.1085/jgp.36.1.39 (1952).

3 Edgar, R. S. & Wood, W. B. Morphogenesis of bacteriophage T4 in extracts of mutant-infected cells. *Proc Natl Acad Sci U S A* **55**, 498-505, doi:10.1073/pnas.55.3.498 (1966).

4 Laemmli, U. K. Cleavage of structural proteins during the assembly of the head of bacteriophage T4. *Nature* **227**, 680-685, doi:10.1038/227680a0 (1970).

5 Enders, J. F., Weller, T. H. & Robbins, F. C. Cultivation of the Lansing Strain of Poliomyelitis Virus in Cultures of Various Human Embryonic Tissues. *Science* **109**, 85-87, doi:10.1126/science.109.2822.85 (1949).

6 Stehelin, D., Varmus, H. E., Bishop, J. M. & Vogt, P. K. DNA related to the transforming gene(s) of avian sarcoma viruses is present in normal avian DNA. *Nature* **260**, 170-173, doi:10.1038/260170a0 (1976).

7 Lane, D. P. & Crawford, L. V. T antigen is bound to a host protein in SV40-transformed cells. *Nature* **278**, 261-263, doi:10.1038/278261a0 (1979).

8 Levine, A. J. The tumor suppressor genes. *Annu Rev Biochem* **62**, 623-651, doi:10.1146/annurev.bi.62.070193.003203 (1993).

9 Moore, P. S. & Chang, Y. Why do viruses cause cancer? Highlights of the first century of human tumour virology. *Nat Rev Cancer* **10**, 878-889, doi:10.1038/nrc2961 (2010).

10 zur Hausen, H. Oncogenic DNA viruses. *Oncogene* **20**, 7820-7823, doi:10.1038/sj.onc.1204958 (2001).

11 Daniel DiMaio, H. in *Fields Virology 6th edtion* Ch. Viruses, Cell Transformation, and Cancer, 153-188 (Philadelphia, PA: Lippincott Williams & Wilkins, 2013).

12 Davison, A. J. *et al.* The order Herpesvirales. *Arch Virol* **154**, 171-177, doi:10.1007/s00705-008-0278-4 (2009).

13 Walker, P. J. *et al.* Changes to virus taxonomy and the Statutes ratified by the International Committee on Taxonomy of Viruses (2020). *Arch Virol* **165**, 2737-2748, doi:10.1007/s00705-020-04752-x (2020).

14 Davison, A. J. in *Human Herpesviruses: Biology, Therapy, and Immunoprophylaxis* (eds A. Arvin *et al.*) Ch. Comparative analysis of the genomes, (2007).

15 Mitchell, M. S., Matsuzaki, S., Imai, S. & Rao, V. B. Sequence analysis of bacteriophage T4 DNA packaging/terminase genes 16 and 17 reveals a common ATPase center in the large subunit of viral terminases. *Nucleic Acids Research* **30**, 4009-4021, doi:10.1093/nar/gkf524 (2002).

16 Baker, M. L., Jiang, W., Rixon, F. J. & Chiu, W. Common ancestry of herpesviruses and tailed DNA bacteriophages. *J Virol* **79**, 14967-14970, doi:10.1128/JVI.79.23.14967-14970.2005 (2005).

17 Davison, A. J. & Davison, M. D. Identification of structural proteins of channel catfish virus by mass spectrometry. *Virology* **206**, 1035-1043, doi:10.1006/viro.1995.1026 (1995).

18 Liu, Y. T., Jih, J., Dai, X., Bi, G. Q. & Zhou, Z. H. Cryo-EM structures of herpes simplex virus type 1 portal vertex and packaged genome. *Nature* **570**, 257-261, doi:10.1038/s41586-019-1248-6 (2019).

19 Booy, F. P., Trus, B. L., Davison, A. J. & Steven, A. C. The capsid architecture of channel catfish virus, an evolutionarily distant herpesvirus, is largely conserved in the absence of discernible sequence homology with herpes simplex virus. *Virology* **215**, 134-141, doi:10.1006/viro.1996.0016 (1996).
20 Davison, A. J. *et al.* A novel class of herpesvirus with bivalve hosts. *J Gen Virol* **86**, 41-53, doi:10.1099/vir.0.80382-0 (2005).
21 Davison, A. J. Evolution of the herpesviruses. *Vet Microbiol* **86**, 69-88, doi:10.1016/s0378-1135(01)00492-8 (2002).
22 Philip E. Pellett, B. R. in *Fields Virology 6th edtion* Ch. Herpesviridae, 1802-1822 (Philadelphia, PA: Lippincott Williams & Wilkins, 2013).
23 Searles, R. P., Bergquam, E. P., Axthelm, M. K. & Wong, S. W. Sequence and genomic analysis of a Rhesus macaque rhadinovirus with similarity to Kaposi's sarcoma-associated herpesvirus/human herpesvirus 8. *J Virol* **73**, 3040-3053, doi:10.1128/JVI.73.4.3040-3053.1999 (1999).
24 McGeoch, D. J., Cook, S., Dolan, A., Jamieson, F. E. & Telford, E. A. Molecular phylogeny and evolutionary timescale for the family of mammalian herpesviruses. *J Mol Biol* **247**, 443-458, doi:10.1006/jmbi.1995.0152 (1995).
25 Richard Longnecker, F. N. in *Human Herpesviruses: Biology, Therapy, and Immunoprophylaxis* (eds A. Arvin *et al.*) Ch. Introduction to the human γ-herpesviruses, (2007).
26 Gao, S. J. *et al.* Seroconversion to antibodies against Kaposi's sarcoma-associated herpesvirus-related latent nuclear antigens before the development of Kaposi's sarcoma. *N Engl J Med* **335**, 233-241, doi:10.1056/NEJM199607253350403 (1996).
27 Cesarman, E., Chang, Y., Moore, P. S., Said, J. W. & Knowles, D. M. Kaposi's sarcoma-associated herpesvirus-like DNA sequences in AIDS-related body-cavity-based lymphomas. *N Engl J Med* **332**, 1186-1191, doi:10.1056/NEJM199505043321802 (1995).
28 Soulier, J. *et al.* Kaposi's sarcoma-associated herpesvirus-like DNA sequences in multicentric Castleman's disease. *Blood* **86**, 1276-1280 (1995).
29 Helenius, A. in *Fields Virology 6th edtion* Ch. Virus Entry and Uncoating, 87-103 (Philadelphia, PA: Lippincott Williams & Wilkins, 2013).
30 Whelan, S. in *Fields Virology 6th edtion* Ch. Viral Replication Strategies, 105-126 (Philadelphia, PA: Lippincott Williams & Wilkins, 2013).
31 Hunter, E. in *Fields Virology 6th edtion* Ch. Virus Assembly, 127-152 (Philadelphia, PA: Lippincott Williams & Wilkins, 2013).
32 Booy, F. P. *et al.* Liquid-crystalline, phage-like packing of encapsidated DNA in herpes simplex virus. *Cell* **64**, 1007-1015, doi:10.1016/0092-8674(91)90324-r (1991).
33 Gong, D. *et al.* DNA-Packing Portal and Capsid-Associated Tegument Complexes in the Tumor Herpesvirus KSHV. *Cell* **178**, 1329-1343 e1312, doi:10.1016/j.cell.2019.07.035 (2019).
34 Yuan, S. *et al.* Cryo-EM structure of a herpesvirus capsid at 3.1 A. *Science* **360**, doi:10.1126/science.aao7283 (2018).
35 Yu, X., Jih, J., Jiang, J. & Zhou, Z. H. Atomic structure of the human cytomegalovirus capsid with its securing tegument layer of pp150. *Science* **356**, doi:10.1126/science.aam6892 (2017).

36 Homa, F. L. *et al.* Structure of the pseudorabies virus capsid: comparison with herpes simplex virus type 1 and differential binding of essential minor proteins. *J Mol Biol* **425**, 3415-3428, doi:10.1016/j.jmb.2013.06.034 (2013).
37 Li, Z. *et al.* CryoEM structure of the tegumented capsid of Epstein-Barr virus. *Cell Res* **30**, 873-884, doi:10.1038/s41422-020-0363-0 (2020).
38 Dai, X. *et al.* Structure and mutagenesis reveal essential capsid protein interactions for KSHV replication. *Nature* **553**, 521-525, doi:10.1038/nature25438 (2018).
39 Newcomb, W. W., Homa, F. L., Thomsen, D. R., Ye, Z. & Brown, J. C. Cell-free assembly of the herpes simplex virus capsid. *J Virol* **68**, 6059-6063, doi:10.1128/JVI.68.9.6059-6063.1994 (1994).
40 Zhou, Z. H. *et al.* Four levels of hierarchical organization, including noncovalent chainmail, brace the mature tumor herpesvirus capsid against pressurization. *Structure* **22**, 1385-1398, doi:10.1016/j.str.2014.05.019 (2014).
41 Dai, X. *et al.* CryoEM and mutagenesis reveal that the smallest capsid protein cements and stabilizes Kaposi's sarcoma-associated herpesvirus capsid. *Proc Natl Acad Sci U S A* **112**, E649-656, doi:10.1073/pnas.1420317112 (2015).
42 Yu, X. *et al.* Biochemical and structural characterization of the capsid-bound tegument proteins of human cytomegalovirus. *J Struct Biol* **174**, 451-460, doi:10.1016/j.jsb.2011.03.006 (2011).
43 Mettenleiter, T. C. Intriguing interplay between viral proteins during herpesvirus assembly or: the herpesvirus assembly puzzle. *Vet Microbiol* **113**, 163-169, doi:10.1016/j.vetmic.2005.11.040 (2006).
44 Bechtel, J., Grundhoff, A. & Ganem, D. RNAs in the virion of Kaposi's sarcoma-associated herpesvirus. *J Virol* **79**, 10138-10146, doi:10.1128/JVI.79.16.10138-10146.2005 (2005).
45 Newcomb, W. W. *et al.* The Primary Enveloped Virion of Herpes Simplex Virus 1: Its Role in Nuclear Egress. *mBio* **8**, doi:10.1128/mBio.00825-17 (2017).
46 Gatherer, D. *et al.* High-resolution human cytomegalovirus transcriptome. *Proc Natl Acad Sci U S A* **108**, 19755-19760, doi:10.1073/pnas.1115861108 (2011).
47 Plaisance-Bonstaff, K. & Renne, R. Viral miRNAs. *Methods Mol Biol* **721**, 43-66, doi:10.1007/978-1-61779-037-9_3 (2011).
48 Stern-Ginossar, N. *et al.* Decoding human cytomegalovirus. *Science* **338**, 1088-1093, doi:10.1126/science.1227919 (2012).
49 Xu, L. & Yuan, Y. Two microPeptides are translated from a KSHV polycistronic RNA in human cells by leaky scanning mechanism. *Biochem Biophys Res Commun* **522**, 568-573, doi:10.1016/j.bbrc.2019.11.087 (2020).
50 Othman, Z. *et al.* Functional analysis of Kaposi's sarcoma-associated herpesvirus vFLIP expression reveals a new mode of IRES-mediated translation. *RNA* **20**, 1803-1814, doi:10.1261/rna.045328.114 (2014).
51 Gomi, Y., Imagawa, T., Takahashi, M. & Yamanishi, K. Comparison of DNA sequence and transactivation activity of open reading frame 62 of Oka varicella vaccine and its parental viruses. *Arch Virol Suppl*, 49-56, doi:10.1007/978-3-7091-6259-0_6 (2001).
52 Lukac, D. M., Renne, R., Kirshner, J. R. & Ganem, D. Reactivation of Kaposi's sarcoma-associated herpesvirus infection from latency by expression of the ORF 50 transactivator, a homolog of the EBV R protein. *Virology* **252**, 304-312, doi:10.1006/viro.1998.9486 (1998).

53 Davison, A. J., Dargan, D. J. & Stow, N. D. Fundamental and accessory systems in herpesviruses. *Antiviral Res* **56**, 1-11, doi:10.1016/s0166-3542(02)00107-9 (2002).
54 Newcomb, W. W. *et al.* Assembly of the herpes simplex virus capsid: characterization of intermediates observed during cell-free capsid formation. *J Mol Biol* **263**, 432-446, doi:10.1006/jmbi.1996.0587 (1996).
55 Tatman, J. D., Preston, V. G., Nicholson, P., Elliott, R. M. & Rixon, F. J. Assembly of herpes simplex virus type 1 capsids using a panel of recombinant baculoviruses. *J Gen Virol* **75 (Pt 5)**, 1101-1113, doi:10.1099/0022-1317-75-5-1101 (1994).
56 Trus, B. L. *et al.* The herpes simplex virus procapsid: structure, conformational changes upon maturation, and roles of the triplex proteins VP19c and VP23 in assembly. *J Mol Biol* **263**, 447-462, doi:10.1016/s0022-2836(96)80018-0 (1996).
57 Heming, J. D., Conway, J. F. & Homa, F. L. Herpesvirus Capsid Assembly and DNA Packaging. *Adv Anat Embryol Cell Biol* **223**, 119-142, doi:10.1007/978-3-319-53168-7_6 (2017).
58 Chang, Y. *et al.* Identification of herpesvirus-like DNA sequences in AIDS-associated Kaposi's sarcoma. *Science* **266**, 1865-1869, doi:10.1126/science.7997879 (1994).
59 Moore, P. S. & Chang, Y. Detection of herpesvirus-like DNA sequences in Kaposi's sarcoma in patients with and those without HIV infection. *N Engl J Med* **332**, 1181-1185, doi:10.1056/NEJM199505043321801 (1995).
60 Blossom A. Damania, E. C. in *Fields Virology 6th edtion* Ch. Kaposi's Sarcoma–Associated Herpesvirus, 2080-2128 (Philadelphia, PA: Lippincott Williams & Wilkins, 2013).
61 Moore, P. S. in *Human Herpesviruses: Biology, Therapy, and Immunoprophylaxis* (eds A. Arvin *et al.*) Ch. KSHV manipulation of the cell cycle and apoptosis, (2007).
62 Robert E. Means, S. M. L., and Jae U. Jung. in *Human Herpesviruses: Biology, Therapy, and Immunoprophylaxis* (eds A. Arvin *et al.*) Ch. Human gammaherpesvirus immune evasion strategies, (2007).
63 Yuan, D. M. L. a. Y. in *Human Herpesviruses: Biology, Therapy, and Immunoprophylaxis* (eds A. Arvin *et al.*) Ch. Reactivation and lytic replication of KSHV, (2007).
64 Ganem, D. in *Human Herpesviruses: Biology, Therapy, and Immunoprophylaxis* (eds A. Arvin *et al.*) Ch. KSHV-induced oncogenesis, (2007).
65 Russo, J. J. *et al.* Nucleotide sequence of the Kaposi sarcoma-associated herpesvirus (HHV8). *Proc Natl Acad Sci U S A* **93**, 14862-14867, doi:10.1073/pnas.93.25.14862 (1996).
66 Lagunoff, M. & Ganem, D. The structure and coding organization of the genomic termini of Kaposi's sarcoma-associated herpesvirus. *Virology* **236**, 147-154, doi:10.1006/viro.1997.8713 (1997).
67 Bruce, A. G. *et al.* Complete genome sequence of Pig-tailed macaque rhadinovirus 2 and its evolutionary relationship with rhesus macaque rhadinovirus and human herpesvirus 8/Kaposi's sarcoma-associated herpesvirus. *J Virol* **89**, 3888-3909, doi:10.1128/JVI.03597-14 (2015).
68 Purushothaman, P., Thakker, S. & Verma, S. C. Transcriptome analysis of Kaposi's sarcoma-associated herpesvirus during de novo primary infection of human B and endothelial cells. *J Virol* **89**, 3093-3111, doi:10.1128/JVI.02507-14 (2015).

69 Krishnan, H. H. *et al.* Concurrent expression of latent and a limited number of lytic genes with immune modulation and antiapoptotic function by Kaposi's sarcoma-associated herpesvirus early during infection of primary endothelial and fibroblast cells and subsequent decline of lytic gene expression. *J Virol* **78**, 3601-3620, doi:10.1128/jvi.78.7.3601-3620.2004 (2004).
70 Dittmer, D. P. Transcription profile of Kaposi's sarcoma-associated herpesvirus in primary Kaposi's sarcoma lesions as determined by real-time PCR arrays. *Cancer Res* **63**, 2010-2015 (2003).
71 Rivas, C., Thlick, A. E., Parravicini, C., Moore, P. S. & Chang, Y. Kaposi's sarcoma-associated herpesvirus LANA2 is a B-cell-specific latent viral protein that inhibits p53. *J Virol* **75**, 429-438, doi:10.1128/JVI.75.1.429-438.2001 (2001).
72 Chang, T. F. S. a. Y. in *Human Herpesviruses: Biology, Therapy, and Immunoprophylaxis* (eds A. Arvin *et al.*) Ch. KSHV gene expression and regulation, (2007).
73 Dittmer, D. *et al.* A cluster of latently expressed genes in Kaposi's sarcoma-associated herpesvirus. *J Virol* **72**, 8309-8315, doi:10.1128/JVI.72.10.8309-8315.1998 (1998).
74 Sun, R. *et al.* Epigenetic Landscape of Kaposi's Sarcoma-Associated Herpesvirus Genome in Classic Kaposi's Sarcoma Tissues. *PLoS Pathog* **13**, e1006167, doi:10.1371/journal.ppat.1006167 (2017).
75 Nakamura, H. *et al.* Global changes in Kaposi's sarcoma-associated virus gene expression patterns following expression of a tetracycline-inducible Rta transactivator. *J Virol* **77**, 4205-4220, doi:10.1128/jvi.77.7.4205-4220.2003 (2003).
76 Sun, R. *et al.* A viral gene that activates lytic cycle expression of Kaposi's sarcoma-associated herpesvirus. *Proc Natl Acad Sci U S A* **95**, 10866-10871, doi:10.1073/pnas.95.18.10866 (1998).
77 Chen, J., Ye, F., Xie, J., Kuhne, K. & Gao, S. J. Genome-wide identification of binding sites for Kaposi's sarcoma-associated herpesvirus lytic switch protein, RTA. *Virology* **386**, 290-302, doi:10.1016/j.virol.2009.01.031 (2009).
78 Chang, P. J. *et al.* Open reading frame 50 protein of Kaposi's sarcoma-associated herpesvirus directly activates the viral PAN and K12 genes by binding to related response elements. *J Virol* **76**, 3168-3178, doi:10.1128/jvi.76.7.3168-3178.2002 (2002).
79 Carroll, K. D., Khadim, F., Spadavecchia, S., Palmeri, D. & Lukac, D. M. Direct interactions of Kaposi's sarcoma-associated herpesvirus/human herpesvirus 8 ORF50/Rta protein with the cellular protein octamer-1 and DNA are critical for specifying transactivation of a delayed-early promoter and stimulating viral reactivation. *J Virol* **81**, 8451-8467, doi:10.1128/JVI.00265-07 (2007).
80 Liang, Y., Chang, J., Lynch, S. J., Lukac, D. M. & Ganem, D. The lytic switch protein of KSHV activates gene expression via functional interaction with RBP-Jkappa (CSL), the target of the Notch signaling pathway. *Genes Dev* **16**, 1977-1989, doi:10.1101/gad.996502 (2002).
81 Lai, I. Y., Farrell, P. J. & Kellam, P. X-box binding protein 1 induces the expression of the lytic cycle transactivator of Kaposi's sarcoma-associated herpesvirus but not Epstein-Barr virus in co-infected primary effusion lymphoma. *J Gen Virol* **92**, 421-431, doi:10.1099/vir.0.025494-0 (2011).
82 Wang, S. E., Wu, F. Y., Yu, Y. & Hayward, G. S. CCAAT/enhancer-binding protein-alpha is induced during the early stages of Kaposi's sarcoma-associated herpesvirus

(KSHV) lytic cycle reactivation and together with the KSHV replication and transcription activator (RTA) cooperatively stimulates the viral RTA, MTA, and PAN promoters. *J Virol* **77**, 9590-9612, doi:10.1128/jvi.77.17.9590-9612.2003 (2003).

83 Yu, Y., Wang, S. E. & Hayward, G. S. The KSHV immediate-early transcription factor RTA encodes ubiquitin E3 ligase activity that targets IRF7 for proteosome-mediated degradation. *Immunity* **22**, 59-70, doi:10.1016/j.immuni.2004.11.011 (2005).

84 Ballestas, M. E., Chatis, P. A. & Kaye, K. M. Efficient persistence of extrachromosomal KSHV DNA mediated by latency-associated nuclear antigen. *Science* **284**, 641-644, doi:10.1126/science.284.5414.641 (1999).

85 Barbera, A. J. *et al.* The nucleosomal surface as a docking station for Kaposi's sarcoma herpesvirus LANA. *Science* **311**, 856-861, doi:10.1126/science.1120541 (2006).

86 Stedman, W., Deng, Z., Lu, F. & Lieberman, P. M. ORC, MCM, and histone hyperacetylation at the Kaposi's sarcoma-associated herpesvirus latent replication origin. *J Virol* **78**, 12566-12575, doi:10.1128/JVI.78.22.12566-12575.2004 (2004).

87 Renne, R. *et al.* Modulation of cellular and viral gene expression by the latency-associated nuclear antigen of Kaposi's sarcoma-associated herpesvirus. *J Virol* **75**, 458-468, doi:10.1128/JVI.75.1.458-468.2001 (2001).

88 Radkov, S. A., Kellam, P. & Boshoff, C. The latent nuclear antigen of Kaposi sarcoma-associated herpesvirus targets the retinoblastoma-E2F pathway and with the oncogene Hras transforms primary rat cells. *Nat Med* **6**, 1121-1127, doi:10.1038/80459 (2000).

89 Friborg, J., Jr., Kong, W., Hottiger, M. O. & Nabel, G. J. p53 inhibition by the LANA protein of KSHV protects against cell death. *Nature* **402**, 889-894, doi:10.1038/47266 (1999).

90 Lan, K., Kuppers, D. A., Verma, S. C. & Robertson, E. S. Kaposi's sarcoma-associated herpesvirus-encoded latency-associated nuclear antigen inhibits lytic replication by targeting Rta: a potential mechanism for virus-mediated control of latency. *J Virol* **78**, 6585-6594, doi:10.1128/JVI.78.12.6585-6594.2004 (2004).

91 Toth, Z. *et al.* Epigenetic analysis of KSHV latent and lytic genomes. *PLoS Pathog* **6**, e1001013, doi:10.1371/journal.ppat.1001013 (2010).

92 Gunther, T. & Grundhoff, A. The epigenetic landscape of latent Kaposi sarcoma-associated herpesvirus genomes. *PLoS Pathog* **6**, e1000935, doi:10.1371/journal.ppat.1000935 (2010).

93 Lu, F. *et al.* Chromatin remodeling of the Kaposi's sarcoma-associated herpesvirus ORF50 promoter correlates with reactivation from latency. *J Virol* **77**, 11425-11435, doi:10.1128/jvi.77.21.11425-11435.2003 (2003).

94 Chen, J. *et al.* Activation of latent Kaposi's sarcoma-associated herpesvirus by demethylation of the promoter of the lytic transactivator. *Proc Natl Acad Sci U S A* **98**, 4119-4124, doi:10.1073/pnas.051004198 (2001).

95 Kang, H., Cho, H., Sung, G. H. & Lieberman, P. M. CTCF regulates Kaposi's sarcoma-associated herpesvirus latency transcription by nucleosome displacement and RNA polymerase programming. *J Virol* **87**, 1789-1799, doi:10.1128/JVI.02283-12 (2013).

96 Li, D., Mosbruger, T., Verma, D. & Swaminathan, S. Complex Interactions between Cohesin and CTCF in Regulation of Kaposi's Sarcoma-Associated Herpesvirus Lytic Transcription. *J Virol* **94**, doi:10.1128/JVI.01279-19 (2020).

97 Giffin, L. & Damania, B. KSHV: pathways to tumorigenesis and persistent infection. *Adv Virus Res* **88**, 111-159, doi:10.1016/B978-0-12-800098-4.00002-7 (2014).

98 An, F. Q. *et al.* Long-term-infected telomerase-immortalized endothelial cells: a model for Kaposi's sarcoma-associated herpesvirus latency in vitro and in vivo. *J Virol* **80**, 4833-4846, doi:10.1128/JVI.80.10.4833-4846.2006 (2006).
99 Jones, T. *et al.* Direct and efficient cellular transformation of primary rat mesenchymal precursor cells by KSHV. *J Clin Invest* **122**, 1076-1081, doi:10.1172/JCI58530 (2012).
100 Engels, E. A. *et al.* Detection and quantification of Kaposi's sarcoma-associated herpesvirus to predict AIDS-associated Kaposi's sarcoma. *AIDS* **17**, 1847-1851, doi:10.1097/00002030-200308150-00015 (2003).
101 Campbell, T. B. *et al.* Relationship of human herpesvirus 8 peripheral blood virus load and Kaposi's sarcoma clinical stage. *AIDS* **14**, 2109-2116, doi:10.1097/00002030-200009290-00006 (2000).
102 Oksenhendler, E. *et al.* High levels of human herpesvirus 8 viral load, human interleukin-6, interleukin-10, and C reactive protein correlate with exacerbation of multicentric castleman disease in HIV-infected patients. *Blood* **96**, 2069-2073 (2000).
103 Robles, R., Lugo, D., Gee, L. & Jacobson, M. A. Effect of antiviral drugs used to treat cytomegalovirus end-organ disease on subsequent course of previously diagnosed Kaposi's sarcoma in patients with AIDS. *J Acquir Immune Defic Syndr Hum Retrovirol* **20**, 34-38, doi:10.1097/00042560-199901010-00005 (1999).

Chapter 2

Methods for the construction and analyzation of mutant Kaposi Sarcoma-associated herpesviruses

“The decision was not based on aptitude.” -*redacted*

Overview and acknowledgements

This chapter outlines the rationale for our experimental procedures and the protocols implemented for the creation and screening of our BAC16 mutant library. This chapter has been submitted with the help of Rachael Burchfield and Marco-Paliza-Carre. Rachael Burchfield was instrumental in the mutagenesis rationale and experimental design, and Marco-Paliza-Carre was instrumental in the cell culture and tittering rationale and experimental design. I am in indebted to them for their help

Creation of the BAC16

The creation of bacterial artificial chromosomes containing the genomes of herpesviruses has eased the ability of scientists to induce targeted mutations and reconstitute mutant viral progeny in vitro[1]. The KSHV BAC16 genome originated from the primary effusion lymphoma cell line JSC-1, which is co-infected with Epstein Barr Virus (EBV)[2]. The KSHV BAC16 was engineered by replacing an artificial GFP-RFP-puro cassette with a GFP-hygromycin cassette linked to the pBeloBAC11 vector flanked by *loxP* sites. The GFP-hygromycin cassette is driven by an eIF1a promoter with an IRES inserted downstream of the GFP coding region and upstream of the hygromycin resistance gene[3,4]. This new artificial chromosome has demonstrated the ability to be introduced via transfection into mammalian cells and produces high viral titer in the supernatant upon induction. Its viability in reverse genetics studies has also been well established in the literature[5-10]. It is worth noting that there are other KSHV BACs, however, the most widely used alternative KSHV BAC, BAC32[11], has been found to contain a long unique sequence region (LUR) duplication in the terminal repeats. This duplication contains KSHV ORFs 18, 17, 16, K7, K6, K5, part of ORF19, and the BAC cassette[12], thus abrogating its use in reverse genetics.

En-Passant mutagenesis and creation of BAC16 mutants

The *En-Passant* mutagenesis method is based off the lambda phage Red-system and allows for the introduction of foreign linear DNA sequences into target plasmids in E. coli[13,14]. The Red system contains three proteins: Exo, Gam, and Beta. When a linear PCR product is electroporated into E. coli, the Gam protein blocks the E. coli RecBCD helicase-nuclease complex from degrading the linear DNA. The 5'->3' exonuclease protein Exo degrades both ends of the PCR product and leaves a single-stranded 3' overhang on both sides. The single stranded binding protein Beta binds to the 3' overhang, protecting it from being degraded, and facilitates annealing of the single strand to complementary DNA during strand invasion. This initial recombination event is mediated by the addition of 40bp of homology to the target at the 5' and 3' end of the PCR product. Homologous recombination between the PCR product and the target results in the insertion of the PCR product and removal of the intervening plasmid sequence. The PCR product contains a marker that allows for selection of colonies that successfully underwent the targeted insertion using selection media (kanamycin). However, to introduce point mutations and deletions in a scarless manner, the selection marker must be removed. This is accomplished by the insertion of additional homology into the forward and reverse PCR primers. A sequence duplication of 20bp directly 3' to the target insertion/deletion

site in the forward primer and a sequence duplication of 20bp directly 5' to the target insertion/deletion site in the reverse primer, as well as an SceI meganuclease site directly downstream of the 3' duplication in the forward PCR primer accomplishes this second task. Thus, introduction of the PCR product into the target results in the duplication of 20bp of the 3' region in the 5' region and the duplication of 20bp of the 5' region in the 3' region. Expression of SceI meganuclease results in a doubled stranded DNA break at the cut site. The concurrent expression of the lambda-red proteins facilitates the second homologous recombination between the 20bp duplication of the 3' region in the 5' region with its homologous sequence downstream of selection marker and the 20bp duplication of the 5' region in the 3' region to recombine with its homologous sequence upstream of the selection marker. This second recombination removes the selection marker and sequence duplications, resulting in scarless deletions or introductions of short insertions. A simplified diagram of this workflow can be found in figure 1.

For the scarless insertion of long sequences, a universal transfer construct is created by cloning. The first step is to clone the insert into a plasmid using PCR and restriction digest. Once the insert has been cloned, a unique restriction site that occurs once in the insert sequence and not in the plasmid or kanamycin cassette is selected. The kanamycin cassette is PCR amplified with primers that add several features. The PCR forward primer adds the unique restriction site to the 5' end of the primer, a 50bp sequence duplication of the sequence directly downstream of the unique restriction site in the insert, and a SceI meganuclease site. The reverse primer should also add the unique restriction site to the 5' of the primer. The PCR product containing the selection marker, 50bp sequence duplication, and SceI site is cloned into the unique restriction site, creating the transfer plasmid. The transfer plasmid is used to create a linear PCR product that is electroporated into E. coli containing the target plasmid. The second PCR reaction should add an additional 50bp of targeting homology directly 5' and 3' to the insert location to the forward and reverse primers respectively, to target the first homologous recombination. The first homologous recombination results in the insertion of the linear universal transfer construct into the target plasmid in E. coli. Expression of the SceI meganuclease creates a double stranded DNA break and allows the 50bp sequence duplication to recombine with the native 50bp sequence downstream of the unique restriction site. This second homologous recombination results in the removal of the selection marker and the scarless insertion of the insert. A simplified diagram of this workflow can be found in figure 2.

This 2-step red recombination method is a versatile site directed mutagenesis procedure for the scarless insertion and deletion of sequences in Bacterial Artificial Chromosomes (BAC's) maintained in Escherichia coli (E. coli). The GS1783 strain of E. coli have the lambda Red proteins successfully inserted into the chromosome under a temperature inducible promoter. Incubation of the bacteria at 42C will induce expression of the Exo, Gam, and Beta proteins. The GS1783 strain also has the SceI meganuclease gene inserted into the chromosome under an arabinose inducible promoter. Addition of arabinose to the medium to a final concentration of 1% will induce expression of the SceI meganuclease[14]. We adopted this approach to mutate each reading frame in a KSHV genome (BAC16). We deleted the entire ORF from start to stop codon for non-overlapping ORFs. For overlapping reading frames, we inserted a short 12-bp sequence

that corresponds to a stop codon in every reading frame (and maintains the topology of the DNA helix) in the non-overlapping 5’ region of the ORF.

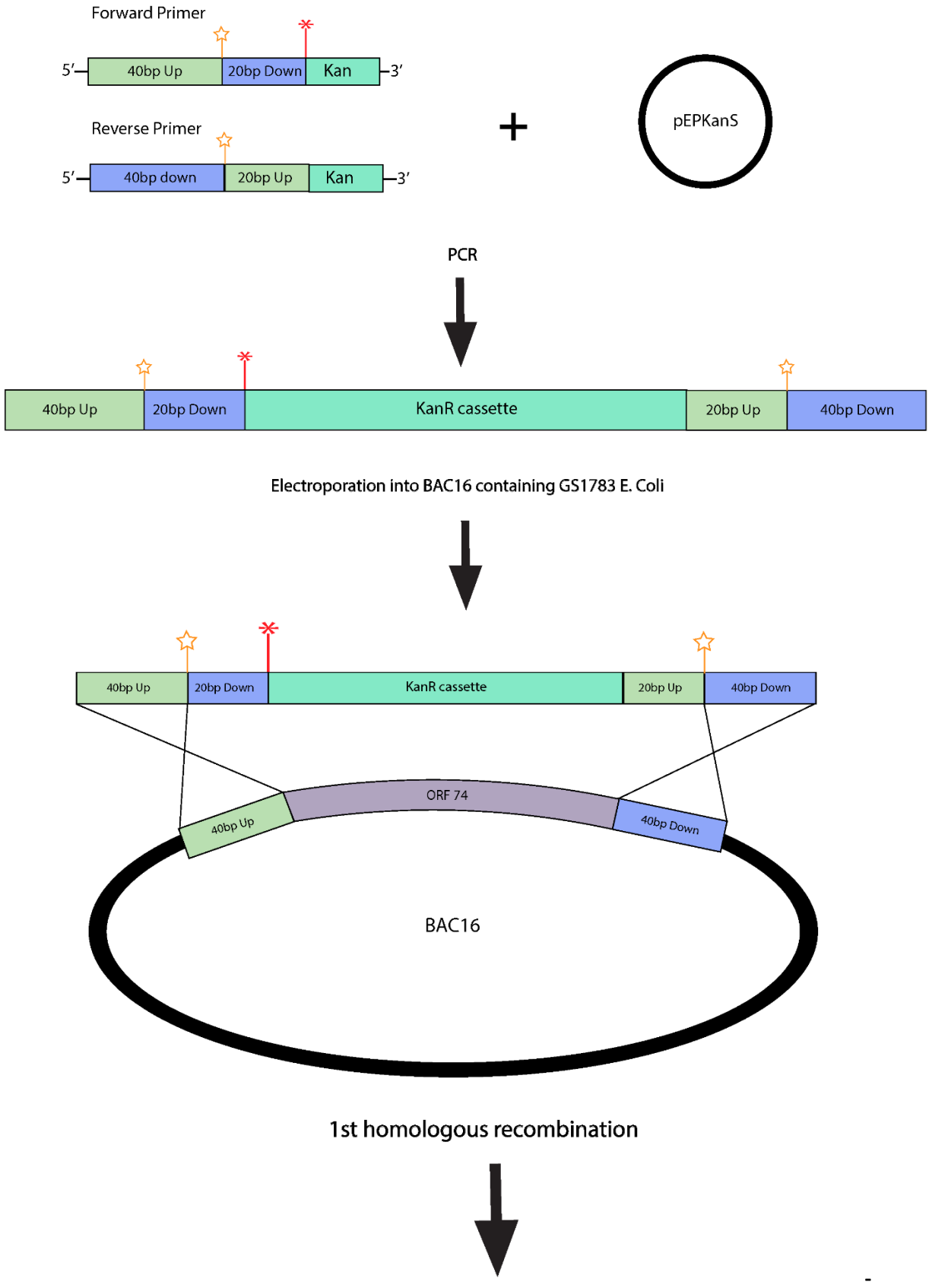
Forward Primer
5′
40bp Up
20bp Down
Kan
3′
Reverse Primer
5′
40bp down
20bp Up
Kan
3′
pEPKanS
PCR
40bp Up
20bp Down
KanR cassette
20bp Up
40bp Down
Electroporation into BAC16 containing GS1783 E. Coli
40bp Up
20bp Down
KanR cassette
20bp Up
40bp Down
ORF 74
40bp Up
40bp Down
BAC16
1st homologous recombination

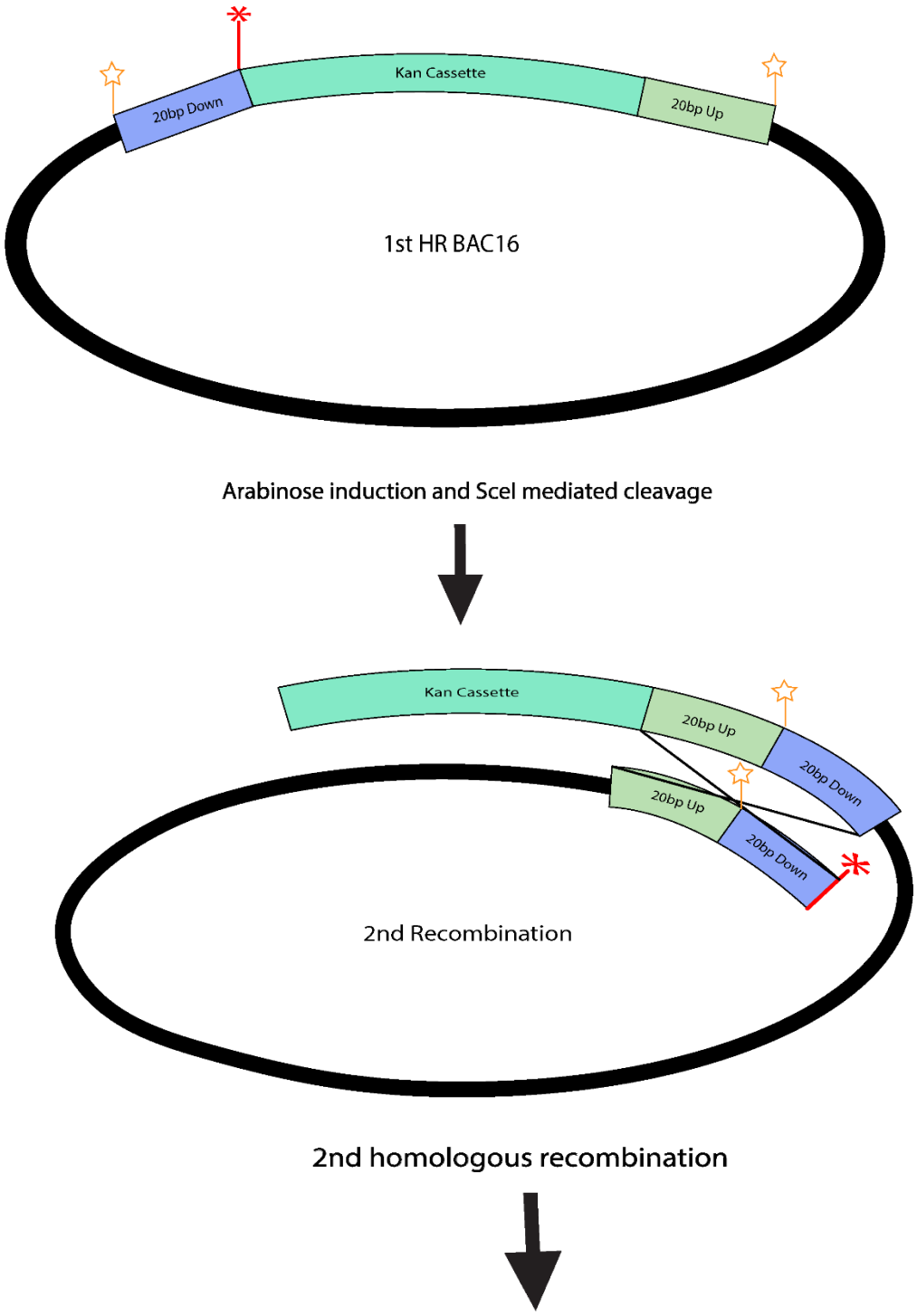
Kan Cassette
20bp Down
20bp Up
1st HR BAC16
Arabinose induction and SceI mediated cleavage
Kan Cassette
20bp Up
20bp Down
20bp Up
20bp Down
2nd Recombination
2nd homologous recombination

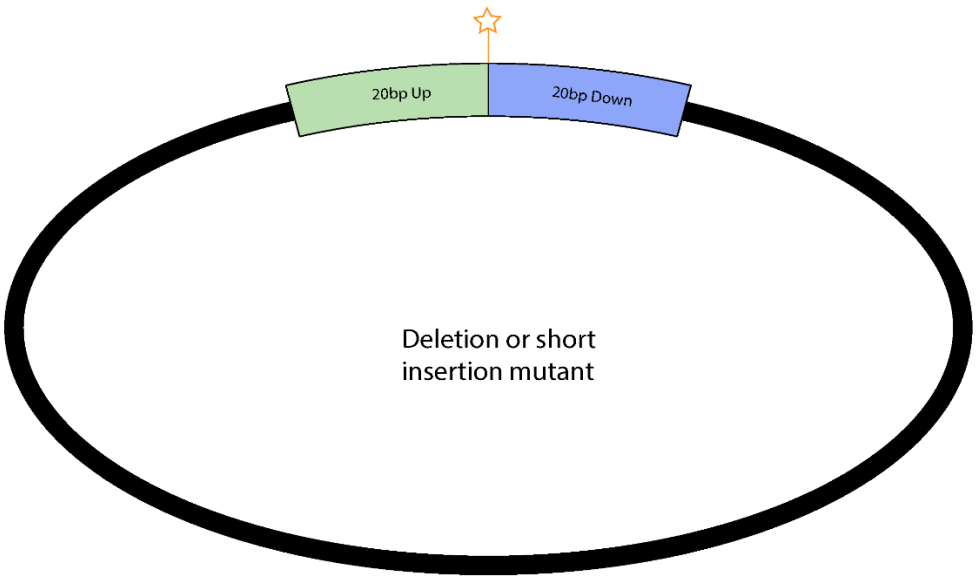

Figure 1: Simplified diagram of BAC16 short insertion/deletion *En Passant* mutagenesis workflow.

The selection cassette created by PCR contains 40bp of homology directly upstream of the ORF annotated start site (40bp up) and 40 bp of homology directly downstream of the annotated stop site (40bp down) to target the 1st HR. 20bp of downstream homology is added to the 5' region (forward primer—20bp down) and 20bp of upstream homology is added in the 3' region (reverse primer—20 up). These 20bp duplications facilitate the 2nd HR. The SceI meganuclease site is marked by a red astricts and the kanamycin cassette is in teal. The 1st HR recombination results in the removal of the intervening sequence (ORF74) and insertion of the PCR product. After SceI-mediated cleavage, the 2nd HR removes the sequence duplications and the kanamycin cassette leaving a scarless deletion. The gold star represents the location of the short insertion sequence for stop codon mutants. There is no sequence placed at the gold star for deletion mutants.

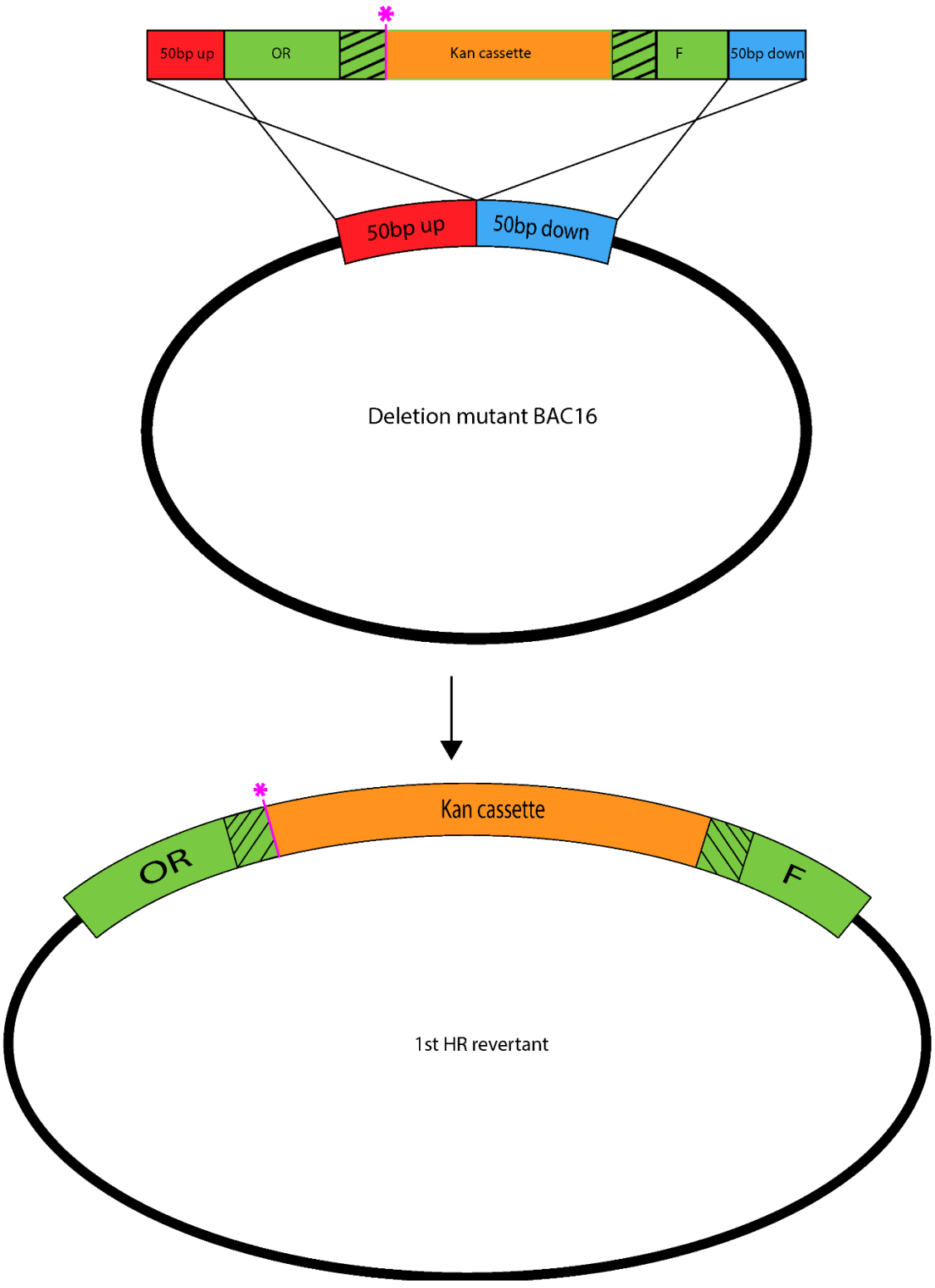
50bp up
OR
Kan cassette
F
50bp down
50bp up
50bp down
Deletion mutant BAC16
Kan cassette
OR
F
1st HR revertant

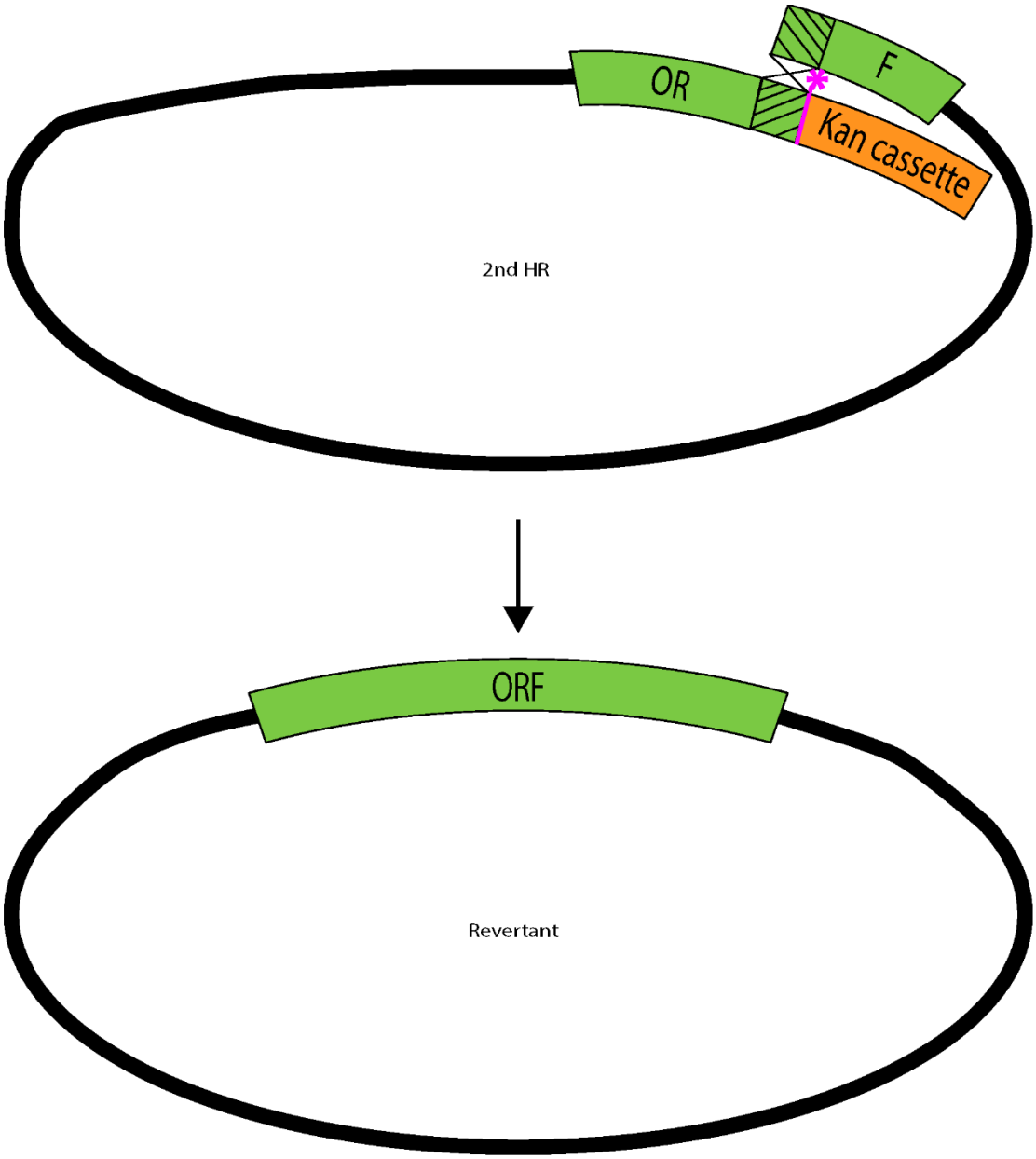

Figure 2: The universal transfer construct for the markerless introduction of long sequences.

The universal transfer construct created by PCR contains 50bp of homology directly upstream (50bp up) and downstream (50bp down) to the deletion locus, a 50bp sequence duplication (black dashed lines), an SceI meganuclease site (pink star), and kanamycin-cassette (orange) inserted into the ORF. The 50bp sequence duplication is made duplicating 50bp of ORF sequence directly downstream of the unique restriction site upstream of the kanamycin cassette (dashed lines). This duplication facilitates the 2nd HR after SceI-mediated cleavage. The 2nd HR removes the sequence duplication and the kanamycin-cassette, leaving the ORF intact.

Mutagenesis rationale

The KSHV genome has been annotated to contain over 80 unique canonical open reading frames[15,16]. In addition, recent mRNA and Riboseq data have expanded our appreciation of the diverse transcriptional and translational repertoire of KSHV[17]. We selected 91 unique ORF's for mutagenesis in our study, including upstream ORFs (uORF)[17]. uORFs are ORFs found in the transcript leader regions (commonly referred to as the 5' untranslated region) and are typically out of frame with the downstream ORF[18]. There are several lines of evidence that strongly suggest uORFs play vital roles in the translational regulation of genes controlling cellular growth, differentiation, and the immune response[18-20]. We included uORFs because of their confirmed ability to be translated into protein products in herpesviruses and yeast[21,22], and the observation that their expression is linked to environmental stress[22].

Our goal was to examine the individual role of each ORF on the viral lifecycle. To do this, we created a library of KSHV mutants where each mutant was characterized by the inactivation of a single ORF. For non-overlapping ORFs, we deleted the entire ORF from the annotated translational start site to the annotated translational stop site. For overlapping ORFs, we inserted a 12-bp sequence corresponding to a stop codon in every reading frame (**TAG**G**TAG**A**TAG**G) in the 5' non-overlapping region of the ORF. The extra guanine base at position 12 of the insertion was added to maintain the topology of the helix. We also made genetic rescues from several mutant viruses by either 1) reinserting the deleted ORF into the mutant genome (figure 2), or 2) deleting the inserted stop codon from the mutant virus (figure 1). These genetic rescues served as controls to indicate the mutant phenotype was due to the mutant genotype, and not a result of other confounding factors.

Screening mutants by restriction digest

KSHV DNA has been observed to undergo spurious genetic rearrangements during propagation in vitro[12] and in-vivo[16]. To assess the integrity of the BAC16 genome after each recombination event induced in GS1783 E. coli, we chose to perform restriction digests using the NheI enzyme (thermo catalog number # FD0974). The predicted digest pattern produced by NheI on the BAC16 (GenBank accession number: MK733609.1) under standard electrophoresis conditions and a 0.8% gel can be found in figure 3. This digest pattern allows good resolution of the repeat regions. The 7575 bp band contains a family of direct repeats, the 6376bp band contains a several families of direct and inverted repeats, and the 5011 bp band contains several families of direct repeats. This digest pattern also produces good resolution for over 40% of the genome and bands that contained significantly more than 1% of the total mass of the genome, which resulted in good staining and visualization using ethidium bromine in the electrophoresis process. We often found large scale duplication or deletion events in and around the repeat regions. Colonies undergoing unexpected bands shifts were discarded. In the table next to figure 3 the 9463bp band is bolded because it contains the terminal repeats. There are typically 30-40 copies of this 803bp sequence in wild type KSHV[23], however, the digest pattern in figure 3 only includes 1 copy of the terminal repeats. In our BAC16 digests, this 9463bp band is shifted into the > 20,000bp region and runs with the largest expected band of 28,862bp.

Plasmid DNA was selectively extracted from E. coli using a standard alkaline lysis procedure[24]. Digests using NheI enzyme from Thermo Fisher were done in 50ul reactions. 80% of plasmid DNA was combined with 5ul of enzyme and buffer, and the reaction was topped off with water. The reaction was carried out at 37C for 24 hours. The entire reaction was run on 0.7% agarose gels at 1.1V/cm for 24 hours and was visualized by ethidium bromide staining.

Screening mutants by PCR and sequencing

For some of our mutants, the insertion and removal of the kan-cassette, and the resulting ORF deletion or stop codon insertion, occurred in restriction digest bands so large that the shifts were unable to be resolved under our electrophoresis conditions. Even for mutations in digest bands that could be resolved, we were still unsure if the mutation occurred in the expected location of digest band. For these reasons, we decided to conduct PCR using primers that flank the mutation site to verify the kan-insertions occurred where we expected in the 1st HR, and that the cassette was removed in the 2nd HR. These primers and their PCR products also afforded us the opportunity to sequence the 12bp stop codon insertion that remained after the removal of the kan-cassette from the genome. Forward and reverse primers were designed to flank the ORF deletion or stop codon insertion sites by 150bp each. Thus, the resulting PCR products were expected to be approximately 1400bp for the 1st HR mutants (because the PCR product also included the selection marker and sequence duplications), and approximately 300bp for the 2nd HR mutants. These expected sizes occurred regardless of if the mutation was a deletion or stop codon insertion. These PCR products provide a more detailed confirmation that the deletion or stop codon insertion occurred at the exact genomic location we expected it to.

Plasmid DNA was selectively extracted from E. coli using a standard alkaline lysis procedure[24]. PCR reactions were carried out in 30ul reactions using the 2X Taq HotStart master mix from Qiagen (catalog# 203445) following the manufactures recommendations and 25 cycles. Reactions contained 1ul of plasmid DNA, forward and reverse primers at a final concentration of 300nM, and were topped off with water. The entire reaction was run on 1% agarose gels at 8V/cm and visualized by ethidium bromide staining. For sequencing, the PCR product was cut from the gel using Qiagen gel extraction kit (catalog number: 28706X4) and sequenced using sanger sequencing and the forward primer.

Creation of the universal transfer construct (ORF74)

Amplification of ORF74 was conducted using the Phusion enzyme from thermo (F-530), forward and reverse pUC19_ORF74 primers (chapter 5 primer table), and BAC16 miniprep DNA. The reaction was run according to the manufacturer's recommendations using a 2-step amplification protocol and the primers added EcoRI and HindIII sites to either end of the PCR product. The PCR products were double digested with NheI and HindIII from NEB (catalog numbers: R3131S and R3104S) for 2 hours and then run on a 1.5% gel at 4V/cm for 2 hours. The bands were cut from the gel using the Qiagen gel extraction kit according to the manufacturer's recommendations. The pUC19 plasmid was double digested with NheI and HindIII for 2 hours and the PCR product was ligated into the vector overnight at room temperature using T-4 ligase (M0202S). Ligation was optimized by varying the molar ratios of insert to vector for the

reaction, and higher ratios of insert to vector were found to increase the ligation efficiency. 2ul of the ligation reaction was transformed into NEB5 alpha E.coli (C2988J) according to the manufactures recommendations. The transformations were plated on LB-Amp plates and incubated at 37C for 24 hours. Colonies were recovered in LB-Amp broth and screened via alkaline lysis and MIu1 digest for 2 hours to confirm insertion of the PCR product into pUC19. The resulting plasmid was named pUC19_ORF74 (chapter 5, plasmid table).

To insert the kanamycin cassette into the middle of ORF74 and create the universal transfer construct, the kan-cassette was PCR amplified out of the pEPKanS plasmid using the ORF74_UTC primers (chapter 5, primer table) with Phusion enzyme using a three-step amplification protocol. The PCR product was digested with the MIu1 enzyme and run on a 1% gel at 4V/cm for 1 hour and the bands were cut from the gel using the Qiagen gel extraction kit according to the manufacturer's recommendations. The pUC19_ORF74 vector was digested with MIu1 and ligated to the PCR product using T-4 ligase at 16C overnight. The ligation reaction was optimized by altering the molar ratio of insert to vector, and higher ratios of insert to vector were found to increase ligation efficiency. 2ul of the ligation reaction was transformed into NEB5-alpha cells according to the manufacturer's recommendations. The transformation reaction was plated on LB-Kan plates and incubated overnight at 37C. Colonies were recovered in LB-Kan broth the next day and screened via alkaline lysis and restriction digest with MIu1 for 2 hours. The resulting plasmid was named ORF74_UTC (chapter 5, plasmid table).

Creation of genetic rescues from BAC16 deletion mutants (ORF74)

Forward and reverse HR1 primers (chapter 5, primer table) were designed to amplify the ORF74_UTC to create a linear PCR product for electroporation and homologous recombination into BAC16-ΔORF74. PCR using the forward and reverse HR1 primers and ORF74_UTC template was conducted with Phusion enzyme using a 3-step amplification protocol. The product was separated on a 1% gel at 8V/cm for 1 hour and extracted using the Qiagen gel extraction kit according to the manufacturer's recommendations. Overnight cultures of BAC16-ΔORF74 were diluted 1:20 and grown at 32C until the they reached early log-phase growth (OD600=0.4) and then transferred to a 42C shaking water bath for 15 minutes. Cultures were then transferred to an ice bath and incubated on an orbital shaker for 25 minutes. After incubation, the cultures were spun down at 4000xg, 4C for 10 minutes and washed with 1ml of 10% glycerol 3 times. The cell pellet was then resuspended in $1/100^{th}$ the original culture volume in 10% glycerol. 50ul of resuspend bacteria was combined with 100ng of PCR product and electroporated at 1.5kV, 200 ohms, 25mF. 250ul of SOC media was added to the reaction directly after electroporation, and the reaction was cultured at 32C for 2 hours. After incubation, the entire reaction was plated on LB-Kan plates. Plates were grown at 30C for 24 hours, colonies were recovered in LB-kan broth at 30C overnight and subjected to alkaline lysis, NheI digest, and PCR screening to confirm the insertion of UTC.

Colonies that successfully passed screening were inoculated in the LB-kan broth and cultured overnight. The next day they were diluted 1:20 in Cm-LB and cultured until they reached early log phase (OD600=0.4). When they reached early log phase, arabinose was added

to a final concentration of 1% and culture was continued at 30C for 50 minutes. Cultures were then transferred to a shaking water bath at 42C for 10 minutes and then moved to 30C for 2 hours. The cultures were then serially diluted, plated on LB-Cm/arabinose plates, and cultured at 30C for 24 hours. After 24 hours, colonies were replica plated onto LB-kan/arabinose plates and cultured for 24 hours at 30C. Colonies that grew on LB-Cm/arabinose plates but not on LB-kan/arabinose plates were selected for alkaline lysis, restriction digest and PCR screening. Sequencing ensured the integrity of the insertion.

Alkaline lysis for plasmid DNA screening

3.5ml LB broth cultures supplemented with chloramphenicol or kanamycin were inoculated from frozen glycerol stocks and the cultured overnight a 30C and 250 rpm. After 20 hours of culture the bacteria were spun out of solution at 4000xg /4C for 10 minutes. The media was decanted, and the pellet was resuspended in one volume of 4C buffer I (50mM Tris, 10mM EDTA, 100ug/ml RNase A). One volume of room temperature buffer II (200mM NaOH, 1% SDS) was added and the tubes were mixed by gentle inversion 10 times and allowed to incubate at room temperature for 2 minutes. 0.5 volumes of 0C bufferN3 (3M K^+ Acetate, pH = 5.2, 4.2M guanidine chloride) was added and the tubes were mixed by gentle inversion 10 times. The lysate was cleared in a bench top centrifuge at 13,000rpm for 10 minutes and the supernatant was transferred to a new tube and spun again at 13,000rpm for 15 minutes. The cleared supernatant was precipitated with 0.6 volumes of room temperature 2-proponal and the DNA was pelleted by centrifugation in a benchtop centrifuge at 13,000rpm for 30 minutes at room temperature. The supernatant was decanted, and the pellet was washed with an excess of 70% ethanol. The residual ethanol was spun down and pipetted out and the tube was dried by evaporation on the bench for 10 minutes. The pellet was then resuspended in a minimal volume of 60C water for 10 minutes.

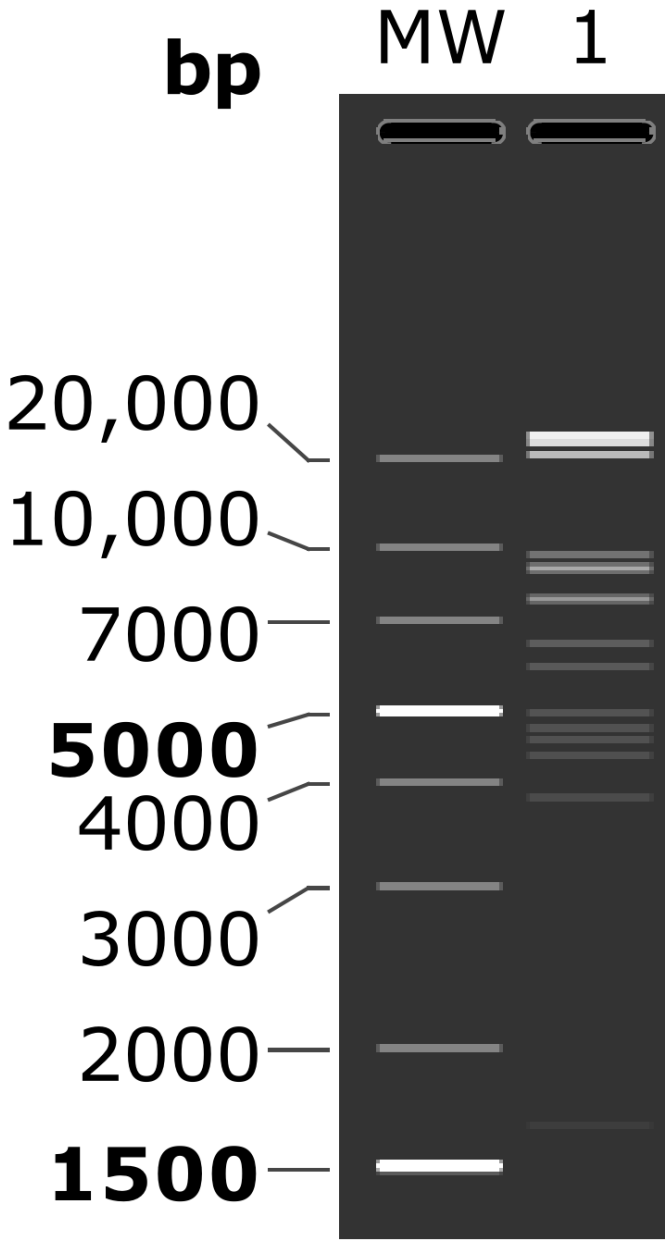

Size (bp)	Site 1	Site 2
28862	18218	47080
25693	52581	78274
20751	83013	103764
9463	**149833**	**4813**
9062	125006	134068
8852	4813	13665
7788	111339	119127
7575	103764	111339
6376	134068	140444
5879	119127	125006
5011	144822	149833
4739	78274	83013
4553	13665	18218
4378	140444	144822
3838	47080	50918
1663	50918	52581

Figure 3: Predicted NheI digest pattern of GenBank accession number: MK733609.1 under standard electrophoresis conditions on a 0.8% agarose gel.

The gene ruler 1kb plus ladder is lane MW. The complete BAC16 genome digest is shown in lane 2. On the right side is a table that lists the expected fragments, their size in base pairs (bp), and the location of their NheI sites in the genome (site 1 and site 2). The digest and table were created using the GenBank accession number: MK733609.1, which only includes one copy of the terminal repeats. The terminal repeats are found in the **bolded 9463bp band** in the table above.

Mutant KSHV-BAC cell line creation

Unlike other herpesviruses, transfection of KSHV-BAC DNA into mammalian cells results in stable latency. The establishment of a pure population of transfected cells is accomplished using section pressure, and the resulting cell lines can be efficiently reactivated with various stimuli to produce significant amounts of infectious cell-free progeny[4,11]. Recently, a cell line believed to be of endothelial origin was created by introducing KSHV ORF50 under the tet-on system[25]. KSHV ORF50 encodes a transcriptional activator whose expression is sufficient to drive the entire lytic cascade of gene expression in KSHV[26-28]. The creation of this cell line, termed iSLK, allows for the efficient and controlled reactivation of latent KSHV infection in-vitro. The value of this inducible system in studying KSHV reactivation and pathogenesis cannot be understated, even considering the discovery that the parental SLK cell line, and thus the iSLK cell line, is a renal carcinoma line and not of endothelial origin[29].

Maxi-prep of BAC DNA from GS1783 E. coli

After mutant BAC16 genomes were created and screened as detailed above, maxi-preps were performed using the NucleoBond BAC 100 kit from Macherey-Nagel (Ref #: 740579) to isolate BAC constructs for transfection into iSLK cells. Briefly, 250ml of LB-Cm was inoculated directly from the glycerol stocks and cultured at 30C for 24 hours. The culture was spun down in an SLA-1500 rotor at 3000xg, 4C for 15 minutes and was resuspended in S1 buffer, lysed in an equal volume of S2 buffer at room temperature for 10 minutes, and neutralized with S3 buffer. The flocculent was spun out of solution at 15,000xg, 4C for 40 minutes and the supernatant was loaded into the column. The column was washed twice with buffer N3 and then eluted with 65C N5 buffer and precipitated with 0.7 volumes of the 2-proponol. The solution was spun in SS-34 rotor at 15,000xg, 4C for 45 minutes and the pellet was washed with an excess of the 70% ethanol twice in an SM-24 rotor at 15,000g, 4C, for 10 minutes. The pellet was resuspended in 65C water on an orbital shaker for several hours.

Transfection of BAC DNA into iSLK cells

Transfection was performed using Lipofectamine 2000 (Invitrgoen cat# 11668027). Briefly, iSLK cells were seeded into 6 well plates at 70% confluence, and 18-24 hours after seeding they were transfected. 2.5ug of DNA was added to 1 volume of Opti-mem (catalog # 31985062) and lipofectamine was diluted (1:26) in 1 volume of Opti-mem. The tubes were incubated at room temperate for 5 minutes, then the lipofectamine tube was added to the DNA tube, and the mixture was incubated for another 20 minutes at room temperature. During the second incubation, the cells were washed with PBS and the media was replaced with complete media without antibiotics. The transfection mixture was added to the wells dropwise and the cells were incubated at 37C 5% CO_2. After 4 hours the media was changed back to complete media with antibiotics.

48 hours after transfection, selection pressure was applied by supplementing the growth media with 1.2mg/ml of hygromycin B, as the BAC16 contains a hygromycin resistance cassette. No colony isolations were performed. Transfected cells were monitored by fluorescence

microscopy as BAC16 contains a GFP expression cassette under a constitutively active promoter. Cells were expanded under selection pressure until approximately 5.0*10^7 transfectants were obtained.

Mutant KSHV-BAC cell line induction

Transfected cells were induced by changing the media to new growth media supplemented with 1ug/ml of doxycycline (to induce ectopic ORF50 expression) and 1mM of butyrate (a histone deacetylase inhibitor to unwind chromatin). Cells were monitored for phenotypic changes from induction for 4 days. A simplified overview of this process can be found in figure 4.

Viral progeny harvest

Induced viral supernatants were cleared of cellular and GFP+ debris by centrifugation and filtration, and cleared supernatants were concentrated over 100-fold using ultracentrifugation. Briefly, the cells were scrapped into the media and the suspension was frozen at -80C. The suspension was thawed, spun at 3200xg, 4C, for 15 minutes and then run through a 0.45um aPES filter. The samples were then concentrated by ultracentrifugation at 13,600rpm in the SureSpin 630 rotor for 3 hours. After the spin, the media was decanted and pipetted out and the pellet was resuspended in 1/100th the initial volume. Aliquots were stored at -80C.

Viral titration

Concentrated supernatants were used to infect 293T cells using spinoculation[3,30]. We chose these conditions for viral tittering because in most cell lines, infection with recombinant KSHV doesn't result in GFP expression in all infected cells, despite GFP being under control of a constitutively active promoter. However, the cell line 293T has been shown to express GFP in virtually all LANA positive cells[3]. Also, centrifugal enhancement of infection significantly increases assay sensitivity, allowing us to detect the presence of minute amounts of infectious virus (detailed later). FACS analysis was used increase the accuracy of our "percentage of GFP+ cells" measurement, and this parameter was used to back-calculate infectious titer using the number of cells at the time of infection. A simplified diagram of our tittering methodology can be found in figure 5. This tittering assay, in combination with the low titer growth analysis assay (see below) were used to determine the presence or absence of infectious progeny in induced mutant cell line supernatants.

Briefly, 293T cells were seeded into 48-well plates at 6*10^4 cells/well and left to incubate at 37C 5%CO2 overnight. The next morning a well was counted on the hemocytometer to ensure accuracy in the final titer calculation (see below). Viral stocks were serially diluted 1:10 in induction media, and excess growth media was aspirated from the wells. 400ul of inoculum was added to wells in duplicate and the plates were spun at 2000xg, 30C for 1 hour and then placed in the 37C, 5% CO2 incubator for 1 hour. At the end of the incubation the inoculum was removed by aspiration and replaced with 500ul of fresh induction media. After 48 hours of incubation the wells were checked for GFP expression. The dilutions where approximately 2-20% of cells expressed GFP were selected for fixing and FACS. The selected wells were washed

with 3ml of PBS + 0.1%BSA, transferred to 15ml conical tubes, and spun at 300xg for 5 minutes at 4C. The cells were fixed in 1ml of 1% paraformaldehyde for 5 minutes at room temperature. After fixation 6ml of PBS + 0.1%BSA was added to tubes. The wash step was repeated twice more with 3ml of PBS + 0.1%BSA. The cells were resuspended in residual wash GFP expression was assessed of the Fortessa X-20 (BD Biosciences). Forward scatted vs side scatted plots were used to gate out cell debris, forward scatter height vs forward scatter area plots were used to gate out single cells, and FITC vs PE plots were used to gate out authentic GFP signal from autofluorescence. A minimum of 20,000 single cell events was taken. The titer was calculated using the following equation where IU stands for Infectious units. All data analysis was done in Flowing Software.

$$IU/ml = ((cell\ count\ at\ infection) * (\%\ single\ cells\ that\ are\ GFP + and\ PE-))/((0.4ml) * (df))$$

*df = dilution factor

Low titer growth analysis

Several mutant viruses produced titers so low that the tittering assay alone was insufficient to determine the presence or absence of infectious viral progeny. This is to say that for some samples, the signal to noise ratio deteriorated to the point that we could not tell the difference between authentic signal generated from cell free progeny, and possible carry-over of GFP+ debris generated from the induction/lysis of transfected cell lines. For these "low titer" samples, we confirmed the presence or absence of infectious viral progeny using and infection and growth-based assay. We infected 293T and naïve iSLK cells with concentrated supernatant using spinoculation (outlined above) and monitored cells by fluorescence microscopy for 100 days. We assumed that if a single infectious particle was present, it would enter cells and the viral genome would be replicated and segregated to daughter cells during mitosis, resulting in an increase in the number of GFP+ cells and thus an increased signal. We also expected the prolonged culture conditions to reduce the noise caused by the carry-over of GFP+ debris from induced supernatants, as the cells had to be passaged several times during the incubation period. This assay, in combination with the tittering assay was used to determine the presence or absence of infectious viral progeny. The ORFs corresponding to mutants that did not produce any infectious progeny in the initial tittering assay, or, produced a titer <1*10^2 IU/ml and the presence of authentic infectious virus was not confirmed by the low titer growth analysis, were determined to be essential.

Multiple step lytic growth curve

To examine the ability of non-essential mutant viruses to undergo multiple rounds of lytic replication, we infected naïve iSLK cells at MOI=0.1 under inducing conditions. We incubated infected cells for 19 days and harvested supernatants at each 3-day interval (1,4,7,10,13,16,19 days post infection) for tittering (outlined above). We calculated the ratio of peak titers in the mutants relative to the BAC16 (peak mutant viral titer)/(peak BAC16 viral titer) and used this metric to separate mutants into four categories based on their growth characteristics. The first group is mutants that exhibited a severely attenuated growth phenotype, defined as over a 100-

fold reduction in mutant peak titer compared to BAC16. The second group is mutants that exhibited a moderately attenuated growth phenotype, defined as a 10-100-fold reduction in mutant peak titer compared to BAC16. The third group is mutants that exhibited no attenuation in growth phenotype, defined as a mutant peak titer that did not very more than 10-fold above or below BAC16 peak titer. The final group is mutants that exhibited an enhanced growth phenotype, defined as a mutant peak titer that was more than 10-fold above BAC16 peak titer.

Induced and spontaneous reactivation growth

We assessed non-essential mutants' ability to produce progeny under growth conditions designed to measure induced and spontaneous reactivation. For these assays, we infected naïve iSLK cells at an MOI=1. For induced reactivation, we cultured infected cells for 2 days under non-inducing conditions, induced infected cells, and collected supernatants at 5 days post infection (3 days post induction). For spontaneous reactivation, we cultured infected cells for 6 days under non-inducing conditions and collected supernatants at 6 days post infection. Supernatants were titered (see above) and the ratio of mutant viral titer to BAC16 titer was calculated (see above).

Electron microscopy

Several viral mutants induced strongly, as determined by cytopathic effect, but did not produce viral progeny. We hypothesized that these mutants were defective in viral capsid maturation and viral particle egress. To test this hypothesis, we fixed the induced cell lines, embedded them in resin, and thin sectioned them for examination using transmission electron microscopy.

Briefly, BAC16-cell lines were thawed and maintained in section media in T75 flasks. When the cells reached 90% confluency the selection media was removed, cells were washed, and 20ml induction media was added. For fixation, the cells were washed and fixed directly inside flasks with a solution containing 1 part 4% glutaraldehyde in 1X PBS and 1 part induction media. Fixation occurred for 2 hours at 37C, 5% CO2. At the end of fixation, cells were scraped into the fixative solution and the suspension was centrifuged for 5 minutes at 250xg, 25C. The fixative solution was aspirated, the pellet was resuspended in 2.5% glutaraldehyde in 0.1M sodium cacodylate pH=7.4 and stored at 4C until secondary fixation and embedding.

For secondary fixation and embedding, the cells were first resuspended in 2% low gelling temperature agarose, spun at 15,000xg for 10 minutes, 25C and then allowed to solidify on ice. The cell pellet was cut from the bottom of the tube with a razor blade and washed twice with 0.1M sodium cacodylate pH=7.2 for 10 minutes on a tilting rack. Secondary fixation occurred in the dark for 1 hour in a solution of 1% Osmium with 1.6% ferricyanide. The cell pellet was then dehydrated in an acetone series; 30%, 50%, 70%, 80% 95%, 100% and infiltrated in a series of acetone:resin mixtures; 3:1, 1:1, 1:3, followed by pure resin overnight. The next day, the sample was embedded twice with resin and DMP-30 accelerant for 30 minutes, placed in mold filled with resin and accelerant and cured at 60C for 48 hours. The cured blocks were hand trimmed and thin sectioned into 100nm sections on mesh copper grids coated with a 0.5% solution of

formvar. The grids were then stained with 2% uranyl acetate for 5 minutes followed by lead citrate for 7 minutes and imagined on a Tecnai 12 scope at 120kV.

Total RNA harvest (ORF74)

iSLK cells were seeded into 96 well plates at 1.25*10^4 cells/well an incubated at 37C 5%CO2 overnight. The next day, cells were counted and infected at MOI=1 in triplicate, spun at 2000xg, 30C for 1 hour, then incubated at 37C, 5%CO2 for 1hour. After incubation the inoculum was removed and the either complete growth medium (non-inducing condition) or induction media (inducing condition) was added and cells were incubated at 37C, 5%CO2. Time points were harvested by aspirating the inoculum, adding 350ul of lysis solution to each well, and pipetting up and down to detach cells. The lysate was transferred to a 1.5mL tube and immediately put on ice or stored at -80C. 350ul 70% EtOH was added to each tube of lysate and pipetted up and down thoroughly until no bilayer was visible and viscosity was reduced. The homogenized lysate was added to the RNA binding column (700ul max) and centrifuged for 15s. 350ul of buffer RW1 (20% ethanol, 900mM guanidine thiocyanate, 10 mM Tris-HCl pH 7.5) was added to the column and centrifuged for 15s. 10ul reconstituted DNaseI (thermo catalog #: EN0521) was mixed with 70ul of DNase dilution solution (10X DNase dilution solution: 100mM Tris HCl, pH 7.5, 25 mM MgCl2, and 5 mM CaCl2) and the diluted DNase I was added to the membrane stack and the digest was conducted at room temperature for 30min. 350ul of buffer RW1(20% ethanol, 900mM guanidine thiocyanate, 10 mM Tris-HCl pH 7.5) was then added and the column was centrifuged for 15s. 500ul of buffer RPE (80% ethanol, 100mM NaCl, 10 mM Tris-HCl pH 7.5) was added and the column centrifuged for 15s. The RPE wash was repeated and centrifuged for 2 minutes. The flow through was discarded and the column was centrifuged for an additional 1 min to remove residual wash solution. The column was eluted by adding 30ul of DEPC treated water to the membrane stack and it was incubated for 10 minutes, then centrifuged for 1 min to elute total RNA. The eluate was mixed 5 times by pipetting, aliquoted, and stored at -80C. All centrifugation steps were conducted at 13600rpm in microcentrifuge, and the collection tube was reused after each wash. RNA concentration and purity were assessed by spectrophotometry and gel electrophoresis was used to assess RNA quality. Samples were run on a 1.5% gel at 8V/cm for 1 hour and imaged with ethidium bromide. All reagents, except DNAse I enzyme, were made in house.

RT-qPCR (ORF74)

Total RNA was diluted to 5ng/µl in water and 25ng was reverse transcribed into cDNA using iScript Reverse Transcriptase Supermix (BioRad catalog number: 1708840) according to the manufacture's recommendations. The samples were diluted 8:25 in water after the reaction was completed. Primer concentrations for qPCR were optimized (350 nM) and standard curves for each primer set were generated to determine reaction efficiencies. qPCR was carried out on 5µl of diluted cDNA solution using SsoAdvanced SYBR Green Master Mix (BioRad catalog number: 1725270). The qPCR program was: 1) 30 seconds at 95 °C, 2) 10 seconds at 95 °C, 3) 20 seconds at 60 °C, 4) repeat steps 2-3 40 times. Melt curve analysis was run on the products of all reactions to ensure specific amplification as demonstrated by the presence of a single peak

(65C –> 95C, 0.5C increments 2-5 s/step). Viral transcript targets were standardized to GAPDH as a loading control and quantified relative to BAC16 levels using the ΔΔCq method. ΔCq values were calculated for each technical replicate and the mean of the technical replicates was taken to find the ΔCq value for each biological replicate. The mean ΔCq for biological replicates was calculated and the ΔΔCq was calculated using BAC16 as the calibrator. All ΔΔCq values were transformed to the relative scale using the formula: $2^{-\Delta\Delta Cq}$. Samples that were not treated with reverse transcriptase were analyzed alongside cDNA samples and their quantities were used to adjust for remaining genomic DNA contamination in the relative quantification of transcripts. We calculated the standard error of the difference in means for ΔCq values by the following formula:

$$Standard\ Error\ of \Delta Cq = \sqrt{\sum(xi - \bar{x})}$$

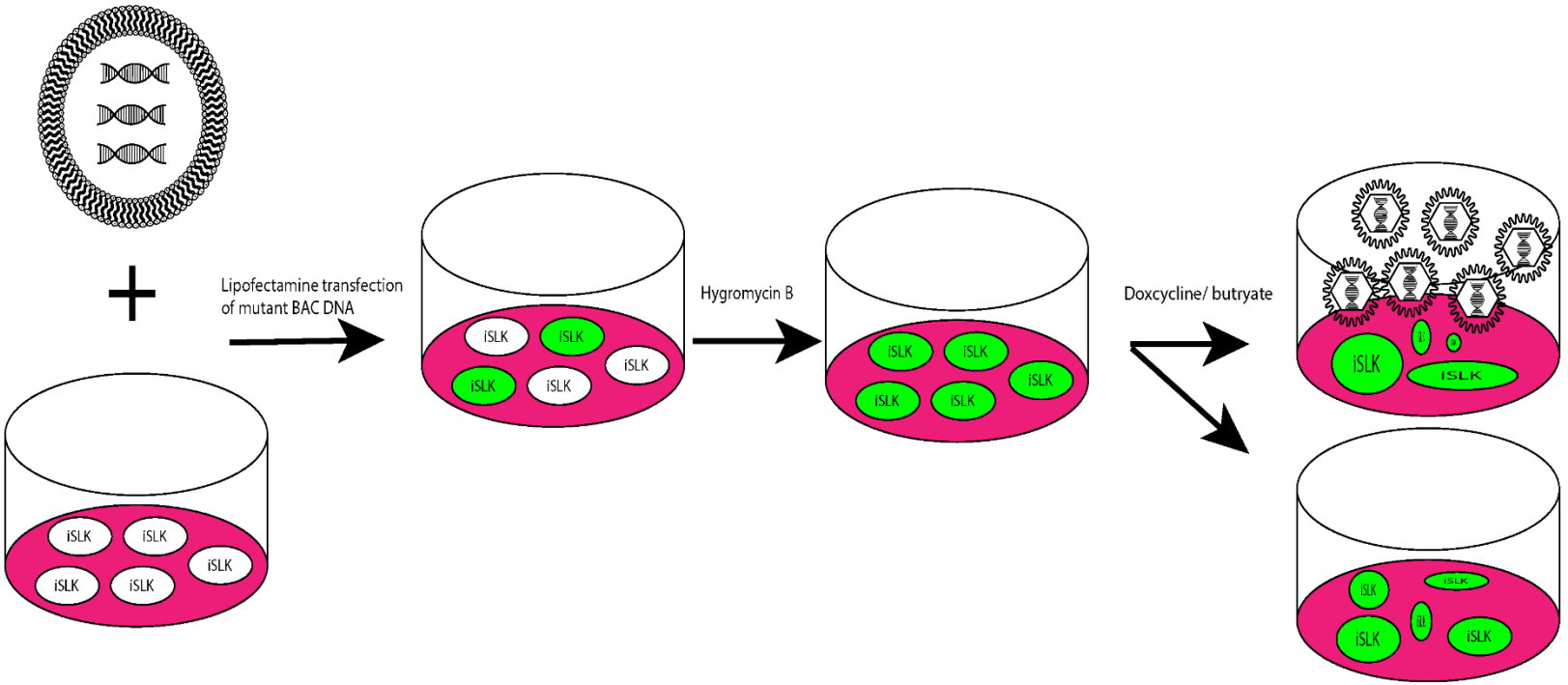

Figure 4: Overview of BAC16-mutant cell line creation and induction process.

Naïve iSLK cells were seeded into 6-well plates and transfected with 2.5ug of mutant or parental BAC16 DNA using lipofectamine 2000. 48 hours after transfection, the media was changed to growth media supplemented with hygromycin to select for transfectants. Transfectants were maintained and expanded under selection pressure. Once transfected cell populations reached 5*10^7 cells, they were induced using doxycycline and butyrate. Induction of transfected cell lines results in phenotypic changes in the cell lines, and either the presence or absence of infectious cell free progeny in the supernatant.

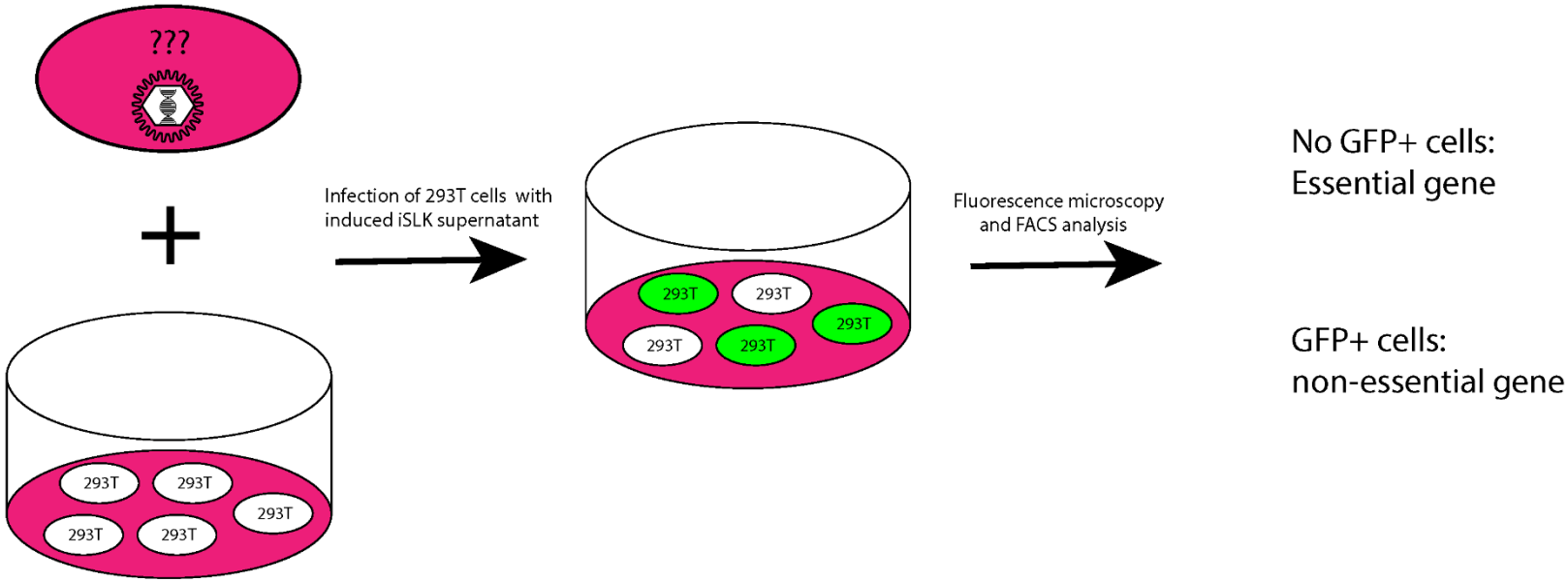

Figure 5: Overview of mutant-BAC16 induced cell supernatant tittering assay.

Cleared and concentrated supernatants from induced mutant BAC16 transfected cell lines were used to infect naïve 293T cells using spinoculation. 48-hours post infection cells were analyzed for GFP expression by fluorescence microscopy and FACS to determine the presence or absence of infectious viral progeny, and the quantity of infectious viral progeny.

References:

1 Messerle, M., Crnkovic, I., Hammerschmidt, W., Ziegler, H. & Koszinowski, U. H. Cloning and mutagenesis of a herpesvirus genome as an infectious bacterial artificial chromosome. *Proc Natl Acad Sci U S A* **94**, 14759-14763, doi:10.1073/pnas.94.26.14759 (1997).

2 Cannon, J. S. *et al.* A new primary effusion lymphoma-derived cell line yields a highly infectious Kaposi's sarcoma herpesvirus-containing supernatant. *J Virol* **74**, 10187-10193, doi:10.1128/jvi.74.21.10187-10193.2000 (2000).

3 Vieira, J. & O'Hearn, P. M. Use of the red fluorescent protein as a marker of Kaposi's sarcoma-associated herpesvirus lytic gene expression. *Virology* **325**, 225-240, doi:10.1016/j.virol.2004.03.049 (2004).

4 Brulois, K. F. *et al.* Construction and manipulation of a new Kaposi's sarcoma-associated herpesvirus bacterial artificial chromosome clone. *J Virol* **86**, 9708-9720, doi:10.1128/JVI.01019-12 (2012).

5 Dunn-Kittenplon, D. D., Kalt, I., Lellouche, J. M. & Sarid, R. The KSHV portal protein ORF43 is essential for the production of infectious viral particles. *Virology* **529**, 205-215, doi:10.1016/j.virol.2019.01.028 (2019).

6 Fu, B. *et al.* Activation of p90 ribosomal S6 kinases by ORF45 of Kaposi's sarcoma-associated herpesvirus is critical for optimal production of infectious viruses. *J Virol* **89**, 195-207, doi:10.1128/JVI.01937-14 (2015).

7 Jain, V. *et al.* A Toolbox for Herpesvirus miRNA Research: Construction of a Complete Set of KSHV miRNA Deletion Mutants. *Viruses* **8**, doi:10.3390/v8020054 (2016).

8 Wang, F., Guo, Y., Li, W., Lu, C. & Yan, Q. Generation of a KSHV K13 deletion mutant for vFLIP function study. *J Med Virol* **90**, 753-760, doi:10.1002/jmv.25009 (2018).

9 Full, F. *et al.* Kaposi's sarcoma associated herpesvirus tegument protein ORF75 is essential for viral lytic replication and plays a critical role in the antagonization of ND10-instituted intrinsic immunity. *PLoS Pathog* **10**, e1003863, doi:10.1371/journal.ppat.1003863 (2014).

10 Zhang, Z. *et al.* The K1 Protein of Kaposi's Sarcoma-Associated Herpesvirus Augments Viral Lytic Replication. *J Virol* **90**, 7657-7666, doi:10.1128/JVI.03102-15 (2016).

11 Zhou, F. C. *et al.* Efficient infection by a recombinant Kaposi's sarcoma-associated herpesvirus cloned in a bacterial artificial chromosome: application for genetic analysis. *J Virol* **76**, 6185-6196, doi:10.1128/jvi.76.12.6185-6196.2002 (2002).

12 Yakushko, Y. *et al.* Kaposi's sarcoma-associated herpesvirus bacterial artificial chromosome contains a duplication of a long unique-region fragment within the terminal repeat region. *J Virol* **85**, 4612-4617, doi:10.1128/JVI.02068-10 (2011).

13 Tischer, B. K., von Einem, J., Kaufer, B. & Osterrieder, N. Two-step red-mediated recombination for versatile high-efficiency markerless DNA manipulation in Escherichia coli. *Biotechniques* **40**, 191-197, doi:10.2144/000112096 (2006).

14 Tischer, B. K., Smith, G. A. & Osterrieder, N. En passant mutagenesis: a two step markerless red recombination system. *Methods Mol Biol* **634**, 421-430, doi:10.1007/978-1-60761-652-8_30 (2010).

15 Blossom A. Damania, E. C. in *Fields Virology 6th edtion* Ch. Kaposi's Sarcoma–Associated Herpesvirus, 2080-2128 (Philadelphia, PA: Lippincott Williams & Wilkins, 2013).

16 Russo, J. J. *et al.* Nucleotide sequence of the Kaposi sarcoma-associated herpesvirus (HHV8). *Proc Natl Acad Sci U S A* **93**, 14862-14867, doi:10.1073/pnas.93.25.14862 (1996).
17 Arias, C. *et al.* KSHV 2.0: a comprehensive annotation of the Kaposi's sarcoma-associated herpesvirus genome using next-generation sequencing reveals novel genomic and functional features. *PLoS Pathog* **10**, e1003847, doi:10.1371/journal.ppat.1003847 (2014).
18 Calvo, S. E., Pagliarini, D. J. & Mootha, V. K. Upstream open reading frames cause widespread reduction of protein expression and are polymorphic among humans. *Proc Natl Acad Sci U S A* **106**, 7507-7512, doi:10.1073/pnas.0810916106 (2009).
19 Kozak, M. An analysis of vertebrate mRNA sequences: intimations of translational control. *J Cell Biol* **115**, 887-903, doi:10.1083/jcb.115.4.887 (1991).
20 Morris, D. R. & Geballe, A. P. Upstream open reading frames as regulators of mRNA translation. *Mol Cell Biol* **20**, 8635-8642, doi:10.1128/MCB.20.23.8635-8642.2000 (2000).
21 Stern-Ginossar, N. *et al.* Decoding human cytomegalovirus. *Science* **338**, 1088-1093, doi:10.1126/science.1227919 (2012).
22 Ingolia, N. T., Ghaemmaghami, S., Newman, J. R. & Weissman, J. S. Genome-wide analysis in vivo of translation with nucleotide resolution using ribosome profiling. *Science* **324**, 218-223, doi:10.1126/science.1168978 (2009).
23 Lagunoff, M. & Ganem, D. The structure and coding organization of the genomic termini of Kaposi's sarcoma-associated herpesvirus. *Virology* **236**, 147-154, doi:10.1006/viro.1997.8713 (1997).
24 Birnboim, H. C. & Doly, J. A rapid alkaline extraction procedure for screening recombinant plasmid DNA. *Nucleic Acids Research* **7**, 1513-1523, doi:10.1093/nar/7.6.1513 (1979).
25 Myoung, J. & Ganem, D. Generation of a doxycycline-inducible KSHV producer cell line of endothelial origin: maintenance of tight latency with efficient reactivation upon induction. *J Virol Methods* **174**, 12-21, doi:10.1016/j.jviromet.2011.03.012 (2011).
26 Nakamura, H. *et al.* Global changes in Kaposi's sarcoma-associated virus gene expression patterns following expression of a tetracycline-inducible Rta transactivator. *J Virol* **77**, 4205-4220, doi:10.1128/jvi.77.7.4205-4220.2003 (2003).
27 Lukac, D. M., Renne, R., Kirshner, J. R. & Ganem, D. Reactivation of Kaposi's sarcoma-associated herpesvirus infection from latency by expression of the ORF 50 transactivator, a homolog of the EBV R protein. *Virology* **252**, 304-312, doi:10.1006/viro.1998.9486 (1998).
28 Sun, R. *et al.* A viral gene that activates lytic cycle expression of Kaposi's sarcoma-associated herpesvirus. *Proc Natl Acad Sci U S A* **95**, 10866-10871, doi:10.1073/pnas.95.18.10866 (1998).
29 Sturzl, M., Gaus, D., Dirks, W. G., Ganem, D. & Jochmann, R. Kaposi's sarcoma-derived cell line SLK is not of endothelial origin, but is a contaminant from a known renal carcinoma cell line. *Int J Cancer* **132**, 1954-1958, doi:10.1002/ijc.27849 (2013).
30 Yoo, S. M. *et al.* Centrifugal enhancement of Kaposi's sarcoma-associated virus infection of human endothelial cells in vitro. *J Virol Methods* **154**, 160-166, doi:10.1016/j.jviromet.2008.07.026 (2008).

Chapter 3

Global phenotypic profiling of a Kaposi Sarcoma-associated herpesvirus

“Just remember, you will never be a real biochemist.” -*redacted*

Overview and acknowledgements

This chapter outlines the creation and phenotypic screening of our KSHV BAC16 mutant virus library and their corresponding cell lines. It is split into two parts. Part I gives an overview of our results and contextualizes our findings in the broader field of herpesvirus biology and general virology. Part II presents a selection of raw data to give the reader a more comprehensive sense of how the library was created and analyzed. It also presents additional phenotypic screening data. This chapter has been submitted with the help of Rachael Burchfield and Marco-Paliza-Carre. Rachael Burchfield created many of the mutant BAC16 viruses, and Marco-Paliza-Carre created many of the BAC16 virus-infected iSLK cell lines. Marco-Paliza-Carre and Fenyong Liu were also instrumental in the data analyses and interpretations presented in part I. I am in indebted to them for their help.

Part I

Abstract

Kaposi's sarcoma-associated herpesvirus (KSHV) is an opportunistic pathogen causing Kaposi's sarcoma. It can establish latent infection, which can be reactivated to engage lytic infection for progeny production. KSHV contains a ~165 kilobase DNA genome predicted to encode at least 90 open reading frames (ORFs). In this report, we generated 91 KSHV mutants, each characterized by the disruption of a single viral ORF. The growth of these mutants in cultured cells was examined to systematically investigate the necessity of each ORF for viral latency, reactivation, and lytic replication. The salient features of our results are (a) 44 ORFs are essential for viral lytic replication in cultured cells and 46 are nonessential; (b) KSHV reactivation can be positively or negatively regulated by specific viral ORFs; and (c) ORFs identified to modulate viral reactivation encode functions modulating both innate and adoptive immune responses. The intersection of viral immunomodulatory genes controlling reactivation suggests that KSHV engages in a concerted effort to communicate and respond to the host immune system using a viral sensory network. Our results imply a novel mechanism in which reactivation of KSHV is actively controlled by the virus in response to its surrounding environment, leading to the opportunistic nature of viral diseases that are strongly correlated to the host's immune status and conditions.

Introduction

Kaposi's sarcoma associated herpesvirus (KSHV) is an oncogenic gamma-herpesvirus which causes Kaposi's sarcoma, primary effusion lymphoma, and multicentric Castleman's disease[1]. The other members of the human herpesvirus family include herpes simplex virus (HSV) 1 and 2, varicella zoster virus (VZV), Epstein Barr virus (EBV), cytomegalovirus (CMV), and human herpesviruses 6 and 7[2]. A hallmark of herpesvirus infection is life-long persistence in a latent state with episodes of reactivation and lytic replication that correlate with the host's immune status and disease progression. During latency, herpesvirus genomes reside as episomes in the nucleus and only a few viral genes are expressed[2]. Onset of reactivation from latency can occur in the presence of certain stimuli and is associated with changes in the host immune status. KSHV reactivation triggers viral lytic replication which proceeds via a highly regulated temporal cascade of gene expression, resulting in viral DNA replication and the assembly and release of infectious virions from the cell[1].

Reactivation and lytic replication of KSHV play important roles in the development of KSHV-associated disease as mechanisms for infection of naïve cells, through oncogenic effects of certain lytic proteins and paracrine signaling[1]. However, the roles of individual viral genes in reactivation and lytic replication are not fully elucidated. Also, little is known about the processes and factors linking KSHV reactivation and changes in the host immune status.

Global studies assaying the essentiality of viral genes in several herpesviruses have been reported but were limited to studying lytic replication and not reactivation or latency[3-7]. KSHV consists of a ~165kb genome that has been predicted to encode at least 90 open reading frames (ORFs) including small and upstream ORFs, and numerous non-coding RNAs including miRNAs and circRNAs[8-14]. To our knowledge, only a handful of KSHV ORFs have been studied using gene inactivation mutants[15-40].

In this report, we performed genome-wide mutational analysis and constructed 91 ORF-inactivating mutants using the KSHV BAC16 construct. BAC16 contains a KSHV genome cloned as a bacterial artificial chromosome (BAC)[38]. Resembling KSHV infection in vivo, virus infection from the BAC16 construct in human iSLK cells typically leads to latency, and reactivation and lytic replication from this system can be induced[41]. We studied ORF-inactivating mutants and investigated the roles of viral ORFs in KSHV latency, reactivation, and lytic replication. Notably, our study is the first global functional profiling of a KSHV genome.

Results

Generation of KSHV mutants and identification of ORFs important for latency

To generate mutant viruses, previous studies used a 2-step red-mediated recombination with BAC16 followed by transfection into iSLK cells, establishment of transfected cell populations, and induction of lytic replication[15-40]. We used this approach to construct 91 BAC16 mutants. Each mutant has an inactivating mutation in a single ORF consisting of either a complete ORF deletion (nonoverlapping ORFs) or an insertion of a stop codon in each frame in the ORF 5' region (overlapping ORFs). Mutant BAC16 DNAs were screened by PCR with primers (Supporting Information Table S1) designed to produce a unique and recognizable product (e.g. a ~300bp PCR product for ΔORF62) (Fig. 1A). Stop codon insertion was confirmed by sequencing. The overall genomic structures of the mutants were further examined to confirm that unexpected genomic rearrangements did not occur (Fig. 1B).

To reconstitute virus, iSLK cells were transfected with mutant or parental BAC16 DNAs and selected with hygromycin B. This produced populations of GFP+ cells as BAC16 contained a GFP expression cassette. To confirm KSHV infection, we also examined the expression of ORF73-encoded latency associated nuclear antigen (LANA) (Fig. 1C). Consistent with the essential role of ORF73 for viral latency[17,42], we could not generate cell populations harboring ΔORF73 even after repeated attempts and growing for more than 62 days (Supporting Information Fig. S1). In contrast, GFP+ and LANA+ cells were found with the remaining 90 mutants, suggesting that these 90 ORFs are dispensable for establishment and maintenance of viral latency (Table 1, Fig. 1C, Fig. 2).

Identification of ORFs essential for virus production

Lytic replication was induced in transfected cell lines by doxycycline and sodium butyrate treatment and the supernatants were harvested 96 hours post-induction and titered on 293T cells (Fig. 1D-E). Forty-seven mutants produced viral progeny, indicating that the mutated ORFs are not essential for KSHV replication in iSLK cells (Table 1). In contrast, 44 mutants did not yield viral progeny even after repeated attempts with independent transfections and extensive induction. To further confirm their no-growth phenotype, rescued BAC clones were derived from several mutants (e.g. ΔORF62) by restoring the mutations with the intact ORF sequence (Fig. 1A-B, Supporting Information Table S2). The rescued mutants (e.g. rORF62) produced progeny and grew as well as BAC16, confirming that the mutation inactivating the ORF causes the no-growth phenotype (Table 1, Supporting Information Table S3).

The majority of the 44 essential ORFs identified are conserved among herpesviruses with key roles in virus production, such as structural, enzymatic, and regulatory functions (Fig. 2, Table 1, Supporting Information Table S3). Strikingly, 10 conserved genes (ORFs 20, 23, 36, 37, 38, 42, 46, 54, 60, and 61) were nonessential in our experiments[2]. In contrast, ORFs 45, 50, 52, 73, and 75, which have no homologues in alpha and beta-herpesviruses, were essential (Table 1, Supporting Information Table S3). The identification of these 44 essential genes suggest that they represent novel and ideal targets for antiviral drug development against KSHV infection.

The growth of mutants with inactivation of nonessential ORFs was further analyzed under multi-step growth conditions for 19 days (Fig 1D, Fig 3A). Based on their peak titers, mutants could be categorized into four major groups: those for which virus production was severely-attenuated (at least 100-fold lower – 9 mutants), partially-attenuated (10 to 100-fold lower – 4 mutants), non-attenuated (within 10-fold – 32 mutants), or enhanced (at least 10-fold

higher – 2 mutants) compared to parental BAC16 (Fig 1D, Fig 3A, Table 1). Notably, inactivation of conserved ORFs 20, 23, 37, and 42 showed no attenuation, while most mutants exhibiting no attenuation and enhanced growth had mutations at γ-herpesvirus or KSHV-specific genes (Fig. 3A, Table 1, Supporting Information Table S3).

Identification of KSHV genes modulating reactivation and latency

To assay virus generated from reactivation and subsequent lytic replication, we infected iSLK cells, induced reactivation at 2 days post-infection (dpi), and harvested the supernatants at 5 dpi for titration. At 2 dpi prior to induction, we barely detected virus from the supernatant collected from BAC16-infected cells, suggesting establishment of viral latency and lack of reactivation. This conclusion is consistent with our observations that the percentage of parental BAC16-infected cells expressing ORF45 (an immediate early gene), K8 (an early gene), or K8.1 (a late gene) was 1.24%, 0.61%, and 0.33% respectively, suggesting that over 98% of BAC16-infected cells were not undergoing lytic replication (Supporting Information Table S4).

We expected to observe changes in virus production due to deficiencies or enhancements in reactivation or subsequent lytic replication. Most mutants generated a titer within 10-fold of parental BAC16 (Fig. 3B). While ΔORF38 and ΔORF46 generated titers more than 50-fold less than BAC16 (Fig. 3B, Supporting Information Fig. S2C and D)**,** they were also attenuated in the lytic multi-step growth analysis, indicating that these ORFs likely do not play a role specific to reactivation (Table 1, Fig. 3A). However, ΔORFK3 and ΔORFK5, which exhibited little change in the multi-step growth analysis (Fig. 3A, Table 1), showed enhanced virus production (Fig. 3B, Supporting Information Fig. S2F and H), implying that ORFK3 and ORFK5 may specifically suppress reactivation but not viral lytic replication.

Increased virus production possibly results from enhanced lytic antigen expression. To test this hypothesis, we measured the expression of viral ORFs 45, K8 and K8.1 proteins under the same conditions. Mutants ΔORFK3 and ΔORFK5 showed an increased percentage of lytic antigen-expressing cells relative to parental BAC16 (Fig. 3D, Supporting Information Fig. S3), indicating that inactivating these genes, which are immunomodulatory factors[43,44], enhanced reactivation at the gene expression level.

Next, we took advantage of our unique system to identify viral ORFs regulating latency and spontaneous reactivation by measuring virus production in the absence of lytic induction. At 6 dpi, the percentage of parental BAC16-infected cells expressing ORF45, K8, or K8.1 was 0.31%, 0.25%, 0.09% respectively, suggesting establishment of latency and lack of reactivation and lytic replication in over 99.5% of infected cells (Supporting Information Table S4). Thus, any change of virus production probably results from alteration of latency and spontaneous reactivation due to the inactivation of the ORF in the mutant.

Consistent with previous observations that ORF50 is necessary and sufficient for reactivation[45,46], ΔORF50 showed a 30-fold decrease in virus production relative to parental BAC16 (Fig. 3C). This confirmed the validity of the experimental system to study spontaneous reactivation. Although many mutants showed no attenuation in virus production, a few (e.g. ΔORF61, and ΔORFK11) exhibited a decrease of approximately 10-fold or more compared to parental BAC16 (Fig. 3C, Supporting Information Fig S4). ΔORF61 was attenuated under multi-step growth and "induced" reactivation conditions (Table 1, Fig. 3A and B). However, ΔORFK11 showed little attenuation in these assays, suggesting that the reduced progeny production under uninduced conditions is due to the specific role of ORFK11 in enhancing

spontaneous reactivation and inhibiting latency (Fig. 3A, Fig. 3B, Supporting Information Fig. S4I).

Interestingly, several mutants (e.g. ΔORF11AA, ΔORF72, ΔORFK3, ΔORFK6, and ΔORFK7) achieved enhanced virus production (Fig. 3C, Supporting Information Fig. S4). ΔORFK7 showed enhanced growth under the multi-step growth conditions and during "induced" reactivation while ΔORFK3 and ΔORFK6 exhibited increased growth only during "induced" reactivation (Fig. 3A-C). In contrast, ΔORF11AA and ΔORF72 show little enhanced growth under these two conditions, suggesting that ORF11AA and ORF72 specifically repress spontaneous reactivation and promote latency. Our results further suggest that ORFK7 represses spontaneous reactivation, and in addition, possibly suppresses viral lytic replication steps.

We then measured the percentage of infected cells expressing ORF45, K8, or K8.1 under these conditions to understand the correlation between viral lytic gene expression and altered levels of reactivation and virus production (Supporting Information Fig. S5). Interestingly, disruption of K6, an immunomodulatory factor encoding a viral chemokine homologue[47,48], increased lytic gene expression and virus production (Fig. 3D-E, Supporting Information Fig. S5P-R). In contrast, disruption of K11, also an immunomodulatory factor involved in IFN transcription responses[49], shows the opposite phenotype - decreased lytic gene expression and virus production (Fig. 3D-E, Supporting Information Fig. S5V-X). The presence of viral genes which either enhance (e.g. K11) or repress (e.g. K6) spontaneous reactivation demonstrates the biological importance of tight viral control over reactivation and implicates these ORFs as critical regulators of latency. Furthermore, our observations suggest that different KSHV immunomodulatory factors affect gene expression to modulate viral reactivation.

Discussion

This is the first genome-wide study to identify viral genes important for KSHV latency, reactivation, and lytic replication. We found that 44 ORFs are essential for successful completion of the viral life cycle. Of these, 33 ORFs are conserved in all herpesvirus subfamilies, six (ORF10, 18, 24, 30, 31, and 66) are conserved among beta and gamma herpesviruses, and five (ORF45, 50, 52, 73, and 75) are gamma herpesvirus-specific[2,50]. Surprisingly, 10 ORFs conserved in all herpesvirus subfamilies were found to be nonessential in KSHV (Table 1), despite some of them being essential in other herpesviruses tested (Supporting Information Table S3)[2,3,51].

Our report is the first global mutagenesis study in a herpesvirus to identify viral ORFs regulating latency or reactivation. Our results suggest that reactivation is regulated positively or negatively by two specific sets of viral genes, which may act as important parts of the latent/lytic switch. For example, some ORFs may repress spontaneous (e.g. ORFs 11AA, 72, and K6) or induced reactivation (e.g. K3 and K5) while others (e.g. ORFK11) enhance spontaneous reactivation (Fig 3, Supporting Information Fig S2-5). ORFK11, an IFN modulator, may enhance spontaneous reactivation through changes in interferon responses while ORF72, a constitutively-expressed cyclin homologue, possibly represses spontaneous reactivation through its effects on cell cycle progression. Our profiling results show that KSHV encodes specific genes that actively turn on and off reactivation, a critical step for viral lytic replication and pathogenesis[5,52-55].

As an opportunistic pathogen, the onset of KSHV lytic replication and its associated diseases correlate with the host's immune status. One hypothesis is that KSHV engages in random spontaneous reactivation to achieve persistent infection and the host immune responses are responsible for controlling the level of reactivation. However, under immunodeficient conditions, viral reactivation is left unchecked and takes off to full blown lytic replication, leading to KSHV diseases. An alternative hypothesis is that KSHV reactivation is not random but tightly and actively regulated by viral factors, which connect reactivation with the host immune status. It is conceivable that these factors, which regulate reactivation, are involved in sensing, interacting, and modulating immune responses.

The alternative hypothesis appears to be supported by our results. Six ORFs (i.e. K3, K4, K5, K6, K7, and K11) known to have immunomodulatory functions were found to promote or suppress virus reactivation and production (Table 1, Fig. 3). Mutants with inactivation in four of these ORFs (i.e. K4, K5, K6, and K11) showed changes in lytic gene expression correlating with changes in virus production (Fig. 3D-E, Supporting Information Fig. S2-S5). These observations further implicate viral immunomodulatory genes in regulating viral reactivation at the gene expression level, even in a cell culture system which lacks adaptive immunity, and many innate immunity factors.

K4 and K6 encode viral chemokine homologues[47,56]. K3 and K5 modulate expression of surface glycoproteins important for immune responses such as MHC and interferon-γ receptor[43,44,57]. K7 and K11 are anti-apoptotic factors involved in autophagy and IFN transcription responses, respectively[49,58,59]. These KSHV factors could play a role in modulating the immune-microenvironment, cell membrane receptor composition, and appropriate downstream signaling pathways to produce an immune-switch for KSHV latency and reactivation. The virally reconfigured pathways serve as a sensory network that allows KSHV to communicate with, and deliberately respond to, changes in host homeostasis. In the presence of immuno-selective/repressive pressure, these virally reconstructed pathways promote latency,

however, under immunocompromised conditions, these pathways promote lytic replication and progeny production.

Our findings suggest that KSHV reactivation is actively regulated by specific genes that sense, interact, and communicate with the immune system. The immune status of the host is the input for this sensory network, and the network output is the decision to reactivate, which is critical for viral pathogenesis. Thus, our results elucidate a possible mechanism for how viral reactivation is correlated with the status of immune status/responses, leading to viral latency with no onset of diseases under immunocompetent conditions and viral active replication with full blown viral diseases under immunodeficient conditions. It will be interesting to determine if other herpesviruses employ similar mechanism to achieve opportunistic infection by encoding immunomodulatory proteins for regulating reactivation and latency. Further studies could provide insight into virus reactivation and production and will facilitate the development of novel strategies for treatment and prevention of the diseases associated with KSHV and other herpesviruses.

Table 1. KSHV ORFs categorized by growth properties of their respective inactivation mutants in human iSLK cells.

	Essential Genes		
44 ORFs	***ORF***	***Conservation***	***Putative Functions***
	73 (D)	γ2	Tethers viral episomes to chromatin
	6 (D)	α, β, γ	Single-stranded DNA-binding protein[24,60]
	7 (S)	α, β, γ	Terminase complex
	8 (S)	α, β, γ	Glycoprotein B
	9 (D)	α, β, γ	DNA polymerase[24,60]
	10 (S)	β, γ	Inhibition of host mRNA nuclear export[40],derived from ORF54[61]
	17 (S)	α, β, γ	Maturational protease and capsid scaffolding protein
	18 (S)	β, γ	Late gene expression[32,62]
	19 (S)	α, β, γ	Portal cap[63], inner tegument protein[64]
	22 (S)	α, β, γ	Glycoprotein H
	24 (S)	β, γ	Late gene expression[31,65]
	25 (S)	α, β, γ	Major capsid protein[66]
	26 (S)	α, β, γ	Triplex capsid protein[66]
	29a (S)	α, β, γ	Terminase complex
	29b (S)	α, β, γ	Terminase complex
	30 (S)	β, γ	Late gene expression[32,62]
	31 (S)	β, γ	Late gene expression[30]
	32 (S)	α, β, γ	Inner tegument protein[63,64]
	33 (S)	α, β, γ	Tegument protein[67], egress[37]
	34 (S)	α, β, γ	Tegument protein, late gene expression[30,31]
	39 (D)	α, β, γ	Glycoprotein M
	40 (D)	α, β, γ	Helicase-primase complex[60]
	41 (S)	α, β, γ	Helicase-primase complex[60]
	43 (S)	α, β, γ	Portal protein[63]
	44 (SC)	α, β, γ	Helicase-primase complex[60]
	45(D)	γ	Tegument protein[68], egress[69], reactivation[70]
	47 (D)	α, β, γ	Glycoprotein L
	50 (D)	γ	RTA, reactivation
	52 (D)	γ	Tegument protein[71]
	53 (D)	α, β, γ	Glycoprotein N
	55 (S)	α, β, γ	Putative tegument protein
	56 (S)	α, β, γ	Primase[60]
	57 (D)	α, β, γ	Regulator of gene expression
	59 (D)	α, β, γ	DNA polymerase processivity factor[60]
	62 (D)	α, β, γ	Triplex capsid protein[66]

	63 (D)	α, β, γ	Tegument protein[67], NLR homolog[72]
	64 (D)	α, β, γ	Large tegument protein[63,67]
	65 (D)	α, β, γ	Small capsid protein
	66 (S)	β, γ	Late gene expression[73]
	67 (S)	α, β, γ	Nuclear egress[74]
	67.5 (S)	α, β, γ	Terminase component (67A)
	68 (S)	α, β, γ	DNA packaging[75]
	69 (D)	α, β, γ	Nuclear egress[74]
	75 (D)	γ	Phosphoribosylformylglycinamidine synthase (vFAGART), tegument protein[67]
Non-Essential Genes (47 ORFs)			
Attenuation	**ORF**	**Conservation**	**Putative function**
Severe (9)	16 (D)	γ	vBCL-2, antiapoptotic[76]
	27 (S)	γ	Putative glycoprotein, tegument protein[67]
	46 (D)	α, β, γ	Uracil-DNA glycosylase
	49 (D)	γ	Co-factor with ORF50 for reactivation[77]
	K8 (D)	U	K-bZIP (KSHV basic leucine zipper)[60,78,79]
	54 (D)	α, β, γ	Deoxyuridine triphosphatase
	58 (D)	γ	Tegument glycoprotein[80]
	60 (D)	α, β, γ	Ribonucleotide reductase; small subunit
	61 (D)	α, β, γ	Ribonucleotide reductase; large subunit[81]
Moderate (4)	4 (D)	γ2	Kaposica, CD46 homologue for complement modulation[82]
	35 (S)	γ	Tegument protein[80]
	36 (S)	α, β, γ	Protein kinase[83]
	38 (S)	α, β, γ	Egress[37]
No Attenuation (32)	K1 (D)	U	KIS (KSHV ITAM signaling protein)[84,85]
	10.1 (S)	U	Unknown function
	11AA (S)	U	Unknown function
	11 (D)	β, γ	Derived from ORF54[61]
	K2 (D)	U	vIL6[86,87]
	2 (D)	γ2	Dihydrofolate reductase
	K3 (D)	U	MIR-1, immunomodulation[44,57]
	70 (D)	γ2	Thymidylate synthase
	K4 (D)	U	vMIP-II (vCCL2), immunomodulation[56,88]
	K4.1 (D)	U	vMIP-III (vCCL3), immunomodulation[89]
	K4.2 (S)	U	Unknown function
	K5 (D)	U	MIR-2, immunomodulation[43,44,57]
	K6 (D)	U	vMIP-I (vCCL1), immunomodulation[47]
	K7 (S)	U	vIAP, antiapoptotic[58,59]
	20 (S)	α, β, γ	Nuclear protein, cell cycle arrest[90]

	21 (S)	α, γ	Thymidine kinase, tegument protein[67]
	23 (S)	α, β, γ	Late gene expression[18], tegument protein[80]
	30.1 (S)	U	Unknown function
	34.1 (S)	U	Unknown function
	37 (S)	α, β, γ	Deoxyribonuclease; DNA maturation and recombination
	42 (S)	α, β, γ	Tegument protein[80]
	48 (D)	γ	Tegument protein[80]
	K9 (S)	U	vIRF1[91], anti-apoptotic[92]
	K10 (D)	U	vIRF4, anti-apoptotic [93]
	K10.5 (D)	U	vIRF-3/LANA2, anti-apoptotic [94,95]
	K11 (S)	U	vIRF-2[49], anti-apoptotic[96]
	K12 (D)	U	Kaposin A[97,98]
	K13/71 (D)	U	vFLIP (FLICE [FADD-like interleukin1 beta-converting enzyme, now called caspase8] inhibitory protein), anti-apoptosis, immunomodulation[99-101]
	72 (D)	γ2	vCyclin[102,103]
	K14 (D)	U	vOX2, immunomodulation[104]
	74 (D)	γ2	vGPCR[105]
	K15 (D)	U	anti-apoptotic, immunomodulation[106,107]
Enhanced Growth (2)	28 (D)	γ	Envelope glycoprotein[67,108]
	K8.1 (D)	U	Envelope glycoprotein[16]

Table 1. KSHV ORFs categorized by growth properties of their respective inactivation mutants in human iSLK cells.

The sequence conservations of these ORFs with those in other herpesviruses of the α, β, γ subfamilies, the genome sequences of which are currently available[8,109-111], is included. ORF functions and the functions of their homologues in other herpesviruses that have been shown or implicated from previous studies is also shown (Supporting Information Table S3)[2]. ORFs unique to KSHV are marked as a "U". D, deletion mutation; S, stop codon mutation.

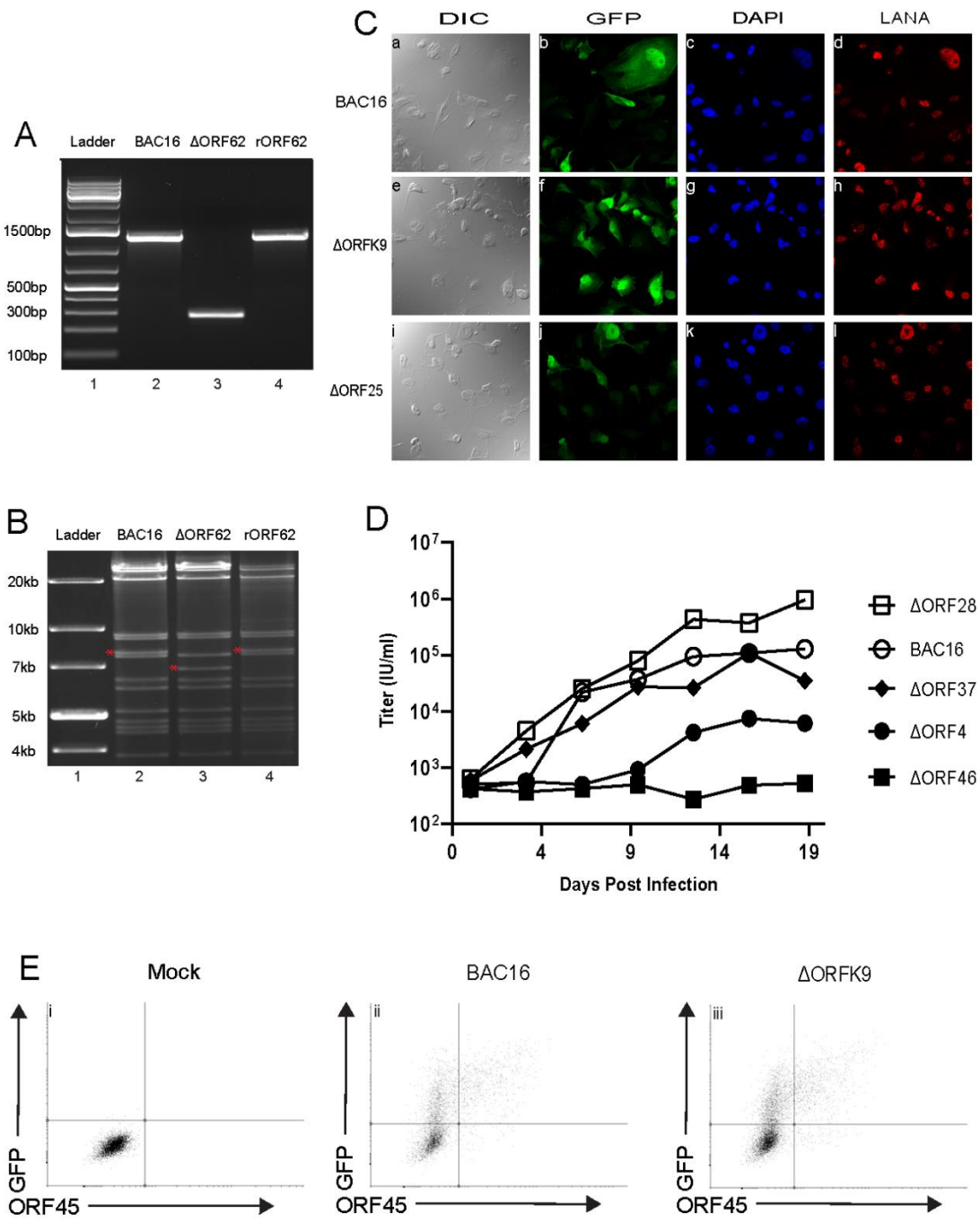

Figure 1. Characterization of KSHV mutants.

(A-B) PCR products (A) and NheI digest (B) of DNAs purified from BAC16, deletion mutant ΔORF62, or rescued mutant rORF62. The red asterisks mark the digest band where ORF62 is expected to be found. (C) Microscopic images of parental and mutant BAC16-transfected iSLK cells under differential interference contrast (DIC) or for expression/staining of GFP, DAPI, and viral LANA. (D) Multi-step growth (MOI=0.1) of mutants and parental BAC16 in iSLK cells. (E) Lytic antigen ORF45 expression in mock-infected, BAC16-infected, and ΔORFK9-infected iSLK cells by flow cytometry. Experimental details can be found in Methods.

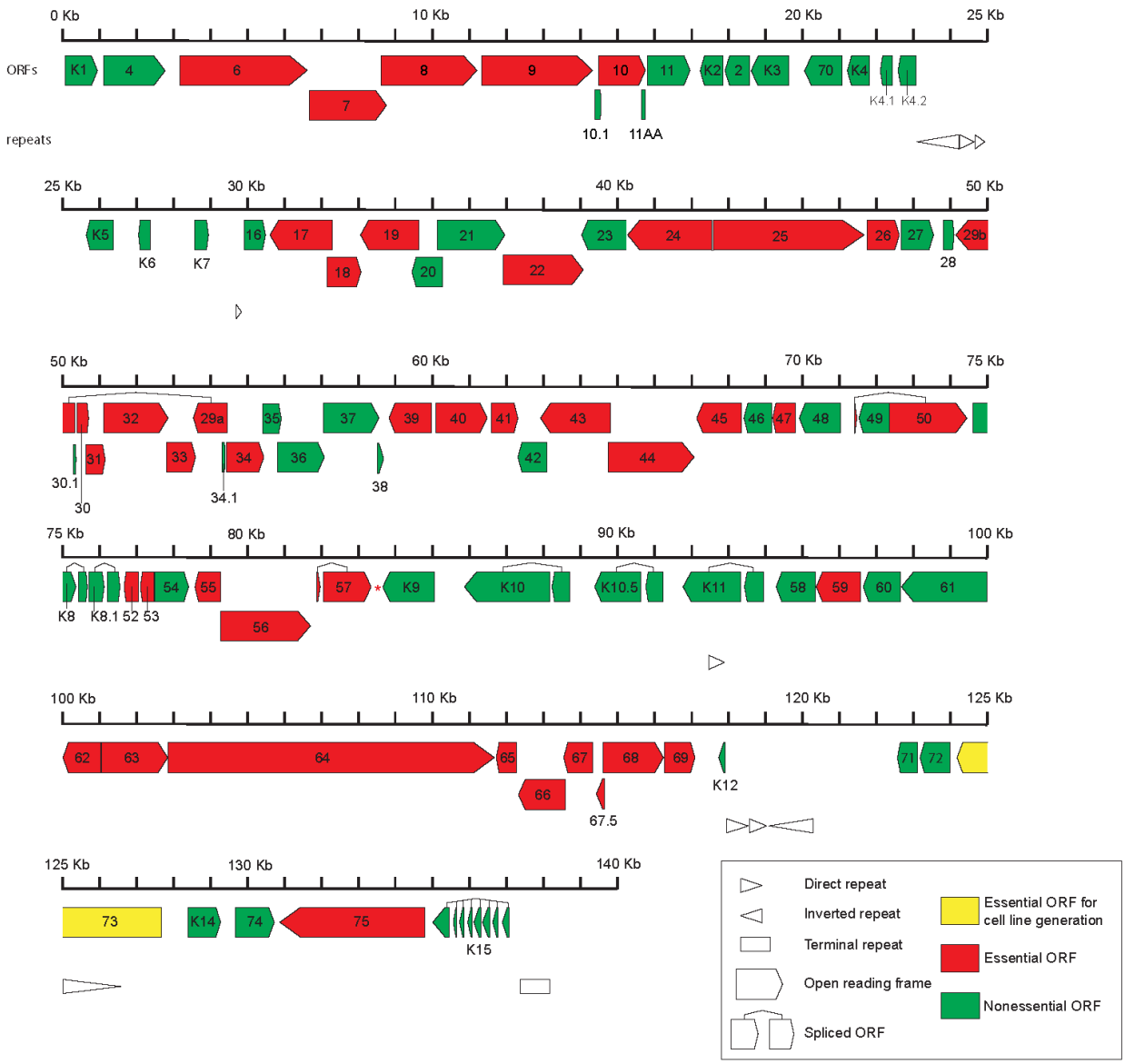

Figure 2. Functional map of KSHV ORFs and their roles in viral growth in human cells.

The genomic locations of KSHV ORFs are indicated by boxed arrows (accession: GQ994935.1). ORFs are colored coded based on the growth properties of their respective gene-inactivated mutants in iSLK cells (Table 1). The red asterisk marks the location where the BAC-backbone was inserted.

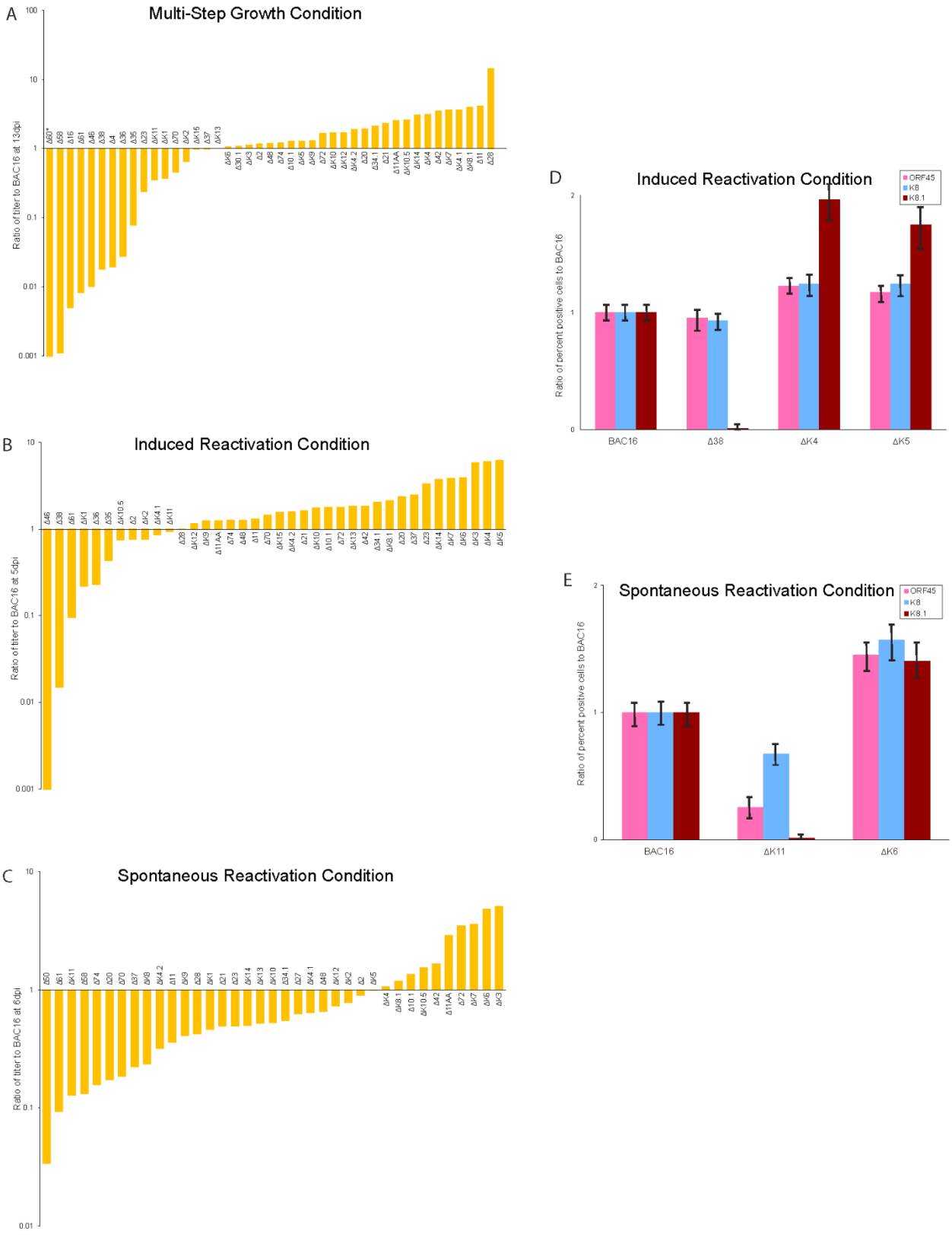

Figure 3. Growth and lytic antigen expression of viral mutants under different conditions.

(A-C). In multi-step growth conditions (A), iSLK cells were infected (MOI=0.1) in inducing conditions in the presence of doxycycline and sodium butyrate. Supernatants were harvested at 13 dpi. In induced reactivation conditions (B), iSLK cells were infected (MOI=1) and induced in the presence of doxycycline and sodium butyrate at 2 dpi, and supernatants were harvested at 5 dpi. In spontaneous reactivation conditions (C), iSLK cells were infected (MOI=1) and maintained in uninduced conditions and supernatants were harvested at 6 dpi. Mutant titers were normalized to BAC16 titers. (D-E). In (D), iSLK cells were infected (MOI=1), induced in the presence of doxycycline and sodium butyrate at 2 dpi and harvested at 4 dpi. In (E), iSLK cells were infected (MOI=1) and maintained in uninduced conditions and harvested at 6 dpi. The harvested cells were fixed, stained for lytic antigens, and analyzed by flow cytometry. The percentages of specific antigen expressing cells for mutants were normalized to those for BAC16. The values are the average of three independent experiments. Error bars represent 1 standard error of the mean.

SUPPORTING INFORMATION

SUPPORTING TABLES

Table S1. Primers for KSHV mutagenesis and PCR.

ORF	Deletion/Insert Primers (5' →3')	PCR Primers (5'→3')
K1	CCTGTCTTTCAGACCTTGTTGGACATCCCGTACAATCAAGCATTCAGGTAAGATAATCTAAGGATGACGACGATAAGTAGGG	CGGCCCTTGTGTAAACCTGTC
	ATTATGTTATAGAGAATATTTAGATTATCTTACCTGAATGCTTGATTGTACGGGATGTCCAACCAATTAACCAATTCTGATTAG	GCACGGTTATACAATGTCCT
2	CTAACGCGGCATACACTAGCCGGTGGTGCCCGAGCGGGAGGCCGCGAGGGTATAGGTAAAAGGATGACGACGATAAGTAGGG	AGGACATTGTATAACCGTGC
	ACACTGTGTGGTTGGTGGTGTTTACCTATACCCTCGCGGCCTCCCGCTCGGGCACCACCGAACCAATTAACCAATTCTGATTAG	GTTGTCTTGTATTGGTCGGT
4	GTACATTAAAAGGACATTGTATAACCGTGCTACTTACAGCCCTAGACTTGCTCCAGTGTTAGGATGACGACGATAAGTAGGG	TATAGTGCGCGGTGTGGCAG
	AAGCAATCATAGCCCTGTCTAACACTGGAGCAAGTCTAGGGCTGTAAGTAGCACGGTTATAACCAATTAACCAATTCTGATTAG	GAGTAGTGTGCCGTGAAGGCT
6	TACACACGGGTTTTTTGTTGTCTTGGCCAATCGTGTCTCCTTGTGTACCCGTAACGATGGAGGATGACGACGATAAGTAGGG	ACAGTCGGTAGTGGAGGAGC
	GACCGCCGCCAGTTCCTTTGCCATCGTTACGGGTACACAAGGAGACACGATTGGCCAAGAAACCAATTAACCAATTCTGATTAG	GCTCTGAAACTTCCCTGTAGTGA
7	GACCTGGATTTGTAGTTGTGTACCCGTAACGATGGCAAAGTAGGTAGATAGGGAACTGGCGGCGGTCTATGCAGGATGACGACGATAAGTAGGG	GAGGAACCGAAACCCGCAGG
	TGGCTAGGGCTGACACATCGGCATAGACCGCCGCCAGTTCCCTATCTACCTACTTTGCCATCGTTACGGGTAAACCAATTAACCAATTCTGATTAG	CCACACTCTTAGGACCAGATGCTT
8	CTGTACCACCACCTGCAATTGAGCAACCACAATGACTCCCTAGGTAGATAGGAGGTCTAGATTGGCCACCCTAGGATGACGACGATAAGTAGGG	CAATCGCTAGACATCAGTCC
	CCAACAGGATGACAGTCCCCAGGGTGGCCAATCTAGACCTCCTATCTACCTAGGGAGTCATTGTGGTTGCTCAACCAATTAACCAATTCTGATTAG	CGTTATCTCCCAGTCACCTA
9	CTACTCGTTACACACAGACACAAATTACCGTCCGCAGATCTGACTCAGACGCGGAAACAGAGGATGACGACGATAAGTAGGG	AGAACAACACGTCGGCAACC

	AAGAGGAAACTTTCTAGGCGCTGTTTCCGCGTCTGAGTCAGATCTGCGGACGGTAATTTGAACCAATTAACCAATTCTGATTAG	GGATTCTTAGCCGCGTGTAGT
10.1	CTTGCGCTATGTGGGACAACTAGAGTCCAACCTGGCAAGCTAGGTAGATAGGAGTGGAGCAAGACGCCAGACAGGATGACGACGATAAGTAGGG	CCACACTCTTAGGACCAGATGCTT
	TATTTTTTTCGAGATCGGCTGTCTGGCGTCTTGCTCCACTCCTATCTACCTAGCTTGCCAGGTTGGACTCTAAACCAATTAACCAATTCTGATTAG	CCACACTCTTAGGACCAGATGCTT
10	AACGTTCATCCTAGGTGACTGGGAGATAACGGTGTCTAACTAGGTAGATAGGTGCCGGTTTACTTGCAGCAGAGGATGACGACGATAAGTAGGG	GCCAGGCACCATACAGCTTC
	AAAGGGGGCCACATGTTAGGCTGCTGCAAGTAAACCGGCACCTATCTACCTAGTTAGACACCGTTATCTCCCAACCAATTAACCAATTCTGATTAG	GATTAGAGATGACGATGTGGCTCGG
11AA	CCACGTAGCGATTAGGGCCGACCGCCACGAGGAACCCATGTAGGTAGATAGGCAATCGTGACTGTCCGAGCAAGGATGACGACGATAAGTAGGG	CAGCTTCTACGACTGCAAGG
	TCTGACTCCTGCGCCATATGTGCTCGGACAGTCACGATTGCCTATCTACCTACATGGGTTCCTCGTGGCGGTAACCAATTAACCAATTCTGATTAG	GTGTGTGTTATGTATTCGGGTGG
11	GCCACGAGGAACCCATGCAATCGTGACTGTCCGAGCACATGTGTCCGGTTCCCACCCACAAGGATGACGACGATAAGTAGGG	TGTTCCCATACGCGCCTGTC
	GAAAGCAATAAAGACAAATGTGTGGGTGGGAACCGGACACATGTGCTCGGACAGTCACGAAACCAATTAACCAATTCTGATTAG	CTGGCGAGCAAGAGAGGGTTT
K2	GTATATTAGTGTTATAAGAAATTTTATGTCACGTCGCTCTGGCTGCTAACGCGGCATACAAGGATGACGACGATAAGTAGGG	CGCGTTCCAGATACCAGCAG
	GCTCGGGCACCACCGGCTAGTGTATGCCGCGTTAGCAGCCAGAGCGACGTGACATAAAATAACCAATTAACCAATTCTGATTAG	GCTGGACCCTCCTCTCTAGTT
2	CTAACGCGGCATACACTAGCCGGTGGTGCCCGAGCGGGAGGCCGCGAGGGTATAGGTAAAAGGATGACGACGATAAGTAGGG	TGGTATCAACCGCAACTACACAG
	ACACTGTGTGGTTGGTGGTGTTTACCTATACCCTCGCGGCCTCCCGCTCGGGCACCACCGAACCAATTAACCAATTCTGATTAG	GTGAGTGGCTGTAGCATTACC
K3	GGTAAACACCACCAACCACACAGTGTGCTCTTATATACTTATCCTGAGAGAGAACCCACAAGGATGACGACGATAAGTAGGG	GATTCATGTAGACAACCCGCTC
	GGGTTAATGCCATGTTTTATTGTGGGTTCTCTCTCAGGATAAGTATATAAGAGCACACTGAACCAATTAACCAATTCTGATTAG	CGTGGGAACTGTGAGTAATGTG
70	GCCCACCACTCTGACCGCACGCTAAACATCGCCCTACCTGGATAGATCCTGGAAGTTTGTAGGATGACGACGATAAGTAGGG	CGCTGTTCTCCTGTAATTGG

	CTCTCCGGGCACAGGGCTTCACAAACTTCCAGGATCTATCCAGGTAGGGCGATGTTTAGCAACCAATTAACCAATTCTGATTAG	GGTGTTGGCCTTCGTAATAA
K4	AGAGATCCGTCGCGTAAATGCGCAGCTGGCAAAGCATTCTAACTCCCCTCGTGTGTCCTCAGGATGACGACGATAAGTAGGG	ACGACGGTTACAGGTCCCTC
	TCGCCGTTTCGCATTTACACGAGGACACACGAGGGGAGTTAGAATGCTTTGCCAGCTGCGAACCAATTAACCAATTCTGATTAG	CATTTGGCAACGCTGGTCTT
K4.1	TATGTCACAGACTCAACACACACGGGCCGTTACGCAACGGACAGTTCTGGCGCCACAACGAGGATGACGACGATAAGTAGGG	CTGGCCGCAATAGCTCAATC
	TGCACCCCTTTGCGCATCATCGTTGTGGCGCCAGAACTGTCCGTTGCGTAACGGCCCGTGAACCAATTAACCAATTCTGATTAG	CCGCTAACAGCACCAAATCCAC
K4.2	ACATAATTTATGCACATAAAAGGATTAGCGCATGCAAATTTAGGTAGATAGGAGCTTTGCCGAAGTTCTCGGAGGATGACGACGATAAGTAGGG	AGGACAGATTTGGGCACAGG
	CAGCGCGCCCCACCGGCTTTCCGAGAACTTCGGCAAAGCTCCTATCTACCTAAATTTGCATGCGCTAATCCTAACCAATTAACCAATTCTGATTAG	CAGGGTGGGTTGTGACAGTT
K5	GGGCGTCACGTCACATATCTCTGTGCACCCAAGTGGTTGTCTCTGCAGCTGGGGTGGAAGAGGATGACGACGATAAGTAGGG	CATTTCTTCCTCGACAGGTCTTC
	TCCCCTTTCCCTTTTTCAGACTTCCACCCCAGCTGCAGAGACAACCACTTGGGTGCACAGAACCAATTAACCAATTCTGATTAG	GCATGTAAGCTGGCGGTTAG
K6	GAGCAGTTGGGCCGCAGTGATATCTTCAACTTTCGACCGTCTGGAGGTGCCAAGTTCGCAAGGATGACGACGATAAGTAGGG	TTATGGATTATTAAGGGTCAGCTTG
	TACGGTTTTCTTTAGACTGTTGCGAACTTGGCACCTCCAGACGGTCGAAAGTTGAAGATAAACCAATTAACCAATTCTGATTAG	CGACGCAATCAACCCACAAT
K7	TCCAAAAATGGGTGGCTAACCTGTCCAAAATATGGGAACATAGGTAGATAGGCTGGAGATAAAAGGGGCCAGAGGATGACGACGATAAGTAGGG	GGAACCAGCTTGGTGATGTG
	CAGTGCTAAACTGACTCAAGCTGGCCCCTTTTATCTCCAGCCTATCTACCTATGTTCCCATATTTTGGACAGAACCAATTAACCAATTCTGATTAG	CAAGCAGTAGCGAACAGTTACG
16	GGTGCTGTGCGCGTGCTATGTTCCCTGGTGACCGTCCACACGCGTAATTCGAGGTCCCCGAGGATGACGACGATAAGTAGGG	GGCAGGACACAACATCTACAAAC
	CATGCAACCATCTACTCTTCCGGGGACCTCGAATTACGCGTGTGGACGGTCACCAGGGAAAACCAATTAACCAATTCTGATTAG	CATTGGCAGTAGCCTCCCTTAA
17	CTCGGTCTCACACACGTATTTTCCGAGCATGGCACAGGGCTAGGTAGATAGGCTGTACGTCGGAGGGTTTGTAGGATGACGACGATAAGTAGGG	TACCGTGGGACACTTGAAATAGAC

	TGGGGCAGGACACAACATCTACAAACCCTCCGACGTACAG CCTATCTACCTAGCCCTGTGCCATGCTCGGAAAACCAATTA ACCAATTCTGATTAG	GCTCTTGGGCG TGGAATGTA
18	GCCGCTGAGCCCGGGGCTTAGGAGGCTCATGTGGCGCTTTT AGGTAGATAGGTTGCAAAATAAGAATTTAAAAGGATGACG ACGATAAGTAGGG	CATTACATCGC TCACTCGGCCC
	GCTCTTGGGCGTGGAATGTATTTAAATTCTTATTTTGCAAC CTATCTACCTAAAAGCGCCACATGAGCCTCCAACCAATTAA CCAATTCTGATTAG	CGGTGAAGTTA CGGTGGCTG
19	GGACCGGCTTGTTCAGGTCCATGACTCACGCGTCCGCGTCT AGGTAGATAGGATTAACGCAGATATCGACGCAGGATGACG ACGATAAGTAGGG	GATCCATTGGC GCGTAGTCTC
	ATCTTCGGTTTTTTGGGTACCTTAGATAGGACCTTTCTGACC TATCTACCTATGTCAGCATTTTCTCTAGCAAACCAATTAAC CAATTCTGATTAG	AGCTCGGACGA CGAATCAAG
20	CGAGTCCGCTCCAAAACCGCCTTCTGCCATGGTACGTCCAT AGGTAGATAGGACCGAGGCCGAGGTTAAGAAAGGATGAC GACGATAAGTAGGG	CGGCAATTCTG TGCCCTAGAG
	CTGGAAGCCTGCTCAGGGATTTCTTAACCTCGGCCTCGGTC CTATCTACCTATGGACGTACCATGGCAGAAGAACCAATTA ACCAATTCTGATTAG	GTGCTTGATTC GTCGTCCGAG
21	TTTCTTAACCTCGGCCTCGGTTGGACGTACCATGGCAGAAT AGGTAGATAGGGGCGGTTTTGGAGCGGACTCAGGATGACG ACGATAAGTAGGG	CCCGTCGTGAT CGAGCTTTG
	TTTCTCCGCCGCGCCCCACCGAGTCCGCTCCAAAACCGCCC CTATCTACCTATTCTGCCATGGTACGTCCAAAACCAATTAA CCAATTCTGATTAG	GGAGCGGGTTA TTGTCGTCG
22	AGTCTAAAGCAGTTAATCACCTAGAGGAGACATGCAGGGT TAGGTAGATAGGCTAGCCTTCTTGGCGGCCCTAGGATGAC GACGATAAGTAGGG	GTCATCGGTTC GCCGCTCTA
	ATATGCATCGCCAGCATGCAAGGGCCGCCAAGAAGGCTAG CCTATCTACCTAACCCTGCATGTCTCCTCTAGAACCAATTA ACCAATTCTGATTAG	GAACAACAGTG GCATCGGGAC
23	CGTACGTTGCGTCCGTCCGCTGGTCTAAGCTATGTTACGAT AGGTAGATAGGGTTCCGGACGTGAAGGCTAGAGGATGACG ACGATAAGTAGGG	GGACACTGCCT TCTCTGGCG
	GCGCCGCGCCCTCTACTAGACTAGCCTTCACGTCCGGAACC CTATCTACCTATCGTAACATAGCTTAGACCAAACCAATTAA CCAATTCTGATTAG	CTTCTAAGGTC AGCTCTGCCTG C
24	CGGGAAAGGTCGTTGCTCCAAGGTCGCCTCCATGGCAGCG TAGGTAGATAGGCTCGAGGGCCCCCTACTACTAGGATGAC GACGATAAGTAGGG	AGTAGTCTGCG TATCGCTCTGC
	TCAGGGAGGCGCTCGGTGGCAGTAGTAGGGGGCCCTCGAG CCTATCTACCTACGCTGCCATGGAGGCGACCTAACCAATTA ACCAATTCTGATTAG	CCTTGCCGAGC AATAGCTGAAA
25	TGGCAGTAGTAGGGGGCCCTCGAGCGCTGCCATGGAGGCG TAGGTAGATAGGACCTTGGAGCAACGACCTTTAGGATGAC GACGATAAGTAGGG	CGTCGTGGTCA ACGGTACAG

	CCTCCGTGGCGAGGTACGGGAAAGGTCGTTGCTCCAAGGT CCTATCTACCTACGCCTCCATGGCAGCGCTCGAACCAATTA ACCAATTCTGATTAG	CAATCTCCGAG CGGCAGTAC
26	TATTAGCTAACCCTTCTAGCGTTGGCTAGTCATGGCACTCT AGGTAGATAGGGACAAGAGTATAGTGGTTAAAGGATGACG ACGATAAGTAGGG	TCTGGACGTAG ACAACACGGAT C
	CGAAGAGTCTGGAGGTGAAGTTAACCACTATACTCTTGTCC CTATCTACCTAGTTGGCTAGTCATGGCACTCAACCAATTAA CCAATTCTGATTAG	GAGCCGTCATC CGTCCTTGC
27	GAGACTTTGGCGGCCTCCTGTTGGTATTCCCCACGCTAACT AGGTAGATAGGGATTTGAAGCGGGGGGGGGGAGGATGAC GACGATAAGTAGGG	TTTACGCTAAG AGTTGGGTGCT TG
	GAATATCAGATGACGCCATACCCCCCCCCCGCTTCAAATCC CTATCTACCTAGTTAGCGTGGGGAATACCAAAACCAATTA ACCAATTCTGATTAG	GGACGACTTAC TTGTGGCAGT
28	CTCAGTTGAGAGTCAGAGAATACAGTGCTAATCAGGGTAG AACGGGGTGTGTGCTATAATAGGATGACGACGATAAGTAG GG	GTTCGCCTCCTC TCCTTTACTGTT A
	TACAGTGCTAATCAGGGTAGAGCCCCCCCCATAGCCATCC ATTATAGCACACACCCCGTTAACCAATTAACCAATTCTGAT TAG	GGTGGAAATCT TCGCGGTGG
29b	AAAGGATGCACTGCCGGCTATTCTGGGTTTCATGCTTCAGT AGGTAGATAGGAAAGACGCCAAGCTTATATTAGGATGACG ACGATAAGTAGGG	TGGGCGTTCCT GAGGTTAAG
	ACGAGTTCACGGATGATATAAATATAAGCTTGGCGTCTTTC CTATCTACCTACTGAAGCATGAAACCCAGAAAACCAATTA ACCAATTCTGATTAG	CCAAGAACAAG AGCCACGCA
30.1	TACGTAGAGCAGGTTAAAGGTCTGTCCCCGAATGCTCTGCT AGGTAGATAGGAGACACGGAAAGACACAAAAAGGATGAC GACGATAAGTAGGG	TCTGAAGCATG AAACCCAGAAT AG
	TAGCCGCTTATGAGCCCCTCTTTTGTGTCTTTCCGTGTCTCC TATCTACCTAGCAGAGCATTCGGGGACAGAAACCAATTAA CCAATTCTGATTAG	CGACCACTTGC TCCCTAAGG
30	GGGAATAAAAGGGGGCGTGTGTGCCGATCGTATGGGTGAG TAGGTAGATAGGCCAGTGGATCCTGGACATGTAGGATGAC GACGATAAGTAGGG	CAGTAAAGGAG AGGAGGCGAAC
	CAAAATCTTTCTCATTCACCACATGTCCAGGATCCACTGGC CTATCTACCTAGTGCCGATCGTATGGGTGAGAACCAATTAA CCAATTCTGATTAG	GGACTCGCCAC ACTCTTCATT
31	TGTGCCGCCTAGACACCGGTGCGAAATGAAGAGTGTGGCG TAGGTAGATAGGAGTCCCTTATGTCAGTTCCAAGGATGAC GACGATAAGTAGGG	CGTGCAGGAAA TAGCCCTGG
	GGTACAGGCAAAACACGCCGTGGAACTGACATAAGGGACT CCTATCTACCTACGCCACACTCTTCATTTCGCAACCAATTA ACCAATTCTGATTAG	GTGATGCAGCA GAAAGGTCCT
32	ACGACTGCATTGCCAAGCGGGTGCGGACAAAATGGATGCG TAGGTAGATAGGCATGCTATCAACGAAAGATAAGGATGAC GACGATAAGTAGGG	ACGGACGGTGA CTGGTTAGAG

	GGTGGCAGCGAGGACCTACGTATCTTTCGTTGATAGCATGC CTATCTACCTAGTGCGGACAAAATGGATGCGAACCAATTA ACCAATTCTGATTAG	GAGATAGAGGT GCAGGCGTTAA AG
33	AAGGAGGATCTGGTGTTCATTCGAGGCCGCTATGGCTAGCT AGGTAGATAGGCGGAGGCGCAAACTTCGGAAAGGATGAC GACGATAAGTAGGG	ACGGACGGTGA CTGGTTAGAG
	TGCATTCCTTGTTTAGGAAATTCCGAAGTTTGCGCCTCCGC CTATCTACCTAGCTAGCCATAGCGGCCTCGAAACCAATTAA CCAATTCTGATTAG	GAGATAGAGGT GCAGGCGTTAA AG
29a	ACCCTCGGACACGAGCGAGCTCAAAGCAAACATGCTGCTC TAGGTAGATAGGAGCCGTCACAGGGAGCGCCTAGGATGAC GACGATAAGTAGGG	CGTTGTCCTCG GACGGTCTG
	TCTCCTGCAGGTTGGCGGCAAGGCGCTCCCTGTGACGGCTC CTATCTACCTAGAGCAGCATGTTTGCTTTGAAACCAATTAA CCAATTCTGATTAG	CTACTGGTCAC CTCCGGGTCA
34.1	ATCCGTGCCGTTTTGGGACAGTGTCGCGTGAATGTCGGGGT AGGTAGATAGGCACTCAGTTCCCACCTCTCTAGGATGACG ACGATAAGTAGGG	GATTTGCTGAC GTGGGCGTG
	GAGACCGCCAAAGACGCCGGAGAGAGGTGGGAACTGAGT GCCTATCTACCTACCCCGACATTCACGCGACACAACCAATT AACCAATTCTGATTAG	CCAGGTGTGTT CTCGCTAAGGT
34	GGCAAGGCGCTCCCTGTGACGGCTGAGCAGCATGTTTGCTT AGGTAGATAGGTTGAGCTCGCTCGTGTCCGAAGGATGACG ACGATAAGTAGGG	TTACATTTCCCA CACCTGCCTC
	TGGTCACCTCCGGGTCACCCTCGGACACGAGCGAGCTCAA CCTATCTACCTAAGCAAACATGCTGCTCAGCCAACCAATTA ACCAATTCTGATTAG	CTCAAACACGG CGCTGCTAC
35	ATACCGGCGATCATCACCATGATCAAGGAGAATGGACTCA TAGGTAGATAGGACCAACTCTAAAAGAGAGTTAGGATGAC GACGATAAGTAGGG	AGTTTCAGGAC GCACAGCATG
	CCTCCAGAGCCGACTTAATAAACTCTCTTTTAGAGTTGGTC CTATCTACCTATGAGTCCATTCTCCTTGATCAACCAATTAA CCAATTCTGATTAG	GCGCTTTAAGA TACGCGGTGG
36	TTGCCCCCGGTGTGCCCTGAAACTCCCTAAGGCTACCCGGT AGGTAGATAGGATTTCAGAGAGACCCTGGGCAGGATGACG ACGATAAGTAGGG	GATTCCCATGC GACAGGAGC
	GATTCAGCTGCCATGTGGACGCCCAGGGTCTCTCTGAAATC CTATCTACCTACCGGGTAGCCTTAGGGAGTTAACCAATTAA CCAATTCTGATTAG	CAGTCTCGAAC CTTGGCGTG
37	AGAAAGCTACTAGAGCGAGACTTTTTCAACCATGGAGGCC TAGGTAGATAGGACCCCCACACCCGCGGACTTAGGATGAC GACGATAAGTAGGG	CCTGTCAACTG TACCATCGGTG
	CCAGATAGTCTTCAGAAAACAAGTCCGCGGGTGTGGGGGT CCTATCTACCTAGGCCTCCATGGTTGAAAAAGAACCAATTA ACCAATTCTGATTAG	GGATTGCGATT GCTCAAGCA
38	GAAGTGCGAAGGACACCTTTCCATATATCAAATGGGATTTT AGGTAGATAGGCTCCTATCTATCTGCAAACGAGGATGACG ACGATAAGTAGGG	GGGATGGAGGA AGAGGGATG

	CGTCTACGGGCTGTGAGGGACGTTTGCAGATAGATAGGAG CCTATCTACCTAAAATCCCATTTGATATATGGAACCAATTA ACCAATTCTGATTAG	GGACGTGAACG CTGTGAAAG
39	ATGGAGGAAGAGGGATGGGTTTATAATGCCAATATATCAG GTTTCTCGGTCTTTTTAACTAGGATGACGACGATAAGTAGG G	GCGGGAGAGCC AATCTGATG
	CCGCAGCGCCGCCTGGCGAAAGTTAAAAAGACCGAGAAAC CTGATATATTGGCATTATAAAACCAATTAACCAATTCTGAT TAG	CCTTTAGAGTA AACCCGGCCAT C
40	GCCCCGGGCAGAAGCCAGAGGTAGTCGACTCATTGACTCA AGCGGAGAGGGGGTGGTGCGAGGATGACGACGATAAGTA GGG	AGGTGAGACCT ACTGTCCCTG
	AAACCCGTCAACTGCCAACTCGCACCACCCCCTCTCCGCTT GAGTCAATGAGTCGACTACAACCAATTAACCAATTCTGATT AG	GGTGATGTGAC GTGGGTTAGG
41	AGAATTCAAGGATCTCAAAAGGGCCTGCCAGATGGCCGGG TAGGTAGATAGGTTTACTCTAAAGGGGGGGACAGGATGAC GACGATAAGTAGGG	GATCGCGGACC TGCTTCAGATG
	AGAATACAAGATCCCCCGAAGTCCCCCCCTTTAGAGTAAA CCTATCTACCTACCCGGCCATCTGGCAGGCCCAACCAATTA ACCAATTCTGATTAG	TCTAAGTGGCC CATCACGGAC
42	AAATACTGTCTAGTTACACCACCCTTCGAGAATGTCCCTGT AGGTAGATAGGGAAAGGGCCCTGGCGAGACTAGGATGAC GACGATAAGTAGGG	CTTCGTCTTCCA GTGGATCGA
	TACTCATTGGCACTCCAGTCAGTCTCGCCAGGGCCCTTTCC CTATCTACCTACAGGGACATTCTCGAAGGGTAACCAATTAA CCAATTCTGATTAG	ATAAGAATACT TGCCTTGCAGG ATC
43	CACTACGCTCCTGACTTTGGCATCCGATGTCATGTTGAGGT AGGTAGATAGGATGAACCCGGGGCTGGGCTCAGGATGACG ACGATAAGTAGGG	ACTCGTATGTC CTCCAGTCG
	AAGGGTGCACTGATATGGACGAGCCCAGCCCCGGGTTCAT CCTATCTACCTACCTCAACATGACATCGGATGAACCAATTA ACCAATTCTGATTAG	CAACCTGTCAA TCTGTTCCACTA C
44	ATACTTGCCTTGCAGGATCTCAAAGAGGGAGATGGACAGC TAGGTAGATAGGTCGGAAGGGTGCACTGATATAGGATGAC GACGATAAGTAGGG	ACTCTGATCTA CTGACCCGTAC C
	ACCCGGGGCTGGGCTCGTCCATATCAGTGCACCCTTCCGAC CTATCTACCTAGCTGTCCATCTCCCTCTTTGAACCAATTAAC CAATTCTGATTAG	CCAACGACTAT TTGACTCGCCA C
45	ACACCTATAATGGTCTGTATTGACACCATTCTTTTATTTAG GCCTTGTACGGGGTTGACCAGGATGACGACGATAAGTAGG G	TGGAAGCATTC TCTCTTCATCGT G
	TGTAAATTTCCGCCCCTAGCGGTCAACCCCGTACAAGGCCT AAATAAAAGAATGGTGTCAAACCAATTAACCAATTCTGAT TAG	CGAAGTTTGAC GGCCTATACTG TA
46	GCTAGGGGCGGAAATTTACAAAGCACACGAGTTATTGCCT GTTGAACTTATTTTCCCTTTAGGATGACGACGATAAGTAGG G	CTGAGCAGCGA GAGCAGTTTC

	CGGAGAGCGCACGCAGGTCAAAAGGGAAAATAAGTTCAACAGGCAATAACTCGTGTGCTTAACCAATTAACCAATTCTGATTAG	CCTCATTAGTCGGGACTCGC
47	CCTAAAGACCGTCTGTTGCAACCATGCGTCCATGTTGAACGGGGCAAATCCGGGTTTCACAGGATGACGACGATAAGTAGGG	GCGAGTCCCGACTAATGAGG
	CCGAACCAGGCAACACAAGGGTGAAACCCGGATTTGCCCCGTTCAACATGGACGCATGGTAACCAATTAACCAATTCTGATTAG	GTCATTGCCACCCAGCTACT
48	GGAAGACGATGGGGGAAATGTGGCATTACCTGACACGGTTGTTCAGTCACATGTACGCTAAGGATGACGACGATAAGTAGGG	CAGTAGCTGGGTGGCAATGAC
	GGGGTTGGGTGGGGAGACCCTAGCGTACATGTGACTGAACAACCGTGTCAGGTAATGCCAAACCAATTAACCAATTCTGATTAG	GGTCACTGGGATCGTAGATTGTTTC
49	ACAAAAATGGCGCAAGATGACAAGGTAAAGATCGACCTTTTGTAAAAACTATGACACGCCAGGATGACGACGATAAGTAGGG	CAGTAGCTGGGTGGCAATGAC
	TCTTACCCTAAGGAGAGAGTGGCGTGTCATAGTTTTTACAAAAGGTCGATCTTTACCTTGAACCAATTAACCAATTCTGATTAG	GGTCACTGGGATCGTAGATTGTTTC
50	ATGTCATTGTAAAAACTATGACACGCCACTCTCTCCTTAGAGTGTTCGCAAGGGCGTCTGAGGATGACGACGATAAGTAGGG	CACGAATCTGGTTGATTGTGAC
	CTGGGAAGTTAACGCAGGCACAGACGCCCTTGCGAACACTCTAAGGAGAGAGTGGCGTGTAACCAATTAACCAATTCTGATTAG	CTGTTCCTTATGTGCCTCCA
K8	GTCGACTATAACCTGGCGTGTAAACGTGTAACCCTGCCAAACGGGAAACAGGTGTCTATCAGGATGACGACGATAAGTAGGG	GGGAGAACCATGCCAGACTTTG
	TTGAGTAACCAGCCGGCCAAGATAGACACCTGTTTCCCGTTTGGCAGGGTTACACGTTTAAACCAATTAACCAATTCTGATTAG	CATCGTGGAACGCACAGGTAA
K8.1	GGACCGAAGTTAATCCCTTAATCCTCTGGGATTAATAACCTGGTGCTAGTAACCGTGTGCAGGATGACGACGATAAGTAGGG	GCGTAAGAAACCCTACATAGTG
	TGTAGTGGTGGCAGAAAATGGCACACGGTTACTAGCACCAGGTTATTAATCCCAGAGGATAACCAATTAACCAATTCTGATTAG	GCATAGACTGGCATGTGATT
52	GTTTGGGGGTTGGGTTGTGGCGTGGTGGCTGGTCCGCGGTGTCAGGTACGCGTAGATGTAAGGATGACGACGATAAGTAGGG	GTAGATGTACGTGTTGGTGATGCTC
	TTGTGAGCATCACCAACACGTACATCTACGCGTACCTGACACCGCGGACCAGCCACCACGAACCAATTAACCAATTCTGATTAG	GTCTGGCTTCATTTGCTCTCGA
53	TAGCTTTCGTCAGCGCTTGTGCGAGTAATCACATGCCAGTTATGAACAACCGCCGAGGCTAGGATGACGACGATAAGTAGGG	TACTGGGACTAGAACGCTCTG

	ACGTTGGATAGACGGCTTGGAGCCTCGGCGGTTGTTCATAACTGGCATGTGATTACTCGCAACCAATTAACCAATTCTGATTAG	GATAGGTTCGACATAGGTTGGCT
54	GGCCACAAATAAAGCCAGGGCCACCGTGGACGCTGTCATTAGCCGCCGCCAAATGCGGCCAGGATGACGACGATAAGTAGGG	GCTGTCGCCACTCGTACAAA
	TCGAATCGCCCTAATAAACTGGCCGCATTTGGCGGCGGCTAATGACAGCGTCCACGGTGGAACCAATTAACCAATTCTGATTAG	GTGCCAAGGTTCGACTGGAC
55	GCCTCGCGGCGGTATGTCGTCTCCATGGTACACCTGGACGTAGGTAGATAGGTGTTGCGGTATAAACCTTTTAGGATGACGACGATAAGTAGGG	ACGTCACCCAGACACACTCC
	AAGCGTGGTTGCCGCGTCCAAAAAGGTTTATACCGCAACACCTATCTACCTACGTCCAGGTGTACCATGGAGAACCAATTAACCAATTCTGATTAG	GCTGTCGCCACTCGTACAAA
56	CACGTCCAGGTGTACCATGGAGACGACATACCGCCGCGAGTAGGTAGATAGGGCGCTGACAGTAAGGGTTATAGGATGACGACGATAAGTAGGG	ACGTCACCCAGACACACTCC
	TGTCGCCACTCGTACAAAAAATAACCCTTACTGTCAGCGCCCTATCTACCTACTCGCGGCGGTATGTCGTCTAACCAATTAACCAATTCTGATTAG	GCTGTCGCCACTCGTACAAA
57	AATATAAGAACCAAAGGACATGGTACAAGCAATGATAGACGGATTGCCAAACCCCATGGCAGGATGACGACGATAAGTAGGG	CACCTTAAACACAACACCAGACC
	TGGAATACGGGAGACACTCTGCCATGGGGTTTGGCAATCCGTCTATCATTGCTTGTACCAAACCAATTAACCAATTCTGATTAG	CCAGGCAATTCTGCGGCTAG
K9	CTCCCTCCCATAACAATACGGTGTAGGCATTTTGTATTATTGTCCCGCAACCAGACTAGCAGGATGACGACGATAAGTAGGG	TGAATGGTAACTGTCTGGACAC
	CACTGGACATTGCGGCGCGAGCTAGTCTGGTTGCGGGACAATAATACAAAATGCCTACACAACCAATTAACCAATTCTGATTAG	GAGAACAAAGCTACGAGGAGG
K10	ACTACAAGATTACATCCGGTTTTATAATTCACATATATGAACCTGAGGTAGATGCGCCCTAGGATGACGACGATAAGTAGGG	CTCTTGACCTGGTAACCCTGG
	CGTGTGGATACCAGTGAATGAGGGCGCATCTACCTCAGGTTCATATATGTGAATTATAAAAACCAATTAACCAATTCTGATTAG	CAGTTGATGATGCCAATGCCG
K10.5	CCACAGCCCGTCAAACCACAGGGACCCTGTTGGCTGACTACAATGCACATGCAGATTCTTAGGATGACGACGATAAGTAGGG	GTCGCCACGCCCACAACATC
	TGACCTCACACTGCTTGATAAAGAATCTGCATGTGCATTGTAGTCAGCCAACAGGGTCCCAACCAATTAACCAATTCTGATTAG	CCCGTTGGCAAACATAGATCCGTC
K11	GGTGGGGGCTCAGGGTTTTGTAGGGAGGGATATGCACAGTTAGGTAGATAGGTTGTTTTTTGAAGAGCCAGAAGGATGACGACGATAAGTAGGG	GCACTGTCCACCCTCTAATACAAG

	ATGACCCAAACCCCGACGGTTCTGGCTCTTCAAAAAACAA CCTATCTACCTAACTGTGCATATCCCTCCCTAAACCAATTA ACCAATTCTGATTAG	CTCACACCAGT TGGTCCCTTTG
58	TCATGGTCAACAAACCAAGAAAAACACATGTATTATTCAA GGTGTCAAATCAGGGGGTTAAGGATGACGACGATAAGTAG GG	GGTAAAGAGTG TGAACGAGTAC AGG
	AAGGTGCCCAAAACCACATTTAACCCCCTGATTTGACACCT TGAATAATACATGTGTTTTAACCAATTAACCAATTCTGATT AG	GTGTGACTGAC GATTTGTGAAG GT
59	GAGCGACAGAGCGCGCTCACTGTCCAGGCGGCACATGGTG GATTGCGGCCGTAGACGCACAGGATGACGACGATAAGTAG GG	GCCGTAGACGC ACAGAGAAATC
	AGCTTTCCTGTGATTTCTCTGTGCGTCTACGGCCGCAATCC ACCATGTGCCGCCTGGACAAACCAATTAACCAATTCTGATT AG	CTTCAGTGCCT GGCAGATCC
60	TTAGGGGAGGTGGAAGTGTGCGACATGGACAGGTTAACCT TGGCCTCACCCGGCTTGCAGAGGATGACGACGATAAGTAG GG	CGTGGGAAACA TCAAGGTGC
	GTCTGTCAGTAGGTAGGTCTCTGCAAGCCGGGTGAGGCCA AGGTTAACCTGTCCATGTCGAACCAATTAACCAATTCTGAT TAG	GCACAGTTCCC TTTGATTCTCAT C
61	AACTGAATCCATTGGCCTCACCCGGCTTGCAGAGACCTACG ACCTTACAGAAACACAGTCAGGATGACGACGATAAGTAGG G	GTCTATGAGAG ATTGGGCACAC
	GAGGCCGCGTGTGGCCCCTGGACTGTGTTTCTGTAAGGTCG TAGGTCTCTGCAAGCCGGGAACCAATTAACCAATTCTGATT AG	GCTCTGTTGTG CTGCTGTTTA
62	TCCCAAGTGAACCTGACAAAATGTCCGGACAGACATGACC ATCCACGCCGGCAATGGACGAGGATGACGACGATAAGTAG GG	GTGGACGCCGC ATATTTAGAGA G
	CTTTTCAAGAGCGTCTGTGCCGTCCATTGCCGGCGTGGATG GTCATGTCTGTCCGGACATAACCAATTAACCAATTCTGATT AG	GGTACATGACG CAGTTGCTGA
63	AGCCGCATTTTCAGCCTGCACCTTCATATCCACGCCGGCAA GGCCATGGCAGCCCAGCCTAGGATGACGACGATAAGTAGG G	GAAACGTACTC CCGGTCTGC
	GCCATTCCCTCCATGTACAGAGGCTGGGCTGCCATGGCCTT GCCGGCGTGGATATGAAGGAACCAATTAACCAATTCTGAT TAG	GTATAACCACC CTGTCCTCTGGT
64	CGCTGGCAGGCCTCCGGAAACTGTTTGTCGAATAGAGGCC CTCCACGGTTGTCCAATCGTAGGATGACGACGATAAGTAG GG	GGTCACCCATA GTACCCATCAG
	CTGGCAAAAAGAAATAGGCAACGATTGGACAACCGTGGAG GGCCTCTATTCGACAAACAGAACCAATTAACCAATTCTGAT TAG	CTGCGAGGCTG CCCTATTAA
65	AGAAGTGGTACTTGTGACTCCACGGTTGTCCAATCGTTGCC TTCCACACAGGCGGGCGAAAGGATGACGACGATAAGTAGG G	GTCACAGCGGT ATATTGGGC

	AGTGTTCCTCCTGAGGCTATTTCGCCCGCCTGTGTGGAAGG CAACGATTGGACAACCGTGAACCAATTAACCAATTCTGATT AG	AAAGCCACATA TTCCTCCACTG
66	TAGGCCGTGCGGTCGCGCTGGTGAGAAGGTCATGGCCCTG TAGGTAGATAGGGATCAGCGCTGGGATCGCTTAGGATGAC GACGATAAGTAGGG	GTTGGAGAGCA AGGTGGACACG
	AACCAAACCAAGACACAAGAAAGCGATCCCAGCGCTGATC CCTATCTACCTACAGGGCCATGACCTTCTCACAACCAATTA ACCAATTCTGATTAG	ACCGTGCTGCA TTCTAACCGTA C
67	GGGGCCTTGCCAGCCCCACCCCGCTGTCGCCATGAGTGTCT AGGTAGATAGGGTTGGTAAGCGTGTAGTGGAAGGATGACG ACGATAAGTAGGG	GAGAGTTGGAA GAGACGCGGG
	ATACCACCCGACACAGTTCGTCCACTACACGCTTACCAACC CTATCTACCTAGACACTCATGGCGACAGCGGAACCAATTA ACCAATTCTGATTAG	CCACCTTGCTCT CCAACACCAG
67.5	GTCTGACCAGCTTCTGCCTCGTGACATGCAAATTTTATTTT AGGTAGATAGGCCCACGATCTATTGTAGATTAGGATGACG ACGATAAGTAGGG	CCACCTTGCTCT CCAACACCAG
	GACAGTAGTTGATGGCGTTCAATCTACAATAGATCGTGGG CCTATCTACCTAAAATAAAATTTGCATGTCACAACCAATTA ACCAATTCTGATTAG	GAGAGTTGGAA GAGACGCGGG
68	TCTACAATAGATCGTGGGAAATAAAATTTGCATGTCACGAT AGGTAGATAGGGGCAGAAGCTGGTCAGACGCAGGATGAC GACGATAAGTAGGG	TTATTCGGGAG CTAACCGCAC
	TGGAACCCAACATGGAGTACGCGTCTGACCAGCTTCTGCCC CTATCTACCTATCGTGACATGCAAATTTTATAACCAATTAA CCAATTCTGATTAG	CACCTTTCATG GCAGTACATTG C
69	ACGCTTGAGCTGGTCCCGGGCCTTCGCACCCCATCCACCGC CTCACATGTAGCCTGTCACAGGATGACGACGATAAGTAGG G	TTATTCGGGAG CTAACCGCAC
	CAGTTGCAATAGGAGCTGGGGTGACAGGCTACATGTGAGG CGGTGGATGGGGTGCGAAGGAACCAATTAACCAATTCTGA TTAG	CACCTTTCATG GCAGTACATTG C
K12	ATTTTATTTTACTGACACTCTTTGGGAGGGCACGCTAGCTG CATTGGGATTGGAGTGAGGAGGATGACGACGATAAGTAGG G	TCGCCTTCAAA CAGAAGCACG
	AACCTGGTGCCCTCCTCCCTCCTCACTCCAATCCCAATGCA GCTAGCGTGCCCTCCCAAAAACCAATTAACCAATTCTGATT AG	GATGTTTCCGTT CTACAGGCGG
K13	CATACATTCTACGGACCAAAAATTAGCAACAGCTTGTTATG GTGCCGGCTTGTATATGTGAGGATGACGACGATAAGTAGG G	TGTCATCCGTG CCCAGTTTC
	TTTTTCCACATCGGTGCCTTCACATATACAAGCCGGCACCA TAACAAGCTGTTGCTAATTAACCAATTAACCAATTCTGATT AG	GTTCTCACGAC CCATCTACCTC
72	AAGGAAAATTTATTTTTCCGCCCTAAACAAAATCACAAGC ATAGAGTGGCGAGCGTATGTAGGATGACGACGATAAGTAG GG	ATGGGTCGTGA GAACACTGC

	CCAGGCTCTAGAGGTAGGCCACATACGCTCGCCACTCTATGCTTGTGATTTTGTTTAGGGAACCAATTAACCAATTCTGATTAG	CTGCGATCTCCATCCTGTGG
73	GGTGGCTTCTAGGGAGGAAAAAGGGGGAGAGGTGTGGCTTCCTCGGGAAATCTGGTCTGAAGGATGACGACGATAAGTAGGG	AAACTGAAGAAGGCGTGTCTGC
	CCATAATTTTACTTTGGTTGTCAGACCAGATTTCCCGAGGAAGCCACACCTCTCCCCCTTAACCAATTAACCAATTCTGATTAG	GAAGTGACTGCCAAACCACAC
K14	TGCTCCCCCGTGGACGACGCCGAGTGCCTCTCGGGGGTCCCTAGATGGACACCCCGTGAAAGGATGACGACGATAAGTAGGG	TGTGTTGAAGGACGGATCAGG
	GGGGTGGGTAAGCACGACGGTTCACGGGGTGTCCATCTAGGGACCCCCGAGAGGCACTCGAACCAATTAACCAATTCTGATTAG	CAAGAAGATCAACGACCACCACTA
74	CGTGGCTAAACAACACCTATACTACTTGTTATTGTAGGCCCCCGCGGATGTCTACGTGCCAGGATGACGACGATAAGTAGGG	TGTGTTGAAGGACGGATCAGG
	AGATTAAATTAAGGGGGAAGGGCACGTAGACATCCGCGGGGGCCTACAATAACAAGTAGTAACCAATTAACCAATTCTGATTAG	CAAGAAGATCAACGACCACCACTA
75	TTATGCGATTAAATGAGGGGTCTGATCCCAAAAGCAATGTGCCTAGAGGGTGCCCCGCCCAGGATGACGACGATAAGTAGGG	TCTAGCCTCCCGTTCCCATG
	ACTACAGAGGGTGTCCCCGGGGGCGGGGCACCCTCTAGGCACATTGCTTTTGGGATCAGAAACCAATTAACCAATTCTGATTAG	AAAGCCCTAACCCAAGTCTGACTAC
K15	ACAACAACTCTATTGTAAGCCCTGTGGATACCTAGTCAAACCCTCCACGACCACAGACTTAGGATGACGACGATAAGTAGGG	GAGCCTTGTGTCGGGAATACTTAG
	AAAAAGGTATCGATGTCAAAAAGTCTGTGGTCGTGGAGGGTTTGACTAGGTATCCACAGGAACCAATTAACCAATTCTGATTAG	TATTACGCAGGCACAGGTTGCTC

Table S1. Primers for KSHV mutagenesis and PCR.

For each ORF, forward primers are listed in the top row and reverse primers in the bottom row.

Table S2. Primers for the construction of rescued KSHV mutants.

	Revertant Primers		
ORF	**Step 1 (5'→3')**	**Step 2 (5'→3')**	**Step 3 (5'→3')**
r59	GAGTCCAAGCTTATGTCGCACACTTCCACC	GAGTCCACGCGTGAGCTATTCGGTGCGAATGTACTCGACGCTGGCATAGCCTTTTATCGAAAAGGATGACGACGATAAGTAGGG	TCGTCTCCAGAACACCCAG
	GAGTCCGAATTCAACGAGTACAGGGCCTTG	GAGTCCACGCGTAACCAATTAACCAATTCTGATTAG	CAGATAACTGAAGAGCGACAGAG
r62	GAGTCCGCATGCTTCCATCAACAGCTTTGTCTGG	GAGTCCCCATGGTCCAGCGCCGGGAACCGGCAGGCCTAAACGTTACTATTTATGCCTCGTTGAGGATGACGACGATAAGTAGGG	TTGTCTGGTGAAGGCTCC
	GAGTCCGAATTCTGAGAGATTGGGCACACATA	GAGTCCCCATGGAACCAATTAACCAATTCTGATTAG	GGGACAGCTCCCAAGTGAA

Table S2. Primers for the construction of rescued KSHV mutants.
The primers are listed according to the steps in construction of the universal transfer construct (UTC). Step 1 inserted the ORF into pUC19. Step 2 inserted the 50 bp sequence duplication and the kanamycin resistance cassette into the unique restriction enzyme site located inside the ORF. Step 3 was used to create the linear UTC for electroporation.

Table S3. KSHV ORFs homologous to HSV, VZV, EBV, HCMV, and MHV-68 ORFs categorized by growth properties of their respective inactivation mutants in cultured cells.

Gene #	KSHV	HSV[112]	VZV[51, 113]	HCMV[3,4,114]	EBV[50]	MHV-68[6,7,115]
1	K1					
2	ORF4					ORF4
3	ORF6	UL29	29	UL57	BALF2[116]	ORF6
4	ORF7	UL28	30	UL56	#BALF3[117]	ORF7
5	ORF8	UL27	31	UL55	BALF4[118]	ORF8
6	ORF9	UL30	28	UL54	BALF5[116]	ORF9
7	10.1					
8	ORF10			UL82 UL83 UL84		ORF10
9	11AA					
10	ORF11			UL82 UL83 UL84	Raji LF2	ORF11
11	K2					
12	ORF2					
13	K3					K3
14	ORF70					
15	K4					
16	K4.1					
17	K4.2					
18	K5					
19	K6					
20	K7					
21	ORF16				BHRF1[119]	
22	ORF17	UL26	33	UL80	#BVRF2[120,121]	ORF17
23	ORF17.5	UL26.5	33.5	UL80.5	BdRF1[121]	
24	ORF18			UL79		ORF18
25	ORF19	UL25	34	UL77	BVRF1	ORF19
26	ORF20	UL24	35	UL76	BXRF1	ORF20
27	ORF21	UL23			BXLF1	ORF21
28	ORF22	UL22	37	UL75	BXLF2[122]	ORF22
29	ORF23	UL21	38	UL88	BTRF1	ORF23
30	ORF24			UL87	‡BcRF1[123,124]	ORF24
31	ORF25	UL19	40	UL86	BcLF1[121]	ORF25*
32	ORF26	UL18	41	UL85	BDLF1[121]	ORF26
33	ORF27				BDLF2	ORF27
34	ORF28				BDLF3[125]	
35	ORF29B	UL15	42/45	UL89.2	BDRF1[126]	ORF29B
36	30.1					
37	ORF30			UL91	*BDLF3.5*	ORF30
38	ORF31			UL92	BDLF4[127]	ORF31

39	ORF32	UL17	43	UL93	BGLF1	ORF32
40	ORF33	UL16	44	UL94	BGLF2[128]	ORF33
41	ORF29A	UL15	42/45	UL89.1	BGRF1[126]	ORF29A
42	34.1					
42	ORF34	UL14	46	UL95	BGLF3	ORF34
43	ORF35				BGLF3.5[129]	ORF35
44	ORF36	UL13	47	UL97	BGLF4[129,130]	ORF36
45	ORF37	UL12	48	UL98	BGLF5[131]	ORF37*
46	ORF38	UL11	49	UL99	BBLF1	ORF38
47	ORF39	UL10	50	UL100	BBRF3	ORF39*
48	ORF40	UL9[132]	51	UL102	BBLF2[116]	ORF40
49	ORF41	UL8	52	UL102	BBLF3[116]	
50	ORF42	UL7	53	UL103	BBRF2[133]	ORF42
51	ORF43	UL6	54	UL104	BBRF1[134]	ORF43
52	ORF44	UL5	55	UL105	BBLF4[116]	ORF44
53	ORF45	UL3[135]			BKRF4[136]	ORF45
54	ORF46	UL2	59	UL114	‡BKRF3[137,138]	ORF46
55	ORF47	UL1	60	UL115	BRKF2	ORF47
56	ORF48				BRRF2[139]	ORF48
57	ORF49				BRRF1[140]	ORF49
58	ORF50				BRLF1[141]	ORF50
59	K8					
60	K8.1					
61	ORF52				BLRF2	ORF52
62	ORF53	UL49A	9A	UL73	BLRF1[142]	ORF53
63	ORF54	UL50	8	UL72	BLLF3	ORF54
64	ORF55	*UL51*	7	UL71	BSRF1[143]	ORF55
65	ORF56	UL52	6	UL70	BSLF1[116]	ORF56*
66	ORF57	UL54	4	UL69	BSLF2/BMLF1[144]	ORF57
67	K9					
68	K10					
69	K10.5					
70	K11					
71	ORF58	*UL43*			BMRF2	ORF58
72	ORF59	UL42	16	UL44	BMRF1[116]	ORF59
73	ORF60	UL40	18		BaRF1[145]	ORF60
74	ORF61	UL39	19	UL45	BORF2[146]	ORF61*
75	ORF62	UL38	20	UL46	BORF1[121]	ORF62
76	ORF63	UL37	21	UL47	BOLF1[147]	ORF63
77	ORF64	UL36	22	UL48	BPLF1[148]	ORF64
78	ORF65	UL35	23	UL48A	BFRF3[121]	*M9/ORF65**
79	ORF66		24	UL49	BFRF2[149]	ORF66*
80	ORF67	UL34	25	UL50	BFRF1[150]	ORF67
81	ORF67.5	UL33	25	UL51	†BFRF1A[126]	

82	ORF68	UL32	26	UL52	†BFLF1[126]	ORF68
83	ORF69	UL31	27	UL53	BFLF2[151]	ORF69
84	K12					
85	K13/ORF71					
86	ORF72					ORF72
87	ORF73					ORF73
88	K14					
89	ORF74					ORF74
90	ORF75				BNRF1	ORF75A ORF75B ORF75C
91	K15				LMP2A	

Table S3. KSHV ORFs homologous to HSV, VZV, EBV, HCMV, and MHV-68 ORFs categorized by growth properties of their respective inactivation mutants in cultured cells.

ORFs in which gene-inactivation mutants failed to grow are marked in red and ORFs in which gene-inactivation mutants were attenuated in growth compared to parental viruses are marked in orange. * Marks the ORFs where the classification assignment between two independent studies disagreed, and the asterisk color indicates the alternative classification[3,4,6,7,51,115]. Italics indicate ORFs that are positional homologs to KSHV ORF's. † Indicates that the ORF's essentiality was assessed as a double mutant. # Indicates essentiality was inferred from knockdown studies. ‡ Indicates two or more studies disagree on essentiality.

Table S4. KSHV lytic antigen expression in BAC16-infected iSLK cells

	Gene expression		
Conditions	**ORF45**	**K8**	**K8.1**
Pre-induced Reactivation	1.24%	0.61%	0.33%
Induced Reactivation	34.03%	26.68%	5.44%
Spontaneous Reactivation	0.31%	0.25%	0.09%

Table S4. KSHV lytic antigen expression in BAC16-infected iSLK cells.
Human iSLK cells were infected with BAC16 (MOI=1). For "Pre-induced reactivation" sample, cells were incubated in normal/uninduced conditions in the absence of doxycycline and sodium butyrate and harvested at 2 dpi. For "Induced reactivation" samples, cells were incubated in normal/uninduced conditions for 2 days, then induced in the presence of doxycycline and sodium butyrate at 2 dpi, and harvested at 5 dpi. For "Spontaneous reactivation" samples, cells were incubated in normal/uninduced conditions and harvested at 6 dpi. The harvested cells were fixed, stained for lytic antigens, and analyzed by flow cytometry. The values are the average from three independent experiments. Each experiment was performed in triplicate. Experimental details are described in Methods.

SUPPORTING FIGURES:

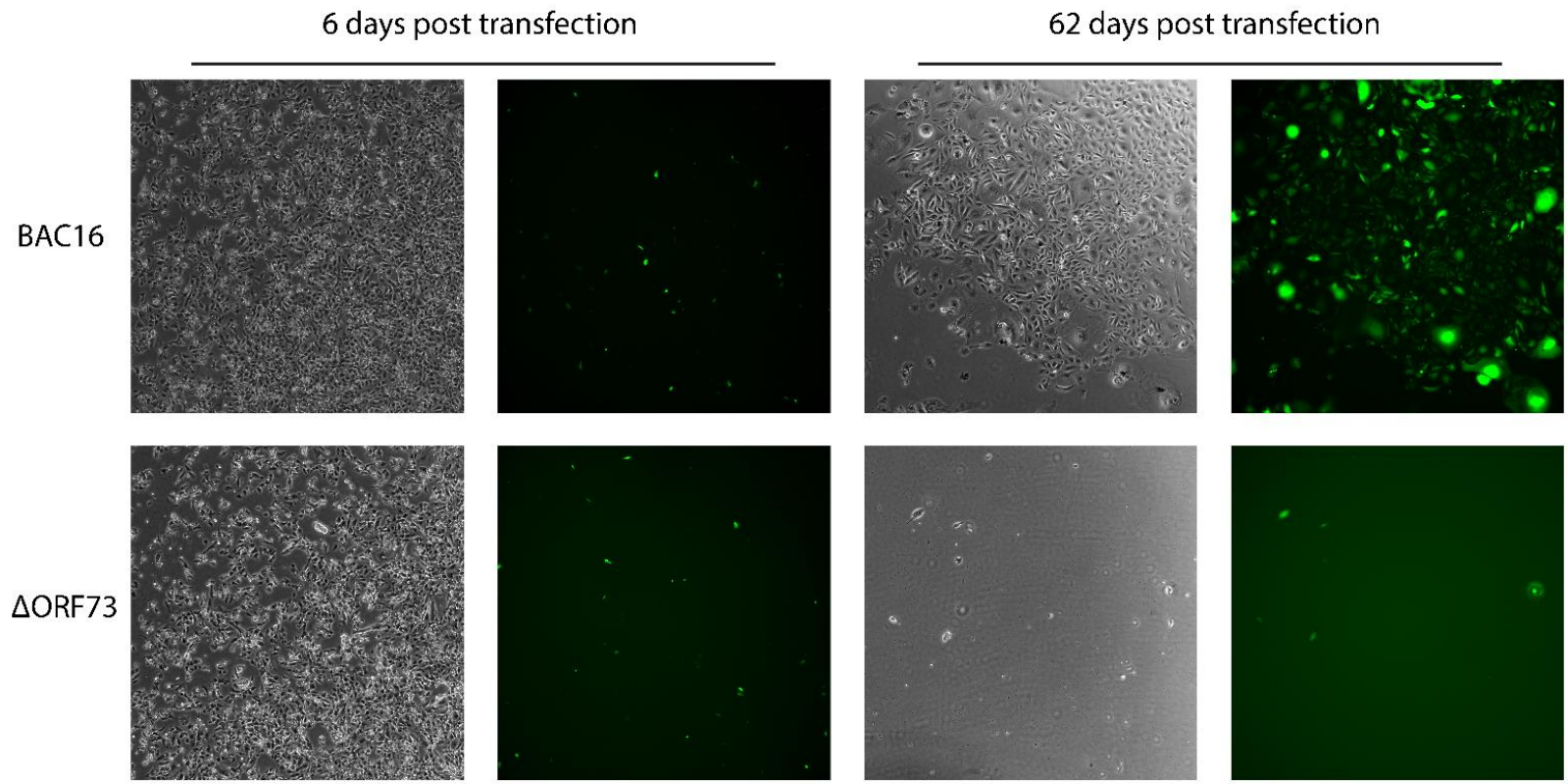

Figure S1. Transfection and selection of BAC16 and ΔORF73 DNAs in iSLK cells.
Cells were imaged using phase contract and fluorescence microscopy to visualize GFP after incubation with hygromycin B (1.2 mg/ml) for 6- and 62-days post transfection.

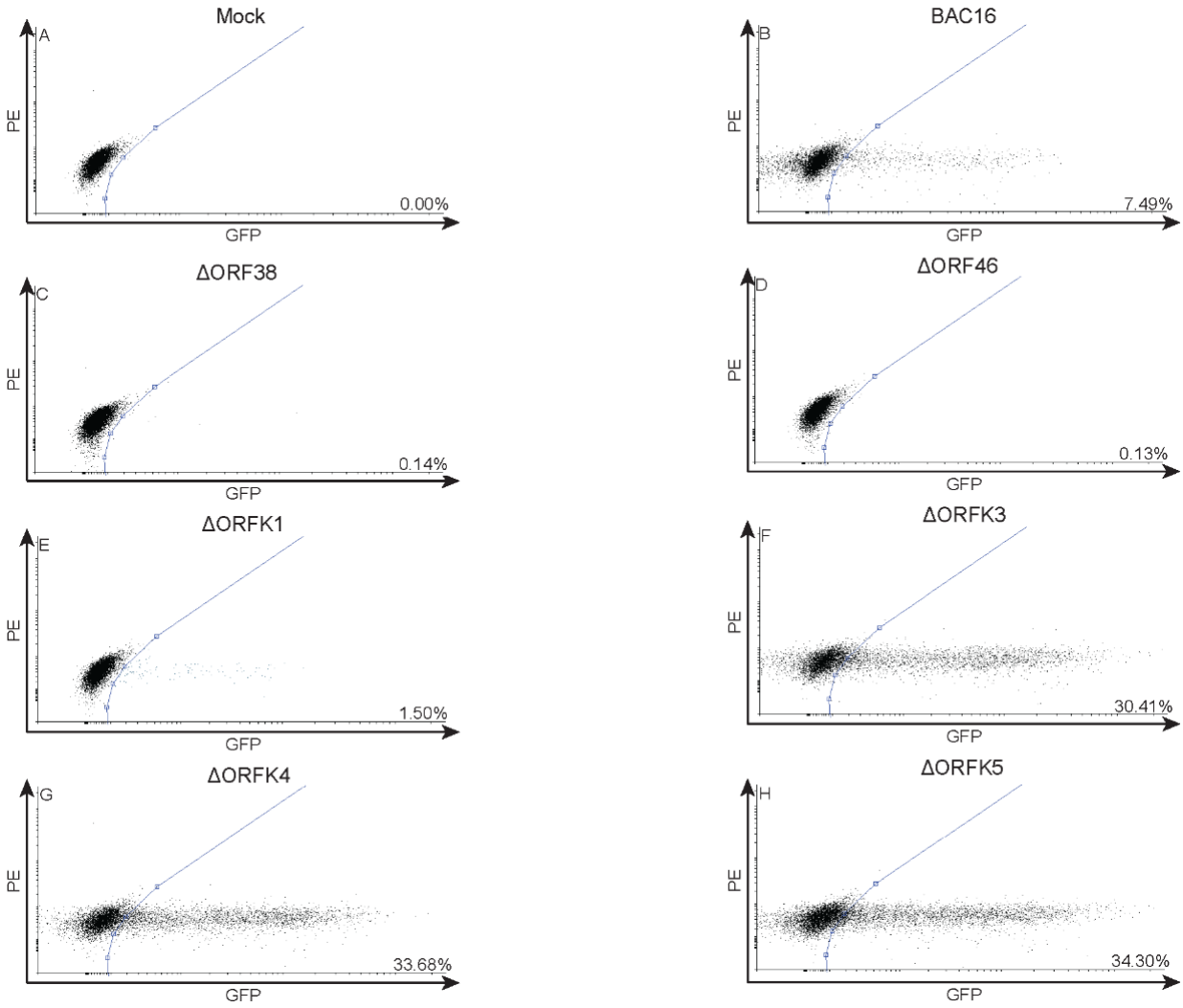

Figure S2. KSHV growth in induced reactivation conditions.

iSLK cells were either mock-infected (Mock) or infected with mutants (ΔORF38, ΔORF46, ΔORFK1, ΔORFK3, ΔORFK4, ΔORFK5) or parental BAC16 (BAC16) (MOI=1), and induced at 2 dpi. At 5 dpi the supernatants were harvested and used to infected 293T cells. Infected cells were fixed and analyzed by flow cytometry for GFP expression. PE (y-axis) was included as an autofluorescence control. The percentage of positive events is listed for each graph. The average of percentages in three independent experiments was used in the ratio calculations for the growth analysis in figure 3B.

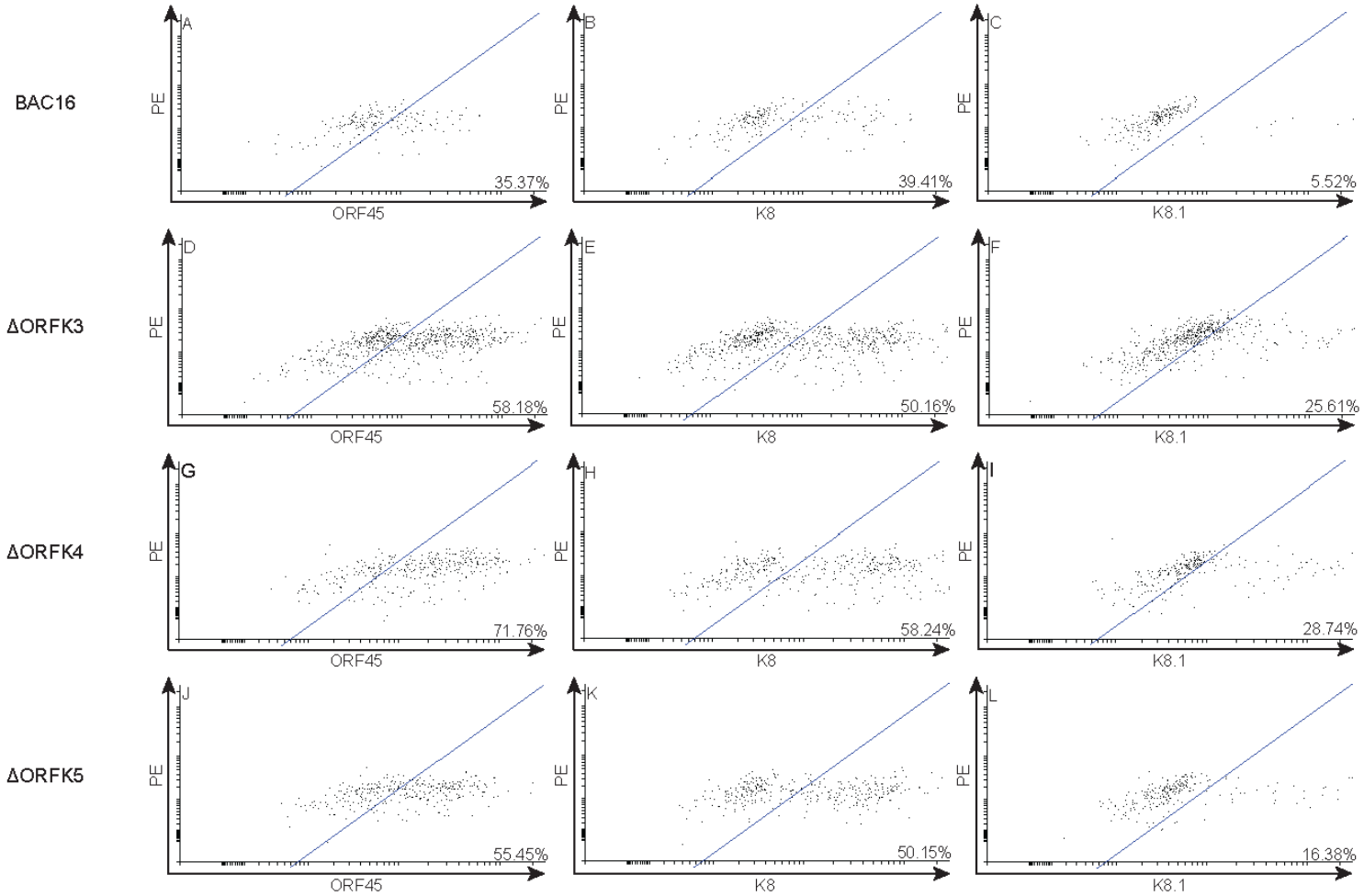

Figure S3. KSHV lytic antigen expression in induced reactivation conditions.

iSLK cells were infected with mutants (ΔORFK3, ΔORFK4, and ΔORFK5) or parental BAC16 (BAC16) (MOI=1), induced in the presence of doxycycline and sodium butyrate at 2 dpi, harvested and stained at 4 dpi, and analyzed by flow cytometry for the expression of viral protein ORF45 (A, D, G, J), K8 (B, E, H, K), and K8.1 (C, F, I, L). PE (y-axis) was included as an autofluorescence control. The percentage of positive events is listed for each graph. The average of percentages in three independent experiments was used in the ratio calculations for the antigen expression ratios in figure 3D.

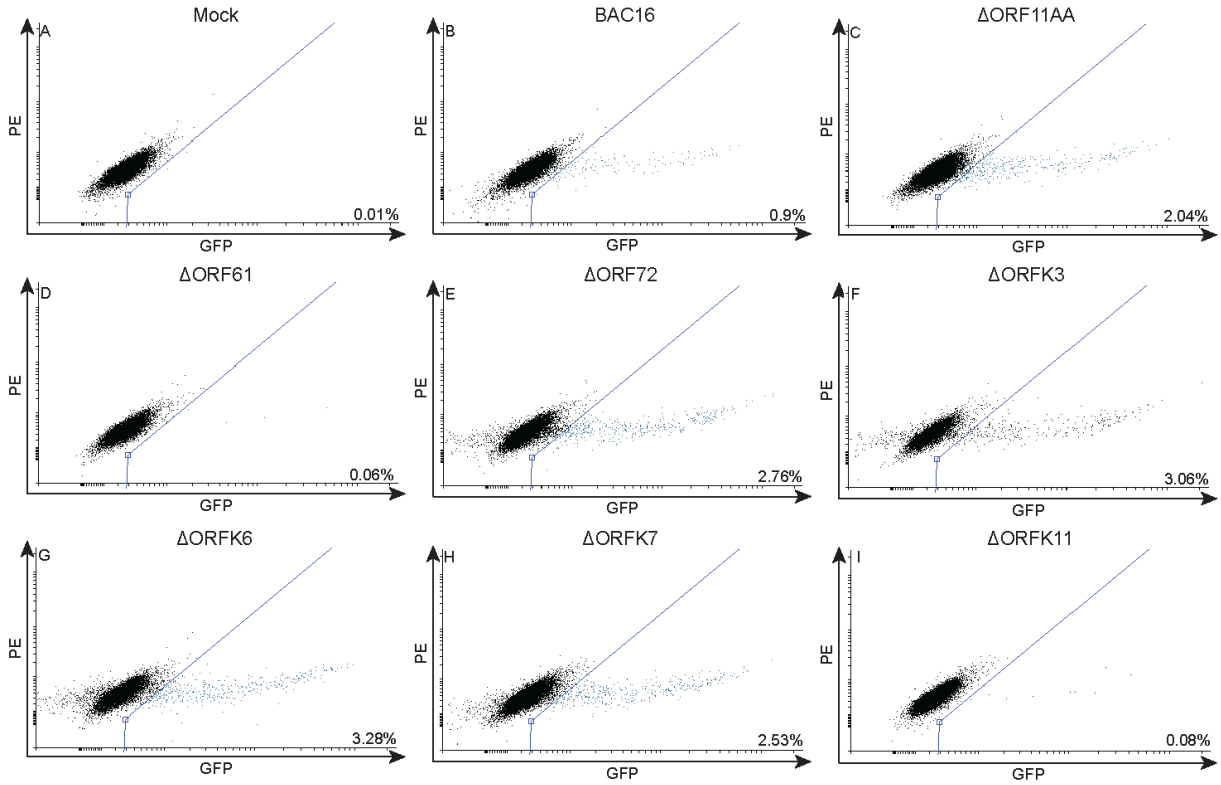

Figure S4. KSHV growth in spontaneous reactivation conditions.

iSLK cells were mock-infected or infected with mutants (ΔORF11AA, ΔORF61, ΔORF72, ΔORFK3, ΔORFK6, ΔORFK7, ΔORFK11) and parental BAC16 (BAC16) (MOI=1) and maintained in normal/uninduced conditions in the absence of doxycycline and sodium butyrate. Supernatants were harvested at 6 dpi and used to infected 293T cells. Infected cells were fixed and analyzed by flow cytometry for GFP expression. PE (y-axis) was included as an autofluorescence control. The percentage of positive events is listed for each graph. The average of percentages in three independent experiments was used in the ratio calculations for the growth analysis in figure 3C.

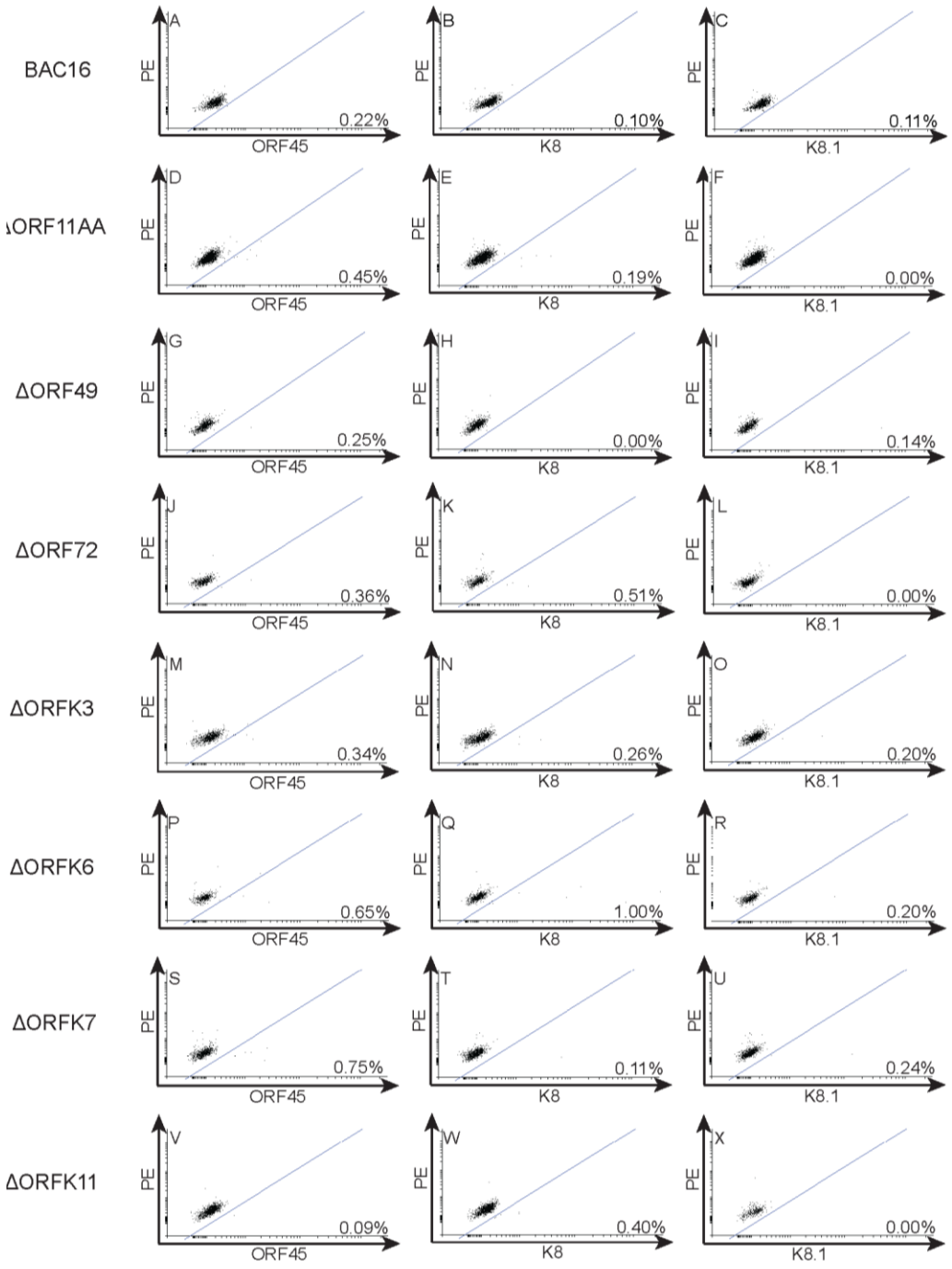

Figure S5. KSHV lytic antigen expression in spontaneous reactivation conditions. iSLK cells were infected with mutants (ΔORF11AA, ΔORF49, ΔORF72, ΔORFK3, ΔORFK6, ΔORFK7, ΔORFK11) and parental BAC16 (BAC16)(MOI=1) in uninduced conditions, and harvested and stained at 6 dpi, and analyzed by flow cytometry for the expression of viral protein ORF45 (A, D, G, J, M, P, S, V), K8 (B, E, H, K, N, Q, T, W), and K8.1 (C, F, I, L, O, R, U, X). PE (y-axis) was included as an autofluorescence control. The percentage of positive events is listed for each graph. The average of percentages in three independent experiments was used in the ratio calculations for the antigen expression ratios in figure 3E.

Reference Part I.

1 Blossom A. Damania, E. C. *Fields Virology* 6th edn, Vol. 2 Chapter 65 (Lippincott and Williams, 2013).

2 Philip E. Pellett, B. R. *Feilds Virology* 6th edn, Vol. 2 Chapter 59 (Lippincott Wilkins 2013).

3 Dunn, W. *et al.* Functional profiling of a human cytomegalovirus genome. *Proc Natl Acad Sci U S A* **100**, 14223-14228, doi:10.1073/pnas.2334032100 (2003).

4 Yu, D., Silva, M. C. & Shenk, T. Functional map of human cytomegalovirus AD169 defined by global mutational analysis. *Proc Natl Acad Sci U S A* **100**, 12396-12401, doi:10.1073/pnas.1635160100 (2003).

5 Zhang, Z. *et al.* Genome-wide mutagenesis reveals that ORF7 is a novel VZV skin-tropic factor. *PLoS Pathog* **6**, e1000971, doi:10.1371/journal.ppat.1000971 (2010).

6 Song, M. J. *et al.* Identification of viral genes essential for replication of murine gamma-herpesvirus 68 using signature-tagged mutagenesis. *Proc Natl Acad Sci U S A* **102**, 3805-3810, doi:10.1073/pnas.0404521102 (2005).

7 Moorman, N. J., Lin, C. Y. & Speck, S. H. Identification of candidate gammaherpesvirus 68 genes required for virus replication by signature-tagged transposon mutagenesis. *J Virol* **78**, 10282-10290, doi:10.1128/JVI.78.19.10282-10290.2004 (2004).

8 Russo, J. J. *et al.* Nucleotide sequence of the Kaposi sarcoma-associated herpesvirus (HHV8). *Proc Natl Acad Sci U S A* **93**, 14862-14867, doi:10.1073/pnas.93.25.14862 (1996).

9 Arias, C. *et al.* KSHV 2.0: a comprehensive annotation of the Kaposi's sarcoma-associated herpesvirus genome using next-generation sequencing reveals novel genomic and functional features. *PLoS Pathog* **10**, e1003847, doi:10.1371/journal.ppat.1003847 (2014).

10 Cai, X. *et al.* Kaposi's sarcoma-associated herpesvirus expresses an array of viral microRNAs in latently infected cells. *Proc Natl Acad Sci U S A* **102**, 5570-5575, doi:10.1073/pnas.0408192102 (2005).

11 Pfeffer, S. *et al.* Identification of microRNAs of the herpesvirus family. *Nat Methods* **2**, 269-276, doi:10.1038/nmeth746 (2005).

12 Tagawa, T. *et al.* Discovery of Kaposi's sarcoma herpesvirus-encoded circular RNAs and a human antiviral circular RNA. *Proc Natl Acad Sci U S A* **115**, 12805-12810, doi:10.1073/pnas.1816183115 (2018).

13 Abere, B. *et al.* Kaposi's Sarcoma-Associated Herpesvirus-Encoded circRNAs Are Expressed in Infected Tumor Tissues and Are Incorporated into Virions. *mBio* **11**, doi:10.1128/mBio.03027-19 (2020).

14 Schifano, J. M., Corcoran, K., Kelkar, H. & Dittmer, D. P. Expression of the Antisense-to-Latency Transcript Long Noncoding RNA in Kaposi's Sarcoma-Associated Herpesvirus. *J Virol* **91**, doi:10.1128/JVI.01698-16 (2017).

15 Walker, L. R., Hussein, H. A. M. & Akula, S. M. Disintegrin-like domain of glycoprotein B regulates Kaposi's sarcoma-associated herpesvirus infection of cells. *J Gen Virol* **95**, 1770-1782, doi:10.1099/vir.0.066829-0 (2014).

16 Luna, R. E. *et al.* Kaposi's sarcoma-associated herpesvirus glycoprotein K8.1 is dispensable for virus entry. *J Virol* **78**, 6389-6398, doi:10.1128/jvi.78.12.6389-6398.2004 (2004).

17 Ye, F. C. *et al.* Disruption of Kaposi's sarcoma-associated herpesvirus latent nuclear antigen leads to abortive episome persistence. *J Virol* **78**, 11121-11129, doi:10.1128/jvi.78.20.11121-11129.2004 (2004).
18 Nishimura, M., Watanabe, T., Yagi, S., Yamanaka, T. & Fujimuro, M. Kaposi's sarcoma-associated herpesvirus ORF34 is essential for late gene expression and virus production. *Sci Rep* **7**, 329, doi:10.1038/s41598-017-00401-7 (2017).
19 Xu, Y. *et al.* A Kaposi's sarcoma-associated herpesvirus/human herpesvirus 8 ORF50 deletion mutant is defective for reactivation of latent virus and DNA replication. *J Virol* **79**, 3479-3487, doi:10.1128/jvi.79.6.3479-3487.2005 (2005).
20 Zhu, F. X., Li, X., Zhou, F., Gao, S. J. & Yuan, Y. Functional characterization of Kaposi's sarcoma-associated herpesvirus ORF45 by bacterial artificial chromosome-based mutagenesis. *J Virol* **80**, 12187-12196, doi:10.1128/JVI.01275-06 (2006).
21 Majerciak, V., Pripuzova, N., McCoy, J. P., Gao, S. J. & Zheng, Z. M. Targeted disruption of Kaposi's sarcoma-associated herpesvirus ORF57 in the viral genome is detrimental for the expression of ORF59, K8alpha, and K8.1 and the production of infectious virus. *J Virol* **81**, 1062-1071, doi:10.1128/JVI.01558-06 (2007).
22 Han, Z. & Swaminathan, S. Kaposi's sarcoma-associated herpesvirus lytic gene ORF57 is essential for infectious virion production. *J Virol* **80**, 5251-5260, doi:10.1128/jvi.02570-05 (2006).
23 Bergson, S. *et al.* The Kaposi's-sarcoma-associated herpesvirus orf35 gene product is required for efficient lytic virus reactivation. *Virology* **499**, 91-98, doi:10.1016/j.virol.2016.09.008 (2016).
24 Peng, C., Chen, J., Tang, W., Liu, C. & Chen, X. Kaposi's sarcoma-associated herpesvirus ORF6 gene is essential in viral lytic replication. *PLoS One* **9**, e99542, doi:10.1371/journal.pone.0099542 (2014).
25 Bala, K. *et al.* Kaposi's sarcoma herpesvirus K15 protein contributes to virus-induced angiogenesis by recruiting PLCγ1 and activating NFAT1-dependent RCAN1 expression. *PLoS Pathog* **8**, e1002927, doi:10.1371/journal.ppat.1002927 (2012).
26 Full, F. *et al.* Kaposi's sarcoma associated herpesvirus tegument protein ORF75 is essential for viral lytic replication and plays a critical role in the antagonization of ND10-instituted intrinsic immunity. *PLoS Pathog* **10**, e1003863, doi:10.1371/journal.ppat.1003863 (2014).
27 Zhang, Z. *et al.* The K1 Protein of Kaposi's Sarcoma-Associated Herpesvirus Augments Viral Lytic Replication. *J Virol* **90**, 7657-7666, doi:10.1128/JVI.03102-15 (2016).
28 Wang, Y., Sathish, N., Hollow, C. & Yuan, Y. Functional characterization of Kaposi's sarcoma-associated herpesvirus open reading frame K8 by bacterial artificial chromosome-based mutagenesis. *J Virol* **85**, 1943-1957, doi:10.1128/JVI.02060-10 (2011).
29 McDowell, M. E., Purushothaman, P., Rossetto, C. C., Pari, G. S. & Verma, S. C. Phosphorylation of Kaposi's sarcoma-associated herpesvirus processivity factor ORF59 by a viral kinase modulates its ability to associate with RTA and oriLyt. *J Virol* **87**, 8038-8052, doi:10.1128/JVI.03460-12 (2013).
30 Brulois, K. *et al.* Association of Kaposi's Sarcoma-Associated Herpesvirus ORF31 with ORF34 and ORF24 Is Critical for Late Gene Expression. *J Virol* **89**, 6148-6154, doi:10.1128/JVI.00272-15 (2015).

31 Davis, Z. H., Hesser, C. R., Park, J. & Glaunsinger, B. A. Interaction between ORF24 and ORF34 in the Kaposi's Sarcoma-Associated Herpesvirus Late Gene Transcription Factor Complex Is Essential for Viral Late Gene Expression. *J Virol* **90**, 599-604, doi:10.1128/jvi.02157-15 (2016).
32 Gong, D. *et al.* Kaposi's sarcoma-associated herpesvirus ORF18 and ORF30 are essential for late gene expression during lytic replication. *J Virol* **88**, 11369-11382, doi:10.1128/JVI.00793-14 (2014).
33 Gelgor, A. *et al.* Viral Bcl-2 Encoded by the Kaposi's Sarcoma-Associated Herpesvirus Is Vital for Virus Reactivation. *J Virol* **89**, 5298-5307, doi:10.1128/jvi.00098-15 (2015).
34 Liang, Q. *et al.* Identification of the Essential Role of Viral Bcl-2 for Kaposi's Sarcoma-Associated Herpesvirus Lytic Replication. *J Virol* **89**, 5308-5317, doi:10.1128/jvi.00102-15 (2015).
35 Kreitler, D. *et al.* The assembly domain of the small capsid protein of Kaposi's sarcoma-associated herpesvirus. *J Virol* **86**, 11926-11930, doi:10.1128/JVI.01430-12 (2012).
36 Sathish, N. & Yuan, Y. Functional characterization of Kaposi's sarcoma-associated herpesvirus small capsid protein by bacterial artificial chromosome-based mutagenesis. *Virology* **407**, 306-318, doi:10.1016/j.virol.2010.08.017 (2010).
37 Wu, J. J. *et al.* ORF33 and ORF38 of Kaposi's Sarcoma-Associated Herpesvirus Interact and Are Required for Optimal Production of Infectious Progeny Viruses. *J Virol* **90**, 1741-1756, doi:10.1128/JVI.02738-15 (2016).
38 Brulois, K. F. *et al.* Construction and manipulation of a new Kaposi's sarcoma-associated herpesvirus bacterial artificial chromosome clone. *J Virol* **86**, 9708-9720, doi:10.1128/JVI.01019-12 (2012).
39 Dunn-Kittenplon, D. D., Kalt, I., Lellouche, J. M. & Sarid, R. The KSHV portal protein ORF43 is essential for the production of infectious viral particles. *Virology* **529**, 205-215, doi:10.1016/j.virol.2019.01.028 (2019).
40 Gong, D. *et al.* A Herpesvirus Protein Selectively Inhibits Cellular mRNA Nuclear Export. *Cell Host Microbe* **20**, 642-653, doi:10.1016/j.chom.2016.10.004 (2016).
41 Myoung, J. & Ganem, D. Generation of a doxycycline-inducible KSHV producer cell line of endothelial origin: maintenance of tight latency with efficient reactivation upon induction. *J Virol Methods* **174**, 12-21, doi:10.1016/j.jviromet.2011.03.012 (2011).
42 Ballestas, M. E., Chatis, P. A. & Kaye, K. M. Efficient persistence of extrachromosomal KSHV DNA mediated by latency-associated nuclear antigen. *Science* **284**, 641-644, doi:10.1126/science.284.5414.641 (1999).
43 Coscoy, L. & Ganem, D. A viral protein that selectively downregulates ICAM-1 and B7-2 and modulates T cell costimulation. *J Clin Invest* **107**, 1599-1606, doi:10.1172/JCI12432 (2001).
44 Ishido, S., Wang, C., Lee, B. S., Cohen, G. B. & Jung, J. U. Downregulation of major histocompatibility complex class I molecules by Kaposi's sarcoma-associated herpesvirus K3 and K5 proteins. *J Virol* **74**, 5300-5309, doi:10.1128/jvi.74.11.5300-5309.2000 (2000).
45 Lukac, D. M., Kirshner, J. R. & Ganem, D. Transcriptional activation by the product of open reading frame 50 of Kaposi's sarcoma-associated herpesvirus is required for lytic viral reactivation in B cells. *J Virol* **73**, 9348-9361, doi:10.1128/jvi.73.11.9348-9361.1999 (1999).

46 Sun, R. *et al.* A viral gene that activates lytic cycle expression of Kaposi's sarcoma-associated herpesvirus. *Proc Natl Acad Sci U S A* **95**, 10866-10871, doi:10.1073/pnas.95.18.10866 (1998).
47 Endres, M. J., Garlisi, C. G., Xiao, H., Shan, L. & Hedrick, J. A. The Kaposi's sarcoma-related herpesvirus (KSHV)-encoded chemokine vMIP-I is a specific agonist for the CC chemokine receptor (CCR)8. *J Exp Med* **189**, 1993-1998, doi:10.1084/jem.189.12.1993 (1999).
48 Nicholas, J. *et al.* Kaposi's sarcoma-associated human herpesvirus-8 encodes homologues of macrophage inflammatory protein-1 and interleukin-6. *Nat Med* **3**, 287-292, doi:10.1038/nm0397-287 (1997).
49 Fuld, S., Cunningham, C., Klucher, K., Davison, A. J. & Blackbourn, D. J. Inhibition of interferon signaling by the Kaposi's sarcoma-associated herpesvirus full-length viral interferon regulatory factor 2 protein. *J Virol* **80**, 3092-3097, doi:10.1128/JVI.80.6.3092-3097.2006 (2006).
50 Richard M. Longnecker, E. K., Jeffrey I. Cohen. *Fields Virology* 6th edn, Vol. 2 Chapter 61 (Lippincott and Williams, 2013).
51 Zhang, Z. *et al.* Genome-wide mutagenesis reveals that ORF7 is a novel VZV skin-tropic factor. *PLoS Pathog* **6**, e1000971, doi:10.1371/journal.ppat.1000971 (2010).
52 Campbell, T. B. *et al.* Relationship of human herpesvirus 8 peripheral blood virus load and Kaposi's sarcoma clinical stage. *AIDS* **14**, 2109-2116, doi:10.1097/00002030-200009290-00006 (2000).
53 Oksenhendler, E. *et al.* High levels of human herpesvirus 8 viral load, human interleukin-6, interleukin-10, and C reactive protein correlate with exacerbation of multicentric castleman disease in HIV-infected patients. *Blood* **96**, 2069-2073 (2000).
54 Fardet, L. *et al.* Human herpesvirus 8-associated hemophagocytic lymphohistiocytosis in human immunodeficiency virus-infected patients. *Clin Infect Dis* **37**, 285-291, doi:10.1086/375224 (2003).
55 Chen, J. *et al.* Activation of latent Kaposi's sarcoma-associated herpesvirus by demethylation of the promoter of the lytic transactivator. *Proc Natl Acad Sci U S A* **98**, 4119-4124, doi:10.1073/pnas.051004198 (2001).
56 Sozzani, S. *et al.* The viral chemokine macrophage inflammatory protein-II is a selective Th2 chemoattractant. *Blood* **92**, 4036-4039 (1998).
57 Li, Q., Means, R., Lang, S. & Jung, J. U. Downregulation of gamma interferon receptor 1 by Kaposi's sarcoma-associated herpesvirus K3 and K5. *J Virol* **81**, 2117-2127, doi:10.1128/JVI.01961-06 (2007).
58 Wang, H. W., Sharp, T. V., Koumi, A., Koentges, G. & Boshoff, C. Characterization of an anti-apoptotic glycoprotein encoded by Kaposi's sarcoma-associated herpesvirus which resembles a spliced variant of human survivin. *EMBO J* **21**, 2602-2615, doi:10.1093/emboj/21.11.2602 (2002).
59 Liang, Q. *et al.* Kaposi's sarcoma-associated herpesvirus K7 modulates Rubicon-mediated inhibition of autophagosome maturation. *J Virol* **87**, 12499-12503, doi:10.1128/JVI.01898-13 (2013).
60 AuCoin, D. P. *et al.* Amplification of the Kaposi's sarcoma-associated herpesvirus/human herpesvirus 8 lytic origin of DNA replication is dependent upon a cis-acting AT-rich region and an ORF50 response element and the trans-acting factors ORF50 (K-Rta) and K8 (K-bZIP). *Virology* **318**, 542-555, doi:10.1016/j.virol.2003.10.016 (2004).

61 Davison, A. J. & Stow, N. D. New genes from old: redeployment of dUTPase by herpesviruses. *J Virol* **79**, 12880-12892, doi:10.1128/JVI.79.20.12880-12892.2005 (2005).
62 Castaneda, A. F. & Glaunsinger, B. A. The Interaction between ORF18 and ORF30 Is Required for Late Gene Expression in Kaposi's Sarcoma-Associated Herpesvirus. *J Virol* **93**, doi:10.1128/JVI.01488-18 (2019).
63 Gong, D. *et al.* DNA-Packing Portal and Capsid-Associated Tegument Complexes in the Tumor Herpesvirus KSHV. *Cell* **178**, 1329-1343 e1312, doi:10.1016/j.cell.2019.07.035 (2019).
64 Dai, X., Gong, D., Wu, T. T., Sun, R. & Zhou, Z. H. Organization of capsid-associated tegument components in Kaposi's sarcoma-associated herpesvirus. *J Virol* **88**, 12694-12702, doi:10.1128/JVI.01509-14 (2014).
65 Castaneda, A. F. *et al.* The gammaherpesviral TATA-box-binding protein directly interacts with the CTD of host RNA Pol II to direct late gene transcription. *PLoS Pathog* **16**, e1008843, doi:10.1371/journal.ppat.1008843 (2020).
66 Dai, X. *et al.* Structure and mutagenesis reveal essential capsid protein interactions for KSHV replication. *Nature* **553**, 521-525, doi:10.1038/nature25438 (2018).
67 Zhu, F. X., Chong, J. M., Wu, L. & Yuan, Y. Virion proteins of Kaposi's sarcoma-associated herpesvirus. *J Virol* **79**, 800-811, doi:10.1128/JVI.79.2.800-811.2005 (2005).
68 Zhu, F. X. & Yuan, Y. The ORF45 protein of Kaposi's sarcoma-associated herpesvirus is associated with purified virions. *J Virol* **77**, 4221-4230, doi:10.1128/jvi.77.7.4221-4230.2003 (2003).
69 Sathish, N., Zhu, F. X. & Yuan, Y. Kaposi's sarcoma-associated herpesvirus ORF45 interacts with kinesin-2 transporting viral capsid-tegument complexes along microtubules. *PLoS Pathog* **5**, e1000332, doi:10.1371/journal.ppat.1000332 (2009).
70 Li, X. *et al.* ORF45-Mediated Prolonged c-Fos Accumulation Accelerates Viral Transcription during the Late Stage of Lytic Replication of Kaposi's Sarcoma-Associated Herpesvirus. *J Virol* **89**, 6895-6906, doi:10.1128/JVI.00274-15 (2015).
71 Li, W. *et al.* Kaposi's Sarcoma-Associated Herpesvirus Inhibitor of cGAS (KicGAS), Encoded by ORF52, Is an Abundant Tegument Protein and Is Required for Production of Infectious Progeny Viruses. *J Virol* **90**, 5329-5342, doi:10.1128/JVI.02675-15 (2016).
72 Gregory, S. M. *et al.* Discovery of a viral NLR homolog that inhibits the inflammasome. *Science* **331**, 330-334, doi:10.1126/science.1199478 (2011).
73 Watanabe, T. *et al.* Kaposi's Sarcoma-Associated Herpesvirus ORF66 Is Essential for Late Gene Expression and Virus Production via Interaction with ORF34. *J Virol* **94**, doi:10.1128/JVI.01300-19 (2020).
74 Luitweiler, E. M. *et al.* Interactions of the Kaposi's Sarcoma-associated herpesvirus nuclear egress complex: ORF69 is a potent factor for remodeling cellular membranes. *J Virol* **87**, 3915-3929, doi:10.1128/JVI.03418-12 (2013).
75 Didychuk, A. L. *et al.* A pentameric protein ring with novel architecture is required for herpesviral packaging. *Elife* **10**, doi:10.7554/eLife.62261 (2021).
76 Cheng, E. H. *et al.* A Bcl-2 homolog encoded by Kaposi sarcoma-associated virus, human herpesvirus 8, inhibits apoptosis but does not heterodimerize with Bax or Bak. *Proc Natl Acad Sci U S A* **94**, 690-694, doi:10.1073/pnas.94.2.690 (1997).

77 Gonzalez, C. M. *et al.* Identification and characterization of the Orf49 protein of Kaposi's sarcoma-associated herpesvirus. *J Virol* **80**, 3062-3070, doi:10.1128/JVI.80.6.3062-3070.2006 (2006).
78 Liu, D., Wang, Y. & Yuan, Y. Kaposi's Sarcoma-Associated Herpesvirus K8 Is an RNA Binding Protein That Regulates Viral DNA Replication in Coordination with a Noncoding RNA. *J Virol* **92**, doi:10.1128/JVI.02177-17 (2018).
79 Rossetto, C., Yamboliev, I. & Pari, G. S. Kaposi's sarcoma-associated herpesvirus/human herpesvirus 8 K-bZIP modulates latency-associated nuclear protein-mediated suppression of lytic origin-dependent DNA synthesis. *J Virol* **83**, 8492-8501, doi:10.1128/JVI.00922-09 (2009).
80 Nabiee, R., Syed, B., Ramirez Castano, J., Lalani, R. & Totonchy, J. E. An Update of the Virion Proteome of Kaposi Sarcoma-Associated Herpesvirus. *Viruses* **12**, doi:10.3390/v12121382 (2020).
81 Cheng, A. Z. *et al.* A Conserved Mechanism of APOBEC3 Relocalization by Herpesviral Ribonucleotide Reductase Large Subunits. *J Virol* **93**, doi:10.1128/JVI.01539-19 (2019).
82 Mullick, J., Bernet, J., Singh, A. K., Lambris, J. D. & Sahu, A. Kaposi's sarcoma-associated herpesvirus (human herpesvirus 8) open reading frame 4 protein (kaposica) is a functional homolog of complement control proteins. *J Virol* **77**, 3878-3881, doi:10.1128/jvi.77.6.3878-3881.2003 (2003).
83 Park, J., Lee, D., Seo, T., Chung, J. & Choe, J. Kaposi's sarcoma-associated herpesvirus (human herpesvirus-8) open reading frame 36 protein is a serine protein kinase. *J Gen Virol* **81**, 1067-1071, doi:10.1099/0022-1317-81-4-1067 (2000).
84 Lee, H. *et al.* Identification of an immunoreceptor tyrosine-based activation motif of K1 transforming protein of Kaposi's sarcoma-associated herpesvirus. *Mol Cell Biol* **18**, 5219-5228, doi:10.1128/MCB.18.9.5219 (1998).
85 Wang, L., Dittmer, D. P., Tomlinson, C. C., Fakhari, F. D. & Damania, B. Immortalization of primary endothelial cells by the K1 protein of Kaposi's sarcoma-associated herpesvirus. *Cancer Res* **66**, 3658-3666, doi:10.1158/0008-5472.CAN-05-3680 (2006).
86 Li, H., Wang, H. & Nicholas, J. Detection of direct binding of human herpesvirus 8-encoded interleukin-6 (vIL-6) to both gp130 and IL-6 receptor (IL-6R) and identification of amino acid residues of vIL-6 important for IL-6R-dependent and -independent signaling. *J Virol* **75**, 3325-3334, doi:10.1128/JVI.75.7.3325-3334.2001 (2001).
87 Aoki, Y. *et al.* Angiogenesis and hematopoiesis induced by Kaposi's sarcoma-associated herpesvirus-encoded interleukin-6. *Blood* **93**, 4034-4043 (1999).
88 Kledal, T. N. *et al.* A broad-spectrum chemokine antagonist encoded by Kaposi's sarcoma-associated herpesvirus. *Science* **277**, 1656-1659, doi:10.1126/science.277.5332.1656 (1997).
89 Stine, J. T. *et al.* KSHV-encoded CC chemokine vMIP-III is a CCR4 agonist, stimulates angiogenesis, and selectively chemoattracts TH2 cells. *Blood* **95**, 1151-1157 (2000).
90 Nascimento, R., Dias, J. D. & Parkhouse, R. M. The conserved UL24 family of human alpha, beta and gamma herpesviruses induces cell cycle arrest and inactivation of the cyclinB/cdc2 complex. *Arch Virol* **154**, 1143-1149, doi:10.1007/s00705-009-0420-y (2009).

91 Burysek, L. *et al.* Functional analysis of human herpesvirus 8-encoded viral interferon regulatory factor 1 and its association with cellular interferon regulatory factors and p300. *J Virol* **73**, 7334-7342, doi:10.1128/JVI.73.9.7334-7342.1999 (1999).
92 Choi, Y. B. & Nicholas, J. Bim nuclear translocation and inactivation by viral interferon regulatory factor. *PLoS Pathog* **6**, e1001031, doi:10.1371/journal.ppat.1001031 (2010).
93 Lee, H. R. *et al.* Kaposi's sarcoma-associated herpesvirus viral interferon regulatory factor 4 targets MDM2 to deregulate the p53 tumor suppressor pathway. *J Virol* **83**, 6739-6747, doi:10.1128/JVI.02353-08 (2009).
94 Marcos-Villar, L. *et al.* Kaposi's sarcoma-associated herpesvirus protein LANA2 disrupts PML oncogenic domains and inhibits PML-mediated transcriptional repression of the survivin gene. *J Virol* **83**, 8849-8858, doi:10.1128/JVI.00339-09 (2009).
95 Joo, C. H. *et al.* Inhibition of interferon regulatory factor 7 (IRF7)-mediated interferon signal transduction by the Kaposi's sarcoma-associated herpesvirus viral IRF homolog vIRF3. *J Virol* **81**, 8282-8292, doi:10.1128/JVI.00235-07 (2007).
96 Burysek, L. & Pitha, P. M. Latently expressed human herpesvirus 8-encoded interferon regulatory factor 2 inhibits double-stranded RNA-activated protein kinase. *J Virol* **75**, 2345-2352, doi:10.1128/JVI.75.5.2345-2352.2001 (2001).
97 Sadler, R. *et al.* A complex translational program generates multiple novel proteins from the latently expressed kaposin (K12) locus of Kaposi's sarcoma-associated herpesvirus. *J Virol* **73**, 5722-5730, doi:10.1128/JVI.73.7.5722-5730.1999 (1999).
98 Kliche, S. *et al.* Signaling by human herpesvirus 8 kaposin A through direct membrane recruitment of cytohesin-1. *Mol Cell* **7**, 833-843, doi:10.1016/s1097-2765(01)00227-1 (2001).
99 Ballon, G., Chen, K., Perez, R., Tam, W. & Cesarman, E. Kaposi sarcoma herpesvirus (KSHV) vFLIP oncoprotein induces B cell transdifferentiation and tumorigenesis in mice. *J Clin Invest* **121**, 1141-1153, doi:10.1172/JCI44417 (2011).
100 Sun, Q., Zachariah, S. & Chaudhary, P. M. The human herpes virus 8-encoded viral FLICE-inhibitory protein induces cellular transformation via NF-kappaB activation. *J Biol Chem* **278**, 52437-52445, doi:10.1074/jbc.M304199200 (2003).
101 Punj, V. *et al.* Kaposi's sarcoma-associated herpesvirus-encoded viral FLICE inhibitory protein (vFLIP) K13 suppresses CXCR4 expression by upregulating miR-146a. *Oncogene* **29**, 1835-1844, doi:10.1038/onc.2009.460 (2010).
102 Ojala, P. M. *et al.* The apoptotic v-cyclin-CDK6 complex phosphorylates and inactivates Bcl-2. *Nat Cell Biol* **2**, 819-825, doi:10.1038/35041064 (2000).
103 Swanton, C. *et al.* Herpes viral cyclin/Cdk6 complexes evade inhibition by CDK inhibitor proteins. *Nature* **390**, 184-187, doi:10.1038/36606 (1997).
104 Salata, C. *et al.* vOX2 glycoprotein of human herpesvirus 8 modulates human primary macrophages activity. *J Cell Physiol* **219**, 698-706, doi:10.1002/jcp.21722 (2009).
105 Bais, C. *et al.* G-protein-coupled receptor of Kaposi's sarcoma-associated herpesvirus is a viral oncogene and angiogenesis activator. *Nature* **391**, 86-89, doi:10.1038/34193 (1998).
106 Choi, J. K., Lee, B. S., Shim, S. N., Li, M. & Jung, J. U. Identification of the novel K15 gene at the rightmost end of the Kaposi's sarcoma-associated herpesvirus genome. *J Virol* **74**, 436-446 (2000).
107 Glenn, M., Rainbow, L., Aurade, F., Davison, A. & Schulz, T. F. Identification of a spliced gene from Kaposi's sarcoma-associated herpesvirus encoding a protein with

similarities to latent membrane proteins 1 and 2A of Epstein-Barr virus. *J Virol* **73**, 6953-6963, doi:10.1128/JVI.73.8.6953-6963.1999 (1999).
108 Mortazavi, Y. *et al.* The Kaposi's Sarcoma-Associated Herpesvirus (KSHV) gH/gL Complex Is the Predominant Neutralizing Antigenic Determinant in KSHV-Infected Individuals. *Viruses* **12**, doi:10.3390/v12030256 (2020).
109 de Jesus, O. *et al.* Updated Epstein-Barr virus (EBV) DNA sequence and analysis of a promoter for the BART (CST, BARF0) RNAs of EBV. *J Gen Virol* **84**, 1443-1450, doi:10.1099/vir.0.19054-0 (2003).
110 McGeoch, D. J. *et al.* The complete DNA sequence of the long unique region in the genome of herpes simplex virus type 1. *J Gen Virol* **69 (Pt 7)**, 1531-1574, doi:10.1099/0022-1317-69-7-1531 (1988).
111 Murphy, E. *et al.* Coding potential of laboratory and clinical strains of human cytomegalovirus. *Proc Natl Acad Sci U S A* **100**, 14976-14981, doi:10.1073/pnas.2136652100 (2003).
112 Bernard Roizman, D. M. K., Richard J. Whitley. *Fields Virology* 6th edn, Vol. 2 Chapter 60 (Lippincott and Williams, 2013).
113 Ann M. Arvin, D. G. *Feilds Virology* 6th edn, Vol. 2 Chapter 63 (Lippincott and Williams, 2013).
114 Edward S. Mocarski, J., Thomas Shenk, Paul D. Griffiths, Robert F. Pass. *Fields Virology* 6th edn, Vol. 2 Chapter 62 (Lippincott and Williams, 2013).
115 Virgin, H. W. t. *et al.* Complete sequence and genomic analysis of murine gammaherpesvirus 68. *J Virol* **71**, 5894-5904, doi:10.1128/JVI.71.8.5894-5904.1997 (1997).
116 Fixman, E. D., Hayward, G. S. & Hayward, S. D. trans-acting requirements for replication of Epstein-Barr virus ori-Lyt. *J Virol* **66**, 5030-5039, doi:10.1128/JVI.66.8.5030-5039.1992 (1992).
117 Chiu, S. H. *et al.* Epstein-Barr virus BALF3 has nuclease activity and mediates mature virion production during the lytic cycle. *J Virol* **88**, 4962-4975, doi:10.1128/JVI.00063-14 (2014).
118 Herrold, R. E., Marchini, A., Fruehling, S. & Longnecker, R. Glycoprotein 110, the Epstein-Barr virus homolog of herpes simplex virus glycoprotein B, is essential for Epstein-Barr virus replication in vivo. *J Virol* **70**, 2049-2054, doi:10.1128/JVI.70.3.2049-2054.1996 (1996).
119 Marchini, A., Tomkinson, B., Cohen, J. I. & Kieff, E. BHRF1, the Epstein-Barr virus gene with homology to Bc12, is dispensable for B-lymphocyte transformation and virus replication. *J Virol* **65**, 5991-6000, doi:10.1128/JVI.65.11.5991-6000.1991 (1991).
120 Larrat, S. *et al.* Inhibition of Epstein-Barr virus replication by small interfering RNA targeting the Epstein-Barr virus protease gene. *Antivir Ther* **14**, 655-662 (2009).
121 Henson, B. W., Perkins, E. M., Cothran, J. E. & Desai, P. Self-assembly of Epstein-Barr virus capsids. *J Virol* **83**, 3877-3890, doi:10.1128/JVI.01733-08 (2009).
122 Oda, T., Imai, S., Chiba, S. & Takada, K. Epstein-Barr virus lacking glycoprotein gp85 cannot infect B cells and epithelial cells. *Virology* **276**, 52-58, doi:10.1006/viro.2000.0531 (2000).
123 Gruffat, H., Kadjouf, F., Mariame, B. & Manet, E. The Epstein-Barr virus BcRF1 gene product is a TBP-like protein with an essential role in late gene expression. *J Virol* **86**, 6023-6032, doi:10.1128/JVI.00159-12 (2012).

124 Jochum, S., Moosmann, A., Lang, S., Hammerschmidt, W. & Zeidler, R. The EBV immunoevasins vIL-10 and BNLF2a protect newly infected B cells from immune recognition and elimination. *PLoS Pathog* **8**, e1002704, doi:10.1371/journal.ppat.1002704 (2012).
125 Borza, C. M. & Hutt-Fletcher, L. M. Epstein-Barr virus recombinant lacking expression of glycoprotein gp150 infects B cells normally but is enhanced for infection of epithelial cells. *J Virol* **72**, 7577-7582, doi:10.1128/JVI.72.9.7577-7582.1998 (1998).
126 Pavlova, S. *et al.* An Epstein-Barr virus mutant produces immunogenic defective particles devoid of viral DNA. *J Virol* **87**, 2011-2022, doi:10.1128/JVI.02533-12 (2013).
127 Watanabe, T. *et al.* The Epstein-Barr Virus BDLF4 Gene Is Required for Efficient Expression of Viral Late Lytic Genes. *J Virol* **89**, 10120-10124, doi:10.1128/JVI.01604-15 (2015).
128 Hung, C. H. *et al.* Interaction Between BGLF2 and BBLF1 Is Required for the Efficient Production of Infectious Epstein-Barr Virus Particles. *Front Microbiol* **10**, 3021, doi:10.3389/fmicb.2019.03021 (2019).
129 Watanabe, T. *et al.* Roles of Epstein-Barr virus BGLF3.5 gene and two upstream open reading frames in lytic viral replication in HEK293 cells. *Virology* **483**, 44-53, doi:10.1016/j.virol.2015.04.007 (2015).
130 Murata, T. *et al.* Efficient production of infectious viruses requires enzymatic activity of Epstein-Barr virus protein kinase. *Virology* **389**, 75-81, doi:10.1016/j.virol.2009.04.007 (2009).
131 Feederle, R., Bannert, H., Lips, H., Muller-Lantzsch, N. & Delecluse, H. J. The Epstein-Barr virus alkaline exonuclease BGLF5 serves pleiotropic functions in virus replication. *J Virol* **83**, 4952-4962, doi:10.1128/JVI.00170-09 (2009).
132 Malik, A. K., Martinez, R., Muncy, L., Carmichael, E. P. & Weller, S. K. Genetic analysis of the herpes simplex virus type 1 UL9 gene: isolation of a LacZ insertion mutant and expression in eukaryotic cells. *Virology* **190**, 702-715, doi:10.1016/0042-6822(92)90908-8 (1992).
133 Masud, H. *et al.* Epstein-Barr Virus BBRF2 Is Required for Maximum Infectivity. *Microorganisms* **7**, doi:10.3390/microorganisms7120705 (2019).
134 Pavlova, S. *et al.* An Epstein-Barr virus mutant produces immunogenic defective particles devoid of viral DNA. *Journal of virology* **87**, 2011-2022, doi:10.1128/jvi.02533-12 (2013).
135 Baines, J. D. & Roizman, B. The open reading frames UL3, UL4, UL10, and UL16 are dispensable for the replication of herpes simplex virus 1 in cell culture. *J Virol* **65**, 938-944, doi:10.1128/JVI.65.2.938-944.1991 (1991).
136 Masud, H. *et al.* Epstein-Barr Virus BKRF4 Gene Product Is Required for Efficient Progeny Production. *J Virol* **91**, doi:10.1128/JVI.00975-17 (2017).
137 Su, M. T. *et al.* Uracil DNA glycosylase BKRF3 contributes to Epstein-Barr virus DNA replication through physical interactions with proteins in viral DNA replication complex. *J Virol* **88**, 8883-8899, doi:10.1128/jvi.00950-14 (2014).
138 Fixman, E. D., Hayward, G. S. & Hayward, S. D. Replication of Epstein-Barr virus oriLyt: lack of a dedicated virally encoded origin-binding protein and dependence on Zta in cotransfection assays. *J Virol* **69**, 2998-3006, doi:10.1128/JVI.69.5.2998-3006.1995 (1995).

139 Watanabe, T. *et al.* The Epstein-Barr virus BRRF2 gene product is involved in viral progeny production. *Virology* **484**, 33-40, doi:10.1016/j.virol.2015.05.010 (2015).
140 Yoshida, M. *et al.* The Epstein-Barr Virus BRRF1 Gene Is Dispensable for Viral Replication in HEK293 cells and Transformation. *Sci Rep* **7**, 6044, doi:10.1038/s41598-017-06413-7 (2017).
141 Feederle, R. *et al.* The Epstein-Barr virus lytic program is controlled by the co-operative functions of two transactivators. *EMBO J* **19**, 3080-3089, doi:10.1093/emboj/19.12.3080 (2000).
142 Lake, C. M. & Hutt-Fletcher, L. M. Epstein-Barr virus that lacks glycoprotein gN is impaired in assembly and infection. *J Virol* **74**, 11162-11172, doi:10.1128/jvi.74.23.11162-11172.2000 (2000).
143 Yanagi, Y. *et al.* Initial Characterization of the Epstein(-)Barr Virus BSRF1 Gene Product. *Viruses* **11**, doi:10.3390/v11030285 (2019).
144 Gruffat, H. *et al.* Epstein-Barr virus mRNA export factor EB2 is essential for production of infectious virus. *J Virol* **76**, 9635-9644, doi:10.1128/jvi.76.19.9635-9644.2002 (2002).
145 Cohen, J. I. & Lekstrom, K. Epstein-Barr virus BARF1 protein is dispensable for B-cell transformation and inhibits alpha interferon secretion from mononuclear cells. *J Virol* **73**, 7627-7632, doi:10.1128/JVI.73.9.7627-7632.1999 (1999).
146 Cheng, A. Z. *et al.* Epstein-Barr virus BORF2 inhibits cellular APOBEC3B to preserve viral genome integrity. *Nat Microbiol* **4**, 78-88, doi:10.1038/s41564-018-0284-6 (2019).
147 Masud, H. *et al.* The BOLF1 gene is necessary for effective Epstein-Barr viral infectivity. *Virology* **531**, 114-125, doi:10.1016/j.virol.2019.02.015 (2019).
148 Whitehurst, C. B. *et al.* Knockout of Epstein-Barr virus BPLF1 retards B-cell transformation and lymphoma formation in humanized mice. *mBio* **6**, e01574-01515, doi:10.1128/mBio.01574-15 (2015).
149 Aubry, V. *et al.* Epstein-Barr virus late gene transcription depends on the assembly of a virus-specific preinitiation complex. *J Virol* **88**, 12825-12838, doi:10.1128/JVI.02139-14 (2014).
150 Farina, A. *et al.* BFRF1 of Epstein-Barr virus is essential for efficient primary viral envelopment and egress. *J Virol* **79**, 3703-3712, doi:10.1128/JVI.79.6.3703-3712.2005 (2005).
151 Granato, M. *et al.* Deletion of Epstein-Barr virus BFLF2 leads to impaired viral DNA packaging and primary egress as well as to the production of defective viral particles. *J Virol* **82**, 4042-4051, doi:10.1128/JVI.02436-07 (2008).

Part II

Overview

Part II is designed to give the reader a more detailed look at how the KSHV BAC16 mutant virus library was created. It also contains a selection of mutants designed to give the reader a more comprehensive sense of our screening observations and is split into sections. Section I outlines the creation of KSHV BAC16 mutant viruses in E. coli. Section II outlines the creation of KSHV BAC16 mutant virus cell lines, general phenotypes observed from viral reactivation, and supplemental observations about reactivation in the BAC16-iSLK mutant library. Section III is a detailed analysis of induction phenotypes for KSHV BAC16 mutant virus cell lines that did not produce infectious progeny. Many of these "essential" KSHV BAC16 mutant virus cell lines were also examined using transmission electron microscopy (TEM) to elucidate viral capsid formation, maturation, and viral egress. A more detailed analysis of viral capsid maturation can be found in Chapter 4: *Kaposi Sarcoma Associated Herpesvirus Open Reading Frame 19 Is Essential for Viral Capsid Maturation during Lytic Infection*

Section I: Creation of a BAC16 mutant virus library

ORF29b and k4.2 1st homologous recombination

We found that optimization of the initial PCR reaction, which amplified out the kan-cassette, and added 60bp of sequence homology for use in the 1st and 2nd homologous recombination reactions, needed considerable optimization. We found a variety of optimization steps, ranging from altered primer and polymerase concentrations to the addition of reducing agents like DMSO, were required for efficient amplification. The need for a specific optimization strategy did not depend on primer length, and thus we hypothesize that the base content of primers, and by extension, the strength of homo and heterodimers formed in solution, dictated the optimization strategy (data not shown). The results of the kan-cassette PCR reaction for primers designed to insert a stop codon in ORF29b and k4.2 can be found in figure 1(chapter 3 part I, supplementary table 1). Primers for ORF29b and k4.2 were diluted serially from 500nM to 100nM in 100nM increments. The top two bands in every lane of the gel that run as a 4500bp band and a weaker staining 12,000bp band represent the pEPKanS supercoiled plasmid and nicked plasmid, respectively. At the bottom of the gel, the smeared band that runs as 200bp band represents primer dimers and their resulting amplification products. The sharp bands in the middle of the gel that run as a 1100bp band represent the PCR product of interest; the 994bp kan-cassette plus the 60bp of homolog added to either end of the product from the forward and reverse primers, the 18bp SceI meganuclease site, and the 12bp that corresponds to the inserted stop sequence (chapter 3 part I, supplementary table 1). In both primer sets, the 200nM primer concentration produced the best amplification results in terms of product band brightness and the removal of the primer-dimer band at the bottom of the gel. While the ORF29b primers produced amplification product in all primer dilution reactions, k4.2 only produced amplification product in the primer concentrations from 300nM-100nM.

These PCR products were cut from the gel using the Qiagen gel extraction kit and 100ng of product was electroporated into early-log phase BAC16 containing GS1783. The reaction was recovered immediately in SOC medium, cultured at 30C for 2 hours, and the entire reaction was

plated on LB-kan plates and incubated at 30C for 24 hours. Colonies were recovered in liquid LB-kan and screened via alkaline lysis, PCR, and restriction digest using NheI. Figure 2 shows the results of the NheI digest for 5 individual colonies from the ORF29b and k4.2 electroporation reaction. All ORF29b colonies show a shift of the 3800bp band up into the 4800bp region (figure 2). This shift corresponds to the insertion of the 994bp Kan-cassette, 40bp of sequence duplication for the second recombination, the 18bp SceI meganuclease site, and the 12bp stop sequence, at nt. 50226 of the MK733609.1 sequence. In colony ORF29b #5 we also observed a shift of the 6400bp band down by about 400bp, so that it runs slightly larger than the 5900bp band. The 6400bp band contains several direct repeat regions and one inverted repeat region. We hypothesize that during the 1st homologous recombination, a large-scale off-target deletion took place. This is an example of a colony that was thrown out because of a bad NheI screen. Importantly, ORF29b colonies 1-4 show a banding pattern that matches the BAC16 digest on the far-right side of the gel, aside from the expected shift in the 3800bp band, verifying their genomic integrity and the fidelity of the 1st recombination reaction. The k4.2 primers inserted the 997bp Kan-cassette, 40bp of sequence duplication for the second recombination, the 18bp SceI meganuclease site, and the 12bp stop sequence, at nt. 23085 of the MK733609.1 sequence. This insertion is unable to be visualized on the gel when compared to the BAC16 digest because it occurs in the 29,000bp band. An insertion of a single kilobase into a band this large is unresolvable under our current electrophoresis conditions. However, we do know that this colony has undergone a recombination event that inserted the kan-cassette somewhere in the BAC or in the host genome, because it was able to grow under selection pressure. Importantly, it can be observed that colony k4.2 #5 has undergone a large off-target insertion or duplication in the 6400bp band. This event has caused the band to shift up to right below the 7600bp band, representing an insertion or duplication of an approximately 700bp sequence. Considering the number and nature of repeat regions in the 6400bp band, we hypothesize that this shift represents a large off-target duplication event. The remaining k4.2 colonies 1-4 show a banding pattern that matches the BAC16 digest on the far-right side of the gel, verifying their genomic integrity and the fidelity of the 1st recombination reaction.

To verify the location of the kan-cassette insertion, we conducted PCR using mini-prep BAC DNA from ORF29b and k4.2 colonies 1-4. For these reactions we used two sets of primer pairs. The first set corresponded to forward and reverse primers that anneal to the BAC16 sequence and flank the insertion site. The second pair contains a forward primer that anneals to the BAC upstream of the insertion site, and a reverse primer that anneals inside the kan cassette. Figure 3a shows the results of the PCR reactions for ORF29b 1-4. The PCR reactions using ORF29b F/R PCR primer pair yielded the expected size band at 1400bp for colonies 1-4 (Figure 3a, lanes 2-5). This band represents the 994bp Kan-cassette, the 40bp duplication for the 2nd homologous recombination, the 18bp SceI meganuclease site, the 12bp stop insertion, and an additional 305bp of sequence that flanks the first homologous recombination insertion site (chapter 3 part I, supplementary table 1). The BAC16 DNA yielded the expected band size of approximately 300bp when combined with the ORF29b F/R PCR primer pair, indicating that the insertion is not present in BAC16 DNA, as it has not undergone the first recombination event (Figure 3a, lane 6). The no template control for the ORF29b F/R PCR primer pair is also

negative as expected (Figure 3a, lane7). These results confirm that an insertion of the expected size has taken place at the expected location in the BAC genome. To verify that the increased band size observed in lanes 2-5 is in fact due to the insertion of the kan-cassette, and not a genomic duplication product or rearrangement event, we conducted PCR using the ORF29b-F/KanR primer set (chapter 3 part I, supplementary table 1). The KanR primer is 748bp downstream of the kan-cassette start site, and the ORF29b-F primer is 163bp upstream of the 1st homologous recombination insertion site. Adding in half of the 40bp duplication for the 2nd homologous recombination and the 12bp stop insertion gives a product length of approximately 900bp. This is the length of the PCR product observed for ORF29b colonies 2-4 (Figure 3a, lanes 9-11). ORF29b colony 1 (Figure 3a, lane 8) did not produce a PCR product. This sample was discarded because it could not be confirmed that the 1100bp insertion observed in Figure 3a, lane 2 was in due to the kan-cassette, and not some other duplication or insertion event. The no template control was negative for the 29b-F/KanR primer set as well (Figure 3a, lane 12).

Figure 3b show the results of the PCR reactions for k4.2 colonies 1-4. The PCR reactions using k4.2 F/R PCR primer pair yielded the expected size band at 1400bp for colonies 1-4 (chapter 3 part I, supplementary table 1) (Figure 3b, lanes 2-5). This band represents the 994bp kan-cassette, the 40bp duplication for the 2nd homologous recombination, the 18bp SceI meganuclease site, the 12bp stop insertion on both sides of the insert, and an additional 291bp of sequence that flanks the first homologous recombination insertion site. There is a slight amplification product of 300bp for k4.2 colony 4 (Figure 3b, lane 5). This is product is unexpected and may indicate contamination of k4.2 colony 4 with “wild-type” BAC16 containing GS1783 E. coli. However, we believe cross contamination of k4.2 colony 4 with “wild-type” BAC16 containing GS1783 E. coli. is unlikely for the following reasons: 1) well isolated individual colonies were selected for screening, and 2) all screened colonies were grown under kanamycin selection pressure, and BAC16 containing GS1783 E. coli do not contain a kanamycin resistance cassette. However, out of an abundance of caution, this sample was discarded. The BAC16 DNA yielded the expected band size of 300bp when combined with the k4.2 F/R PCR primer pair, indicating that the insertion is not present in BAC16 DNA which has not undergone the first recombination event (Figure 3b, lane 6), and the no template control lane is negative for amplification (Figure 3b, lane 7). To verify that the increased band size observed in lanes 2-5 of figure 3b is in fact due to the insertion of the kan-cassette, and not a genomic duplication product or rearrangement event, we conducted PCR using the k4.2-F/ KanR primer set. The KanR primer is 748bp downstream of the Kan-cassette start site, and the k4.2-F primer is 139bp upstream of the 1st homologous recombination insertion site. Adding in half of the 40bp duplication for the 2nd homologous recombination and the 12bp stop insertion gives a product length of approximately 900bp (chapter 3 part I, supplementary table 1). This is the length of the PCR product observed for k4.2 colonies 1-4 (Figure 3b, lanes 8-11). The no template control was negative for the k4.2-F/ KanR primer set as well (Figure 3b, lane 12).

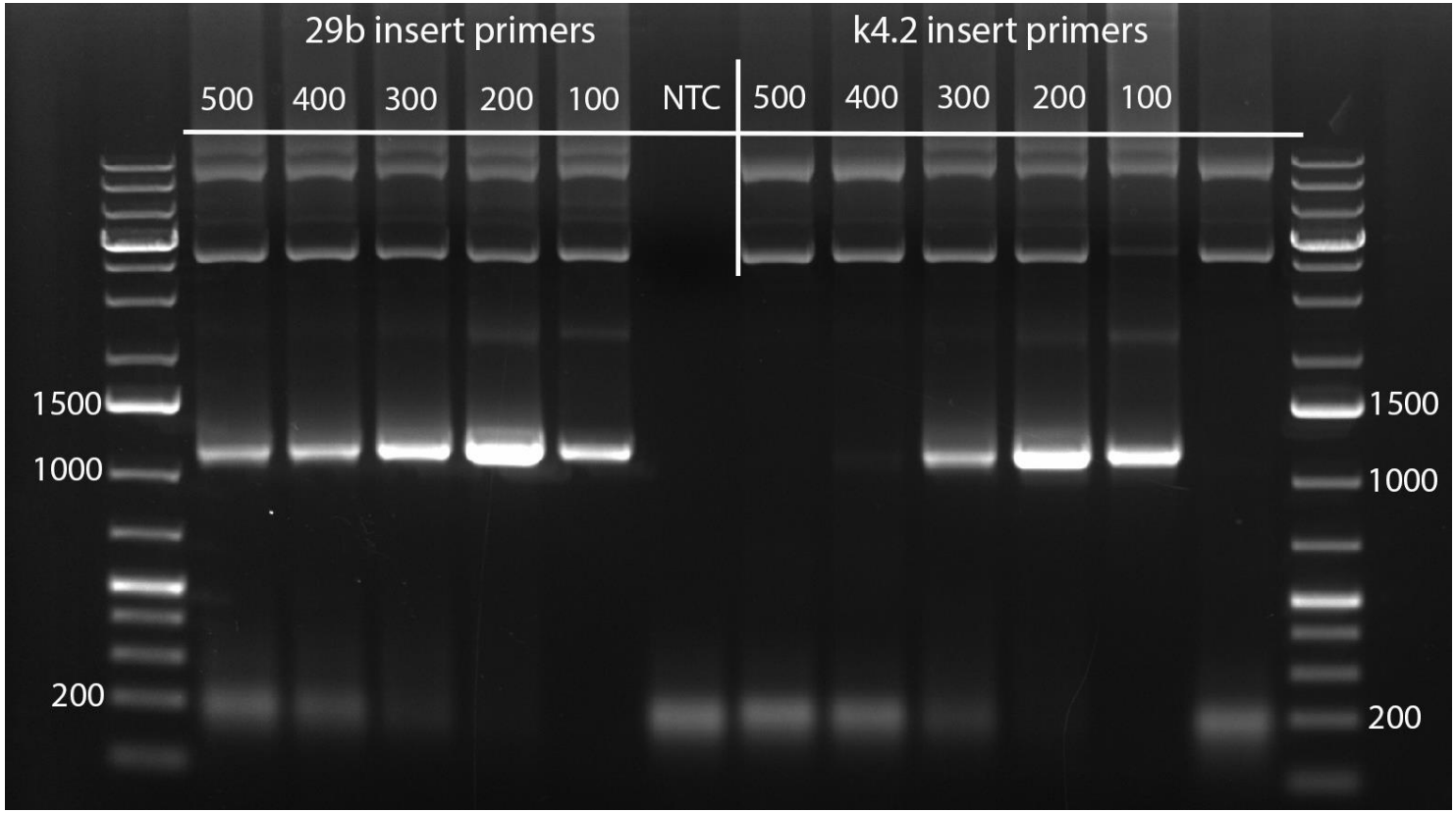

Figure 1: 29b and k4.2 insert PCR optimization.

Lane 1 is the 1kb plus gene ruler. Lane 2-6 are the PCR products for pEPKanS mini-prep DNA combined with different nanomolar concentrations of 29b insert primers. Lane 7 is the no template control for the 29b insert primers. Lane 8-12 are the PCR products for pEPKanS mini-prep DNA combined with different nanomolar concentrations of k4.2 insert primers. Lane 13 is the 1kb plus gene ruler.

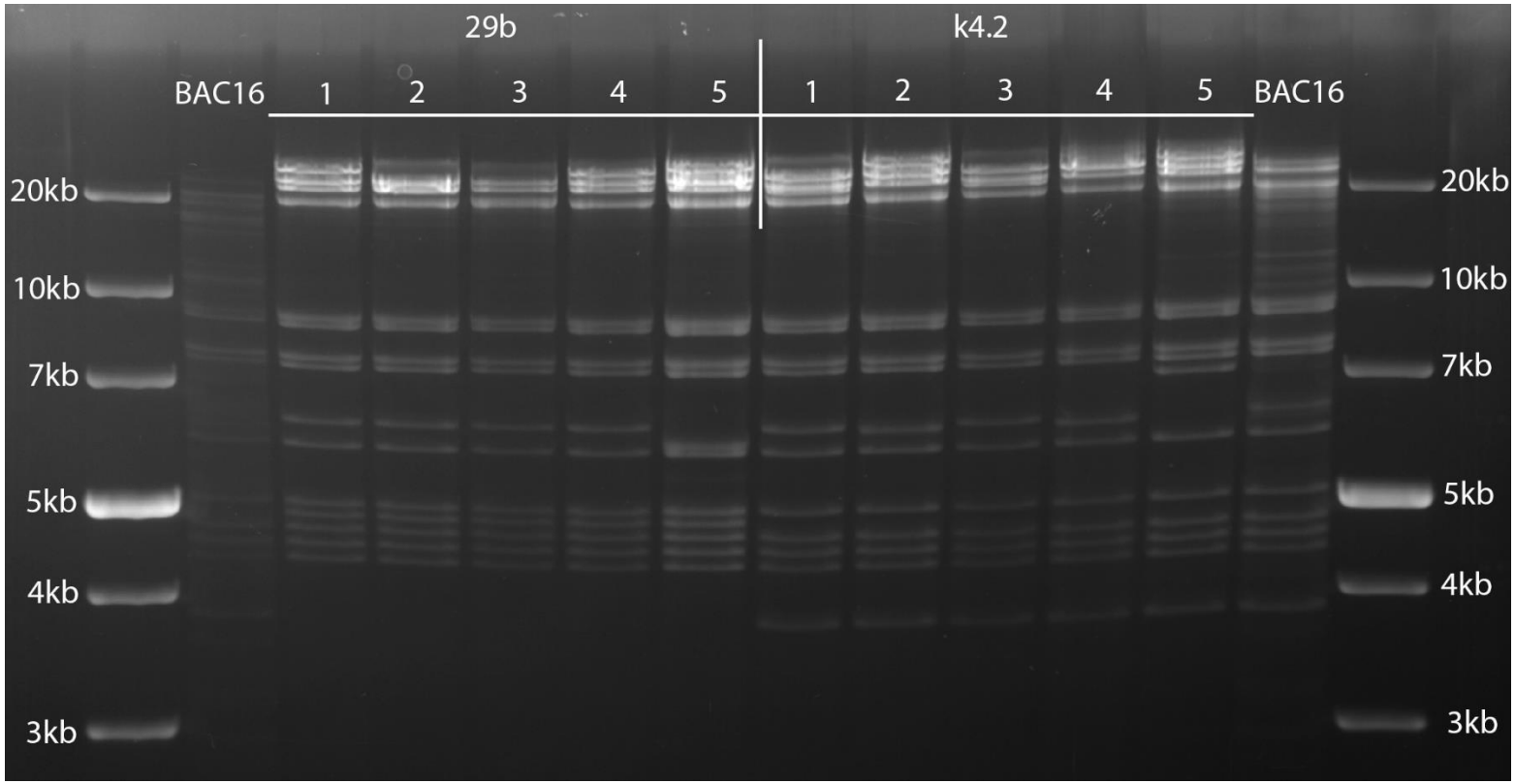

Figure 2: NheI digest products for ORF29b and k4.2 1st HR colonies 1-5.

Lane 1 is the 1kb plus ladder from gene ruler. Lane 2 is the BAC16. Lane 3-7 are ORF29b colonies 1-5 respectively. Lanes 8-12 are k4.2 colonies 1-5 respectively. Lane 13 is the BAC16. Lane 14 is the 1kb plus ladder from gene ruler.

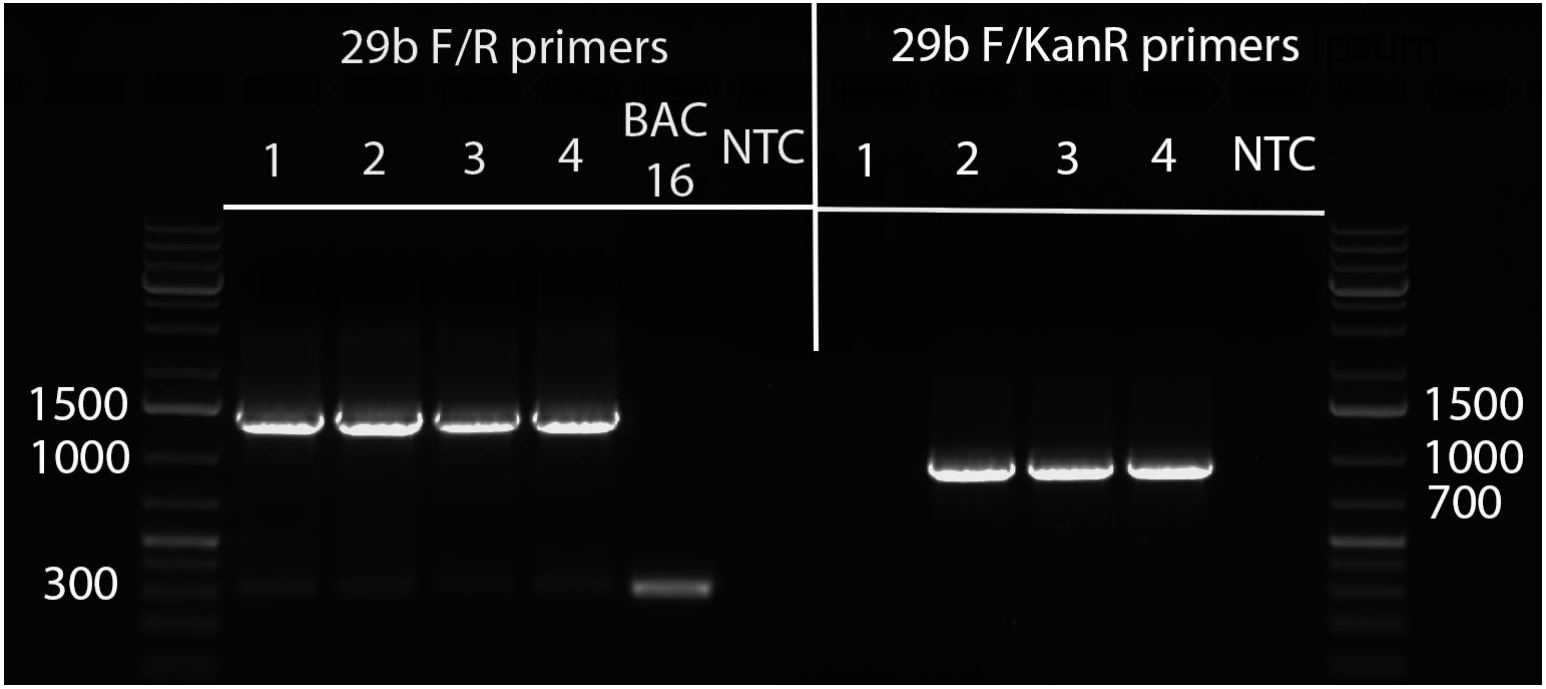

Figure 3a: PCR reaction products of the 29b 1st HR clones #1-4 with 29b F/R and 29b F/KanR primer sets:

Lane 1 is the 1kb plus ladder from gene ruler. Lane 2-5 is the PCR reaction product using the ORF29b F/R primer set for the 1st HR colonies 1-4. Lane 6 is the PCR reaction product using the ORF29b F/R primer set on BAC16 DNA, and lane 7 is the ORF29b F/R primer set no template control. Lane 8-11 is the PCR reaction product using the ORF29b F/KanR primer set for the 1st HR colonies 1-4 and lane 12 is the ORF29b F/KanR primer set no template control. Lane 13 is the 1kb plus ladder from gene ruler.

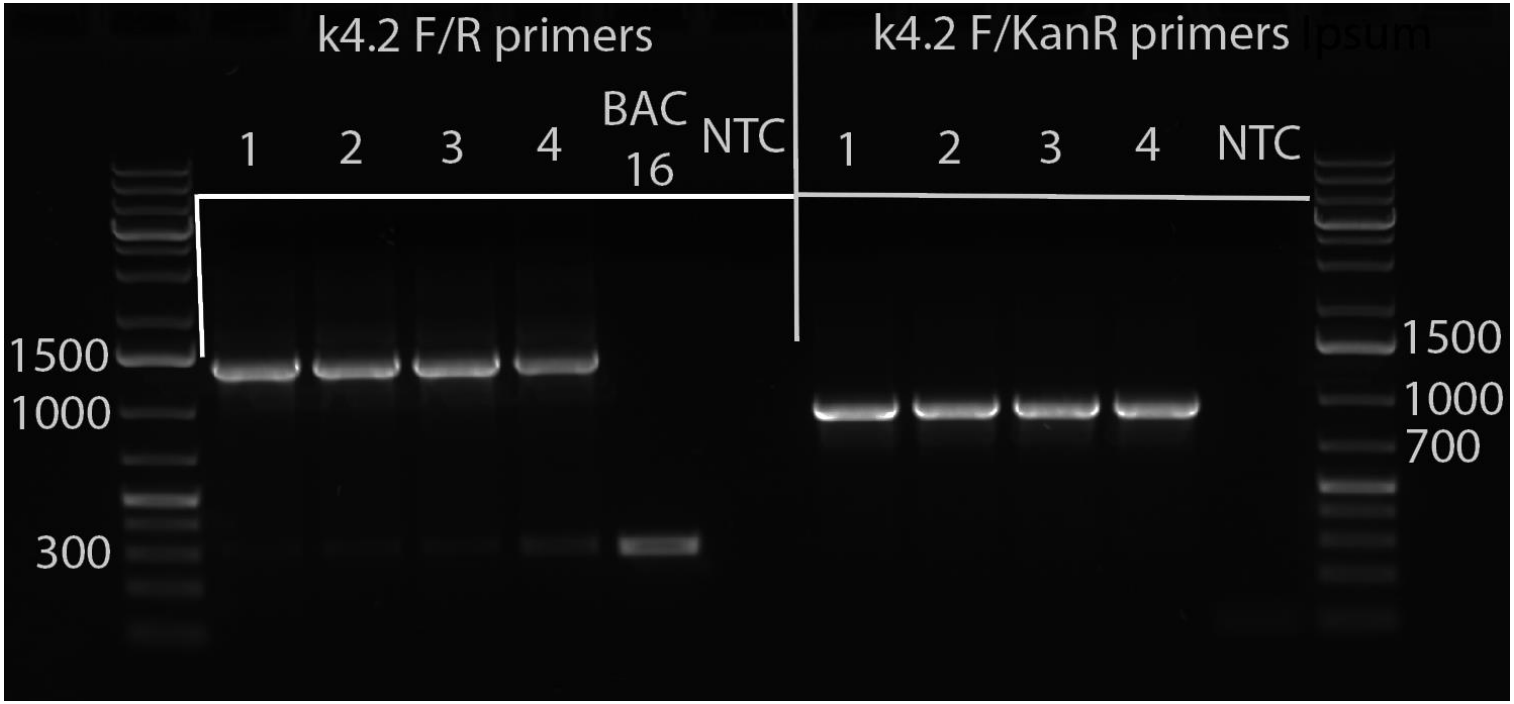

Figure 3b: PCR reaction products of the k4.2 1st HR clones #1-4 with k4.2 F/R and k4.2 F/KanR primer sets:

Lane 1 is the 1kb plus ladder from gene ruler. Lane 2-5 is the PCR reaction product using the k4.2 F/R primer set for the 1st HR colonies 1-4. Lane 6 is the PCR reaction product using the k4.2 F/R primer set on BAC16 DNA, and lane 7 is the k4.2 F/R primer set no template control. Lane 8-11 is the PCR reaction product using the k4.2 F/KanR primer set for the 1st HR colonies 1-4 and lane 12 is the k4.2 F/KanR primer set no template control. Lane 13 is the 1kb plus ladder from gene ruler.

ORF29b and k4.2 2nd homologous recombination

The 1st HR colony #1 for k4.2 and #3 for ORF29b were selected to undergo the 2nd HR. These two colonies were grown to early log phase in Kan-LB broth, arabinose was added to a final concentration of 1% to induce expression of the SceI meganuclease, and the cultures were grown for an additional 45 mins at 30C. After the 45-minute incubation, the cultures were moved to a 42C water bath for 15 minutes, and then moved back to 30C for an additional 2 hours. At the end of the incubation, the cultures were serially diluted and plated on CM+ arabinose LB agar plates and grown for 24 hours at 30C. Isolated colonies were selected and replica-plated on Kan+ arabinose LB agar plates and grown again for 24 hours at 30C. Colonies that were negative for growth on the Kan+ arabinose LB agar plates were recovered in CM-LB broth and screened via alkaline lysis, restriction digest and PCR.

The results of the NheI digest for second homologous recombination clones are shown in figure 4. As expected, K4.2 clone 1c (figure 4, lane 3) and 1h (figure 4, lane 4) have a digest pattern that matches the BAC16 digest (figure 4, lane 2). This data is still inconclusive as the removal of the kan-cassette, the 40bp sequence duplication, and the duplication of the 12bp stop sequence leads to the removal of about 1100bp from the 28kb band. A 1.1kb removal from a band this size is unable to be resolved in our electrophoresis (refer to figure 2, lanes 8-12). Colony k4.2-1f shows a digest pattern where one of the three expected bands in the 26-30kb region has shifted downward and now runs at approximately 18kb (figure 4, lane 5). One 29kb band contains two direct repeat regions and a single inverted repeat region, and another 29kb band corresponds to the terminal repeats which are composed of a long stretch of 803bp tandem repeats (see chapter 2, figure 3). Either of these bands could have undergone a significant deletion event during the second homologous recombination that caused them to shift down into the 18kb region for k4.2-1f. For this reason, we discarded the k4.2-1f colony.

All the ORF29b-3 clones (29b-3i, 29b-3j, 29b-3m, and 29b-3n) show the removal of the 4800bp band and the reappearance of the 3800bp band after the second homologous recombination (compared Figure 4 lanes 6-9 to figure 2 lanes 3-7). This shift resulted from the removal of the 1100bp kan-cassette and the 40bp sequence duplications. ORF29b-3 clones ORF29b-3i, and ORF29b-3n show a digest pattern that matches the BAC16 digest (Figure 4, lane 2). ORF29b-3j shows a digest pattern where one of the three expected bands in the 26-30kb region has shifted downward and now runs at approximately 17kb (Figure 4, lane 7). This band has shifted slightly lower than the band for k4.2-1f (Figure 4, lane 5), indicating a slightly larger deletion event when compared to k4.2-1f. We hypothesize that these band shifts occurred from the terminal repeat region, and that the removal of different numbers of terminal repeats caused the different size band shifts in k4.2-1f and ORF29b-3j (Figure 4, lanes 5 and 7). ORF29b-3m shows a shift in the 6400bp band to where it can no longer be resolved/visualized (Figure 4, lanes 8). All the 2nd HR clones for ORF29b-3 and k4.2-1 should match the digestion pattern of the BAC16 (Figure 4, lane 2) because they are only expected to contain a short 12bp insertion in either the 3800bp band (ORF29b) or the 29kb band (k4.2). An insertion this small is unable to be resolved using our current electrophoresis conditions.

To verify that the kan-cassette was removed from the insertion location, we conducted PCR using ORF29b F/R and k4.2 F/R primers that flank the insertion sites. The results of the PCR are found in figure 5. The k4.2 F/R primer pair flank the insertion site and create a 291bp product in the BAC16 (unedited) genome, and a 313bp product for k4.2-1 clones that have successfully undergone the second homologous recombination to remove the kan-cassette and the 40bp duplication, leaving a scarless insertion of the 12bp stop sequence. The 2nd HR clones k4.2-1c, k4.2-1f, k4.2-1h have a major PCR product of approximately 300bp (Figure 5, lanes 2-4) indicating the removal of kan-cassette. It is also evident that the PCR product of the clones is shifted upward in the gel when compared to the BAC16 PCR product (Figure 5, lane 5). This slight shift upwards is the result of the 12bp stop insertion at the target site. There is also a weak 650bp amplification product in Figure 5, lanes 2-3, however, this is likely due to non-specific amplification considering that the expected band size is 1400bp if the kan-cassette was not removed (figure 3b, lanes 2-5).

The ORF29b primer pair flank the insertion site and create a 305bp product in the BAC16 (unedited) genome, and a 317bp product in the ORF29b-3 clones that have successfully undergone the second homologous recombination to remove the Kan-cassette and the 40bp duplication, leaving a scarless insertion of the 12bp stop sequence. The 2nd HR clones 29b-3i, 29b-3j, 29b-3m, 29b-3n have a major PCR product of slightly larger than 300bp (Figure 5, lanes 8-11) indicating the removal of kan-cassette. It is also evident that the PCR product of the clones is shifted upward in the gel when compared to the BAC16 PCR product (Figure 5, lane 12). This slight shift upwards is the result of the 12bp stop insertion at the target site. There are also two weak bands at 650bp and 950bp seen in Figure 5, lanes 8-10, however, these bands are likely due to non-specific amplification considering that the expected band size is 1400bp if the kan-cassette was not removed (figure 3a, lanes 2-5).

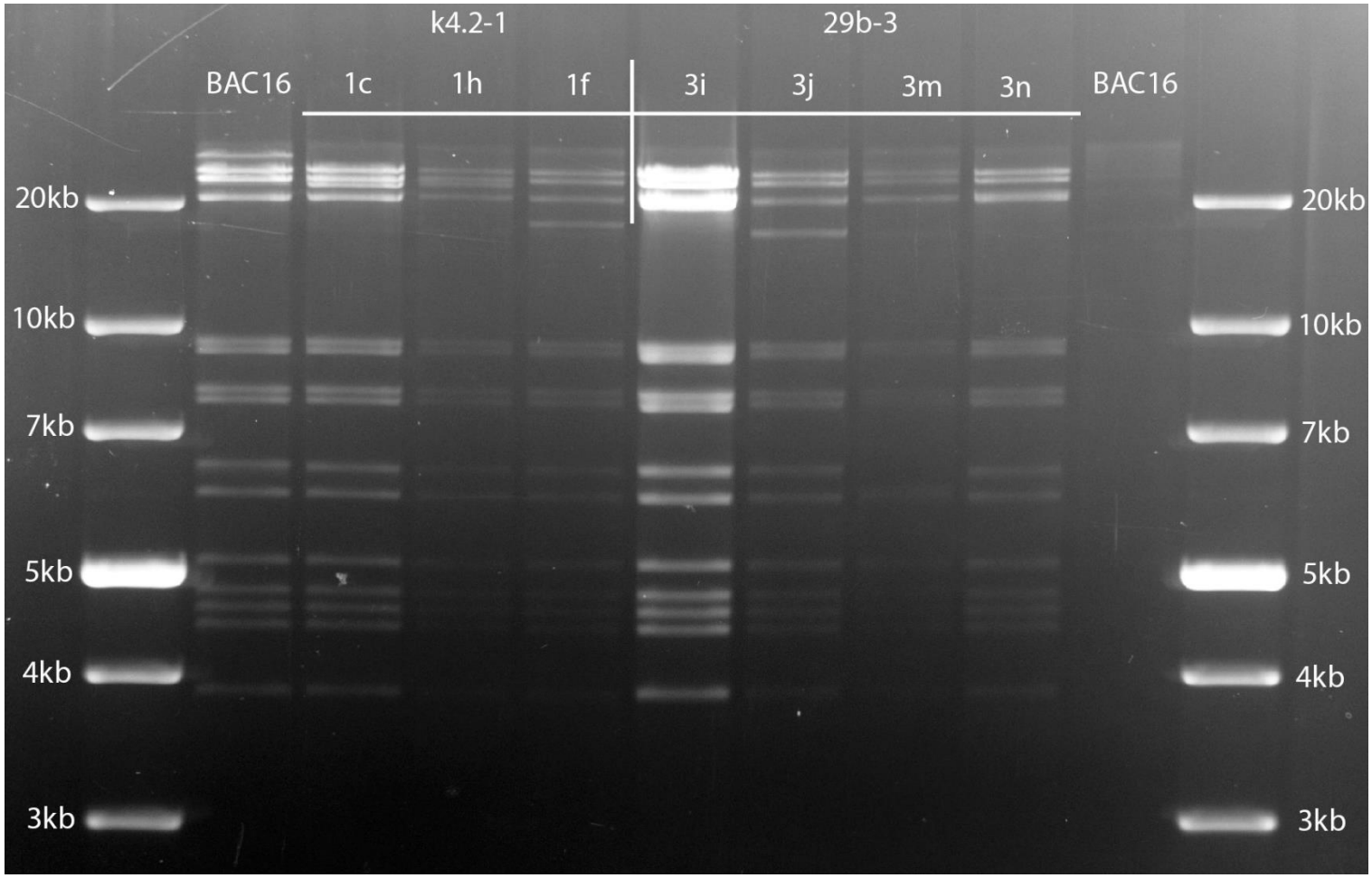

Figure 4: NheI digest of 29b-3 and k4.2-1 2nd HR clones.

Lane 1 is the 1kb plus ladder from gene ruler. Lane 2 is the BAC16. Lane 3-5 are k4.2-1 colonies 1c, 1h, and 1f respectively. Lanes 6-9 are ORF29b-3 colonies 3i, 3j, 3m respectively. Lane 10 is the BAC16. Lane 11 is the 1kb plus ladder from gene ruler.

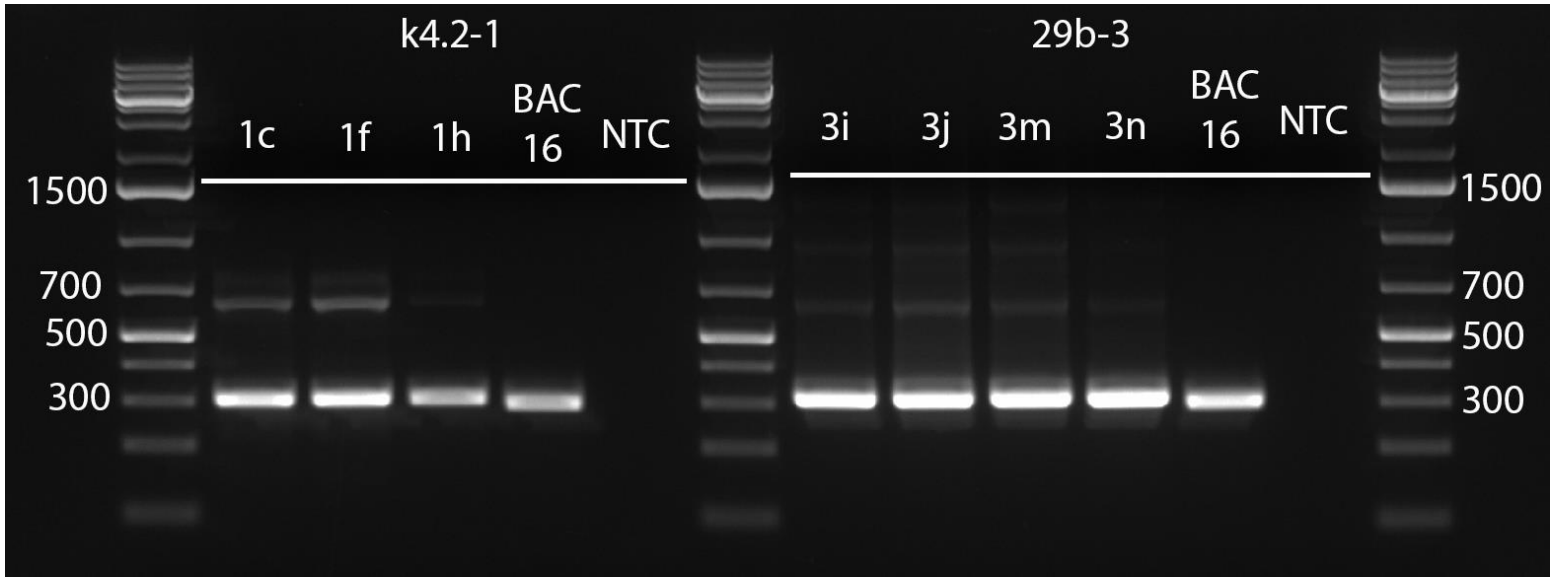

Figure 5: PCR of k4.2-1 and 29b-3 2nd HR clones.

Lane 1 is the 1kb plus gene ruler. Lane 2-4 is the PCR product from the k4.2-1 2nd HR clones using the k4.2 F/R primers. Lanes 5 and 6 are PCR products of the BAC16 and NTC using the k4.2 F/R primers. Lane 7 is the 1kb plus gene ruler. Lane 8-11 is the PCR product from the ORF29b-3 2nd HR clones using the ORF29b F/R primers. Lanes 12 and 13 are the PCR products of the BAC16 and NTC using the ORF29b F/R primers. Lane 14 is the 1kb plus gene ruler.

Section II: Creation of mutant-BAC16 iSLK cell lines and general phenotypic observations

Cell lines harboring BAC16, K6 and ORF73

Creation of mutant virus cell lines was accomplished by transfection of BAC DNA into iSLK cells using lipofectamine 2000 (see chapter 2). Transfection of BAC DNA into iSLK cells resulted in significant cell death prior to the application of selection pressure, despite the absence of detectable GFP expression (figure 6-BAC16, compare pre-transfection and 48 hours post-transfection). Selection pressure was applied 2 days after transfection and cells were maintained under selection pressure. We typically observed the first detectable signs of GFP expression over 1 week after transfection (figure 6-BAC16, figure 7-Δk6, figure 8-ΔORF73). Overall, very few cells became GFP+, with an average of 10 cells becoming GFP+ after transfection (overall transfection efficiency of < 0.002%). Cells that did become GFP+ started out swollen, with a distorted morphology (figure 6-BAC16 and figure 7-Δk6 at the 12-day timepoint, and figure 8-ΔORF73 at the 8-day timepoint). Despite their morphology these cells remained GFP+, did not detach from the bottom of the flask, and eventually began to divide (figure 6-BAC16 at the 24-day timepoint, and figure 7-Δk6 at the 19-day timepoint). For the parental BAC16 virus and 90 of the 91 mutant viruses, we were able to expand this minute number of initial transfectants into large populations were all cells harbored the viral genome as determined by GFP expression (figure 6-BAC16 and figure 7-Δk6, 40-days timepoint).

Despite this success, we were unable to create and expand stable populations of cells harboring the ΔORF73 virus (part I-figure 2 yellow box, part I-figure S1, part II-figure 8-ΔORF73). While the initial transfection of ΔORF73 virus resulted in GFP+ cells that were resistant to selection pressure (figure 8-ΔORF73 at the 12 and 21-days timepoint), these cells failed to divide into populations of GFP+ cells (figure 8-ΔORF73, 21 and 36-days post transfection). It is also important to note that the original GFP+ cells that resulted from the transfection of ΔORF73 BAC-DNA into iSLK cells eventually died, likely by apoptosis (figure 8-ΔORF73, 21, 36 and 40-days post transfection). While we did observe what appeared to be GFP+ debris at longer timepoints in the ΔORF73 BAC-DNA transfected sample (figure 8-ΔORF73, 40-days post transfection GFP merge photo), there were no intact cells in the sample and the debris was also RFP+ (figure 8-ΔORF73, 40-days post transfection RFP merge photo). These data led us to interpret the fluorescence observed at 40-days post transfection as autofluorescence (figure 8-ΔORF73, 40-days post transfection GFP and RFP merge photos). We attempted the transfection of ΔORF73 virus several times using multiple independently prepared BAC DNA's, however, we were never able to expand the initial population of GFP+ cells, and the initial GFP+ cells eventually died. This yielded our first ORF category; ORF is essential for cell line generation (part I-figure 2, yellow box, part I-figure S1, figure 9).

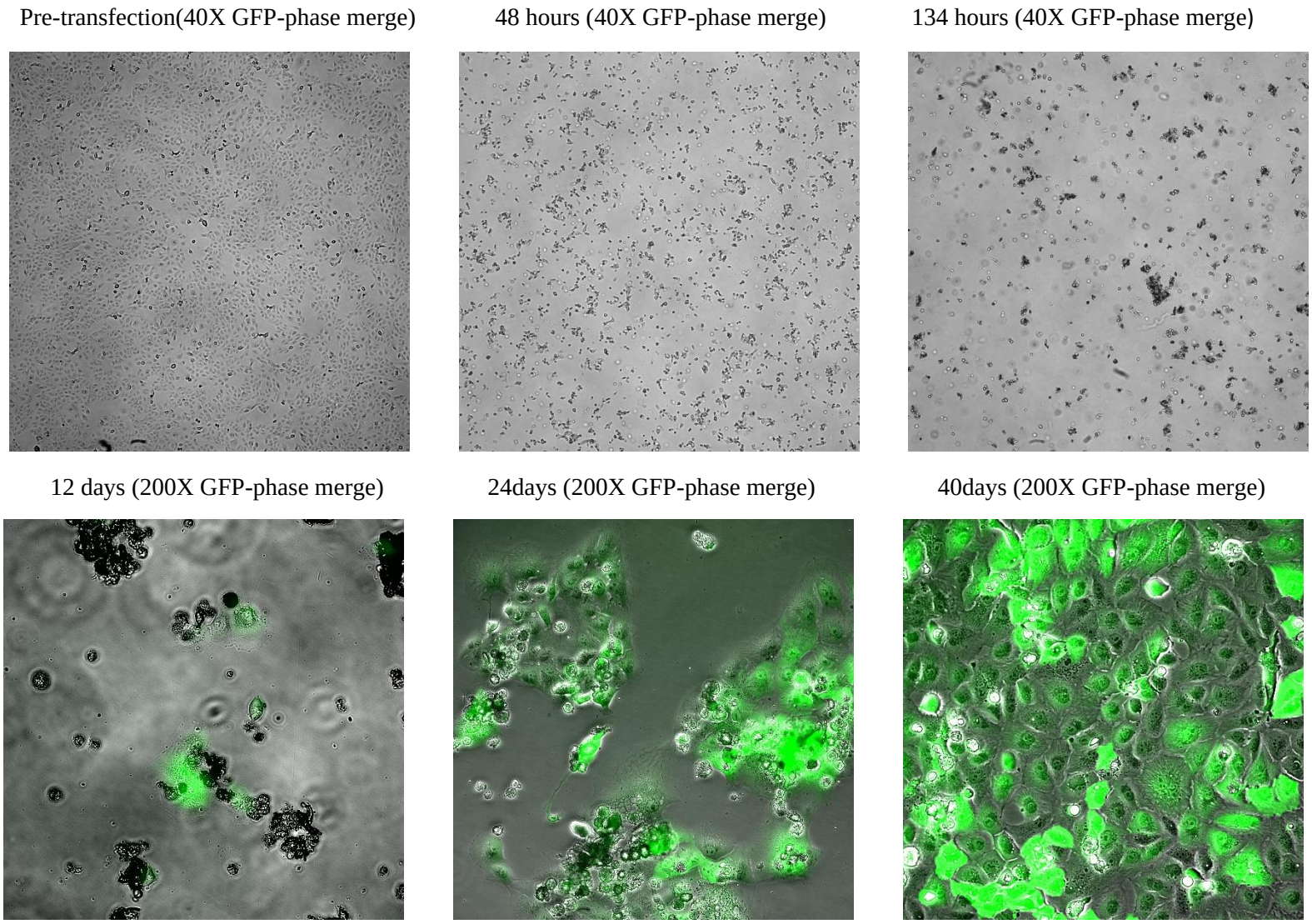

Figure 6: BAC16 transfection into niave iSLK cells at various times post transfection. Total magnification and color chanels listed for each photo. Each photo is a merge of GFP and phase chanels.

Pre-transfection(40X GFP-phase merge)

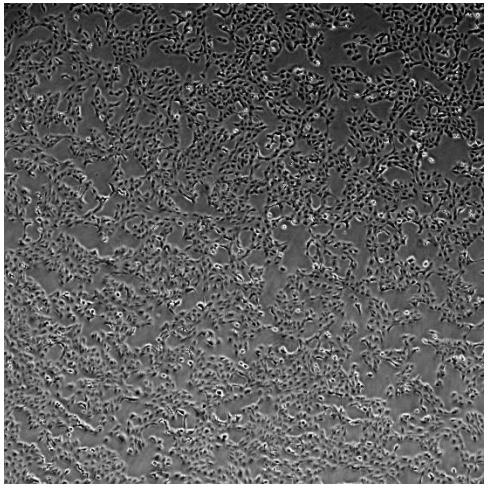

8 days (40X GFP-phase merge)

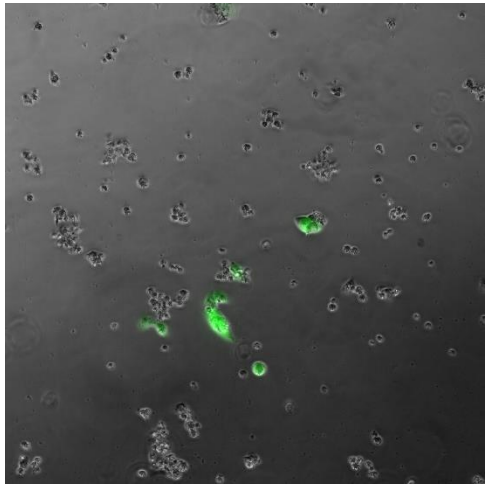

19 days (40X GFP-phase merge)

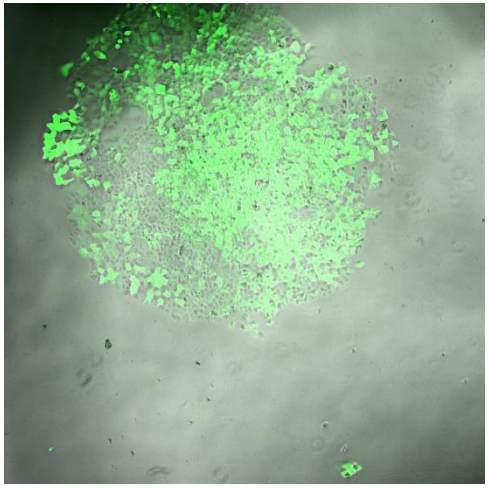

40 days (40X GFP-phase merge)

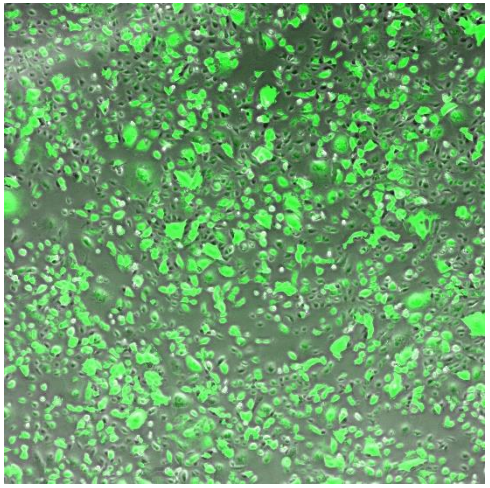

Figure 7: Δk6 transfection into niave iSLK cells at various times post transfection. Total magnification and color chanels listed for each photo. Each photo is a merge of GFP and phase chanels.

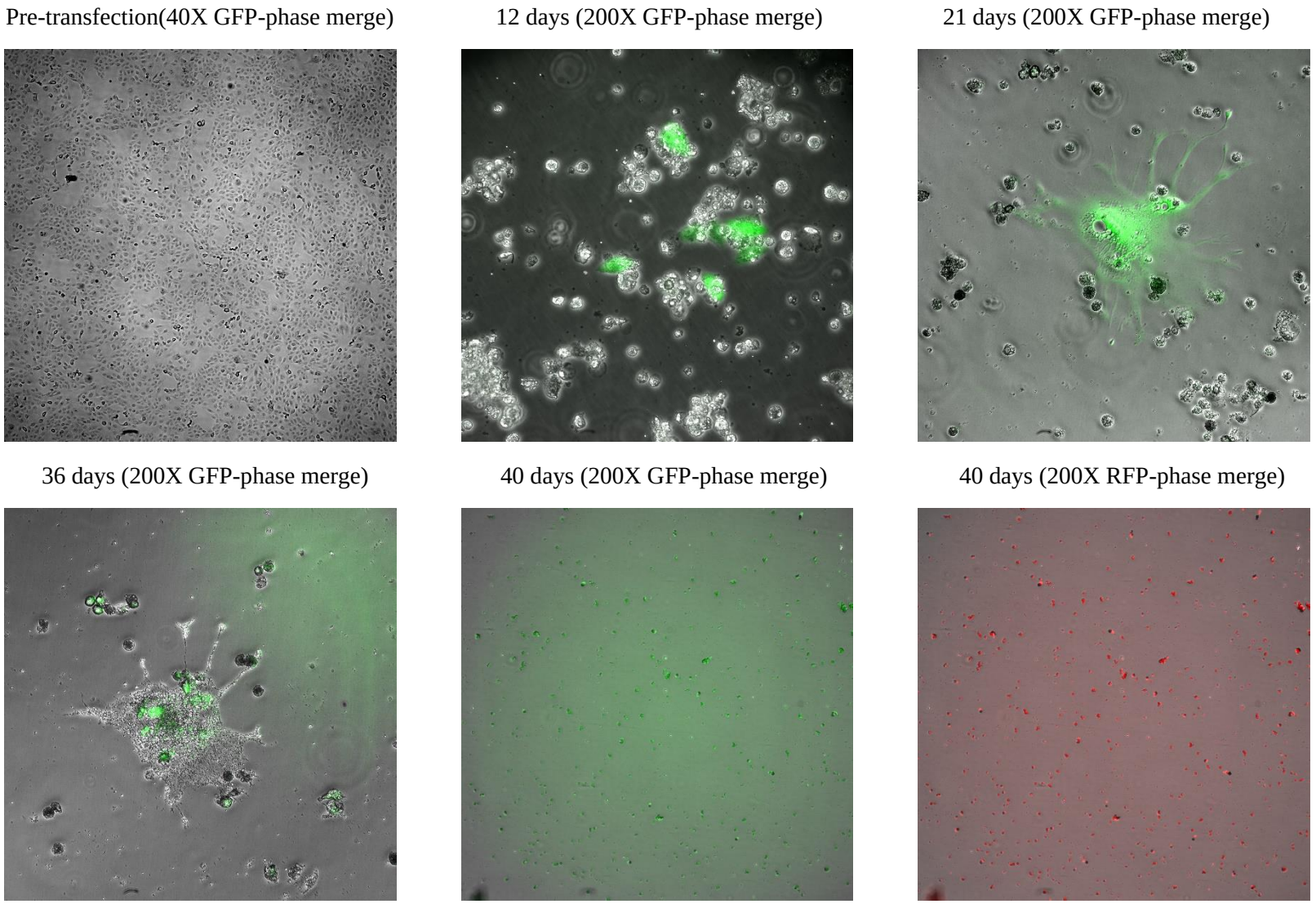

Figure 8: ΔORF73 transfection into niave iSLK cells at various times post transfection. Total magnification and color chanels listed for each photo. Each photo is a merge of GFP or RFP and phase chanels

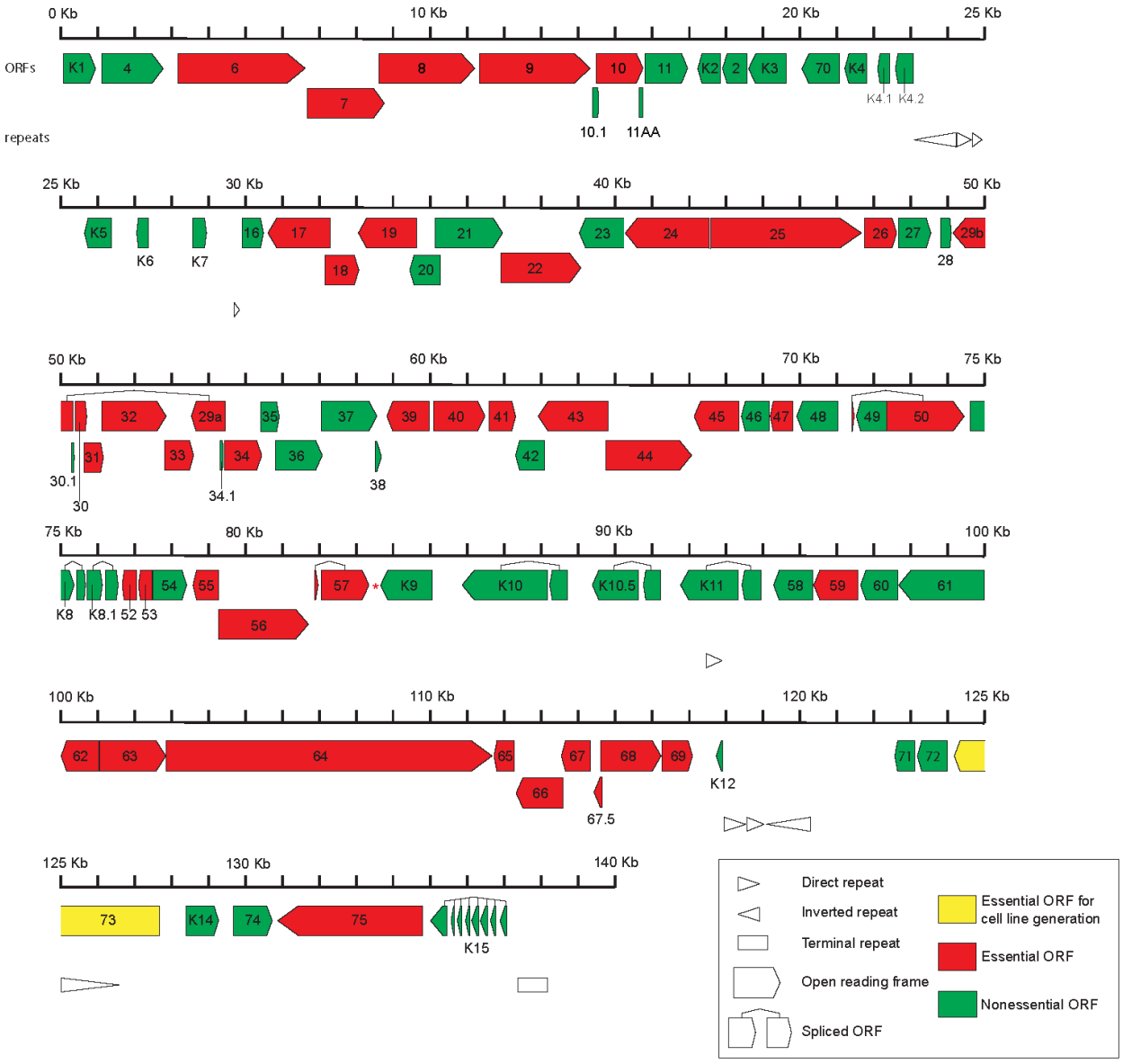

Figure 9: Genome map of KSHV:

ORFs mutated in this study are indicated by boxed arrows, and the arrow indicates the direction of the ORF. ORFs are color coded according to their in ability to generate cell lines and infectious progeny. ORFs colored by yellow boxes can not generate cell lines when mutated, ORFs colored by red boxes can not generate infectious progeny when mutated, and ORFs colored by green boxes can generate infectious progeny when mutated.

Induction phenotype classification of BAC16-iSLK cell lines

General induction phenotype for BAC16 transfected cells was characterized by the rounding, swelling and detachment of cells, as well as the elongation/distortion of morphology for cells that remianed attached to the flask. We observed about a 50% reduction in confluence over the 4-day induction period for BAC16 transfected cells (figure 10-BAC16). For mutant-BAC16 transfected cells, we observed a variety of induction phenotypes. One way we characterized induction phenotype was by the stregnth of the phenotype. Some mutant-BAC16 transfected cell lines induced "like BAC16" transfected cells (figure 11-Δk1). Mutant transfected cell lines that induced "like BAC16" where characterized by significant rounding and swelling of cells, most of which remained partially attached to the flask. We also observed a significant population of cells that displayed an elongated phenotype and remained completeley attached to the flask (figure 14-Δk1). Some mutant-BAC16 transfected cells induced "stronger than BAC16" transfected cells (figure 12-**Δ**k6). Stronger induction phenotype was characterized by a complete, or almost complete, clearing of the monolayer (confluency under 20%). Mutant cell lines in the "stronger than BAC16" category showed virtually no cells that remianed attached to the flask at the end of the induction period, and the majority of rounded/swelling cells had lysed (figure 12-Δk6). We rarley observed elongated cells in the "stronger than BAC16" induction phenotype category. Some mutant-BAC16 transfected cells induced "weaker than BAC16" transfected cells (figure 13-**Δ**ORF39). "Weaker than BAC16" induction phenotype was characterized by a significant reduction, or absence, of rounding and swelling cells when compared to the stronger indiuction phenotypes (figure 13-**Δ**ORF39 comapred to figure 12-**Δ**k6 and figure 11-Δk1, and figure 10-BAC16). Mutants in this category were often characterized by the elongation and distortion of morphology for attached cells, a slight reduction or no reduction in confluency, and sometimes a "swiss-cheese"–like colony morphology (figure 13-**Δ**ORF39).

Some mutant-BAC16 transfected cell lines displayed induction phenotypes that were distinct from BAC16 induced cells. One prominent phenotype we observed in several cell lines was designated "clustering". The "clustering" phenotype was characterized by a "like BAC16" induction phentoype strength, however the colony arrangement of rounding and swelling cells was unique. Instead of seeing the rounding and swelling of cells evenly distributed over the flask, rounding and swelling cells clustered together in distinct foci (figure 14-**Δ**k11 compared to figure 10-BAC16). Another prominent feature of the clustering phenoypte is that the foci of rounding and swelling cells occured on-top of a layer of elongated cells (compare figure 14, 3 days to 4 days). These cell lines often displayed a "swiss-cheese" like colony morphology of rounding and swelling cells that arose from a layer of elongated cells (figure 14-**Δ**k11 and figure 18-**Δ**ORF67)

General Induction phenotype observations

Variability in induced cell line titers

We observed significant differences in viral titer from induced cell lines that were transfected with the same BAC DNA. We created four separate cell lines from "wildtype"

BAC16 DNA, and their induced titers ranged from 1*10^6 IU/ml to 1*10^8 IU/ml. We tested the hypothesis that the variability in cell free progeny generation from cell lines created from the same BAC DNA was due to variability in transfection efficiencies. To do this we created new cell lines by infecting naïve iSLKs with a fixed number of infectious viral particles harvested from each of the "wildtype" BAC16 transfected cell lines. This is to say we infected naïve iSLK cells with cell free progeny at an MOI=1. After infection we applied selection pressure and expanded infected cells into stable populations, induced, harvested, and tittered their supernatants. We only observed a 2-fold variation in titers when cell lines were generated from a fixed number of viral particles (figure 15). Creation of cell lines by infection with a fixed number of viral particles (infection at MOI=1) yielded much closer titers compared to cell lines created by transfection with the same BAC DNA. For this reason, we choose not to report the titers of mutant virus cell lines, as the relative and absolute titers may be misleading. We attribute this variability in titers from cell lines generated by transfection to the fact that each cell line was created from a different number(s) of cells that initially received the BAC DNA successfully and were able to divide (number of successful transfection events), as well as differences in the number of viral genomes each successful transfectant received during transfection.

Induction and virus generation from non-essential mutants

We often needed to generate additional mutant virus stocks from non-essential mutant cell lines during our studies. It was not uncommon for us to observe log-fold changes in cell-free virus generation from the same cell line (generated from the same transfection event) during independent induction events. Virtually all the cell lines displayed lower titers from the second induction event. We calculated fold-changes in titer by (1st induction titer/2nd induction titer) (figure 16). This is to say that cell lines displaying lower titers for the second induction event are represented by large positive fold changes in the graph (figure 16). We do not know the cause of this variability, as each cell line was created from a single transfection experiment. One hypothesis is that the establishment of long-term latency in iSLK cells by mutant-BAC16 viruses is a process that takes many months to fine tune. The longer the transfectants are in culture, the more pronounced and entrenched latency becomes. Mutant-cell lines that generated less progeny from the second induction event (aka large fold changes in figure 16) may have an important reactivation factor lacking. It is important to note that BAC16 transfected cell lines rarely yielded discrepancies in titer from independent induction events, and the discrepancies that were observed were never over 10-fold (data not shown).

Essentiality characterization using conventional tittering and low titer analysis experiments

44 mutant ORF virus cell lines produced no GFP+ signal in fluorescence microscopy and FACS analysis when their induced supernatants were tittered on 293T cells using spinoculation (part I-table 1, part I-figure 2). Note that ORF29 is spliced and represents two distinct mutants. One ORF29 mutant is mutated the upstream transcript, leaving the downstream transcript intact, and the second ORF29 mutant is mutated in the downstream transcript, leaving the upstream transcript intact (see section III, subsection I below). It is important to note that some mutant ORF virus cell lines produced very low levels of GFP+ signal in fluorescence microscopy and/or

FACS analysis when their induced supernatants were tittered on 293T cells. The level of GFP expression was so low that we used an infection and growth-based assay to verify the authenticity of the GFP signal. This is to say we verified the GFP signal was coming from infection of 293T cells with cell free progeny virions, and not from the carry-over of GFP+ debris from induced supernatants (figure 13) (see chapter 2).

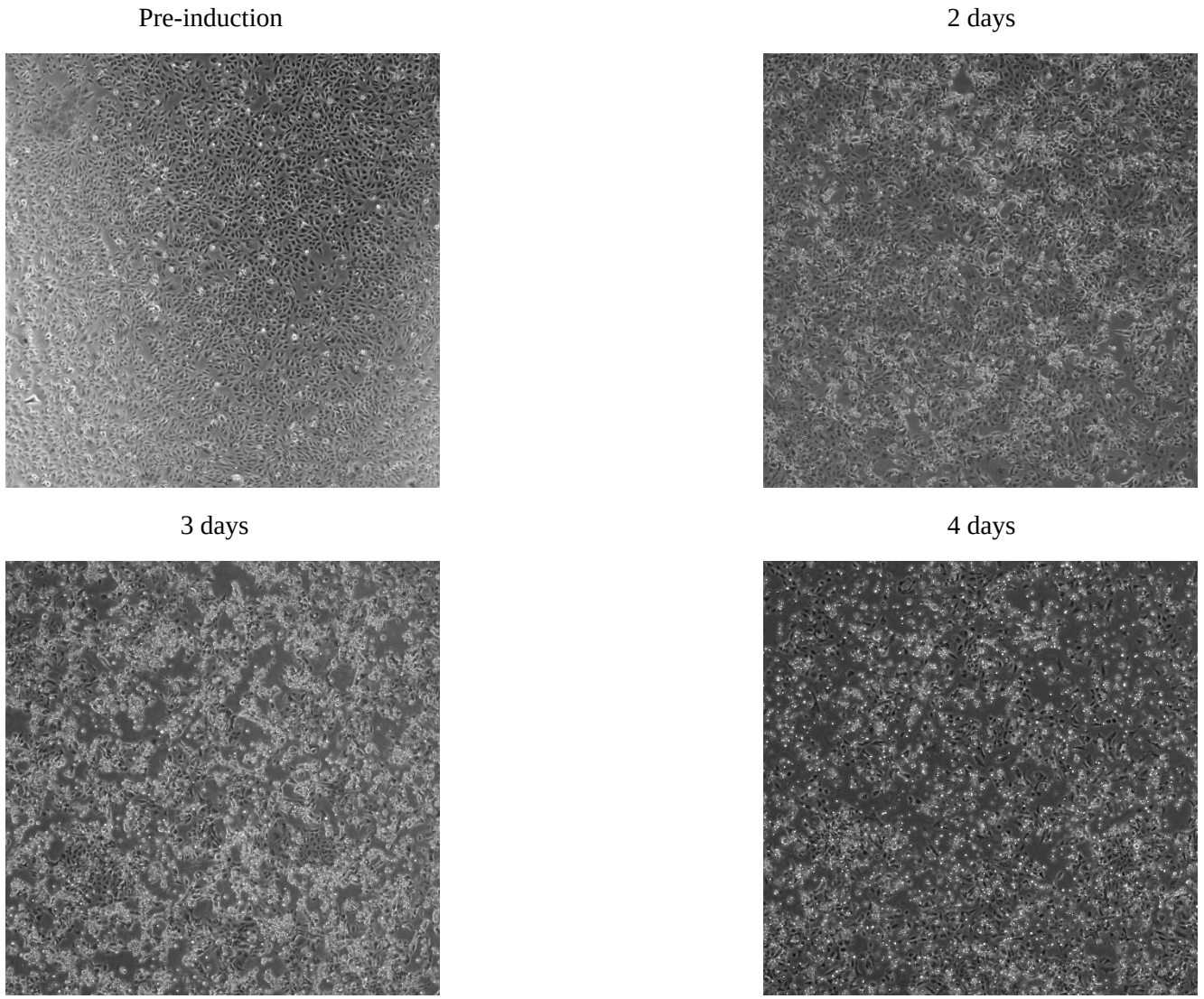

Figure 10: Induced BAC16-iSLK cells at various times post induction. All photos are in phase contrast and have a total magnification of 40X.

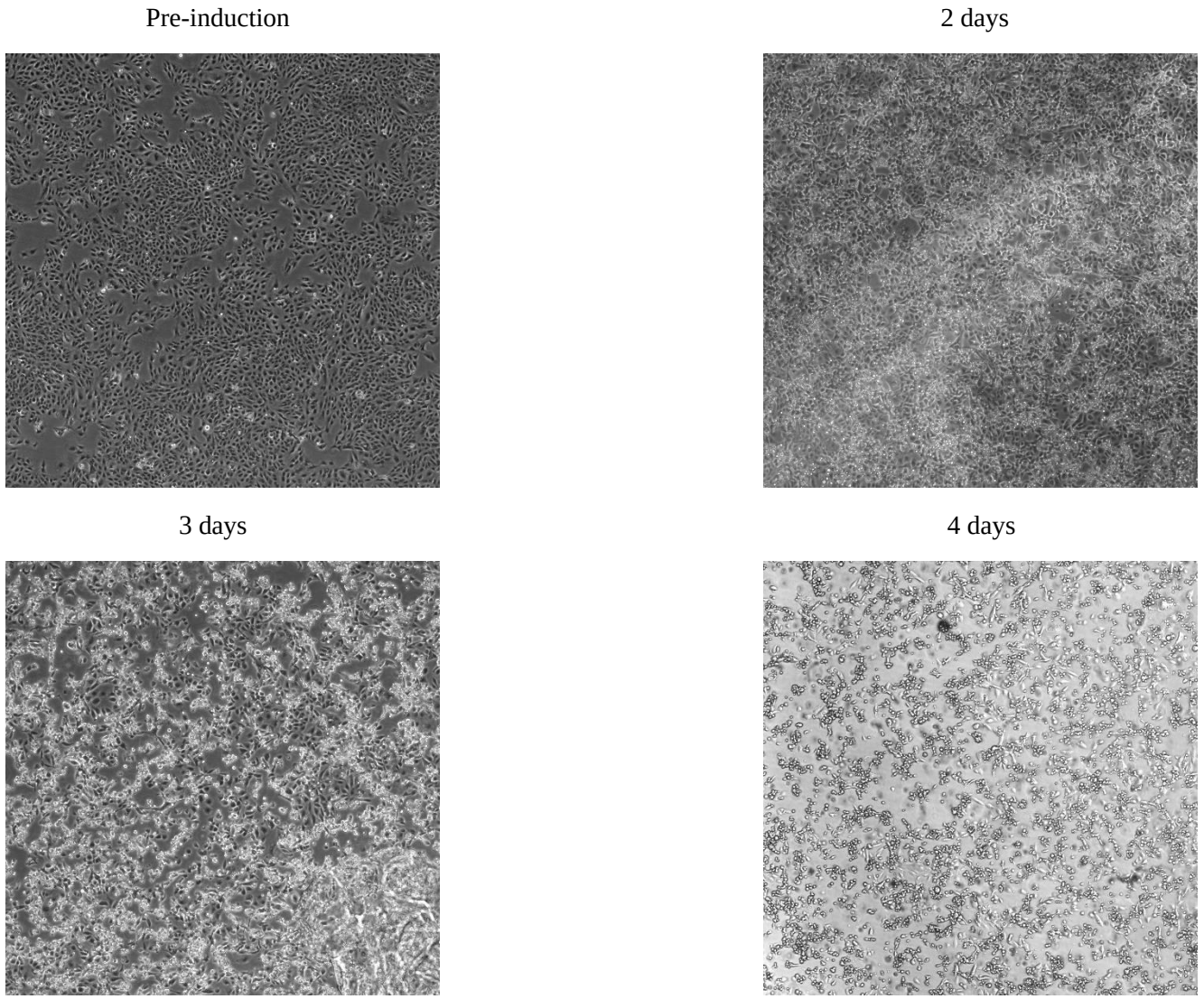

Figure 11: Induced Δk1-iSLK cells at various times post induction. All photos are in phase contrast and have a total magnification of 40X. Induction phenotype is “like BAC16”.

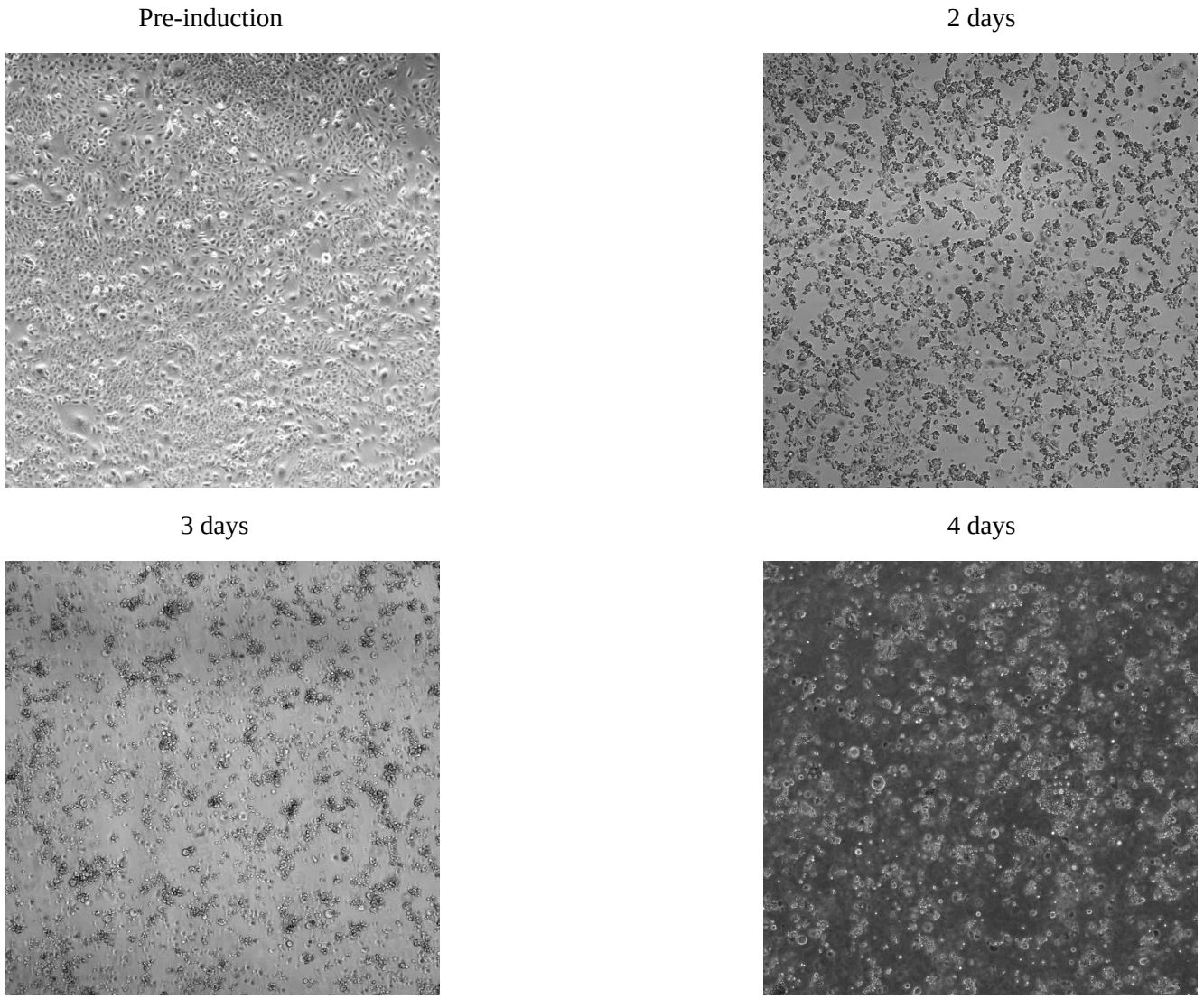

Figure 12: Induced Δk6-iSLK cells at various times post induction. All photos are in phase contrast and have a total magnification of 40X. Induction phenotype is “stronger than BAC16”.

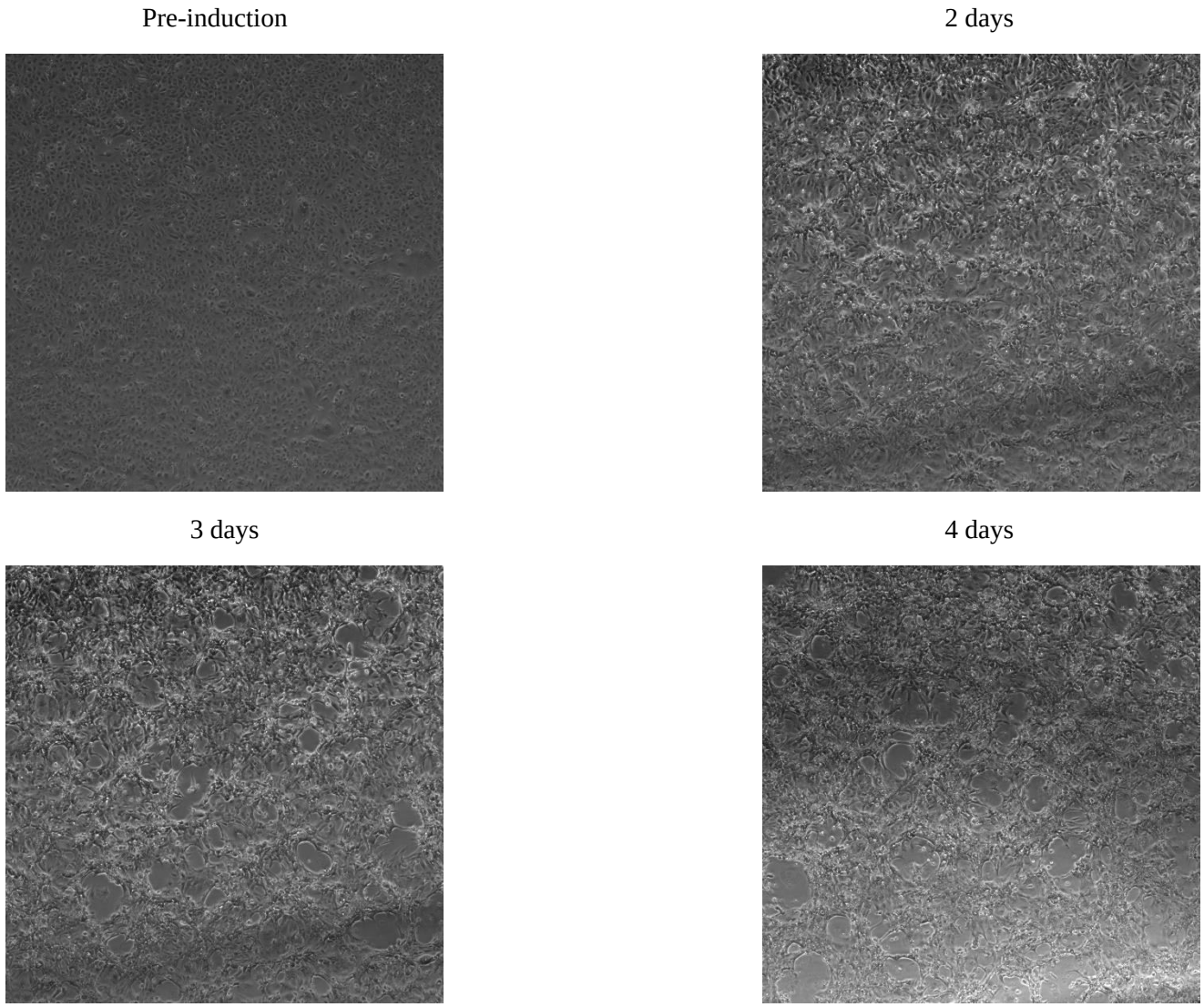

Figure 13: Induced ΔORF39-iSLK cells at various times post induction. All photos are in phase contrast and have a total magnification of 40X. Induction phenotype is “weaker than BAC16”.

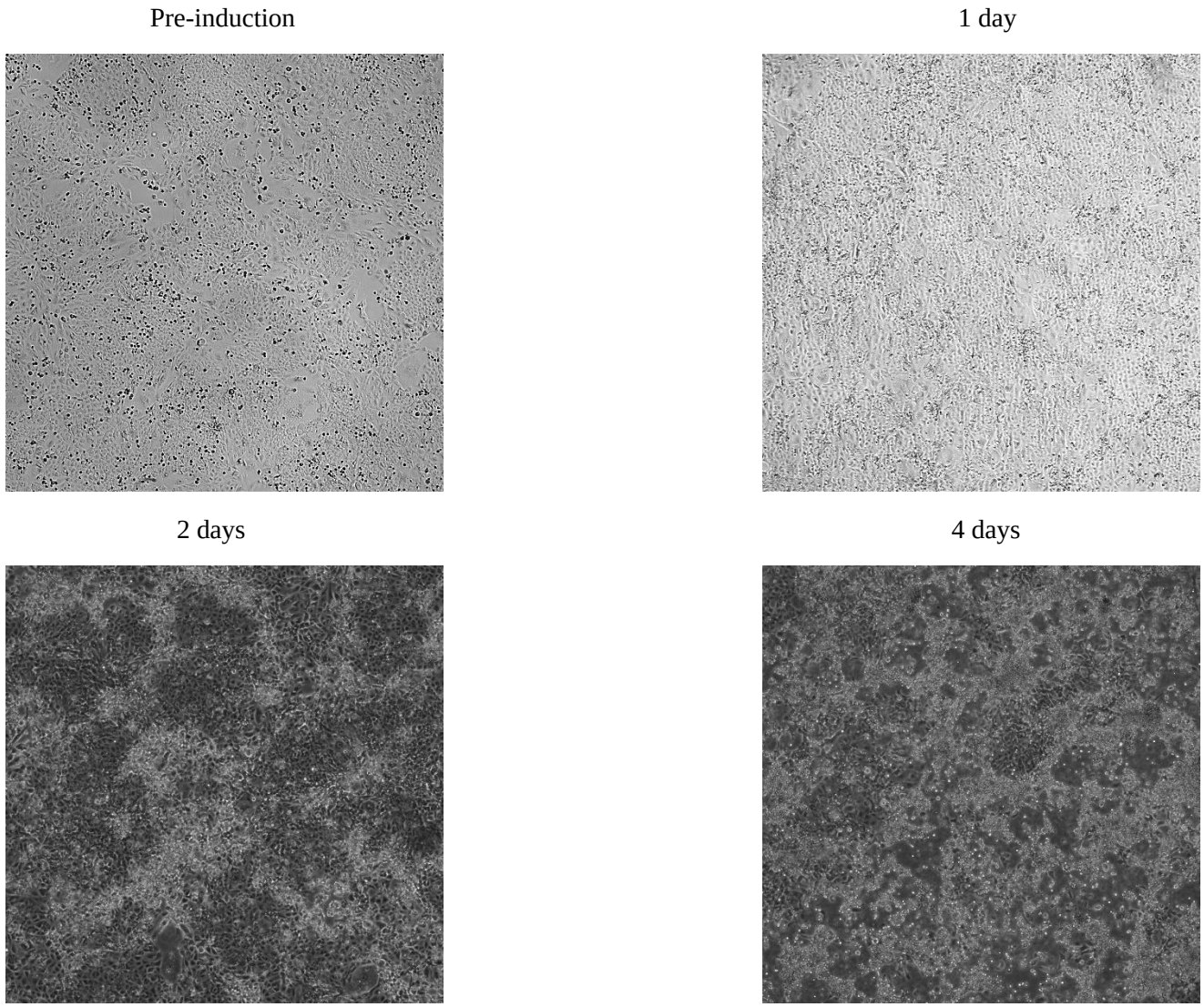

Figure 14: Induced **Δ**k11-iSLK cells at various times post induction. All photos are in phase contrast and have a total magnification of 40X. Induction phenotype is “clustering”.

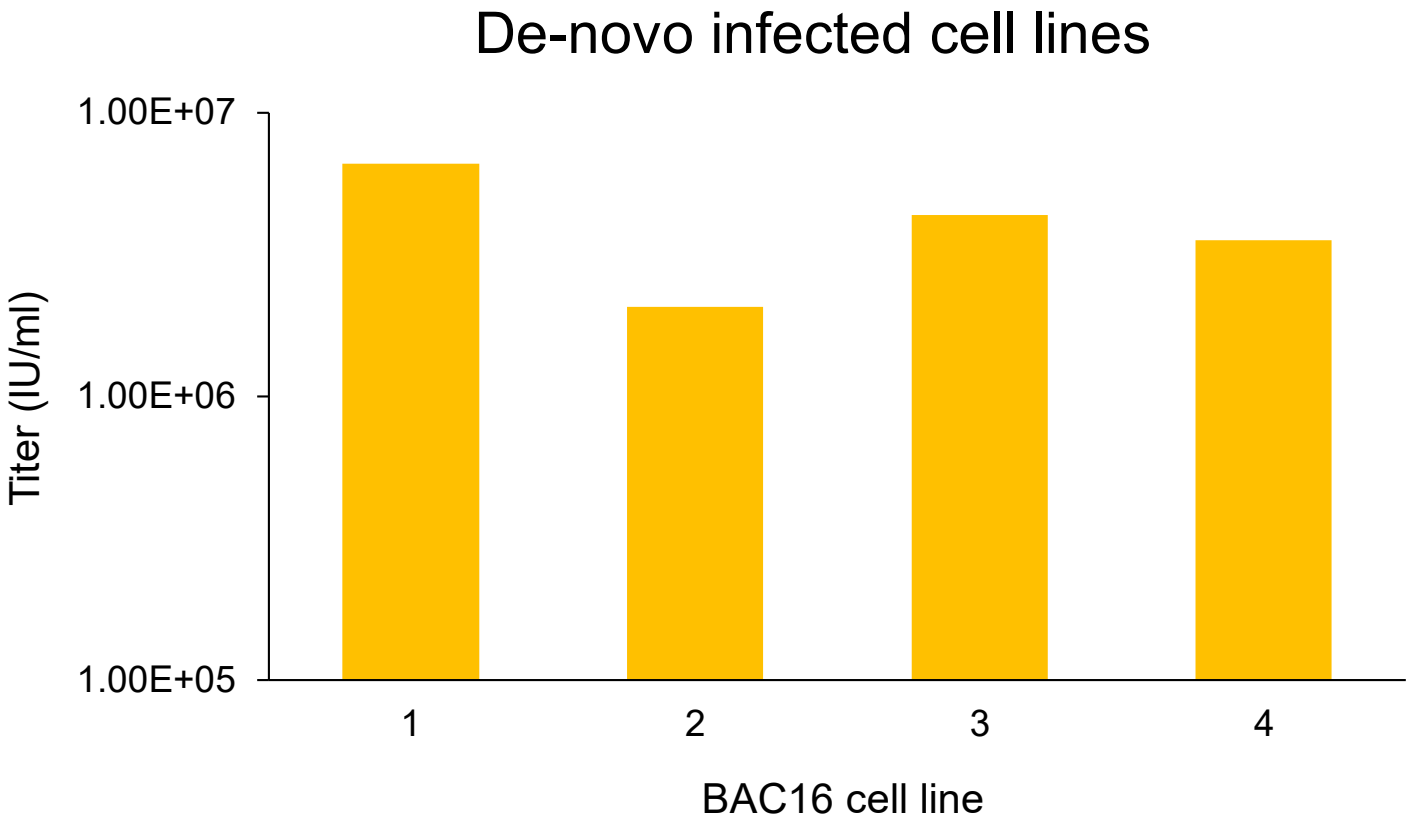

Figure 15: Titers from cell lines created by infection of naïve iSLK cells with "wildtype" BAC16 viruses at an MOI=1. Each BAC16 virus used came from an independently transfected cell line.

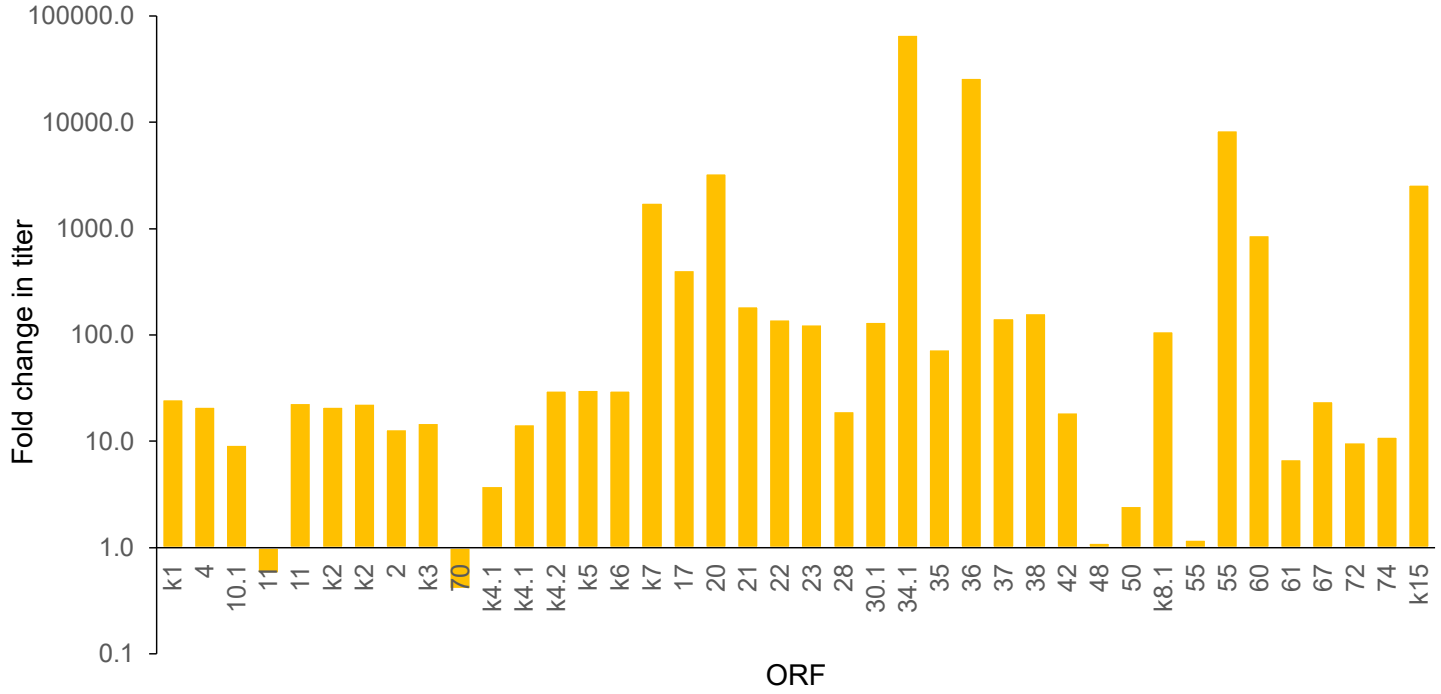

Figure 16: Fold changes in titer observed for the same cell line. The titer obtained from the original induction experiment is divided by the titer obtained from the second induction experiment for each cell line. This is to say that mutant-ORF cell lines that generated significantly reduced titers from the second induction event display large fold changes. ORFs graphed twice represent two cell lines created by transfection with independently prepared BAC DNAs containing the same mutation.

Section III: Phenotypic analysis of essential mutants

Global deletion and stop codon analysis of the JSC-1 derived KSHV BAC 16 genome yielded 44 ORF's that do not produce infectious progeny from transfected cell lines (part I-table 1, part I-figure 2, part II-figure 9). We decided to examine the role of these mutations in reactivation, and capsid assembly and maturation using induction phenotype analysis and transmission electron microscopy (TEM). This section is split into subsections based on the putative functional roles of each KSHV ORF. Subsection I are ORFs speculated to play a role in DNA packaging, capsid maturation, and nuclear egress. Subsection II are ORFs speculated to play a role in DNA replication. Subsection III are ORFs speculated to be core capsid components. Subsection IV are ORFs speculated to play a role in reactivation, and specifically, late gene expression.

Subsection I: DNA packaging, capsid maturation, and nuclear egress

KSHV ORF68:

To examine the role of KSHV ORF68 in reactivation and capsid maturation, we induced the ΔORF68 mutant cell line using sodium butyrate and doxycycline and observed its ability to reactivate for 4 days. The 5' end of ORF68 overlaps with 5' end of ORF67A, so we inserted the 12bp stop sequence at nt. 114596 to make the ΔORF68 mutant. This stop sequence is 9 nucleotides downstream of the annotated start site of ORF68, however, this insertion was still made in a region that overlaps with ORF67A. The insertion occurs 29bp downstream of the ORF67A annotated start site (accession number GQ994935.1) in the opposite orientation. We observed little to no cytopathic effect 2 days post induction, however, a low to moderate level of cell rounding and elongation become evident 3 days post induction. We observed a decrease in confluence from 100% to around 60-70% by 4 days post induction indicating moderate amounts of cell death. The remaining attached cells show an elongated phenotype (figure 17). We categorized this induction phenotype as "weaker than BAC16".

KSHV ORF67:

To examine the role of KSHV ORF67 in reactivation and capsid maturation, we induced the ΔORF67 mutant cell line using sodium butyrate and doxycycline and observed its ability to reactivate for 4 days. The 3' end of ORF67 overlaps with the 5' end of ORF66, so we inserted the 12bp stop sequence at nt. 114319 to make the ΔORF67 mutant. This insertion is 9 nucleotides downstream of the annotated start site and is in a region that does not overlap with other annotated coding regions in the genome (accession number GQ994935.1). We observed little to no cytopathic effect 2 days post induction. However, 2-3days post induction showed a dramatic increase in the number of rounding and swelling cells.By 4 days post induction virtually all the cells were rounded. We observed a decrease in confluence from 100% to around 30-40% by 4-days post induction, indicating significant amounts of cell death. However, we did not observe a base-layer of elongated cells. All attached cells were rounded and displayed a

unique colony morphology at 4dpi (figure 18). We categorized this induction phenotype as "clustering".

KSHV ORF29:

KSHV ORF29 is a spliced transcript containing the ORF29b and ORF29a exons. The intervening seqeuence contains ORF30, ORF31, ORF32, and ORF33 on the opposite strand (figure 9). The ORF29b exon does not overlap with any annotated ORF's, however, we inserted a 12bp stop codon at nt. 50226, which is 9 nucletodies dowstream of the annoated 5' splice-acceptor site (figure 9). The ORF29a exon overlaps with a known polycistronic transcipt encoding ORF34-ORF37. Specifically, ORF29a overlaps the ORF34 start codon, and a 29 amino acid upstream ORF (uORF) called 34.1 (figure 9). We inserted a 12bp stop codon at nt. 54484, which is 9 neclutodies downstream of the annoated start site of ORF29 and overlaps the uORF by 2 nucleotides and the known ORF34-ORF37 transcipt by 109 bp. It should be noted that the stop is inserted upstream of the the ORF34 start codon (in the 5' leader seqeunce of the transcript) and in the reverse orientaion (accession number GQ994935.1). To examine the role of KSHV ORF29 in reactivation and capsid maturation we induced the ΔORF29b mutant cell line using sodium butyrate and doxycycline and observed its ability to reactivate for 4 days. We observed virtually no induction phenotype, and cells continued to grow throughout the induction treatment. Cellular morphology was significantly distorted at 4 days post induction; however, we did not observe any rounding or elongation of cells. The distortion in cellular morphology at 4 days post induction was likely due to the cells overgrowing the monolayer, and not authentic cytopathic effect induced from viral reactivation. Confluence was well over 100% at 4 days post induction, indicating no significant amounts of cell death occurred (figure 19). We classified this induction phenotype as "weaker than BAC16".

Despite observing no cytopathic effect from induction, we imagined the induced cells under the electron microscope. We observed the nuclei of the induced cells very closely and were able to find a handful of nuclei that contained capsid structures. We observed B-capsid structures in the 2 days post induction sample. These capsid structures contained the characteristic ring structure made from scaffolding protein inside of the capsids (figure 20). We believe these are B-capsids because their morphology is more angular as opposed to the more circular pro-capsid species (figure 21).

KSHV ORF7:

To examine the role of KSHV ORF7 in reactivation and capsid maturation we induced the ΔORF7 mutant cell line using sodium butyrate and doxycycline and observed its ability to reactivate for 4 days. ORF7 3' region overlaps with ORF8 5' region, so we inserted the 12bp stop at nt. 6618, which is 9 nucleotides downstream of the annoated start site of ORF7 (accession number GQ994935.1). This insertion does not overlap with other annoated ORFs. We observed significant cytopathic effect characterized by the rounding and swelling of cells by 2 days post induction. This effect was amplified by 4 days post induction with over 50% of the attached cells showing a rounded phenotype. We did not observe a significant amount of elongating cells. The

confluence was reduced from 100% to about 50% over the induction period, indicating significant amounts of cell dealth occurred (figure 22). We classified this induction phenotype as “like BAC16”.

We imaged these cells using an electron microscope and found that the cell nuclei contained large amounts of B-capsids that were scattered throughout the nucleus by 2 days post induction (figure 23). These capsids were angular in shape and contained the characteristic ring structure in the center of the capsid formed by the scaffolding protien (figure 23). By 3 days post induction, capsid structures began to aggreate at the nuclear periphery near the inner nuclear membrane, and by 4 days post induction the number of capsids aggregating near the inner nuclear membrane increased (figure 24). More capsids were observed in nuclei of ΔORF7 (50-100 capsids per nucleues) than in any other sample, and the number of nuclei that contained capsids was also larger than any other sample. KSHV ORF7 is been putativley assinged as part of the viral terminase complex responsible for packaging replicated viral DNA into nascent capsids. Thus, we hypothesize that proper capsid loading is an essential step in nuclear egress.

KSHV ORF32:

To examine the role of KSHV ORF32 in reactivation and capsid maturation we induced the ΔORF32 mutant cell line using sodium butyrate and doxycycline and observed its ability to reactivate for 4 days. The 5’ end of ORF32 overlaps with 3’ end of ORF31, so we inserted the 12bp stop sequence at nt. 51230 to make the ΔORF32 mutant. This stop sequence is 9 nucleotides downstream of the annotated start site of ORF32, however, this insertion was still made in a region that overlaps with ORF31. The insertion occurs 25bp upstream of the ORF31 annotated stop site (accession number GQ994935.1). We observed little to no cytopathic effect 2 days post induction. However, a moderate level of cell rounding/swelling and cell elongation became evident 2 days post induction. These phenotypes progressed through the monolayer through 4 days post induction. We observed a decrease in confluence from 65% to less than 10% by 4 days post induction indicating significant amounts of cell death, and the remaining attached cells show an elongated phenotype (figure 25). We classified this induction phenotype as “like BAC16”.

We viewed all 4 days of induction extensively under TEM; however, we never encountered any capsid species in the nucleus or cytoplasm of induced cells. We did occasionally come across what appeared to be sites of capsid nucleation (figure 26, red box), and sometimes capsid-like structures could be observed (figure 26, red arrows). However, these capsid-like structures lacked defined edges and shape. KSHV ORF32 is putatively assigned as an inner tegument protein that is part of the capsid associated tegument complex (CATC) which caps the tips of pentons at the icosahedral vertices. Thus, we hypothesize that this putative inner tegument protein is an important capsid formation and stability component.

KSHV ORF67.5/67A:

To examine the role of KSHV ORF67.5/67A in reactivation and capsid maturation we induced the ΔORF67.5/67A mutant cell line using sodium butyrate and doxycycline and

observed its ability to reactivate for 4 days. The 5' end of ORF67.5/67A overlaps with 5' end of ORF68, so we inserted the 12bp stop sequence at nt. 114574 to make the Δ ORF67.5/67A mutant. This stop sequence is 51 nucleotides downstream of the annotated start site of ORF67.5/67A and does not overlap with other annotated ORFs (accession number GQ994935.1). We observed virtually no CPE during the 4-day induction course for this mutant. During the induction period cells continued to grow, and by 4 days post induction they had clearly overgrown the monolayer. This overgrowth contributed to the loss of normal iSLK cuboidal morphology, presumably due to overcrowding. There was no rounding/detachment of cells, and no elongation of cells, which are the characteristic cytopathic effects from induction (figure 27). Thus, we characterized this induction phenotype as "weaker than BAC16".

KSHV ORF69:

To examine the role of KSHV ORF69 in reactivation and capsid maturation we induced the ΔORF69 mutant cell line using sodium butyrate and doxycycline and observed its ability to reactivate for 4 days. ORF69 does not overlap with any flanking ORFs so we deleted the entire ORF from the annotated start site to the annotated stop site to make the ΔORF69 mutant. This corresponds to a deletion of 909 nucleotides; from nt 116257-117165 (accession number GQ994935.1). We observed slight elongation of cells by 2-days post induction, and by 3-days post induction the elongation phenotype was evident, and cells began to round and swell. By 4 days post induction virtually all the cells were rounded, and we observed a decrease in confluence from 70% to around 5% indicating significant amounts of cell death (figure 28). Thus, we classified this induction phenotype as "stronger than BAC16".

We viewed this sample under the TEM and found significant amounts of capsid structures in the nuclei of induced ΔORF69 cells. We first observed capsid structures scattered throughout the nuclei of infected cells at 2- and 3-days post induction (figure 29). By day 4 capsids began to aggregate in clusters around the nuclear periphery, but never in proximity to the inner nuclear membrane. Thus, we hypothesize the ORF69 is important for bridging contact between the capsid and the inner nuclear membrane. Despite observing all three capsid species (A/B/C), most capsid structures were B-capsids (figure 29). This makes us speculate that ORF69 may play a role in genome packaging as well.

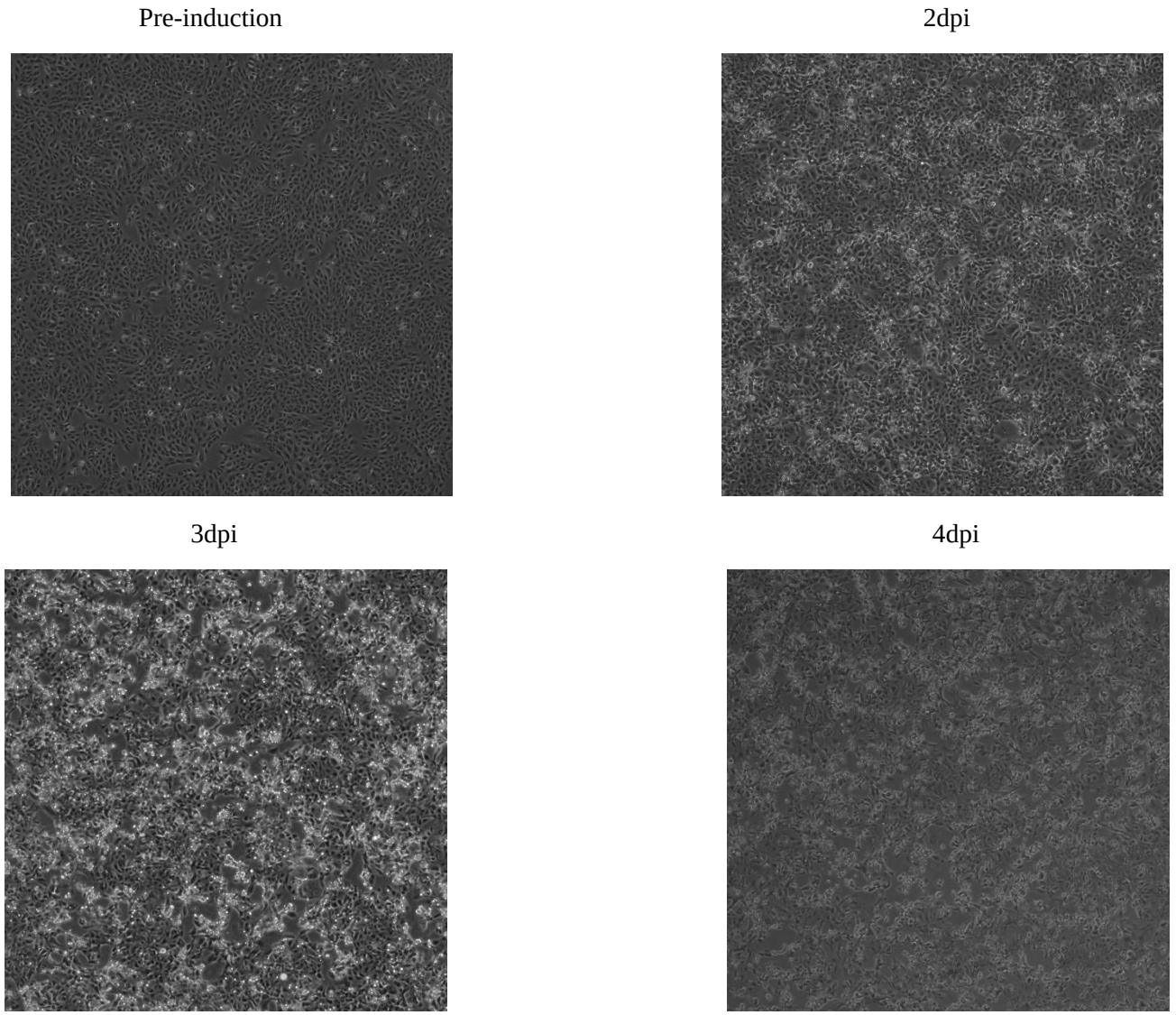

Figure 17: Phase microscopy of ΔORF68 mutant cell-line before and after induction with sodium butyrate and doxycycline.

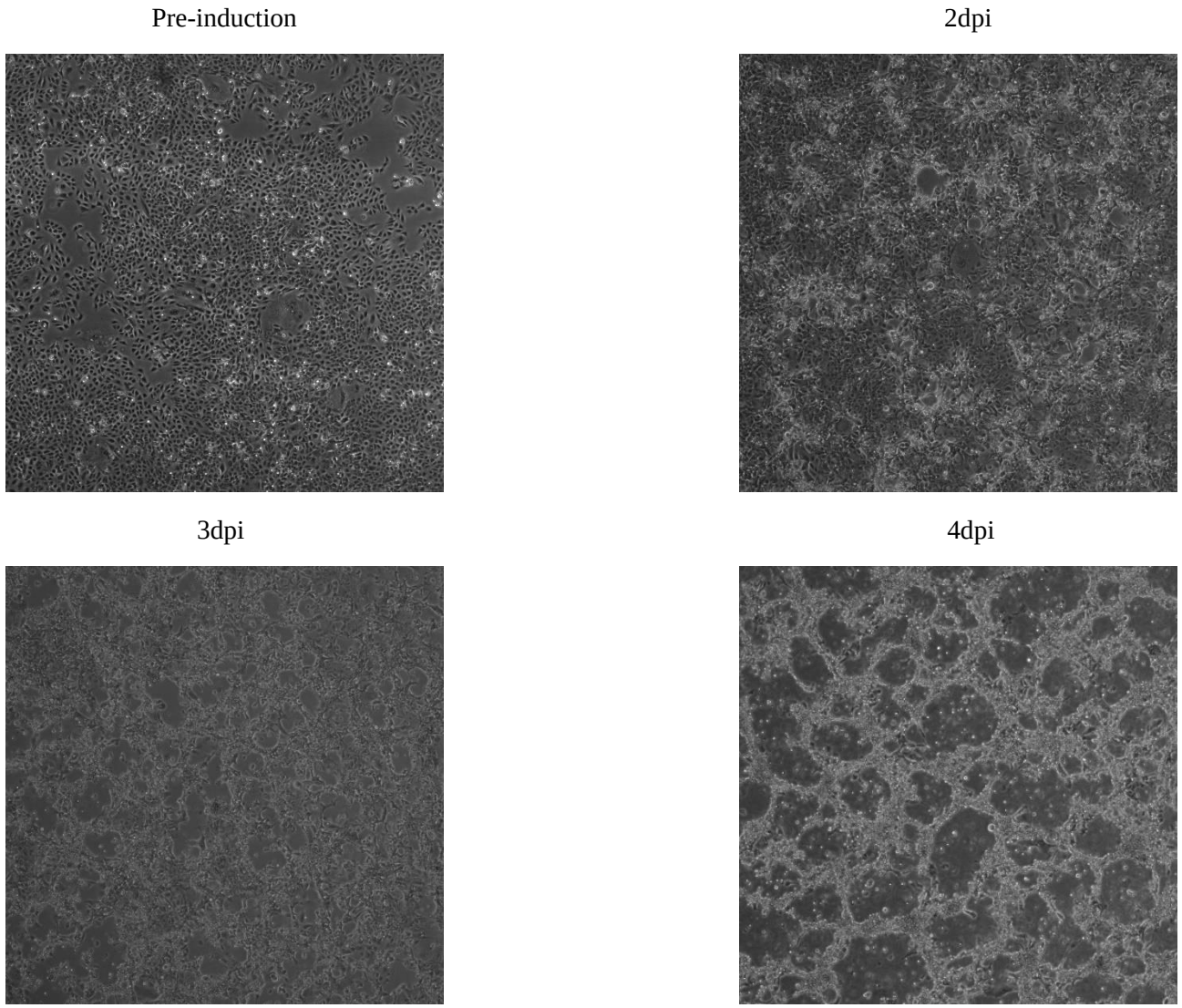

Figure 18: Phase microscopy of ΔORF67 mutant cell-line before and after induction with sodium butyrate and doxycycline.

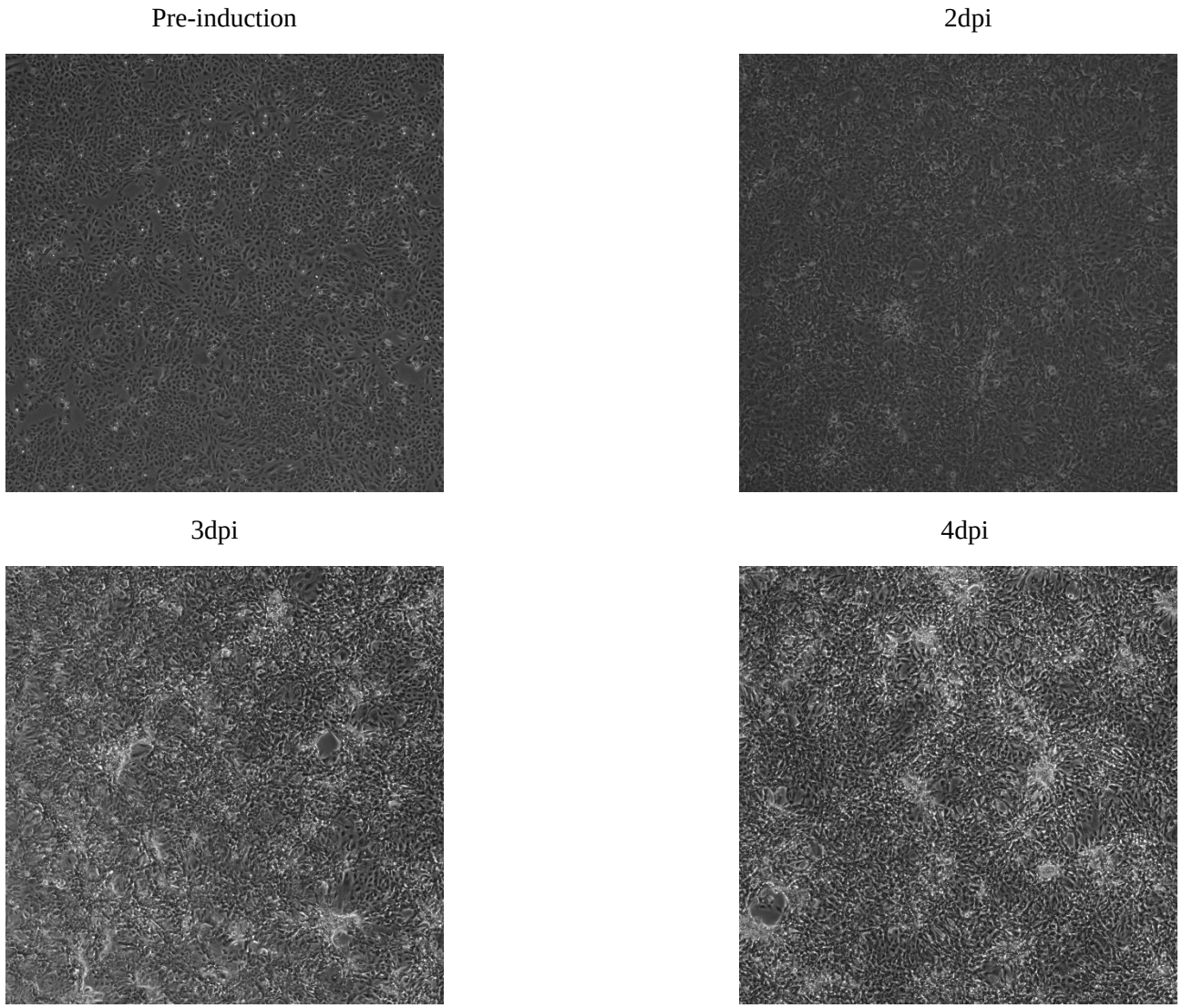

Figure 19: Phase microscopy of ΔORF29b mutant cell-line before and after induction with sodium butyrate and doxycycline.

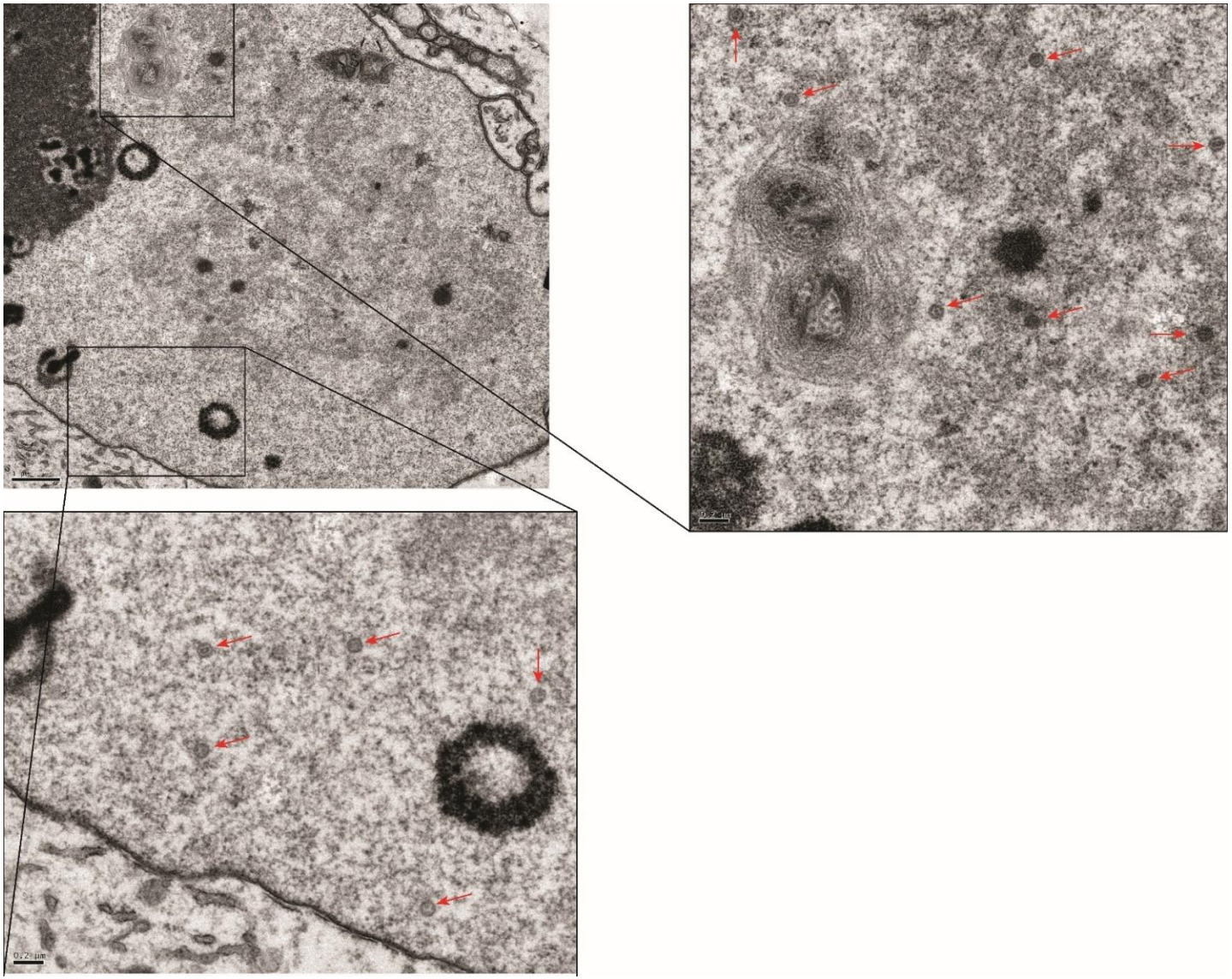

Figure 20: TEM of ΔORF29b mutant cell-line at 2 days post induction. Red arrows indicate capsid structures. Scale bars are in micrometers.

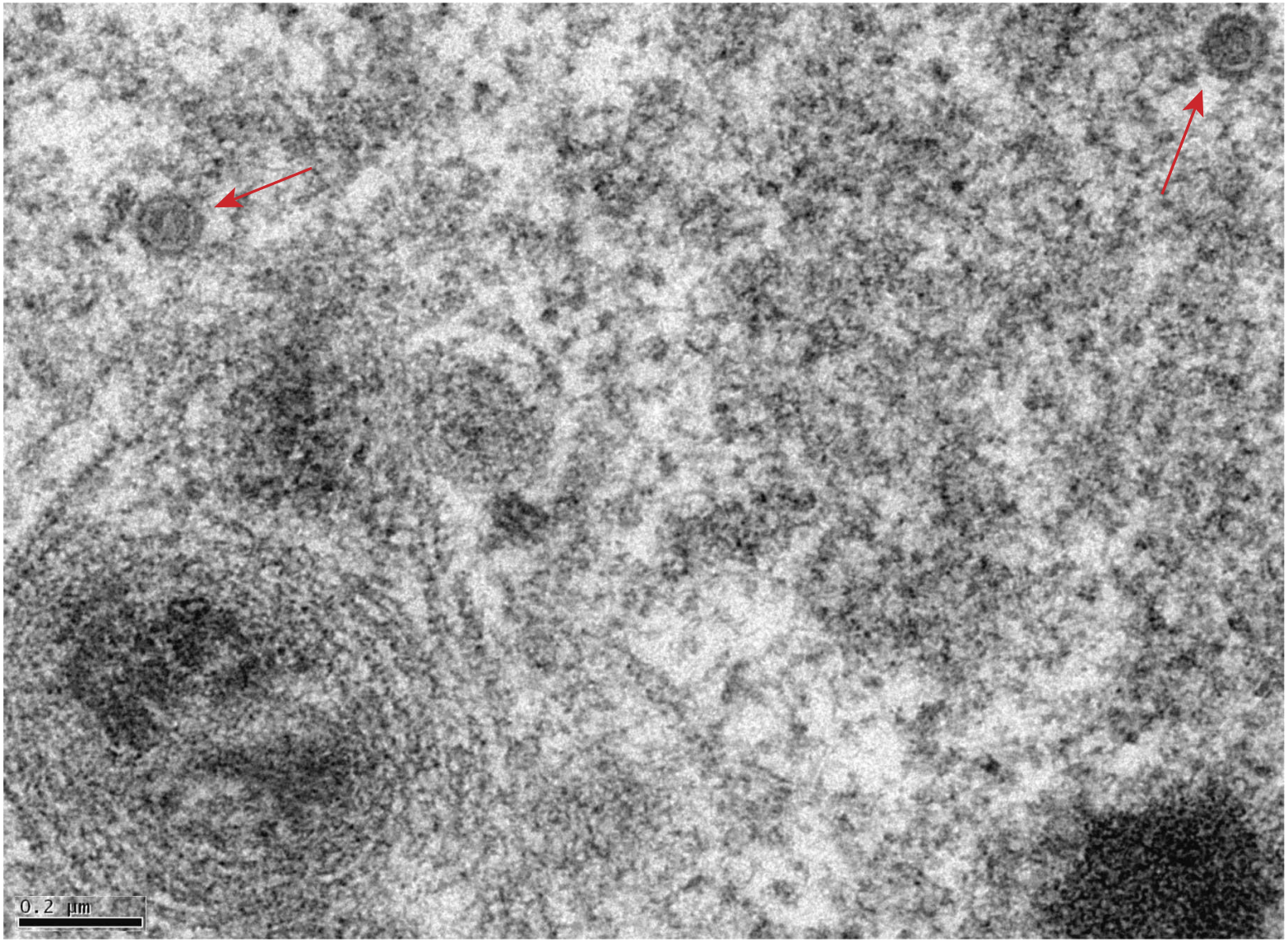

Figure 21: TEM of angular shape of capsids in the ΔORF29b mutant cell-line at 2 days post induction. Red arrows indicate capsid structures. Scale bars are in micrometers

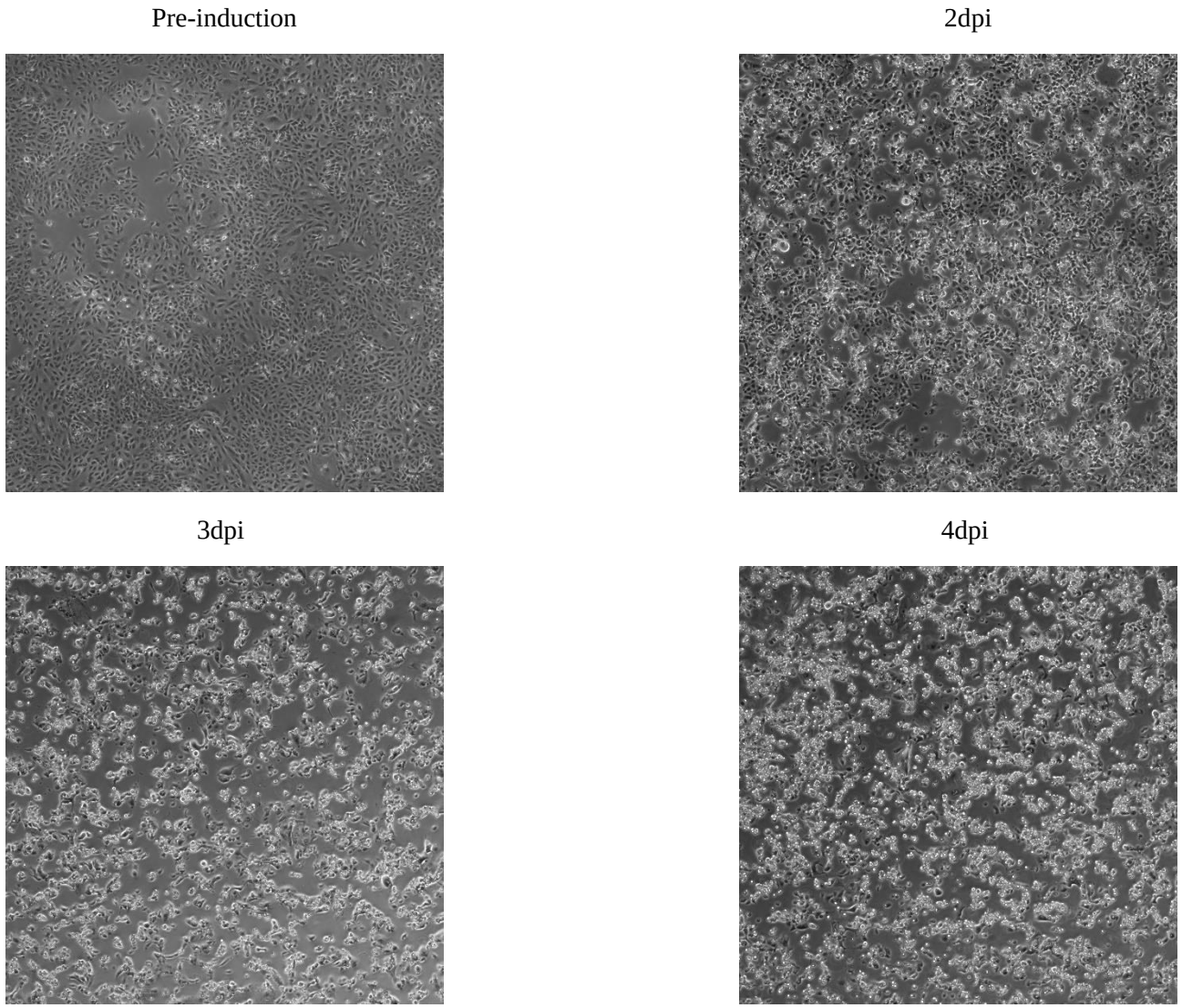

Figure 22: Phase microscopy of ΔORF7 mutant cell-line before and after induction with sodium butyrate and doxycycline

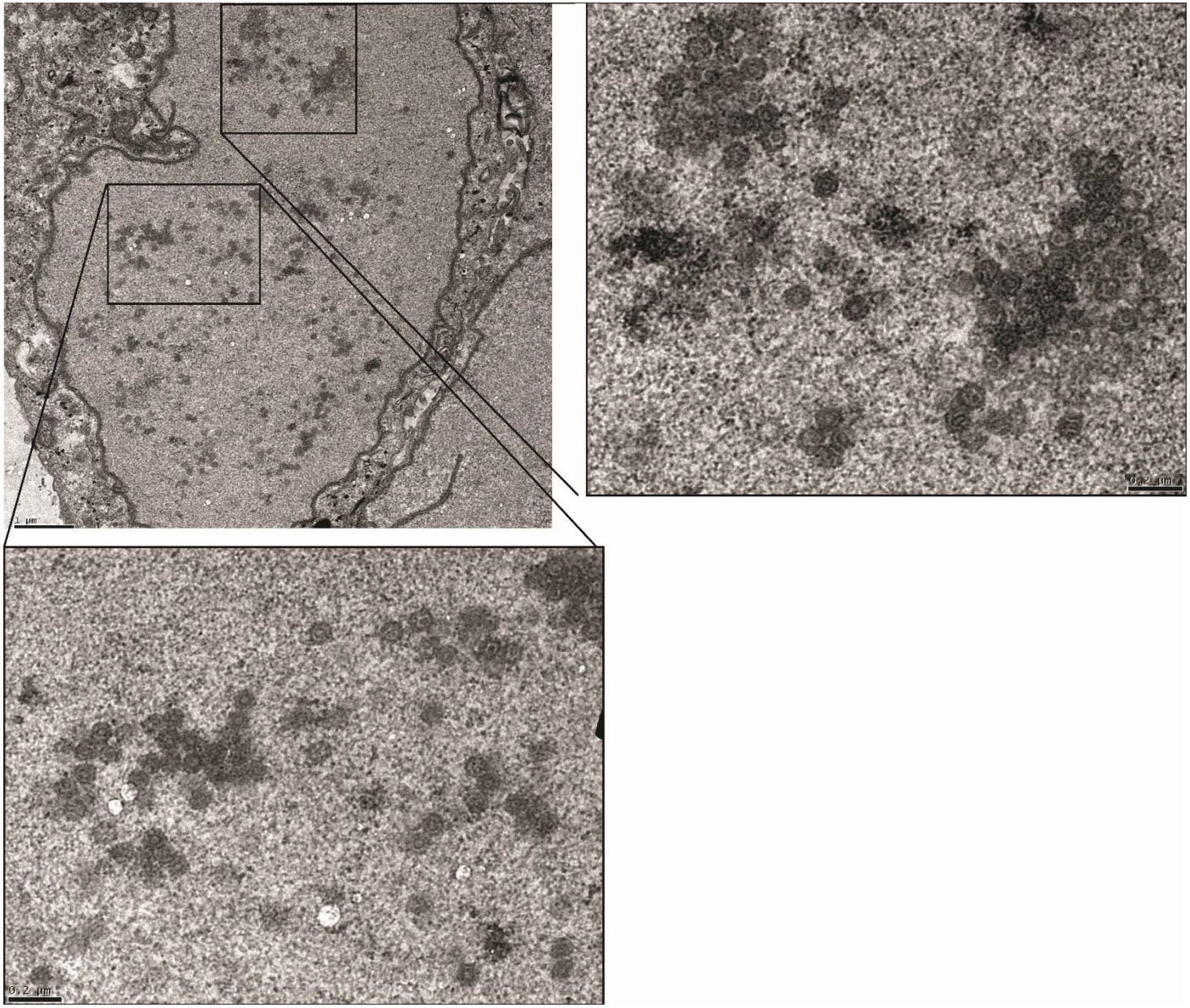

Figure 23: TEM of angular shape of capsids in the ΔORF7 mutant cell-line at 2 days post induction. Scale bars are in micrometers.

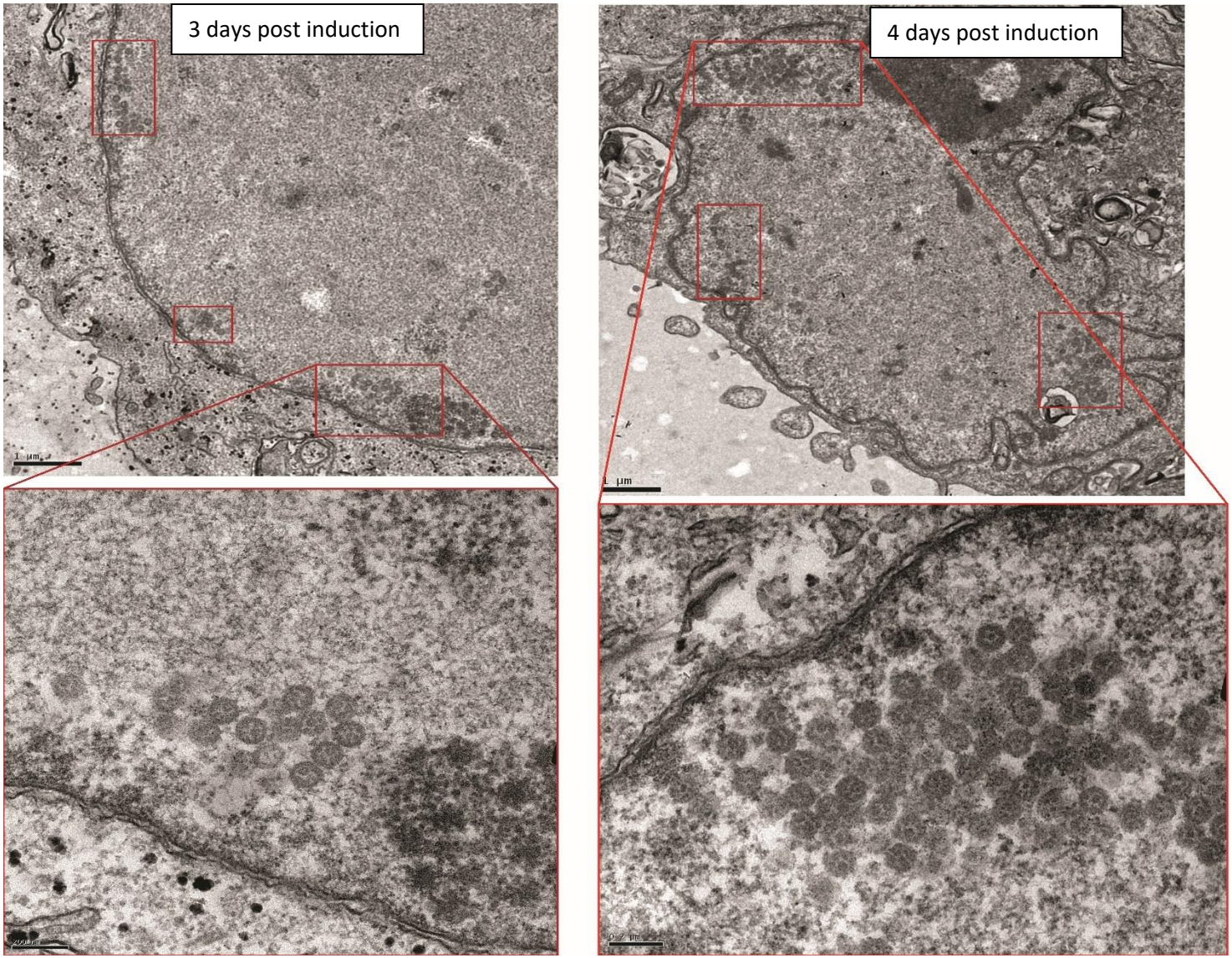

Figure 24: TEM of capsids aggregating along the inner nuclear membrane in the ΔORF7 mutant cell-line at 3 and 4 days post induction. Scale bars are in micrometers. Red boxes indicate locations of capsid aggregation.

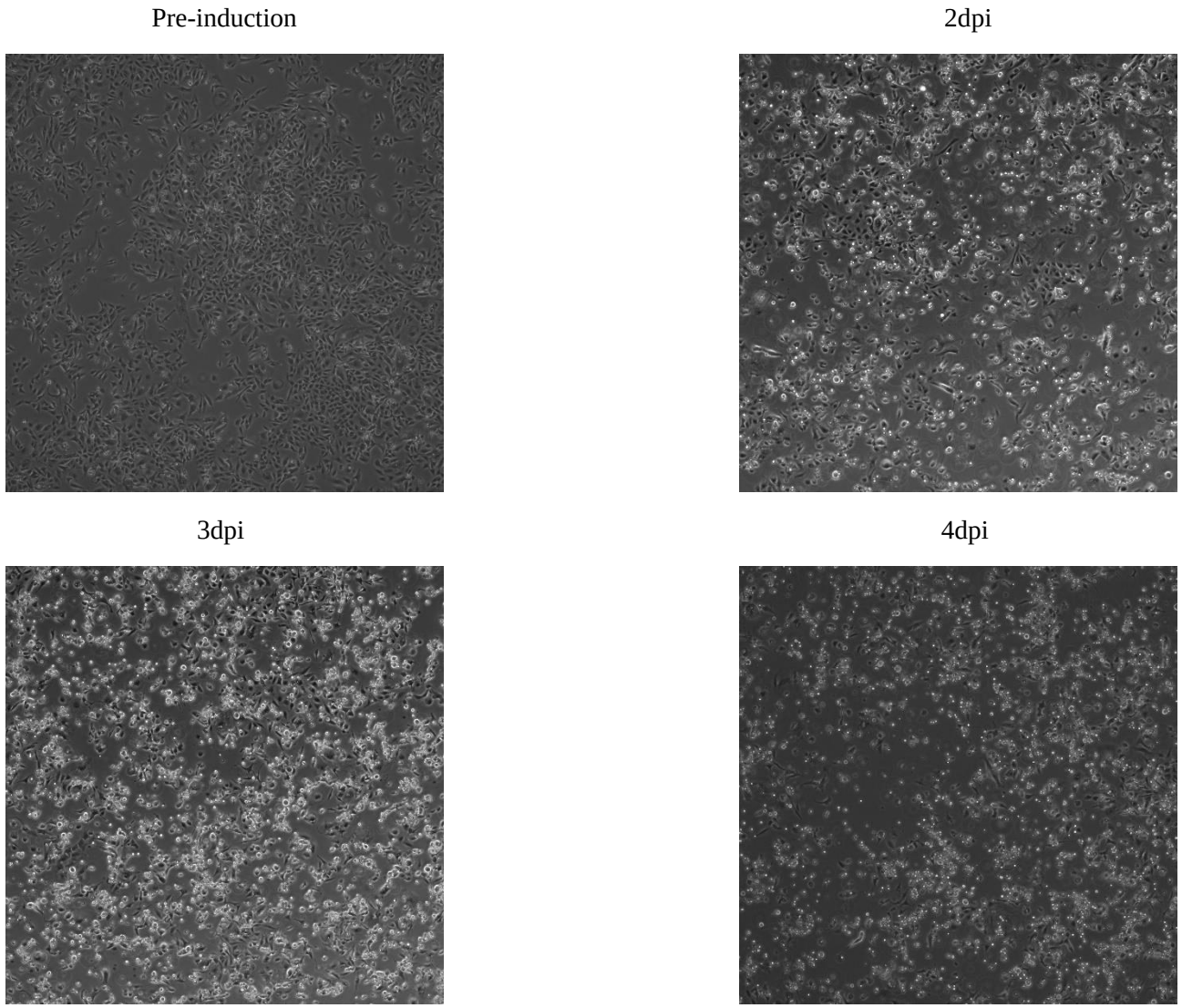

Figure 25: Phase microscopy of ΔORF32 mutant cell-line before and after induction with sodium butyrate and doxycycline.

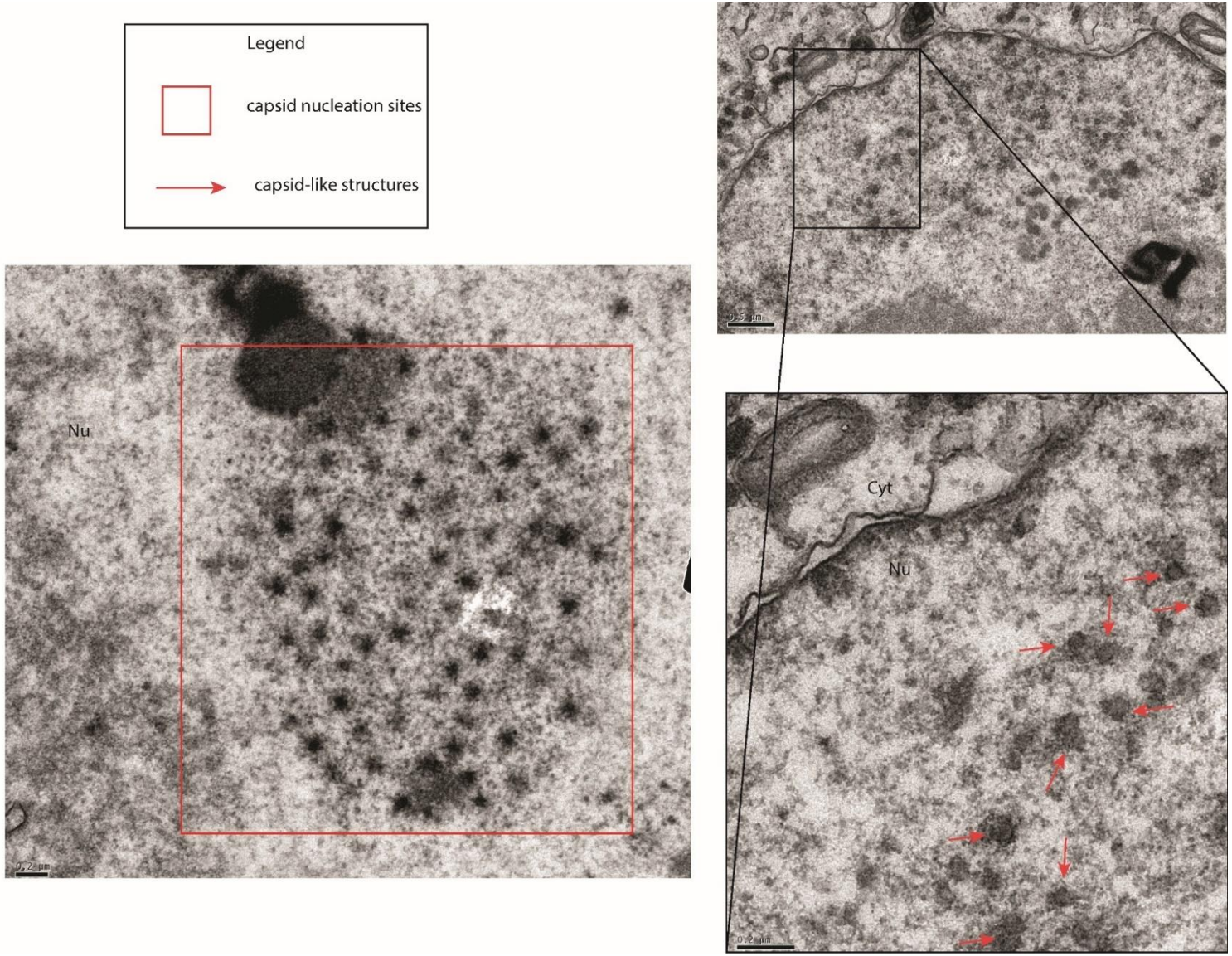

Figure 26: TEM of induced ORF32 cell lines. Capsid assembly sites are indicated by a red box. Partially formed capsids are indicated by red arrows.

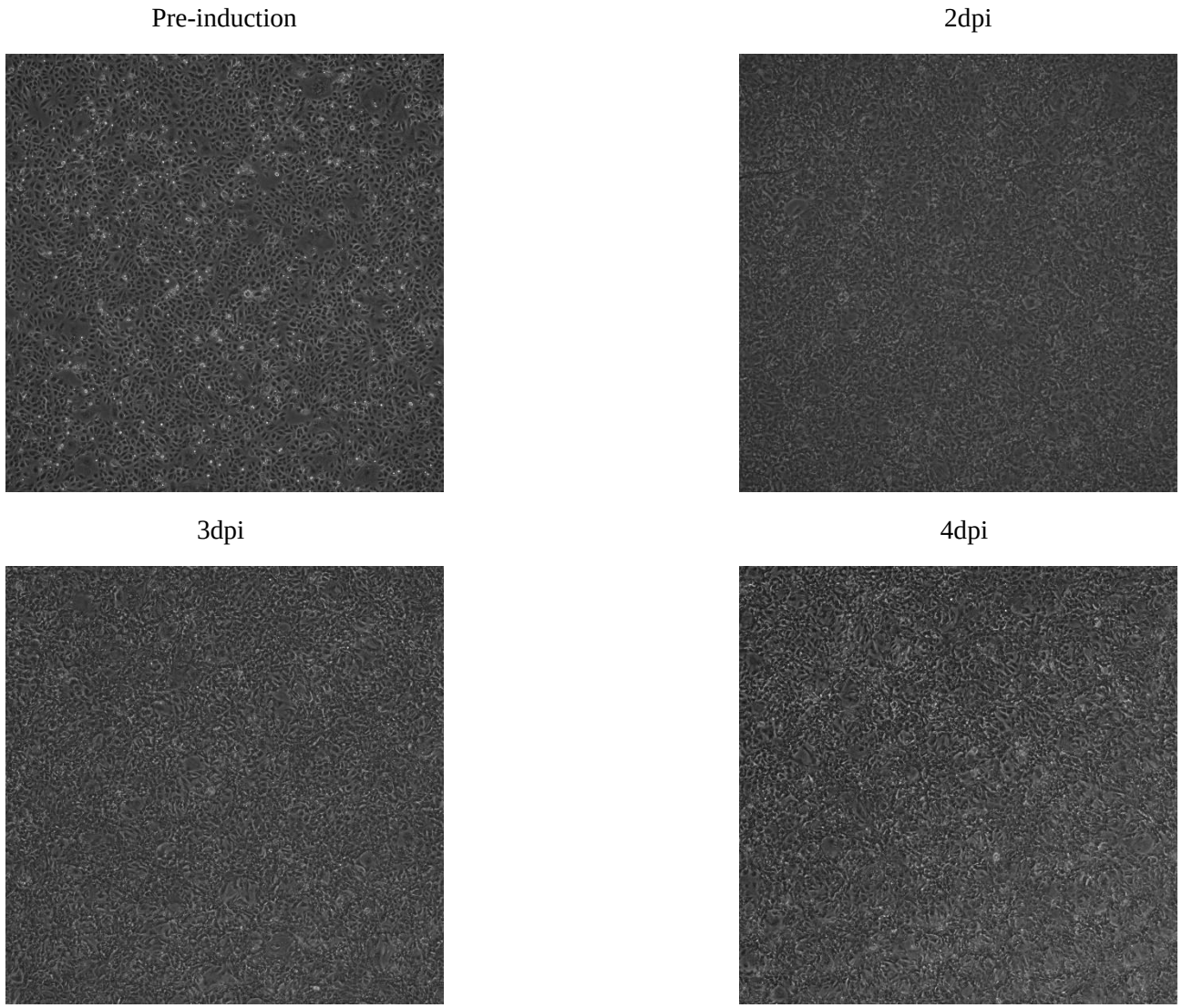

Figure 27: Phase microscopy of ΔORF67.5/67A mutant cell-line before and after induction with sodium butyrate and doxycycline.

Pre-induction

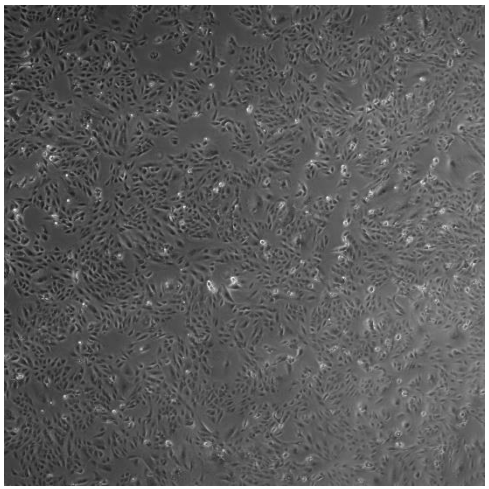

2dpi

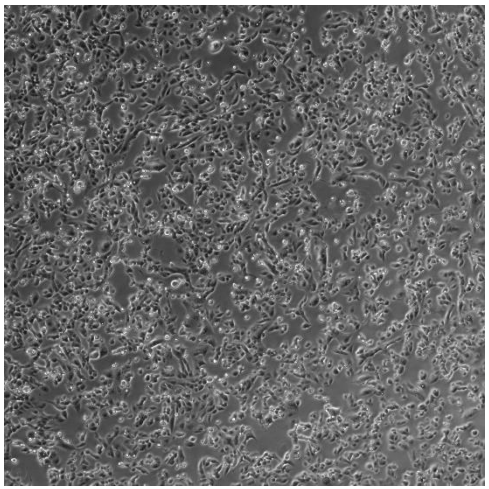

3dpi

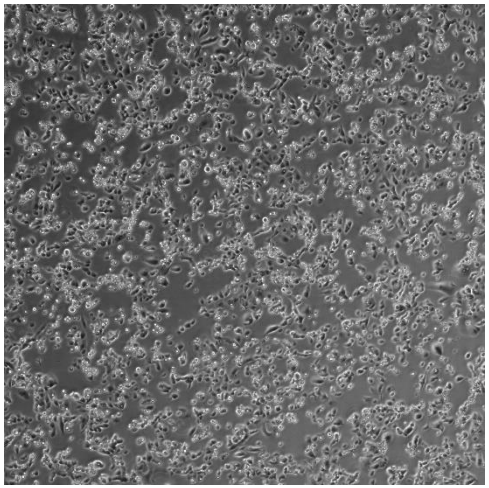

4dpi

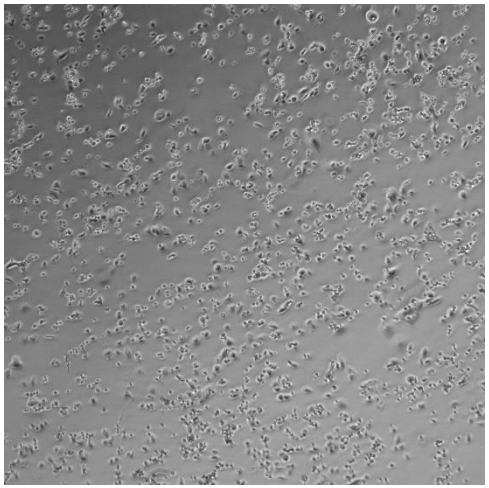

Figure 28: Phase microscopy of ΔORF69 mutant cell-line before and after induction with sodium butyrate and doxycycline.

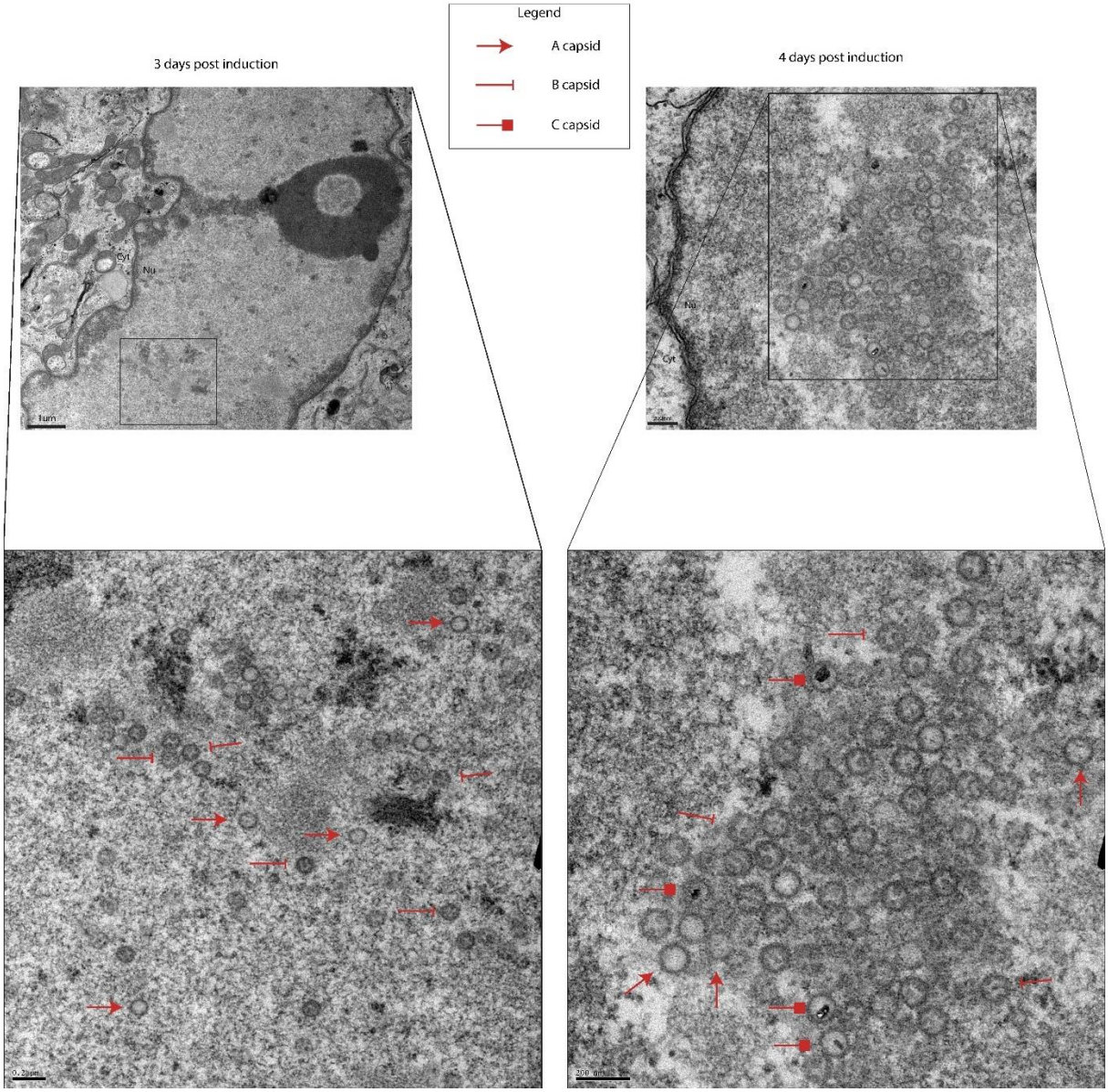

Figure 29: TEM of capsids aggregating in nuclei of ΔORF69 mutant cell-line at 3 and 4 days post induction. Scale bars are in micrometers. Red arrows indicate A capsids, red flat-headed arrows indicate B capsids, and red boxed arrows indicate C capsids.

Subsection II: DNA replication

KSHV ORF6:

To examine the role of KSHV ORF6 in reactivation we induced the ΔORF6 mutant cell line using sodium butyrate and doxycycline and observed its ability to reactivate for 4 days. We deleted from nucleotide 3194-6592 (3399 nucleotides) to make the ΔORF6 mutant (accession number GQ994935.1). This deletion removes ORF6 from the annotated start site to the annotated termination site. We observed slight rounding of cells 2-days post induction, and this rounding and swelling progressed to a moderate level through day 4 of induction. Elongation of attached cells became evident 2-days post induction and continued to progress through the monolayer through 4 days post induction as well. The degree of elongation was not as pronounced as some of the other mutants described in the DNA packaging section but was significant enough to note here. We observed a decrease in confluence from 100% to about 60% by 4 days post induction, indicating that a moderate amount of cell death from induction (figure 30). We classified this induction phenotype as "like-BAC16" We viewed all 4 days of induction for this sample extensively under TEM, however, we never encountered any capsid species in the nucleus or cytoplasm of cells.

KSHV ORF9:

To examine the role of KSHV ORF9 in reactivation we induced the ΔORF9 mutant cell line using sodium butyrate and doxycycline and observed its ability to reactivate for 4 days. We deleted from nucleotide 11344-14382 (3039 nucleotides) to make the ΔORF9 mutant (accession number GQ994935.1). This deletion removes ORF9 from the annotated start site to the annotated termination site. We observed slight rounding of cells 2-days post induction, however, this rounding and swelling did not progress significantly between 2-4 days of induction. Elongation of attached cells only became slightly evident at 4-days post induction. We observed no decrease in confluence from induction, indicating there was virtually no cell death from induction (figure 31). We classified this induction phenotype as "weaker than BAC16". We viewed all 4 days of induction for this sample extensively under TEM, however, we never encountered any capsid species in the nucleus or cytoplasm of cells.

KSHV ORF40:

To examine the role of KSHV ORF40 in reactivation we induced the ΔORF40 mutant cell line using sodium butyrate and doxycycline and observed its ability to reactivate for 4 days. We deleted from nucleotide 60124-61497 (1374 nucleotides) to make the ΔORF40 mutant (accession number GQ994935.1). This deletion removes ORF40 from the annotated start site to the annotated termination site. We observed slight rounding of cells 2-days post induction, and this rounding and swelling progressed weakly through 3-days post induction. Elongation of attached cells never became evident in this sample, even at 4-days post induction. We observed a decrease in confluence from 95%-65% indicating there was a moderate amount of cell death from induction (figure 32). We classified this induction phenotype as "like-BAC16". We viewed

all 4 days of induction for this sample extensively under TEM, however, we never encountered any capsid species in the nucleus or cytoplasm of cells.

KSHV ORF41:

To examine the role of KSHV ORF41 in reactivation we induced the ΔORF41 mutant cell line using sodium butyrate and doxycycline and observed its ability to reactivate for 4 days. The 3' end of ORF41 overlaps the 3' end of ORF42 by 8 nucleotides, so we inserted the 12bp stop codon at nucleotide 61652 to make the ΔORF41 mutant (accession number GQ994935.1). This stop codon is 9 nucleotides downstream of the annotated start site of ORF41 and does not overlap with any other annotated coding region. We observed a moderate amount of rounding and swelling of cells by 3-days post induction. The rounding and swelling of cells appeared to be coming from a base-layer of elongated cells, and this phenotype progressed through 4-days post induction (figure 33). We classified this induction phenotype as "clustering". We viewed all 4 days of induction for this sample extensively under TEM, however, we never encountered any capsid species in the nucleus or cytoplasm of cells.

KSHV ORF44:

To examine the role of KSHV ORF44 in reactivation we induced the ΔORF44 mutant cell line using sodium butyrate and doxycycline and observed its ability to reactivate for 5 days. The 5' end of ORF44 overlaps the 5' end of ORF43 by 62 nucleotides, so we inserted the 12bp stop codon at nucleotide 64717 to make the ΔORF44 mutant (accession number GQ994935.1). This stop codon is 9 nucleotides downstream of the annotated start site of ORF44, however, it overlaps with ORF43 and is 53bp downstream of the annotated start site of ORF43 in the reverse orientation. We observed virtually no rounding and swelling or elongation of cells through the 5-day induction period (figure 34). Thus, we classified this induction phenotype as "weaker than BAC16". We viewed all 5 days of induction for this sample extensively under TEM, however, we never encountered any capsid species in the nucleus or cytoplasm of cells.

KSHV ORF59:

To examine the role of KSHV ORF59 in reactivation we induced the ΔORF59 mutant cell line using sodium butyrate and doxycycline and observed its ability to reactivate for 4 days. We deleted ORF59 from the annotated start site to the annotated stop site to make the ΔORF59 mutant. This corresponds to a deletion of 1191bp, removing nucleotide 111705-112895 (accession number GQ994935.1). We observed virtually no rounding and swelling or elongation of cells through the 4-day induction period (figure 35). Thus, we classified this induction phenotype as "weaker than BAC16". We viewed all 4 days of induction for this sample extensively under TEM, however, we never encountered any capsid species in the nucleus or cytoplasm of cells.

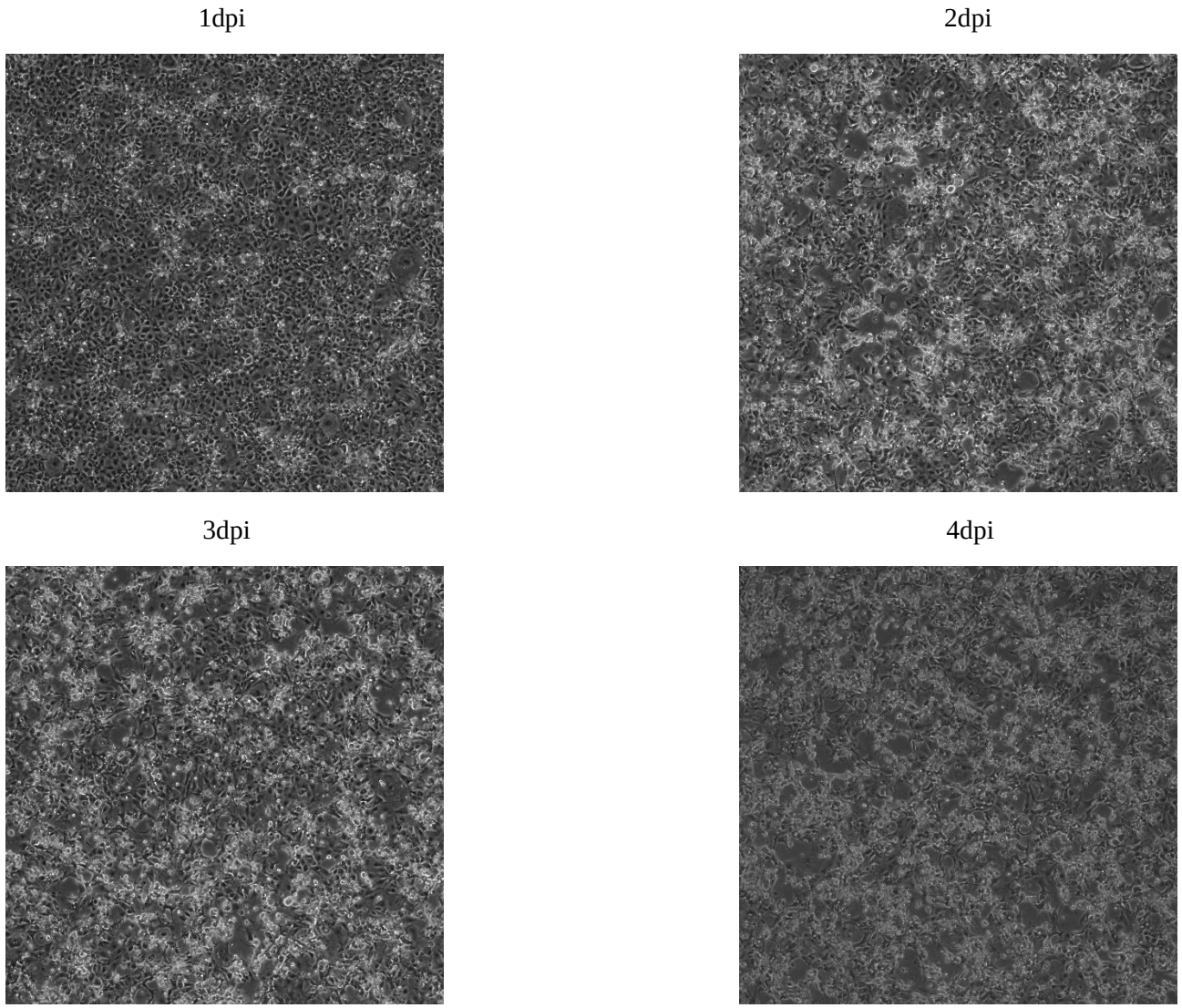

Figure 30: Phase microscopy of ΔORF6 mutant cell-line after induction with sodium butyrate and doxycycline.

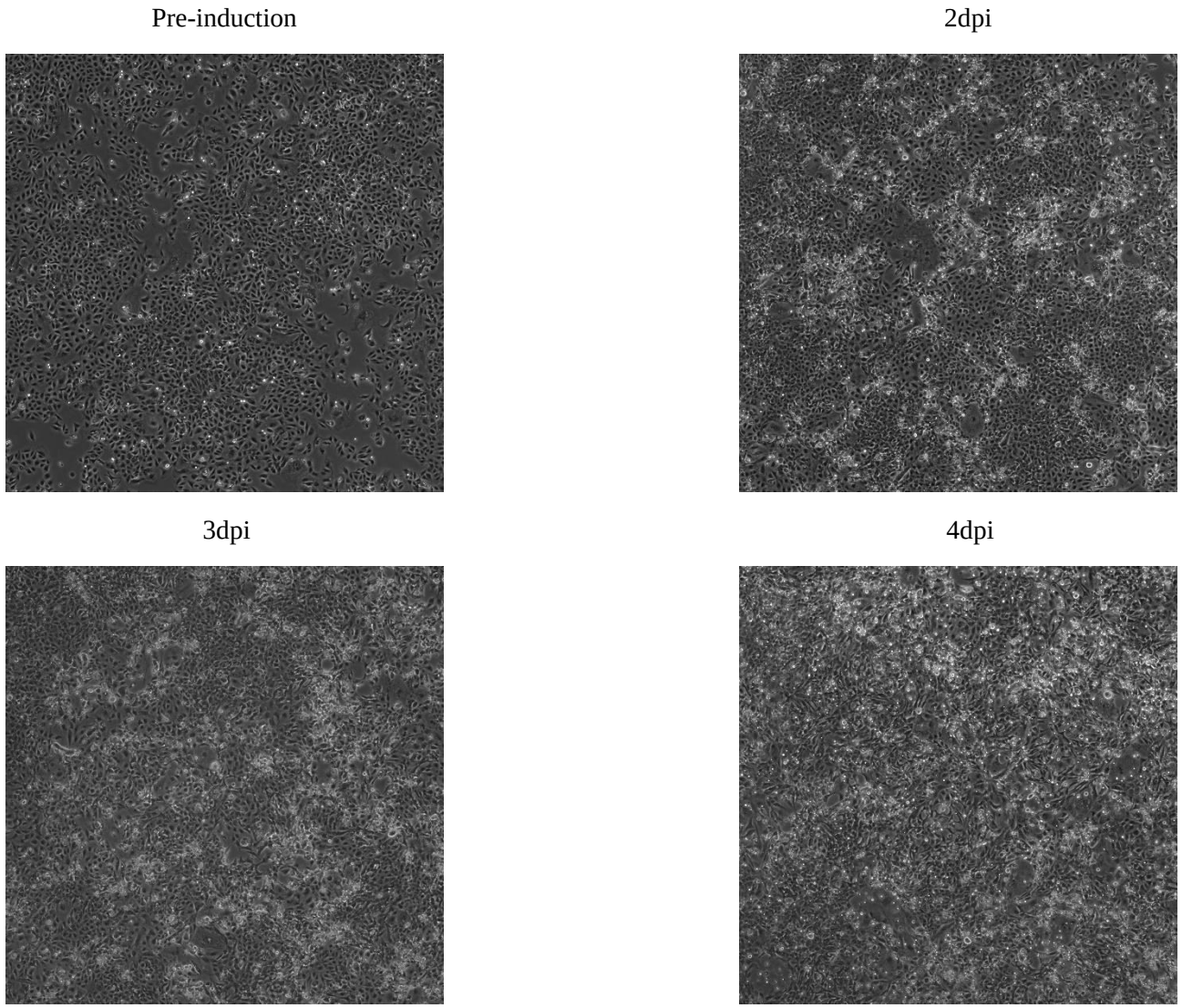

Figure 31: Phase microscopy of ΔORF9 mutant cell-line before and after induction with sodium butyrate and doxycycline.

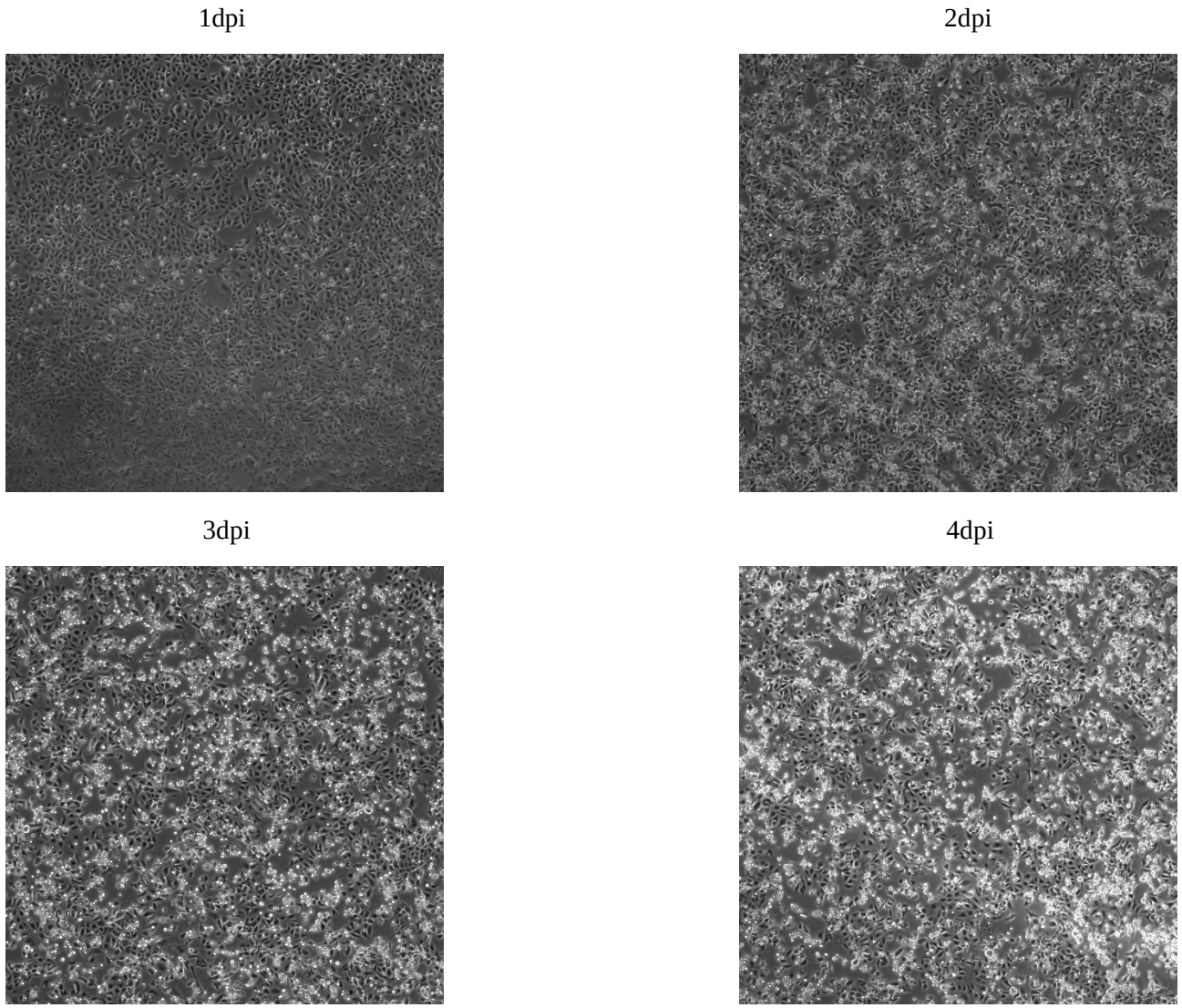

Figure 32: Phase microscopy of ΔOR40 mutant cell-line after induction with sodium butyrate and doxycycline.

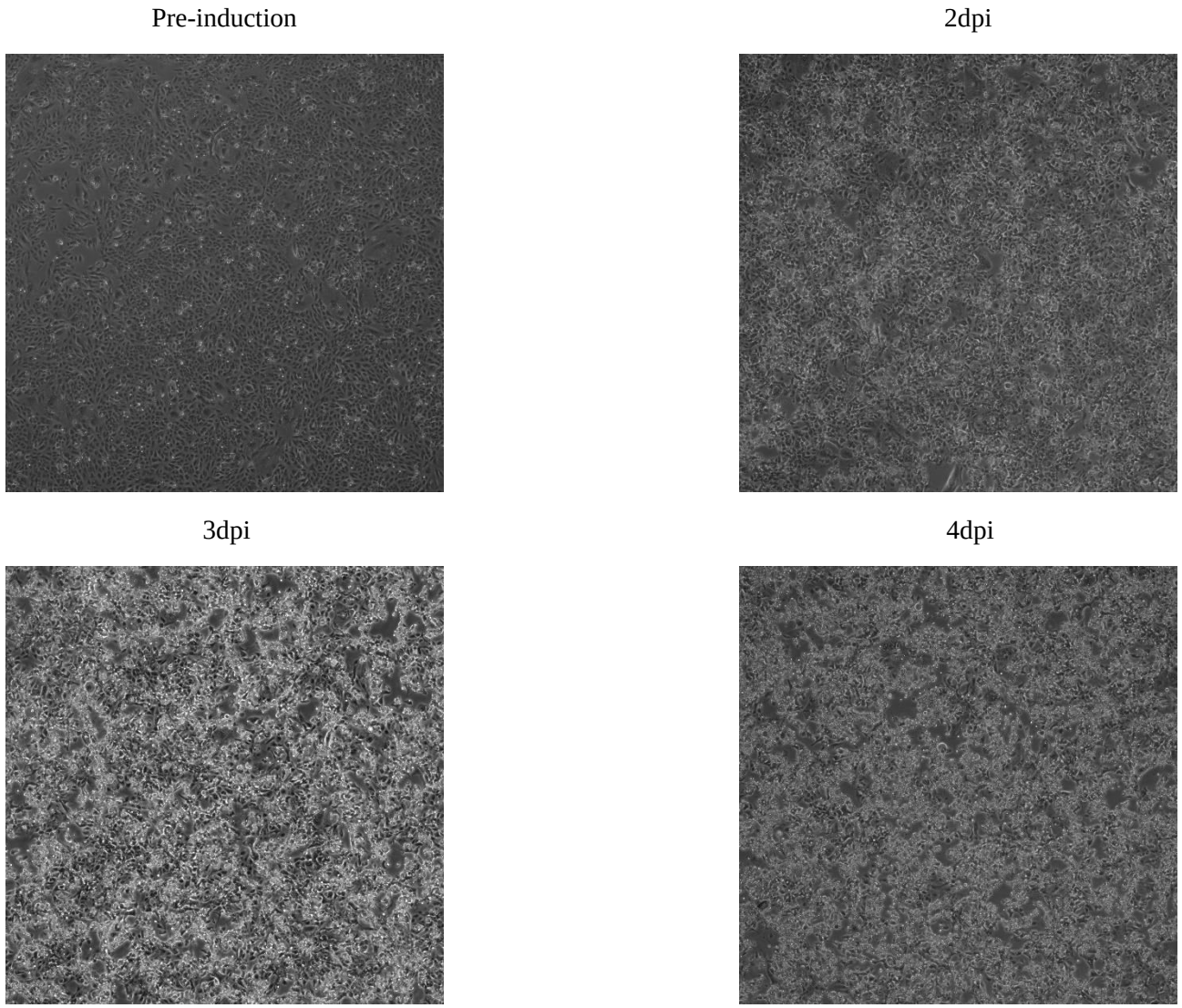

Figure 33: Phase microscopy of ΔOR41 mutant cell-line before and after induction with sodium butyrate and doxycycline.

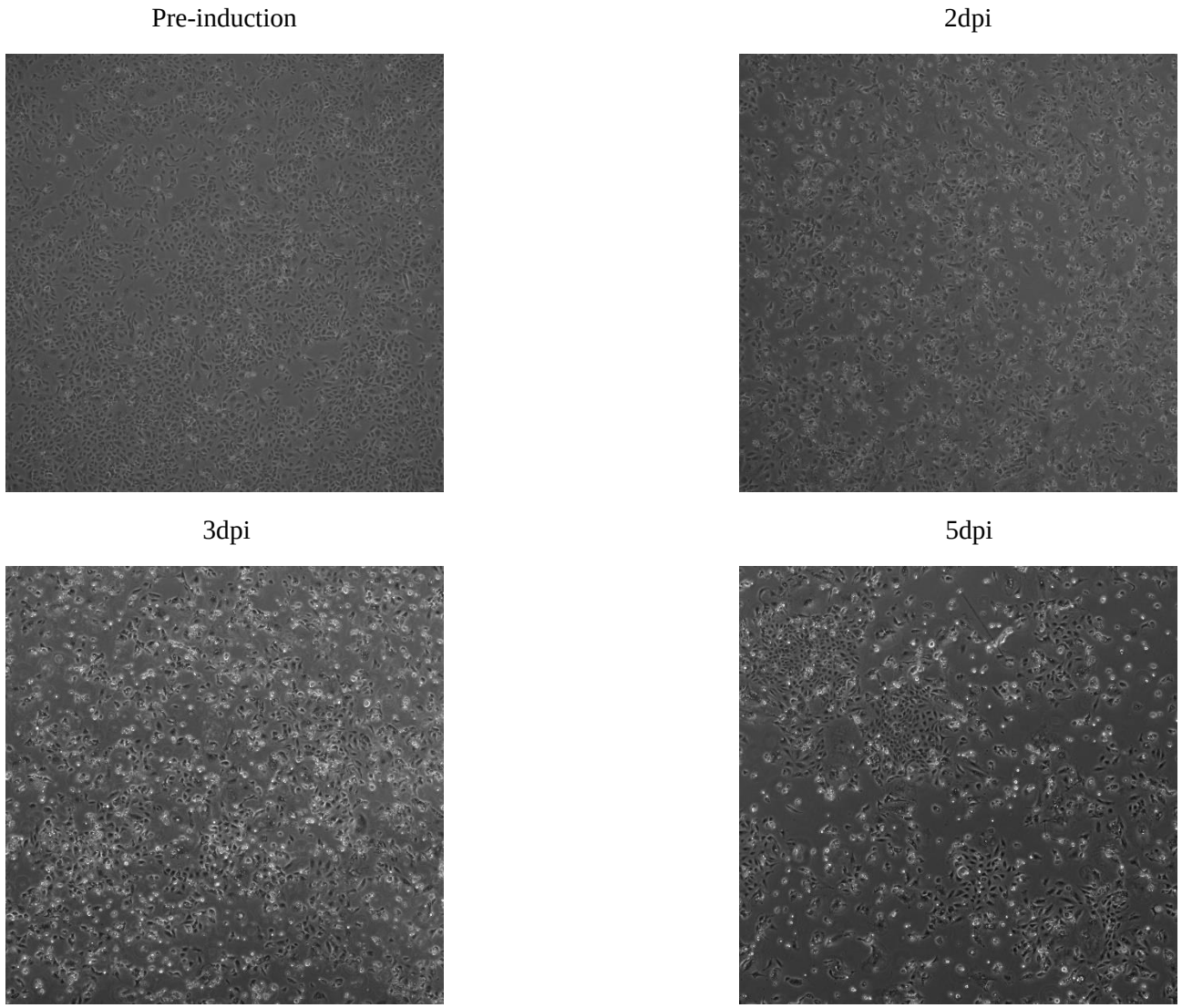

Figure 34: Phase microscopy of ΔOR44 mutant cell-line before and after induction with sodium butyrate and doxycycline.

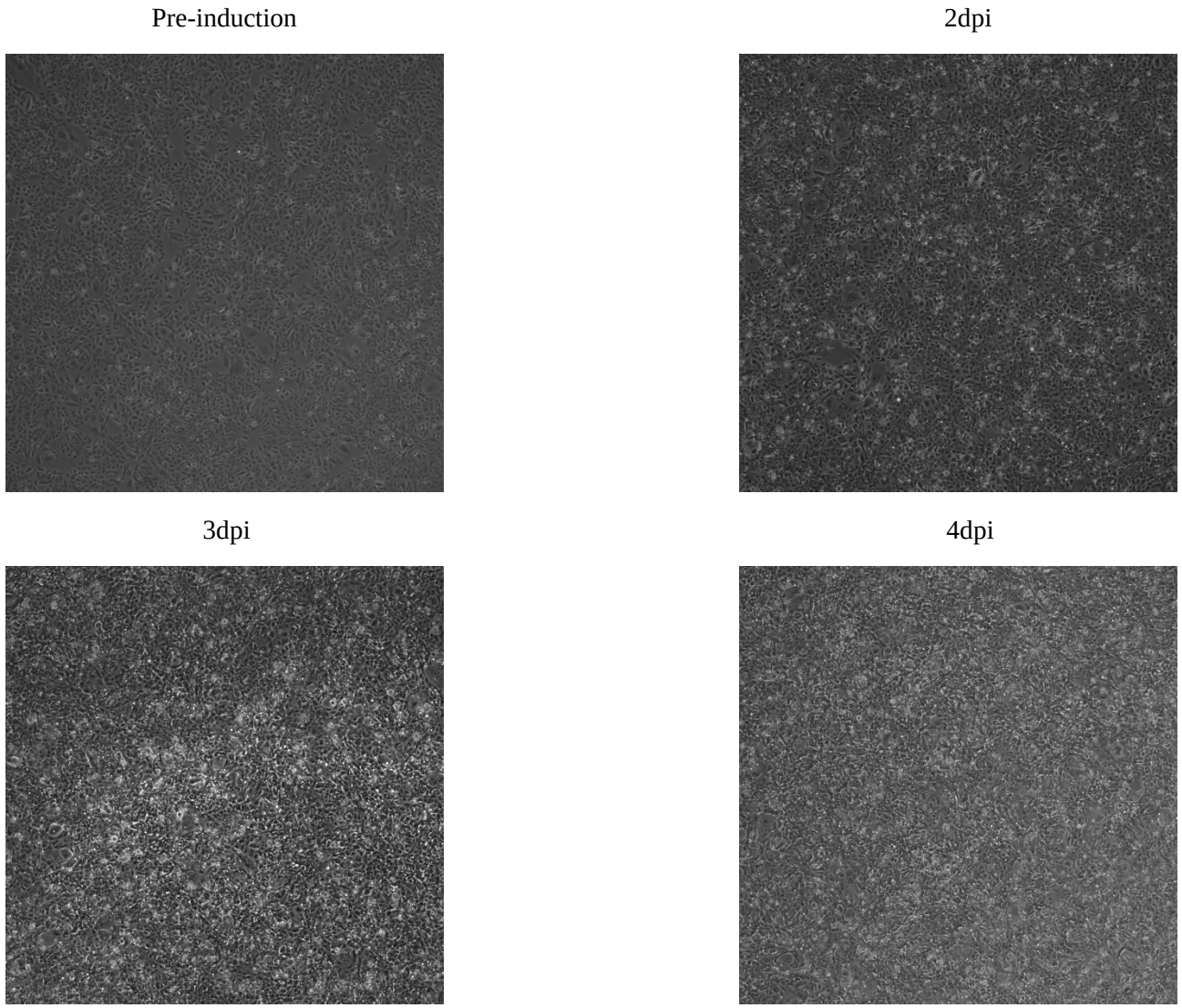

Figure 35: Phase microscopy of ΔOR59 mutant cell-line before and after induction with sodium butyrate and doxycycline.

Subsection III: Core capsid components

KSHV ORF25:

To examine the role of KSHV ORF25 in reactivation and capsid formation we induced the ΔORF25 mutant cell line using sodium butyrate and doxycycline and observed its ability to reactivate for 4 days. The 5' end of ORF25 overlaps the 5' end of ORF24 by 2 nucleotides, so we inserted the 12bp stop codon 9 nucleotides downstream of the annotated start site at nucleotide 42604 to make the ΔORF25 mutant (accession number GQ994935.1). We observed small amounts of rounding and swelling cells by 3-days post induction. However, by 4-days post induction a significant elongation phenotype was observed and virtually no rounding cells were observed. The elongation of cells into patches that looked like Swiss cheese was evident. This phenotype is reminiscent of the clustering induction phenotype, except here there are no rounding and swelling cells. We observed a decrease in confluence from 100% to about 85% by 4-days post induction, indicating small amounts of cell death from induction (figure 36). Thus, we classified this induction phenotype as "weaker than BAC16". We viewed all 4 days of induction for this sample extensively under TEM, however, we never encountered any capsid species in the nucleus or cytoplasm of cells.

KSHV ORF62:

To examine the role of KSHV ORF62 in reactivation and capsid formation we induced the ΔORF62 mutant cell line using sodium butyrate and doxycycline and observed its ability to reactivate for 4 days. We removed from nucleotide 100018 to 1010013 (995 nucleotides) to make the ΔORF62 mutant (accession number GQ994935.1). This deletion removes ORF62 from the annotated start site to the annotated termination site. We observed moderate amounts of rounding and swelling cells by 4-days post induction. The elongation of cells was not as pronounced as other samples, but morphology distortions in the remaining attached cells was evident enough to note here. We observed a decrease in confluence from 100% to about 70% by 4-days post induction, indicating that there was a small amount of cell death from induction (figure 37). Thus, we classified this induction phenotype as "like-BAC16". We viewed all 4 days of induction for this sample extensively under TEM, however, we never encountered any capsid species in the nucleus or cytoplasm of cells.

KSHV ORF65:

To examine the role of KSHV ORF65 in reactivation and capsid formation we induced the ΔORF65 mutant cell line using sodium butyrate and doxycycline and observed its ability to reactivate for 4 days. We removed from nucleotide 111750 to 112262 (513 nucleotides) to make the ΔORF65 mutant (accession number GQ994935.1). This deletion removes ORF65 from the annotated start site to the annotated termination site. We observed large amounts of rounding and swelling cells by 2-days post induction. By 4-days post induction the monolayer was virtually cleared of attached cells. We did not observe any noticeable elongation of attached cells. We observed a decrease in confluence from 100% to about 10% by 4-days post induction, indicating there was massive amounts of cell death from induction (figure 38). Thus, we classified this

induction phenotype as “stronger than BAC16”. We viewed all 4 days of induction for this sample extensively under TEM, however, we never encountered any capsid species in the nucleus or cytoplasm of cells.

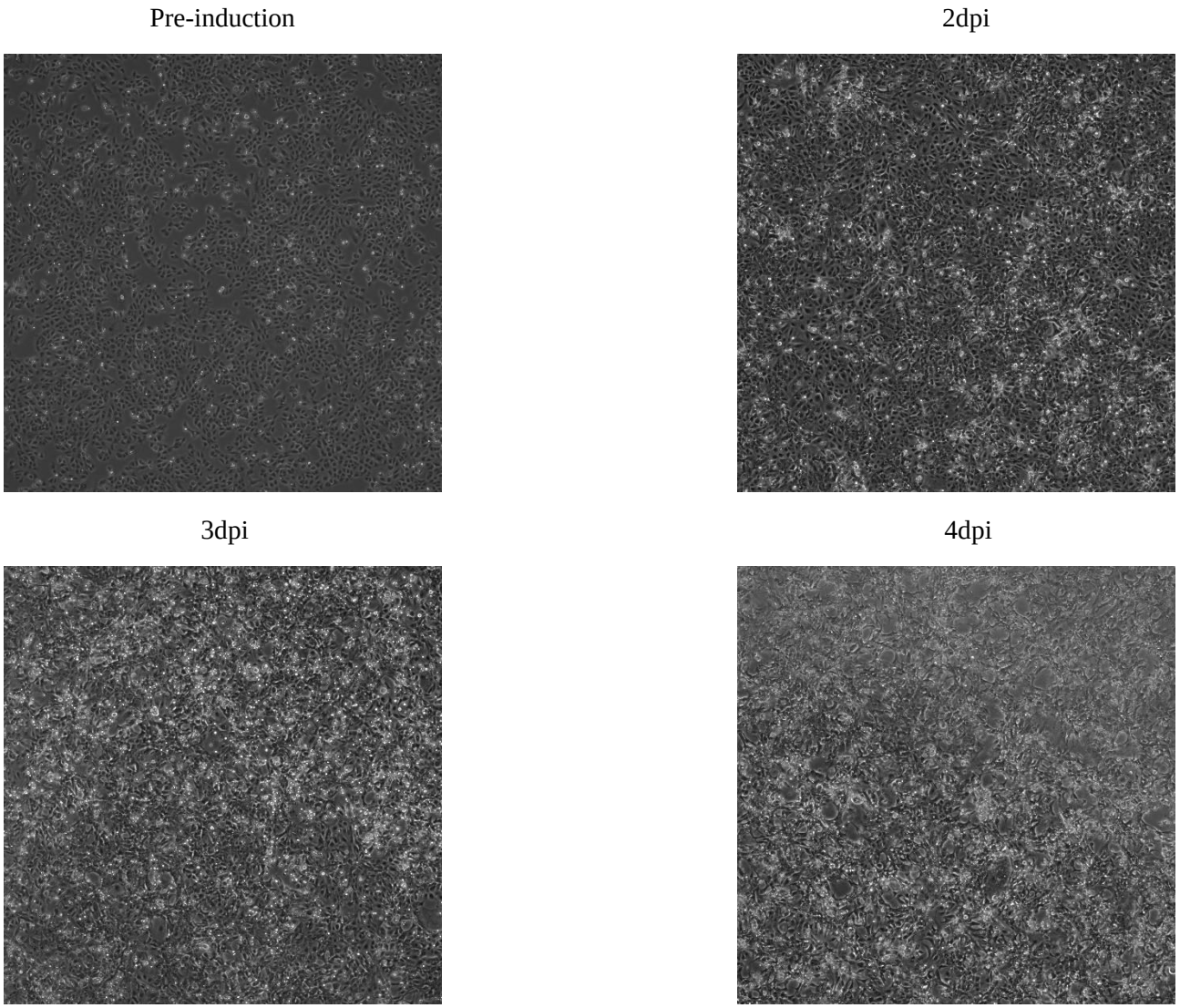

Figure 36: Phase microscopy of ΔOR25 mutant cell-line before and after induction with sodium butyrate and doxycycline.

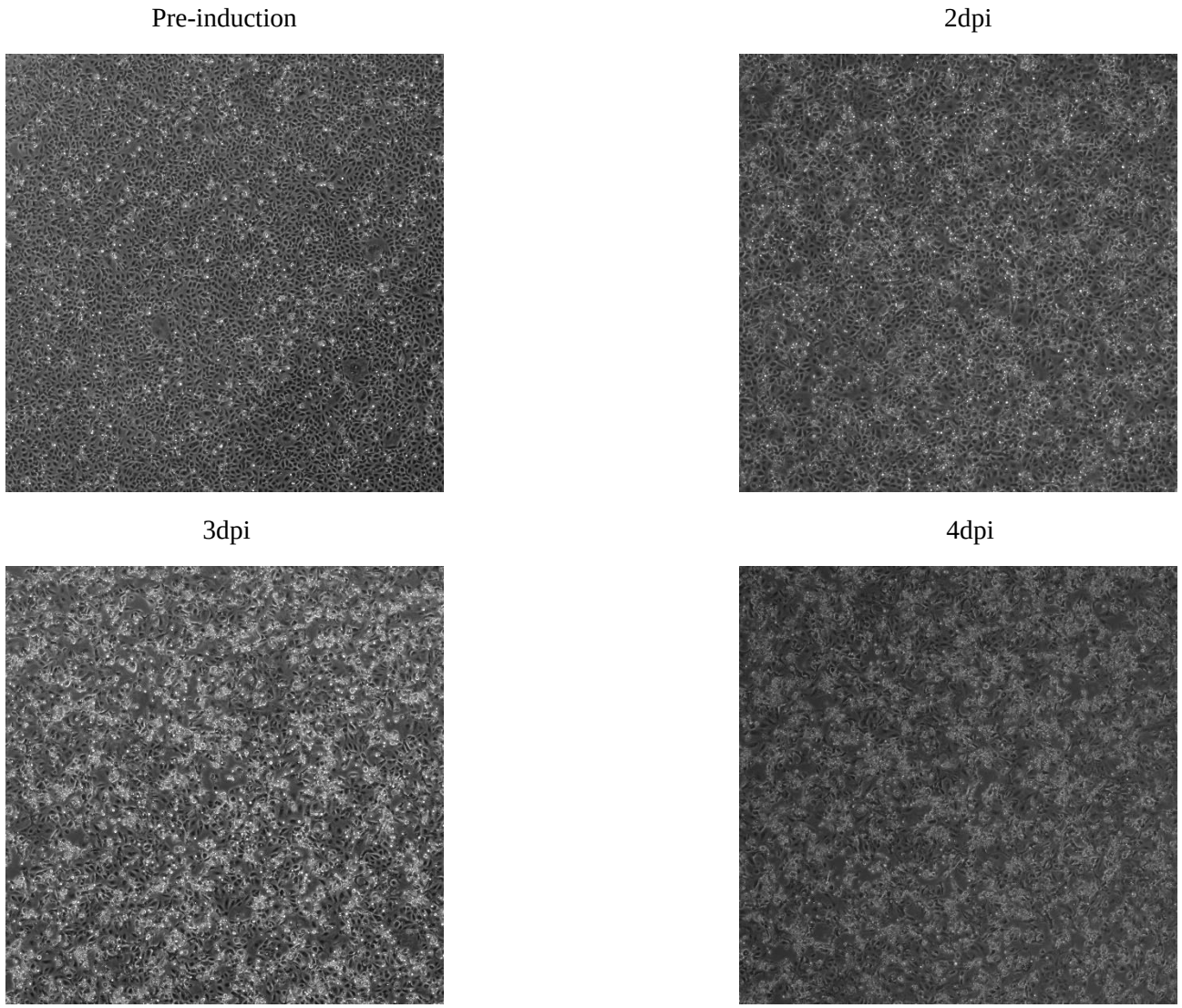

Figure 37: Phase microscopy of ΔOR62 mutant cell-line before and after induction with sodium butyrate and doxycycline.

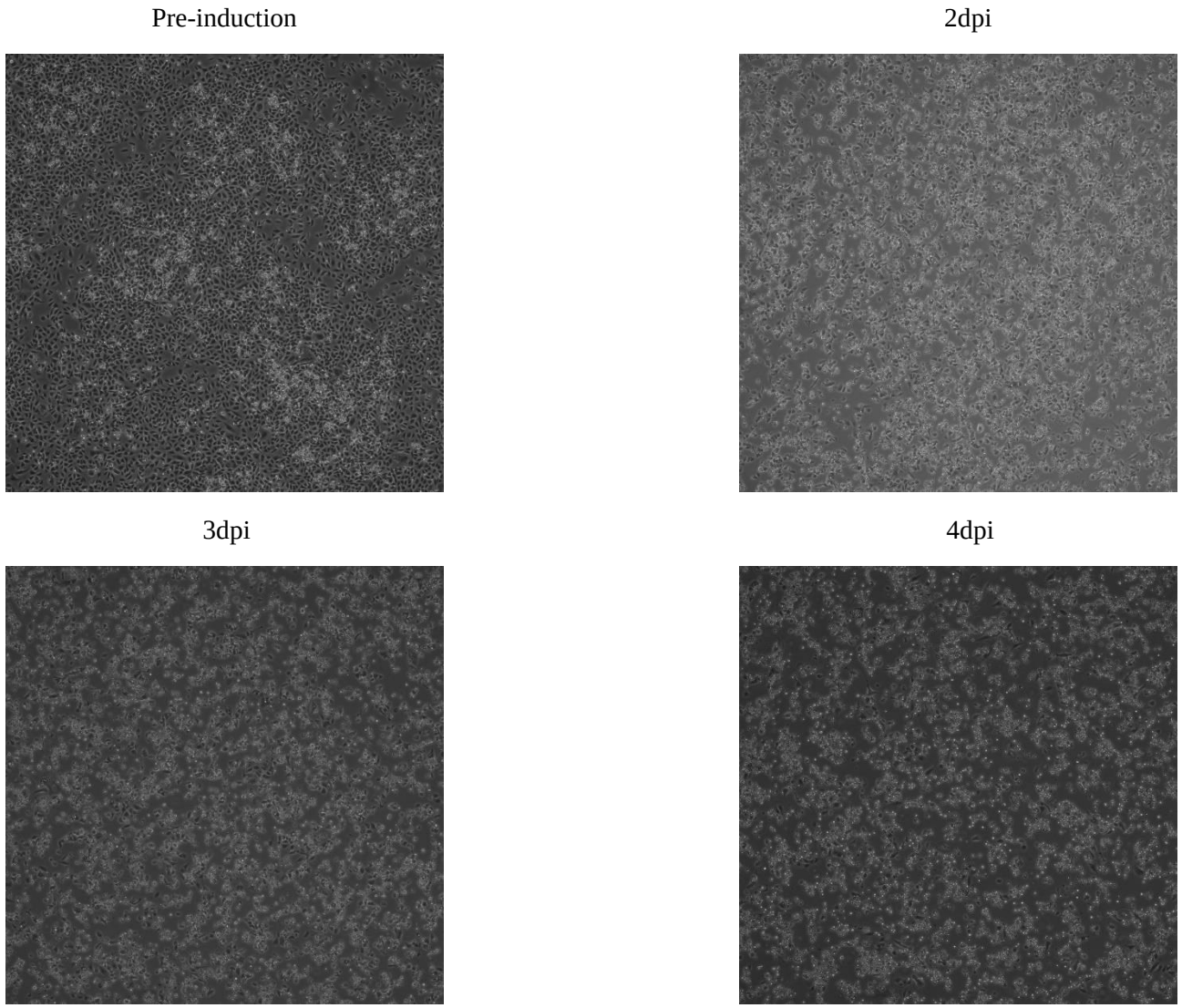

Figure 38: Phase microscopy of ΔOR65 mutant cell-line before and after induction with sodium butyrate and doxycycline.

Subsection IV: Reactivation and late gene expression

KSHV ORF18:

To examine the role of KSHV ORF18 in reactivation we induced the ΔORF18 mutant cell line using sodium butyrate and doxycycline and observed its ability to reactivate for 4 days. The 3' end of ORF18 overlaps the 3' end of ORF19 by 3 nucleotides and the 5' end of ORF18 overlaps the 5' end of ORF17 by 59 nucleotides. We inserted the 12bp stop codon 69 nucleotides downstream of the annotated start site for ORF18 at nucleotide 32311 to make the ΔORF18 mutant (accession number GQ994935.1). This insertion does not overlap either flanking ORF. We observed virtually no rounding and swelling of cells throughout the 4-day induction time course. By 4 days post induction there was a minor amount of elongation/distortion of attached cell morphology, but it was not very pronounced. We observed no decrease in confluence from induction, indicating that there was virtually no cell death, and cells began to overgrow the monolayer by 4-days post induction (figure 39). Thus, we classified this induction phenotype as "weaker than BAC16".

KSHV ORF31:

To examine the role of KSHV ORF31 in reactivation we induced the ΔORF31 mutant cell line using sodium butyrate and doxycycline and observed its ability to reactivate for 4 days. The 5' end of ORF31 overlaps the 3' end of ORF30 by 94 nucleotides and the 3' end of ORF31 overlaps the 5' end of ORF32 by 34 nucleotides. We inserted the 12bp stop codon 105 nucleotides downstream of the annotated start site for ORF31 at nucleotide 50685 to make the ΔORF31 mutant (accession number GQ994935.1). This insertion does not overlap either flanking ORF. We observed virtually no CPE characterized by rounding and swelling of cells throughout the 4-day induction time course. By 3-days post induction there was a significant amount of elongation/distortion of attached cell morphology that was observed, and it continued to progress through 4-days post induction. We observed a slight decrease in confluence from 100% to 90% from induction, indicating that there was very little cell death (figure 40). Thus, we categorized this induction phenotype as "weaker than BAC16.

KSHV ORF34:

To examine the role of KSHV ORF34 in reactivation we induced the ΔORF34 mutant cell line using sodium butyrate and doxycycline and observed its ability to reactivate for 4 days. The 3' end of ORF34 overlaps the 5' end of ORF35 by 20 nucleotides. We inserted the 12bp stop codon 9 nucleotides downstream of the annotated start site for ORF34 at nucleotide 54500 to make the ΔORF34 mutant (accession number GQ994935.1). We observed virtually no CPE characterized by rounding and swelling of cells throughout the 4-day induction time course. However, by 2-days post induction, there was a major amount of elongation/distortion of attached cell morphology that was observed, and it continued to progress through 4-days post induction. Cells began to bunch-up and form a Swiss-cheese like pattern. We observed a slight decrease in confluence from 100% to 90% indicating that there was very little cell death (figure 41). This induction phenotype was like the "clustering" phenotype, expect that it lacked a

significant layer of rounding and swelling cells. Because this induction phenotype was like "weaker than BAC16" and "clustering" we approach categorization with caution. Ultimately, we decided to categorize this induction phenotype as "weak clustering".

KSHV ORF66:

To examine the role of KSHV ORF66 in reactivation we induced the ΔORF66 mutant cell line using sodium butyrate and doxycycline and observed its ability to reactivate for 4 days. The 5' end of ORF66 overlaps the 3' end of ORF67 by 67 nucleotides, so we inserted the 12bp stop codon 9 nucleotides downstream of the annotated start site for ORF66 at nucleotide 113570 to make the ΔORF66 mutant (accession number GQ994935.1). This inserted stop codon is 58 nucleotides upstream of the 3' termination codon of ORF67, and presumably results in a truncated form of ORF67. We observed virtually no rounding and swelling of cells throughout the 4-day induction time course. We also observed minor elongation/distortion of attached cell morphology that began to appear 4-days post induction. We observed no decrease in confluence from induction indicating no cell death, and cells began to overgrow the monolayer by 4-days post induction (figure 42). Thus, we categorized this induction phenotype as "weaker than BAC16".

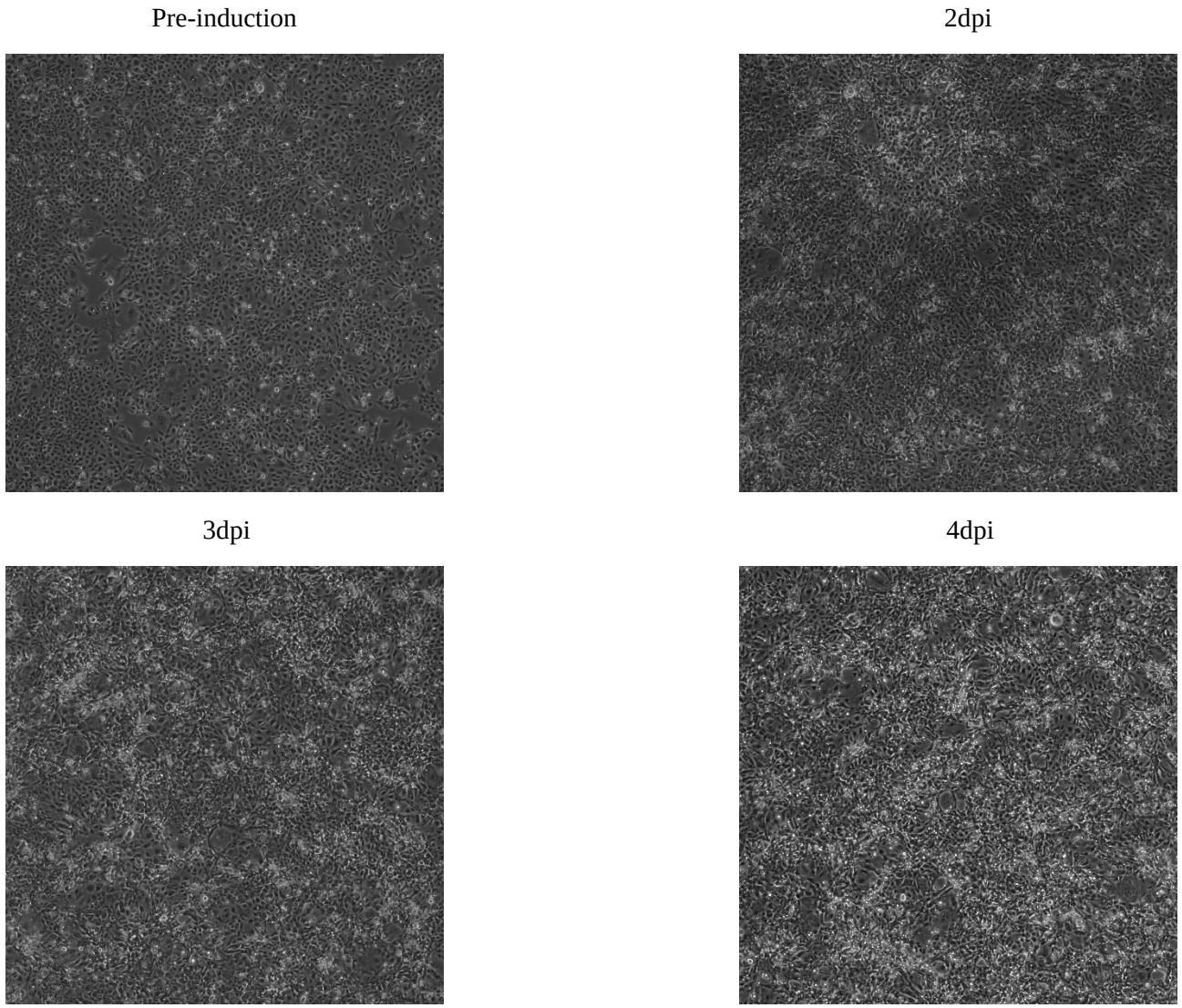

Figure 39: Phase microscopy of ΔOR18 mutant cell-line before and after induction with sodium butyrate and doxycycline.

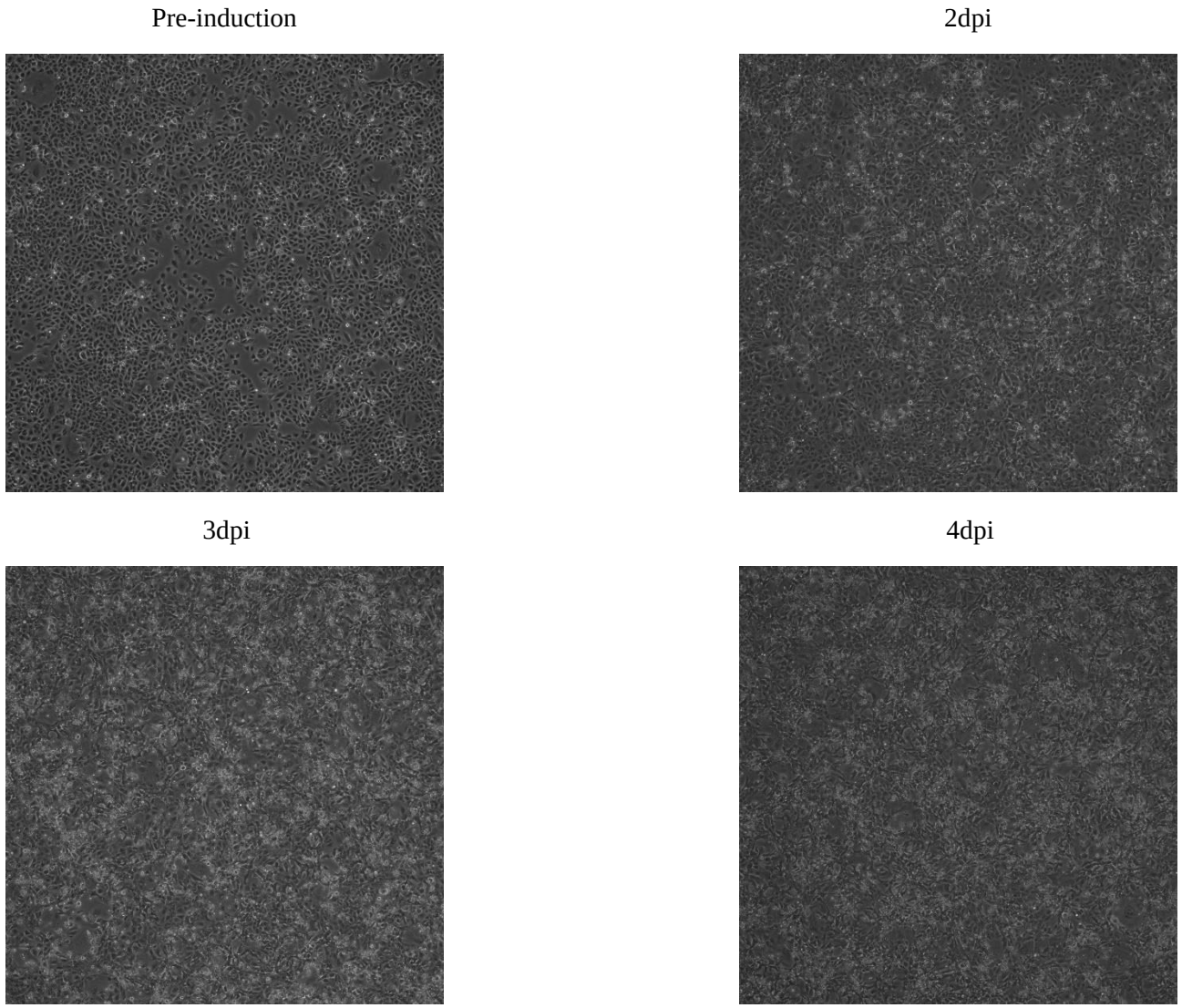

Figure 40: Phase microscopy of ΔOR31 mutant cell-line before and after induction with sodium butyrate and doxycycline.

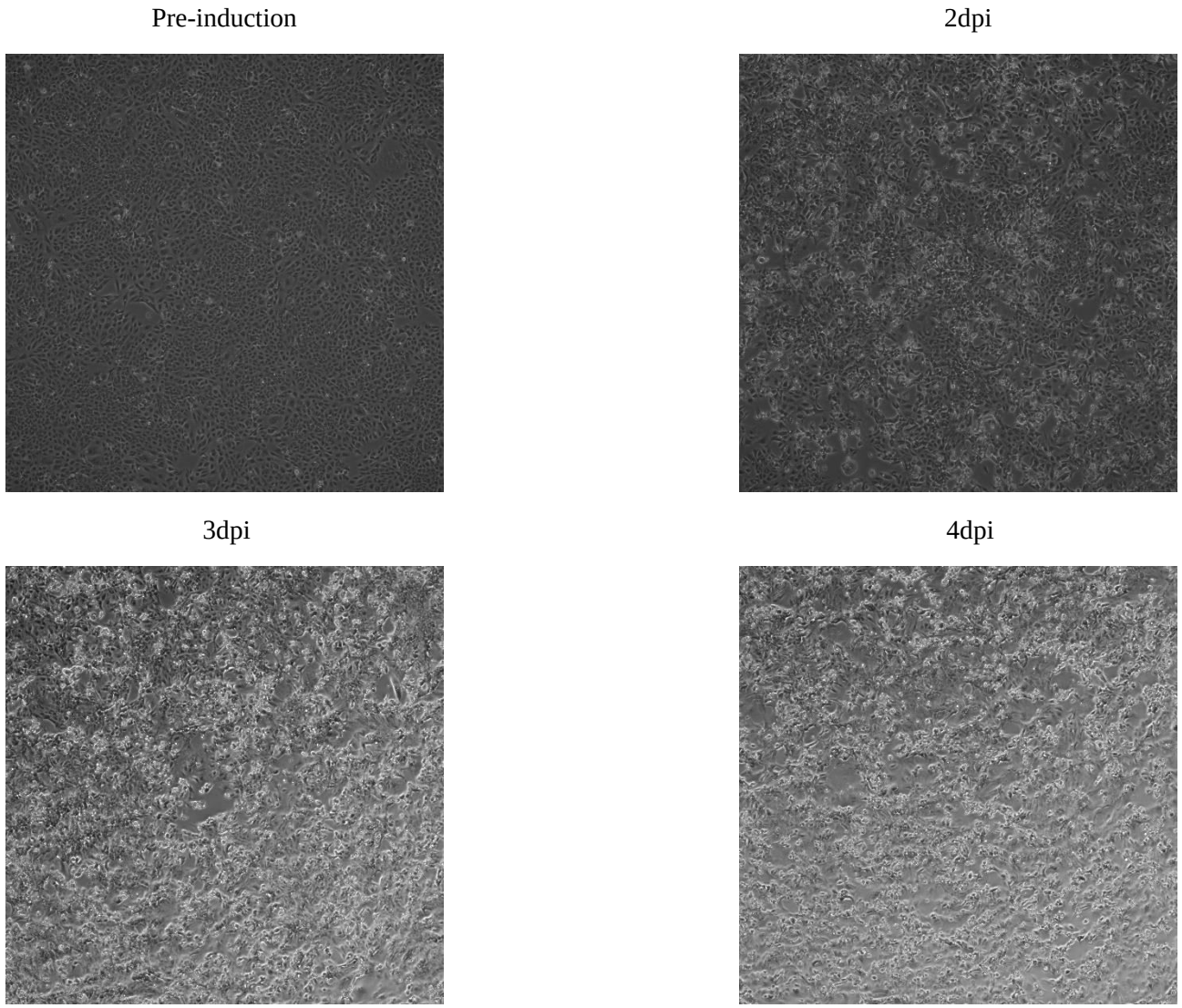

Figure 41: Phase microscopy of ΔOR34 mutant cell-line before and after induction with sodium butyrate and doxycycline.

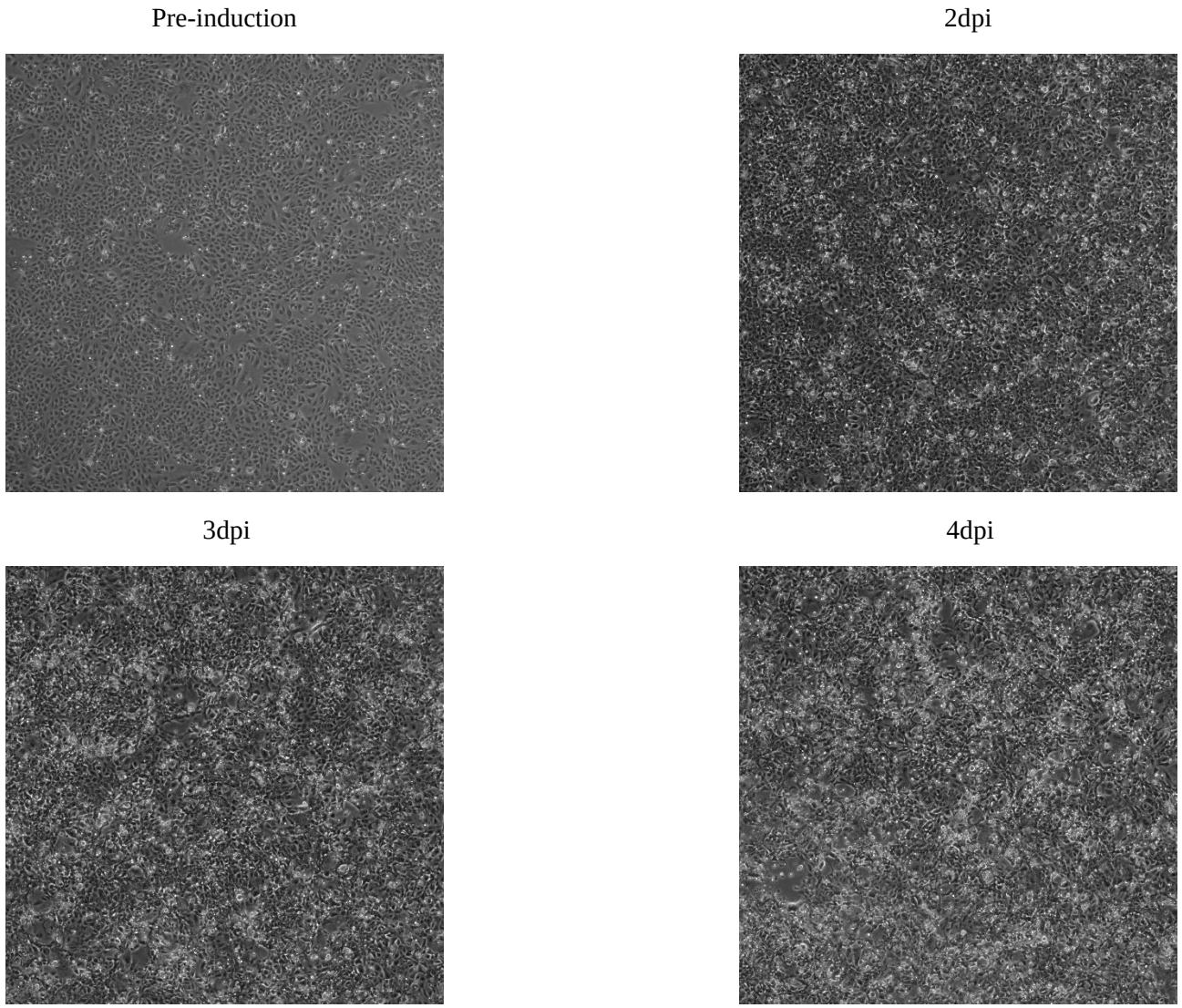

Figure 42: Phase microscopy of ΔOR66 mutant cell-line before and after induction with sodium butyrate and doxycycline.

Chapter 4

Kaposi Sarcoma-associated herpesvirus open reading frame 19 is essential for viral capsid maturation during lytic infection

"Forever trust in who you are." -*redacted*

Overview:

This chapter outlines the creation of the stop-ORF19 mutant (ΔORF19) and its genetic rescue (res-ORF19). This chapter also includes the results of phenotypic analyses covering several key lifecycle steps including viral latency, reactivation, lytic gene expression and viral lytic DNA replication, progeny production, and capsid formation. This chapter is split into two parts. The main text includes the results of the phenotypic analyses and provides context to our findings in the broader field of herpesvirus biology. The appendix section provides the reader with a more detailed look at the creation of the stop-ORF19 and res-ORF19 viruses, their corresponding cell lines, and provides several other interesting phenotypic findings. I am indebted to Fenyong Liu for his help in the design and analyses presented herein.

Abstract:

Kaposi sarcoma-associated herpesvirus (KSHV) open reading frame 19 (ORF19) is conserved throughout human herpesviruses, however, very little is known about the role KSHV ORF19 plays in the viral lifecycle. In this study we investigated the role of KSHV ORF19 in the establishment and maintenance of viral latency, reactivation, viral lytic gene expression, lytic DNA replication, capsid formation, and progeny production. We created a KSHV ORF19 inactivation mutant (stop-ORF19) from a bacterial artificial chromosome containing the KSHV genome (BAC16), and we rescued the stop-ORF19 virus genotype (res-ORF19). stop-ORF19 virus was able to establish latency as determined by the expansion of transfected cell lines and the lack of infectious progeny in the cell and culture supernatant. stop-ORF19 virus had no defect in DNA replication and segregation during viral latency and induction confirmed stop-ORF19 was able to reactivate from latency. stop-ORF19 had no defect in lytic viral DNA replication. Tittering of induced cells and supernatants showed that stop-ORF19 virus produced no infectious progeny, while res-ORF19 virus produced progeny and grew like BAC16 virus. Transmission electron microscopy of induced stop-ORF19 virus infected cells revealed the accumulation of empty A-capsids that were retained in the nucleus, indicating that KSHV ORF19 plays a critical role in KSHV capsid maturation and viral egress. Our results provide biological evidence complementing cryogenic electron microscopy (cryo-EM) structural data that indicate KSHV ORF19 helps retain the packaged genome inside of mature capsids by capping the portal vertex.

Introduction:

Kaposi sarcoma-associated herpesvirus (KSHV) is a human *Gammaherpesvirinae* in the *Rhadinovirus* genus. KSHV has been identified as the etiologic agent of Kaposi Sarcoma, Primary Effusion Lymphoma, and a subset of Multicentric Castleman's Disease[1]. KSHV infection is initiated through binding of viral glycoproteins to host cell receptors, endocytosis of viral particles, and transport to the nucleus. KSHV DNA enters the nucleus through the nuclear pore and latency is established shortly after infection. Latency is a quiescent state where viral DNA is maintained as extrachromosomal episomes tethered to host chromatin[2 3], and only a handful of viral genes are expressed[4 5 6]. During latency, viral DNA replication occurs during cell division using host machinery[7] and replicated episomes are segregated to daughter cells[8].

Reactivation of KSHV from latency is induced by various stimuli and results in the temporally regulated expression of viral genes. Immediate early (IE) genes encode regulatory and transcription factors, delayed early (DE) genes encode proteins controlling viral DNA replication, host transcription, and immune evasion, and late genes (L) encode virion structural proteins. Lytic gene expression results in lytic viral DNA replication and the assembly of viral progeny. Nascent capsids are assembled and packaged with a single, naked, unit length genome inside of the nucleus. Mature capsids are transported to the inner nuclear membrane, bud into the lumen of the nuclear envelope, and fuse with the outer nuclear membrane to release naked capsids into the cytosol[9]. Capsids egress through the cytosol and acquire additional proteins called tegument, as well as a final lipid envelope studded with glycoproteins, ultimately resulting in the release of mature virions from the cell[1].

Herpesvirus capsid formation and maturation is a multi-step process involving a series of structural re-arrangements triggered by diverse stimuli. Capsid formation begins with nucleation of nascent capsomers facilitated by the scaffolding protein, and the assembly of capsomers into a fragile, short-lived, circular procapsid intermediate[10 11]. Procapsids require the activity of the viral protease to mature into a more angular capsid shape, indicating that cleavage events in the lumen of the nascent procapsid are required for angularization[12]. Angular capsids come in three distinct species separatable by density gradient centrifugation; A capsids which contain no internal structure, B capsids which contain the viral protease and several 3' coterminal variants that act as a scaffolding structure, and C capsids where the internal scaffolding is replaced by a single copy of unit length genome[13 14]. Defects in genome packaging lead to the accumulation of either A or B-capsids in the nucleus of infected cells[15]. These observations lead to the belief that C-capsids are formed from the packaging of viral DNA into B-capsids, and that A-capsids result from an abortive packaging event[15].

KSHV ORF19 is a core gene conserved throughout the human herpesviruses. Cryo-EM analysis of KSHV and other herpesvirus virions revealed that the ORF19 protein and its homologues (i.e. HSV-1 UL25) are a component of the Capsid Associated Tegument Complex (CATC) that caps the tips of capsomer pentons located at the icosahedral vertices[16], and subsequent biochemical data support this observation[17]. In addition to caping the penton-containing vertices, KSHV ORF19 has also been located at the vertex containing a portal-like entry into the interior of the capsid[18].

Wild-type KSHV virus has been cloned as a bacterial artificial chromosome (BAC) construct facilitating the application of reverse genetics to study KSHV gene function[19]. We used

2-step red-recombineering to generate a KSHV ORF19 inactivation mutant (stop-ORF19 virus) from a KSHV BAC (BAC16 virus) by inserting stop codons into the ORF. Moreover, a rescue mutant, res-ORF19, was derived from stop-ORF19 virus by repairing the ORF19 inactivation mutation and restoring the wild type sequence at the ORF. stop-ORF19, res-ORF19, and BAC16 viruses were able to establish and maintain latency as judged by the expansion of transfected cell lines, lack of progeny in the cell and culture supernatants, and the ability to replicate latent viral DNA. Induction of stop-ORF19, res-ORF19, BAC16 virus infected cells reveled significant CPE, and RT-qPCR/qPCR confirmed the full cascade of viral lytic gene expression and viral DNA replication occurred. Extensive induction and tittering via fluorescence microscopy revealed that ΔORF19 virus produced no infectious progeny, while res-ORF19 virus produced progeny and grew like BAC16 virus. TEM of induced virus infected cells revealed a log-fold increase in the number of capsids in the nuclei of stop-ORF19 virus infected cells compared to BAC16 and res-ORF19 virus infected cells. Capsid species counting combined with statistical analysis revealed that stop-ORF19 disproportionately accumulated A-capsids in the nuclei of infected cells.

Methods:

Cells:

Human HEK 293T cells were purchased from American Type Culture Collection (ATCC) (Manassas, VA) and iSLK cells were kindly provided by Dr. Brit Glaunslinger [20]. Naïve iSLK and uninfected HEK 293T cells were maintained in high glucose DMEM with pyruvate (Gibco catalog: 11995040) supplemented with 10% heat inactivated FBS (hyclone catalog: SH30088.03) and 1% PenStrep (Gibco catalog: 15140122) (complete medium). iSLK-BAC16, iSLK-stop-ORF19, and iSLK-res-ORF19 transfected cell lines were expanded in complete media supplemented with 1.2mg/ml hygromycin B (Gibco catalog: 10687010) (selection medium). For induction of iSLK-BAC16, iSLK-stop-ORF19, iSLK- res-ORF19 and infected HEK 293T cells, complete media was supplemented with 1ug/ml of doxycycline (sigma catalog: D9891) and 1mM of butyrate (sigma catalog: 303410) (induction medium).

Plasmids:

The KSHV BAC16 was generated previously and was kindly provided by Dr. Brit Glaunsinger[19]. The pEPKanS plasmid was a gift from Nikolaus Osterrieder (Addgene plasmid # 41017). Construction of stop-ORF19 virus from the parental BAC16 was done using 2-step red-mediated recombineering [21] to insert a 12-base pair sequence at nt. 34413 (GenBank: MK733609.1). This insertion corresponds to a stop-codon in every reading frame and results in a C-terminal truncation of ORF19. This truncation removes the entire ORF19 globular domain, leaving only the N-terminal amino acids 1-83 [16]. To create the res-ORF19 virus, we removed the inserted stop-codon from the stop-ORF19 genome using the same method.

To create stop-ORF19 and res-ORF19 viruses, positive selection marker PCR products (NEB catalog: M0530S) were generated with stop-ORF19 or res-ORF19 primers and the pEPKanS plasmid (primer table). The products were separated on agarose and the amplicon was removed using the Qiagen gel extraction kit (Qiagen catalog: 28704). BAC16 or stop-ORF19 containing GS1783 E.coli were grown in LB broth (fisher catalog: BP1426), heat shocked at 42C for 15 minutes, and incubated on ice for 25 minutes. The cultures were spun down, washed three times in 10% glycerol and resuspended in 1:100th of the original culture volume in 10% glycerol. 50ul of resuspended culture was used to electroporate 100ng of positive selection marker PCR product and the suspensions were recovered in SOC media (Invitrogen catalog: 15544) and plated on kanamycin plates. Colonies were screened using alkaline lysis followed by PCR (Qiagen catalog: 201443), restriction digest with NheI (Thermo catalog #FD0974), and sanger sequencing (University of California at Berkeley DNA Sequencing facility). To remove the sequence duplications and kanamycin selection marker, screened colonies were inoculated in LB broth and arabinose was added to final concentration of 1%. The cultures were heat shocked at 42C for 15 minutes and cultured at 30C for an additional 2 hours. Colonies were isolated on arabinose (1%) and chloramphenicol plates and replica plated on kanamycin plates. Colonies negative for growth on kanamycin plates were recovered in LB broth and screened using alkaline lysis followed by PCR, restriction digest, and sanger sequencing. All sequencing was done using PCR products. (Qiagen catalog: 28704) and the PCR forward primer.

Generation of iSLK-BAC16, iSLK-ΔORF19, and iSLK-res-ORF19 transfected cell lines

BAC16, stop-ORF19, and res-ORF19 BAC DNA was isolated from GS1783 E. coli using the nucleobond BAC 100 kit (Macherey-Nagel catalog # 740579) according to the manufacturer's instructions. iSLK cells were seeded into 6 well plates at 90% confluence and incubated at 37C with 5% CO_2 overnight. The next morning, the media was aspirated, cells were washed, and complete media without antibiotic was added. Cells were transfected with 2.5ug of DNA using Lipofectamine 2000 (Invitrogen catalog# 11668030) following the manufactures recommendations. 48 hours after transfection, the media was changed to selection media. Cells were monitored by phase and fluorescence microscopy for up to 90 days. No colony isolations were performed.

RT-qPCR:

iSLK-BAC16, iSLK-stop-ORF19, and iSLK-res-ORF19 transfected cell lines were seeded into 12-well plates at 70% confluence and incubated at 37C 5%CO2 overnight. The next day cells were washed and induced with 2ml of induction media. At 40 hours post induction 1.2ml of cold solution D[22] was added to the wells and the lysates were placed on ice for 15 minutes. 0.1 volume of 2M sodium acetate (pH=4.0) was added followed by 1 volume of phenol-chloroform -isoamyl alcohol (25:24:1) (Invitrogen cat# 15593031), and the aqueous phase was precipitated with 1 volume of isopropyl alcohol. The pellet was washed with 0.3 volumes of solution D, re-precipitated using isopropanol and washed with 70% ethanol. 1ug of RNA was digested with DNase I at 37C for 1 hour (Thermo catalog # EN0525) and 10ng of RNA was reverse transcribed into cDNA using the Bio-Rad iSCRIPT kit (catalog# 1708840). 2.5ng of cDNA was used with 350nM of gene specific primers (primer table 2) in the qPCR reaction with the Bio-Rad SSOAdvanced Universal SYBR Green supermix (catalog# 1725270). Fold changes were calculated using the delta delta Cq method [23].

qPCR:

For latent and lytic genome replication assays, iSLK-BAC16, iSLK-stopORF19, and iSLK-res-ORF19 transfected cell lines were seeded into t75 flasks at 70% confluence and incubated at 37C, 5%CO2 overnight. For latent genome replication, the cells were passaged every 3 days and a sample of cells was harvested every 6 days. For lytic genome replication, the next day the media was changed to induction media and the cells were incubated for 72 hours. Harvested cells were washed three times in TBS and stored at -80C until DNA extraction. For DNA extraction, cells were resuspended at a concentration of 1.5*10^7 cells/ml in TE (pH=8.0), and proteinase K (100ug/ml) plus 10 volumes of lysis buffer (10mM Tris-Cl (pH=8.0), 0.1M EDTA (pH=8.0), 0.5% SDS (w/v), 20ug/ml RNase) was added. The solution was incubated at 50C for 3 hours. The solution was extracted three times with phenol-chloroform -isoamyl alcohol (25:24:1) (Invitrogen cat# 15593031) and DNA was precipitated with ammonium acetate and ethanol. Approximately 10ng of DNA and 350nm of LANA and 18S primers were added to the qPCR reaction using the Bio-Rad SSOAdvanced Universal SYBR Green supermix (catalog# 1725270). Fold changes were calculated using the delta delta Cq method [23].

Virus production and tittering

iSLK-BAC16, iSLK-stop-ORF19, and iSLK-res-ORF19 transfected cell lines were induced using induction media and the supernatant and cells were harvested 4 days post induction. The samples were freeze-thawed, centrifuged at 3200xg for 15 minutes, and then passed through a 0.45um aPES filter. The cleared supernatant was concentrated at 34,000xg for 3 hours and the pellet was resuspended in 1:100 volume of complete medium. For titration, HEK 293T cells were seeded in 48-well plates at 50% confluence and cultured overnight at 37C with 5% CO_2. The next morning serial dilutions of viral stocks were made using induction media. The media was aspirated from cells and 400ul of virus dilutions were added to wells in duplicate. The plates were centrifuged at 2000xg, 30C, for 1 hour and then allowed to incubate at 37C, 5% CO_2 for one hour. After the incubation period the inoculum was removed, 500ul of fresh induction media was added to the wells and the cells were incubated at 37C, 5% CO_2 for 48 hours. After 48 hours the wells were examined by fluorescence microscopy and GFP+ cells were counted and used to calculate viral titer.

Electron microscopy

iSLK-BAC16, iSLK-stop-ORF19, and iSLK-res-ORF19 transfected cell lines were thawed and maintained in section media in T75 flasks. When cells reached 90% confluency the media was changed to induction media. Induced infected cells were fixed directly in flasks with a solution containing 1 part 4% glutaraldehyde (Ted pella catalog number: 18420) in 1X PBS and 1 part induction media for 2 hours at 37C, 5% CO_2. Cells were gently scrapped into the fixative solution and stored in 2.5% glutaraldehyde in 0.1M sodium cacodylate pH=7.4 (EMS sciences catalog number: 16537-15) until secondary fixation and embedding. For secondary fixation and embedding, the cells were resuspended in 2% low gelling temperature agarose, spun down, and allowed to solidify on ice. The cell pellet was cut from the bottom of the tube with a razor blade and washed twice with 0.1M sodium cacodylate pH=7.4 for 10 minutes on a tilting rack. Secondary fixation occurred in the dark for 1 hour in a solution of 1% Osmium in water with 1.6% ferricyanide. The cell pellet was dehydrated in an acetone series; 30%, 50%, 70%, 80% 95%, 100% and infiltrated in a series of acetone:resin mixtures; 3:1, 1:1, 1:3, followed by pure resin overnight. (Eponate-12 kit with DMP-30, Ted Pella catalog: 18010) The next day, the sample was embedded twice with resin and DMP-30 accelerant for 30 minutes, and then cured at 60C for 48 hours. The cured blocks were hand trimmed and thin sectioned into 100nm sections on mesh copper grids coated with a 0.5% solution of formvar. The grids were stained with 2% uranyl acetate for 5 minutes followed by lead citrate for 7 minutes and imagined on a Tecnai 12 scope at 120kV.

Results:

Generation of stop-ORF19 and res-ORF19 viruses

To study the function of KSHV ORF19 in the viral lifecycle we used KSHV BAC16 to create an ORF19 inactivation virus using en-passant mutagenesis. En-passant mutagenesis utilizes a PCR construct to insert targeted, scarless mutations in bacterial artificial chromosomes[21]. Primers are designed to produce a product containing a 20bp sequence duplication of nucleotides 3' to the mutation site in the 5' region, an SceI cleavage site, a selection marker, and a 20bp sequence duplication of the nucleotides 5' to the mutation site in the 3' region. The product is electroporated into GS1783 stain of E.coli which contain the KSHV bacterial artificial chromosome (BAC) clone BAC16[24 19]. Additionally, GS1783 E.coli contain the lambda-red recombination proteins (Exo, Gam, Beta) under a temperature sensitive promoter, and the SceI meganuclease under an arabinose-inducible promoter[24]. Homologous recombination between PCR product and BAC16 is mediated by lambda-red recombination proteins and results in the insertion of the PCR product into BAC16. The selection marker and sequence duplications are removed by SceI-mediated cleavage and a second red-mediated homologous recombination event facilitated by the 5' and 3' sequence duplications, leaving a scarless mutation (Chapter 2)

The ORF19 CDS is in reverse orientation and flanked by overlapping ORFs. ORF20 CDS overlaps ORF19 CDS by 233bp in the 5' region, and ORF18 CDS overlaps ORF19 CDS by 4bp in the 3' region (Figure 1 A-B). Therefore, we used en-passant mutagenesis to insert a stop codon in every reading frame in the non-overlapping 5' region, which results in a C-terminal truncation of ORF19 (1-83). We created the res-ORF19 virus by removing the stop codon from the stop-ORF19 virus using the same methodology. Sanger sequencing confirmed the insertion and orientation of the stop codon in the stop-ORF19 virus, and removal of the stop codon in the res-ORF19 virus (Figure 1C-D). We also examined stop-ORF19 and res-ORF19 virus integrity by NheI restriction digest (Supplemental Figure 1). These data suggest that no off-target rearrangements occurred in the stop-ORF19 and res-ORF19 viruses.

stop-ORF19 virus establishes and maintains viral latency in iSLK cells

Previous studies have shown that infection of iSLK cells with KSHV BACs results in stable latency characterized by the lack of infectious progeny in cells and culture supernatant[20]. We adopted this tractable system to examine the role of ORF19 in establishment and maintenance of viral latency. We transfected stop-ORF19, res-ORF19 and BAC16 viruses into iSLK cells and selected for transfectants using hygromycin. By 45 days post transfection we observed the outgrowth of morphologically normal cells. All cells appeared GFP+, consistent with having retained the viral genome as BAC16 contains a GFP reporter[19] (Figure 2A). Next, we sought to validate the establishment and maintenance of viral latency in our cell lines using two series of experiments. First, to investigate the presence of infectious progeny, infected cells and supernatants were harvested and used to infect 293T cells. These experiments showed that no infectious progeny was produced in cells and supernatants of stop-ORF19, res-ORF19 and BAC16 virus infected cultures at 2, 8, 14, 20, and 26 days after construction of cell lines was completed and selection was removed. These results support the hypothesis that the viruses in these cells are not in the lytic replication cycle.

In the second series of experiments, we examined the maintenance of viral genomes in stop-ORF19, res-ORF19 and BAC16 virus infected cells during a time course of 26 days after construction of the cell line was completed and selection was removed. In these experiments, infected cells were collected at 2, 8, 14, 20, and 26 days and the levels of viral genome copy number were determined by qPCR. We performed two different analyses for this experiment. First, we compared the levels of viral genome copy number in the stop-ORF19 and res-ORF19 cell lines with those of the BAC16 at each time point (figure 2B). Second, we compared the levels of genome copy numbers of each virus to those of the corresponding virus at the 2-day timepoint (figure 2C).

Comparison of mutant with BAC16 genome copy numbers at each time point revealed and interesting trend. stop-ORF19 exhibited an increase in viral genome copy number relative to BAC16 throughout the time course, resulting in approximately 4-fold more genomes by 26 days in culture. res-ORF19 infected cells also showed an increase in viral genome copy number relative to BAC16 throughout time course, resulting in 2.6-fold more genomes by 26 days in culture. To examine if the increase in genome copy number of the mutants relative to BAC16 could be explained by the loss of viral genomes from BAC16 infected cells, we compared the level of genome copy numbers of each virus to those of the corresponding virus at the 2-day timepoint (figure 2C). This analysis revealed BAC16 virus exhibited a decrease in genome copy number throughout the time course. Consistent with this observation, stop-ORF19 virus exhibited a 2-fold increase in viral genome copy number and res-ORF19 virus exhibited a 1.4-fold increase in viral genome copy number after 26 days in this analysis (Figure 2C). We attribute the variability of genome copy numbers in this assay to differences in transfection efficiencies. This is to say that each BAC-virus cell line was formed by a different number of cells that successfully received the viral genome during transfection, and differences in the initial copy number of viral genomes received by each successfully transfected cell (see methods). These data indicate that stop-ORF19, res-ORF19, and BAC16 virus infected cells, on average, have at least as many viral genomes as BAC16 virus infected cells (figure 2B) and that all three viruses replicate latent viral DNA with similar kinetics (figure 2C). These data support the hypothesis that the maintenance of latency is unaffected in stop-ORF19 virus.

stop-ORF19 virus engages in lytic gene expression and lytic genome replication upon induction

Once we verified there were no significant differences in the levels or replication kinetics of stop-ORF19, res-ORF19 and BAC16 viruses in latency, we sought to examine if the viruses could be reactivated by induction. One of the advantages of the KSHV BAC-iSLK system is that iSLK cells contain the KSHV lytic switch protein ORF50 under the tet-on system[20]. Ectopic expression of ORF50 reactivates KSHV from latency and drives the entire lytic cascade of gene expression[25,26]. Thus, the addition of doxycycline and the histone deacetylase inhibitor butyrate to the media results in significant cell-free progeny in this system[19 20].

To examine the ability of stop-ORF19, res-ORF19, and BAC16 viruses to reactivate from latency, we added doxycycline and butyrate to the media and cultured cells for 40 hours. We expected to see viral lytic gene transcription if viruses were reactivated from latency. We extracted total RNA, digested with DNase I, and performed RT-qPCR using gene specific primers for LANA, ORF50, ORF45 and ORF25. We choose these viral targets to act as

surrogates for transcription of latency (LANA), IE (ORF50), DE (ORF45), and L (ORF25) viral transcripts. stop-ORF19, res-ORF19, and BAC16 virus infected cells showed log-fold increases in lytic gene expression relative to non-inducing conditions and one way ANOVA confirmed there were no significant differences in viral lytic gene expression between viruses (Figure 3A). These data indicate that transcription of viral genes, as represented by LANA, ORF50, ORF45, and ORF25, was induced to similar levels in stop-ORF19, res-ORF19, and BAC16 virus infected cells (figure 3A).

We expected expression of viral lytic transcripts to lead to viral lytic DNA replication. To examine the ability of stop-ORF19, res-ORF19, and BAC16 viruses to engage in lytic DNA replication, we induced cell lines harboring these viruses for 72 hours, extracted cellular DNA, and ran qPCR with LANA specific primers. stop-ORF19, res-ORF19, and BAC16 viruses displayed an increase in genome copy number relative to non-inducing conditions by 72 hours post induction (figure 3B). These data indicate viral lytic DNA replication was induced in cell lines harboring stop-ORF19 and res-ORF19 viruses as well as BAC16. Our viral lytic gene expression and viral lytic DNA replication data support the hypothesis that stop-ORF19 and res-ORF19 viruses are reactivated upon induction, and that reactivation was not attenuated compared to BAC16 virus.

stop-ORF19 virus does not produce infectious progeny after extensive induction

After reactivation, lytic gene expression, and viral lytic DNA replication, we expected infected cells to assemble viral capsid and release mature infectious viral particles into the culture media. To examine the ability of stop-ORF19, res-ORF19, and BAC16 viruses to produce infectious progeny, we induced cell lines harboring these viruses and harvested the cells and supernatants for tittering. At 96 hours post induction, stop-ORF19, res-ORF19, and BAC16 virus infected cells all showed cytopathic effect as determined by the rounding and swelling of cells, and a significant reduction in confluence (Figure 4A compared to figure 2A). We collected the cells and culture supernatant and used them to infect 293T cells. 48 hours after infection, the number of GFP+ cells were counted using fluorescence microscopy and used to calculate viral titer. Interestingly, stop-ORF19 virus produced no viral progeny while res-ORF19 virus produced progeny and grew like BAC16 virus (Figure 4B). These results support the hypothesis that disruption of KSHV ORF19 by stop codon insertion in the 5’ region of the CDS results in a mutant that cannot produce infectious viral progeny after extensive induction.

stop-ORF19 virus infected cells accumulate A-capsids in nuclei after induction

Since stop-ORF19 virus was able to replicate viral DNA but failed to produce infectious progeny, we speculated that this mutant may be defective in capsid maturation or viral particle formation. To test this hypothesis, we induced stop-ORF19 virus infected cells and fixed them in glutaraldehyde at 2-, 3- and 4-days post induction. Fixed cells were embedded in resin, sectioned, and examined using TEM. We observed significant numbers of capsid structures in the nuclei of induced stop-ORF19 virus infected cells. At 2 days post induction, we observed primarily A-capsid structures and only a handful of C-capsid structures scattered throughout nuclei (Supplementary figure 2). However, by 4 days post induction, stop-ORF19 virus infected cell nuclei accumulated only A-capsid structures (figure 5). We rarely observed capsid structures in induced res-ORF19 and BAC16 virus infected cells, consistent with the hypothesis that KSHV capsids are efficiently matured, exported out of the nucleus, formed into mature virions, and

released from the cell. When we did locate capsids, there were <10 per nucleus and they were mostly B-capsids (figure 5).

TEM is generally regarded as a qualitative (non-numerical) piece of data. To increase the cogency of this evidence, we added a quantitate aspect by counting the number of capsids in infected cell nuclei. When we counted the total number of capsids in infected cell nuclei (irrespective of area constraints), we observed a log-fold increase in nuclear capsids in stop-ORF19 virus compared to BAC16 virus (table 3). The high absolute number of capsid structures observed in stop-ORF19 virus infected cell nuclei (n=257) compared to the low absolute number of capsid structures observed in BAC16 virus infected cell nuclei (n=15) indicate that capsids produced by stop-ORF19 virus are retained in the nucleus (table 3).

To examine the relative distribution of capsid species between samples, we counted a fixed number of capsids (n=2) in a fixed nuclear area ($1um^2$) in stop-ORF19 and BAC16 virus infected cells and calculated the mean number of each capsid type per area (table 3). The mean number of A-capsids was $1.52/1um^2$ (SD=0.70) in stop-ORF19, compared to $0.40/1um^2$ (SD=0.80) in BAC16. The mean number of B-capsids was $0.19/1um^2$ (SD=0.51) in stop-ORF19, compared to $1.60/1um^2$ (SD=0.80) in BAC16. The mean number of C-capsids was $0.29/1um^2$ (SD=0.50) in stop-ORF19, compared to $0.00/1um^2$ (SD=0.00) in BAC16 (table 3). The high mean number of A-capsids per fixed nuclear area in stop-ORF19 virus infected cells compared to the high mean number of B-capsids per fixed nuclear area in BAC16 virus infected cells support the hypothesis that stop-ORF19 virus infected cells disproportionally accumulate A-type capsids. Together, these quantitative data support the hypothesis stop-ORF19 virus is deficient in capsid maturation and nuclear egress.

Discussion:

The establishment of latency in KSHV infected cells is largely governed by epigenetic changes. Shortly after infection the KSHV genome adopts a transcriptionally active epigenetic state[27] resulting in attenuated viral lytic gene expression[28]. This "initial burst" of lytic gene expression has been hypothesized to prime the cell for the establishment of latency because shortly after it begins, the active epigenetic state is replaced by a repressive state, resulting in viral latency[27]. Our data demonstrate that stop-ORF19 virus was able to establish and maintain latency in iSLK cells as determined by creation of a cell line harboring stop-ORF19 virus and absence of infectious viral progeny in cells and supernatants of infected cultures. Thus, our data support the hypothesis that KSHV ORF19 does not play a role in the early events responsible for the transition from a transcriptionally active to a transcriptionally repressive genomic state in iSLK cells.

During latency the KSHV genome is maintained in the nucleus of infected cells as episomal plasmids, and several host factors serve key roles in latent viral DNA replication[29]. KSHV ORF73 (LANA) has been shown to be essential for the maintenance of latency by tethering viral episomes to host chromatin[30], mediating latent DNA replication[31], and segregating replicated viral DNA during mitosis[8]. However, to our knowledge, no labs have directly examined the roles of other KSHV ORF's in these processes. Our results show that stop-ORF19 virus was able to maintain, replicate and segregate viral DNA under non-inducing conditions with similar efficiencies relative to res-ORF19 and BAC16 viruses as determined by qPCR. These data support the hypothesis that ORF19 is dispensable for the maintenance of viral latency as defined as episomal tethering, latent viral DNA replication, and viral DNA segregation during mitosis in iSLK cells.

While ectopic ORF50 expression is sufficient to reactivate KSHV from latency [25,32] several other viral gene products have been shown to positively or negatively regulate KSHV reactivation [33 34 35], and control lytic DNA replication [36 37]. Reactivation, as measured by the induction of immediate early (ORF50), early (ORF45), and late gene (ORF25) transcription was not enhanced or attenuated in stop-ORF19 virus, and lytic viral DNA replication occurred at least as well in stop-ORF19 virus compared to the BAC16 virus. While it is important to note that ORF50 expression is initially induced exogenously in this system, ORF50 expression from the viral genome is also expected to take place[38]. Our results support the hypothesis that KSHV ORF19 does not play a role in positively or negatively regulating reactivation or lytic DNA replication. Furthermore, our results suggest that ORF19 is dispensable for the expression of viral immediate-early, early, and late genes.

KSHV ORF19 is a core gene conserved throughout the human herpesvirus subfamilies. ORF19 and its homologs bind directly to the capsid exterior as an inner tegument component while forming part of the Capsid Vertex Specific Component (CVSC). The CVSC is a hetero-pentameric complex composed of three conserved proteins; one unit of KSHV ORF32, two units of KSHV ORF19, and two units KSHV ORF64[16,39-41]. Cryo-EM studies of virions have revealed this complex is found at the capsid vertices where it caps the tips of pentons. However, herpesviruses from different subfamilies indicate the stoichiometry of CVSC-penton binding varies significantly. In α herpesviruses, five units of CVSC bind to each of the pentons at the capsid vertices[42-45]. This "full occupation" of CVSC at the capsid vertices has been proposed to

support and reinforce capsid stability after genome packaging[43,46], and atomic force microscopy measurements support this hypothesis in HSV-1[47]. However, in β and γ herpesviruses, the CVSC occupies capsid vertices at significantly reduced frequency. In β herpesviruses, the majority of penton vertices are occupied by a single CVSC unit in HCMV[48] and no CVSC units are found at the penton containing vertices of HHV-6B[49]. For the γ herpesvirus EBV, the average occupancy of CVSC units at penton vertices is one, with portal proximal pentons displaying one copy of the CVSC and portal distal pentons displaying two copies of the CVSC [50]. In the γ herpesvirus KSHV, the average occupancy of CVSC units at penton vertices is closer to two, with portal proximal pentons displaying two copies of the CVSC and portal distal pentons displaying one copy of the CVSC[18]. The lack of association between CVSC occupancy at capsid vertices and viral genome size for β and γ herpesviruses argue against the hypothesis that KSHV ORF19 and its homologs in β and γ herpesviruses function to stabilize the capsid once the genome has been loaded. The identification of β herpesvirus-specific inner tegument components [49,51,52], and the mapping of core capsid component interactions in γ herpesviruses[53-55], indicate that capsid structural integrity is obtained independently of KSHV ORF19 and its homologs. Despite the variability of penton-vertex occupancy by CSVC's, all studies agree that the portal vertex contains the full register of CSVCs, and that the CSVC component KSHV ORF19 (and its homologs) have their head domains extending over the portal opening like a cap [18,48,50,56]. Our observation of a significant number of C-capsids 2 days post induction (Supplemental figure 3, table 3) show that KSHV C-capsids can be formed in the absence of ORF19. These data indicate the KSHV ORF19 is not essential to maintain capsid stability during genome packaging. While it is tempting to speculate that the disappearance of C-capsids overtime (figure 5) in induced stop-ORF19 virus infected cell nuclei is the result of the breakdown of unstable C-capsids lacking ORF19, this rationale is countered by our observation of significant numbers of A-capsids in infected stop-ORF19 cell nuclei. The concurrent disappearance of C-capsids and enrichment of A-capsids overtime supports the interpretation that capsids lacking ORF19 result in the expulsion of packaged DNA through the uncapped portal.

Herpesvirus nuclear egress is mediated by primary envelopment at the inner nuclear membrane (INM), transport through the perinuclear space, and fusion of primary enveloped nucleocapsids at the outer nuclear membrane (ONM), resulting in the release of naked capsids into the cytosol. The genes that make up the herpesvirus nuclear egress complex (NEC) are conserved throughout herpesvirus subfamilies. This complex is essential for primary envelopment and nuclear egress of capsids, however, the recruitment mechanism of nascent capsids to the NEC embedded INM and the molecular interactions governing the engulfment of capsids for transport through the lumen of the nuclear membrane remain largely unknown [57]. A mutant PrV virus lacking UL25 (KSHV ORF19) was shown to be defective in nuclear egress of C-capsids, outlining a possible role for KSHV ORF19 and its homologs in primary envelopment[58]. Biochemical analysis confirms that components of the HSV-1 CVSC UL25 and UL17 (KSHV ORF19 and KSHV ORF32) directly interact with the NEC in the context of viral infection[59], and cryo-electron tomographs indicate HSV-1 capsids undergoing primary envelopment make contact with inner nuclear membrane-anchored NEC largely through the CVSC[60]. Despite this evidence, studies in PrV indicate part of the NEC (UL31) associates with capsids in the absence of UL25 (KSHV ORF19)[61]. This observation combined with the evidence that the NEC forms hexagonal lattices in in-vitro budding assays and crystallization experiments hints at alternative NEC-capsid contact points [62,63]. In-vitro biochemical data support the

hypothesis that KSHV ORF19 interacts with a component of the KSHV NEC (KSHV ORF69)[17]. However, proper capsid loading is generally regarded to be a prerequisite for nuclear egress, and this hypothesis is a possible confounder in our speculations on the role of KHSV ORF19 in nuclear egress from our data. It is worth noting that the enrichment of A-capsids in induced ΔORF19 virus infected cells occurs around the edges of the nucleus (Figure 5), but not directly proximal to the INM. This leads to the hypothesis that ORF19 is not responsible for capsid transport to the edges of the nuclear membrane, however, direct contact with the INM mediated through the NEC is not possible in the absence of ORF19. This hypothesis is also supported by the fact that we did not observe any capsids in the cytoplasm of induced ORF19 virus infected cells. Whether or not KSHV ORF19 interacts with the NEC in the context of viral infection, and whether this interaction (if it does occur) plays a significant role in the engulfment of capsids at the INM remains to be seen. Mapping the molecular interactions between KSHV ORF19 and the NEC using alanine scanning and/or linker insertion studies in the globular and helix domain of ORF19 in the context of viral infection will help elucidate the role of ORF19 in nuclear egress.

FIGURES AND TABLES

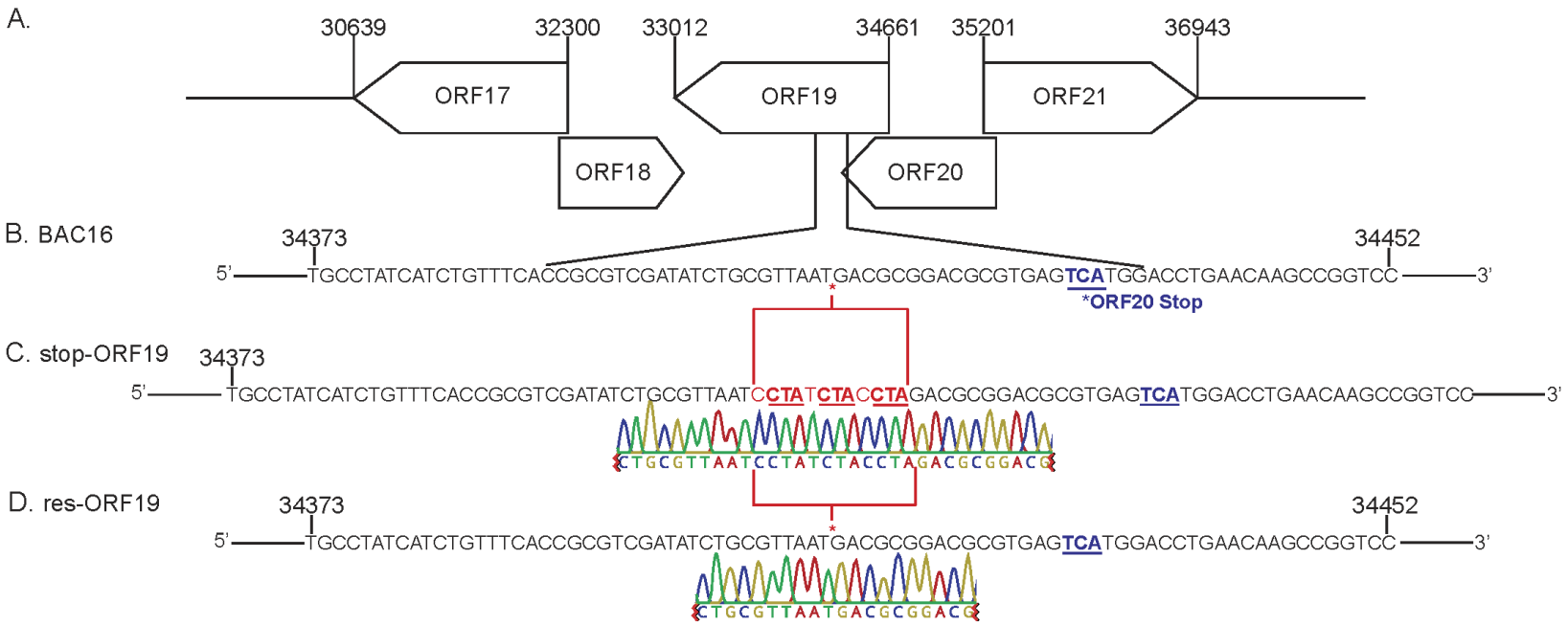

Figure 1: Construction of stop-ORF19 and res-ORF19 viruses.

(A) Schematic of the coding regions surrounding ORF19 in the KSHV genome (GenBank: MK733609.1). (B) The sequence from the parental BAC16 used to design mutagenesis primers is shown. The red asterisk marks the location of stop codon insertion for creation of the stop-ORF19 genome, and the blue underline marks the location of the ORF20 stop codon. (C) The sequence of the stop-ORF19 genome is shown with the 12-bp insertion in red, and stop codons underlined. Sanger sequencing data confirming the orientation and integrity of stop codon insertion in the stop-ORF19 genome is shown directly underneath the sequence. (D) The res-ORF19 virus was created by removing the 12-bp insertion from the stop-ORF19 genome. Sanger sequencing data confirming the removal of the 12-bp insertion from the stop-ORF19 genome and integrity of the mutation site.

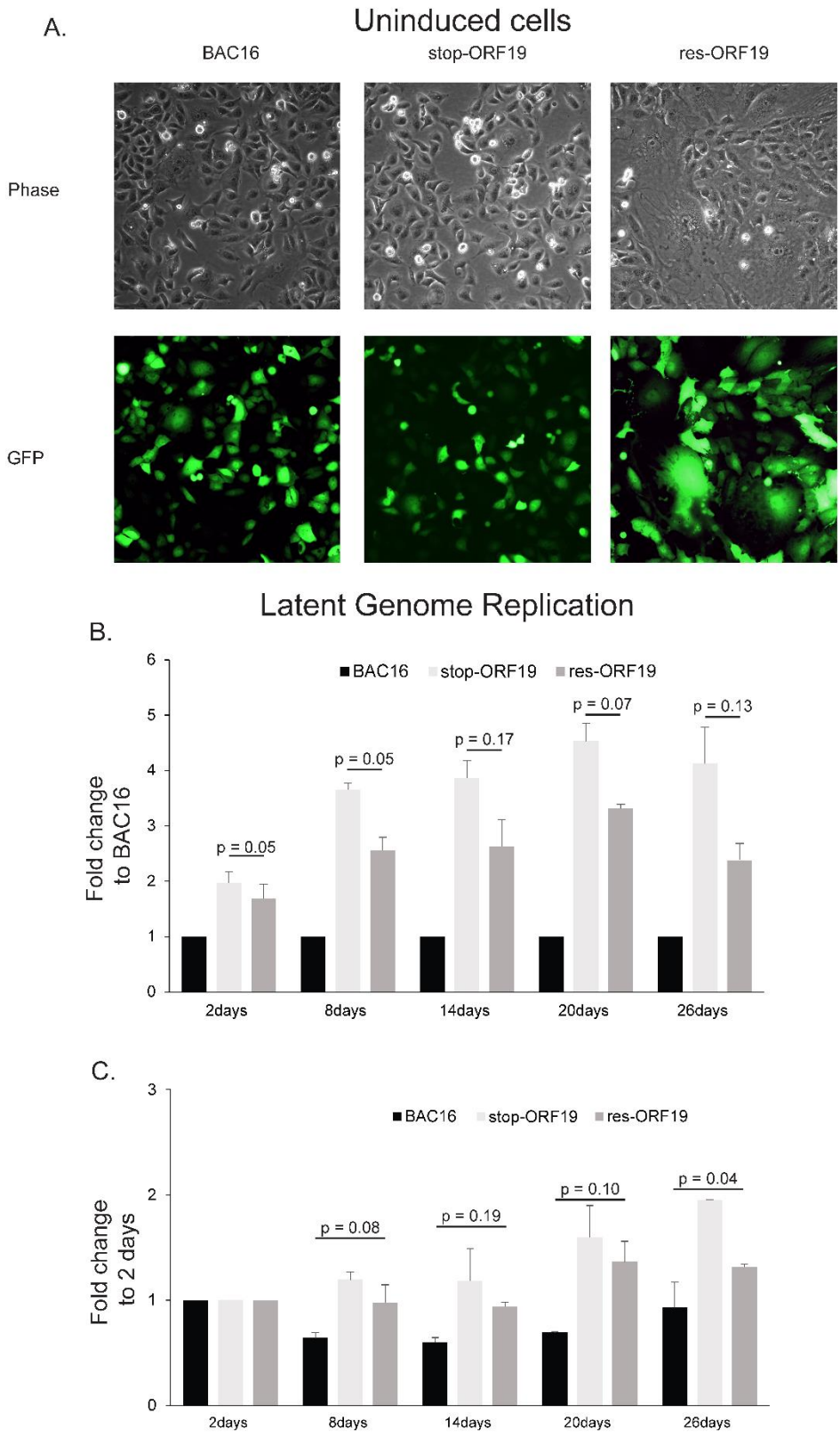

Figure 2: stop-ORF19 establishes latency and replicates viral DNA in iSLK cells.

(A) Phase-contrast and GFP photos of iSLK-BAC16, iSLK-stop-ORF19, and iSLK-res-ORF19 cells under hygromycin selection. Total magnification 200X. (B-C) Latent viral genome replication under non-inducing conditions in iSLK-BAC16, iSLK-stop-ORF19, and iSLK-res-ORF19 cells. Total DNA was harvested and subjected to qPCR using LANA and 18S primers. (B) Fold change to BAC16 is shown and p-values for Students 2-talied, unpaired T-test are reported. (C) Fold change to 2-days is shown and p-values for one way ANOVA are reported. All bars represent the average of 2 independent experiments and error bars indicate 1 standard error of the mean. All fold changes were calculated using $\Delta\Delta$Cq method

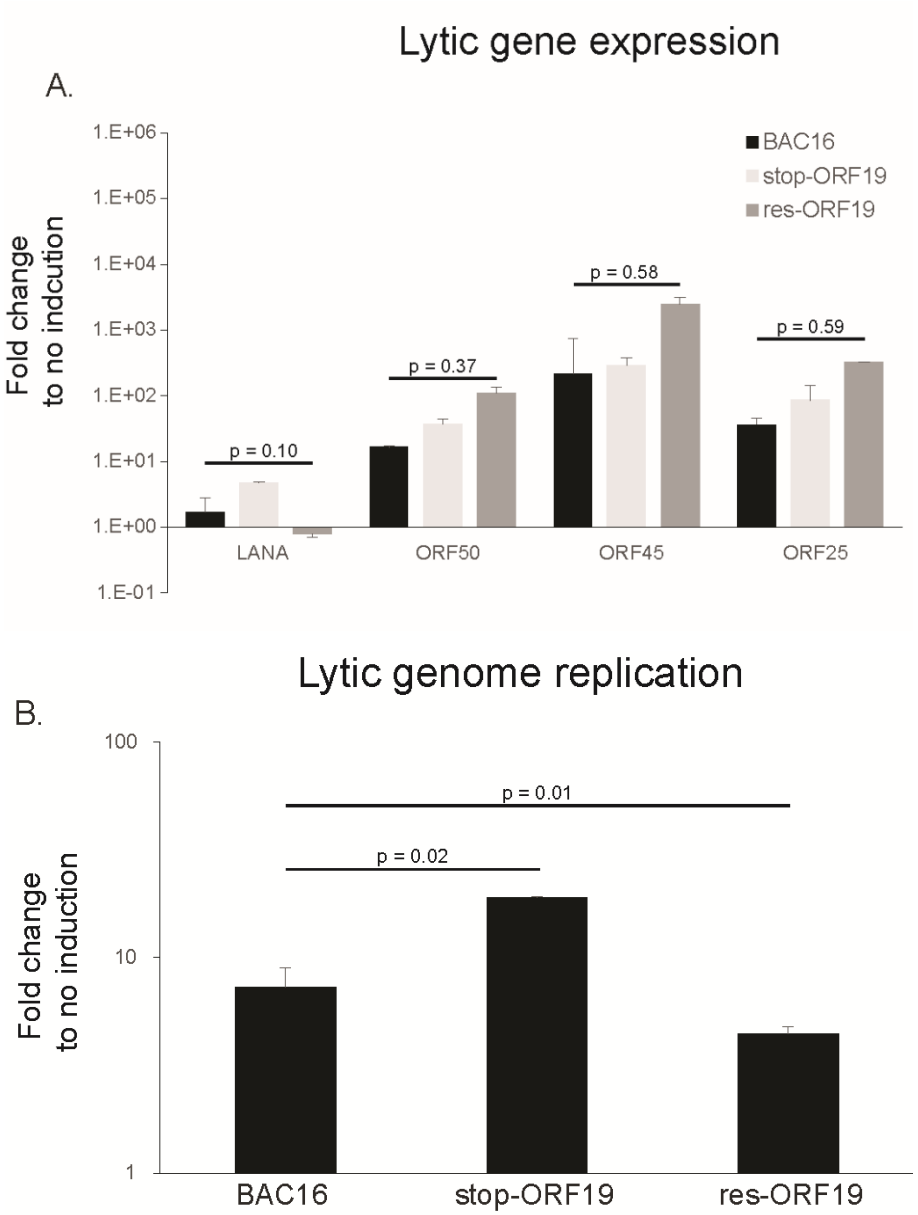

Figure 3: stop-ORF19 virus reactivates from latency and undergoes lytic viral DNA replication.

(A) Lytic gene expression in iSLK-BAC16, iSLK-stop-ORF19, and iSLK-res-ORF19 cells after treatment with sodium butyrate and doxycycline for 40 hours. Fold change to no induction is shown. Total RNA was harvested and digested with DNase I, reverse transcribed to cDNA, and quantified by qPCR using 18S and gene-specific primers. p-values for one way ANOVA are reported. (B) Viral genome replication in iSLK-BAC16, iSLK-stop-ORF19, and iSLK-res-ORF19 cells after induction with sodium butyrate and doxycycline for 72 hours. Fold change to no induction is shown. Total DNA was harvested and quantified by qPCR using LANA and 18S primers. All bars represent the average of 2 independent experiments, error bars indicate 1 standard error of the mean. p-values for Students 2-tailed, unpaired T-test are reported. All fold changes were calculated using ΔΔCq method.

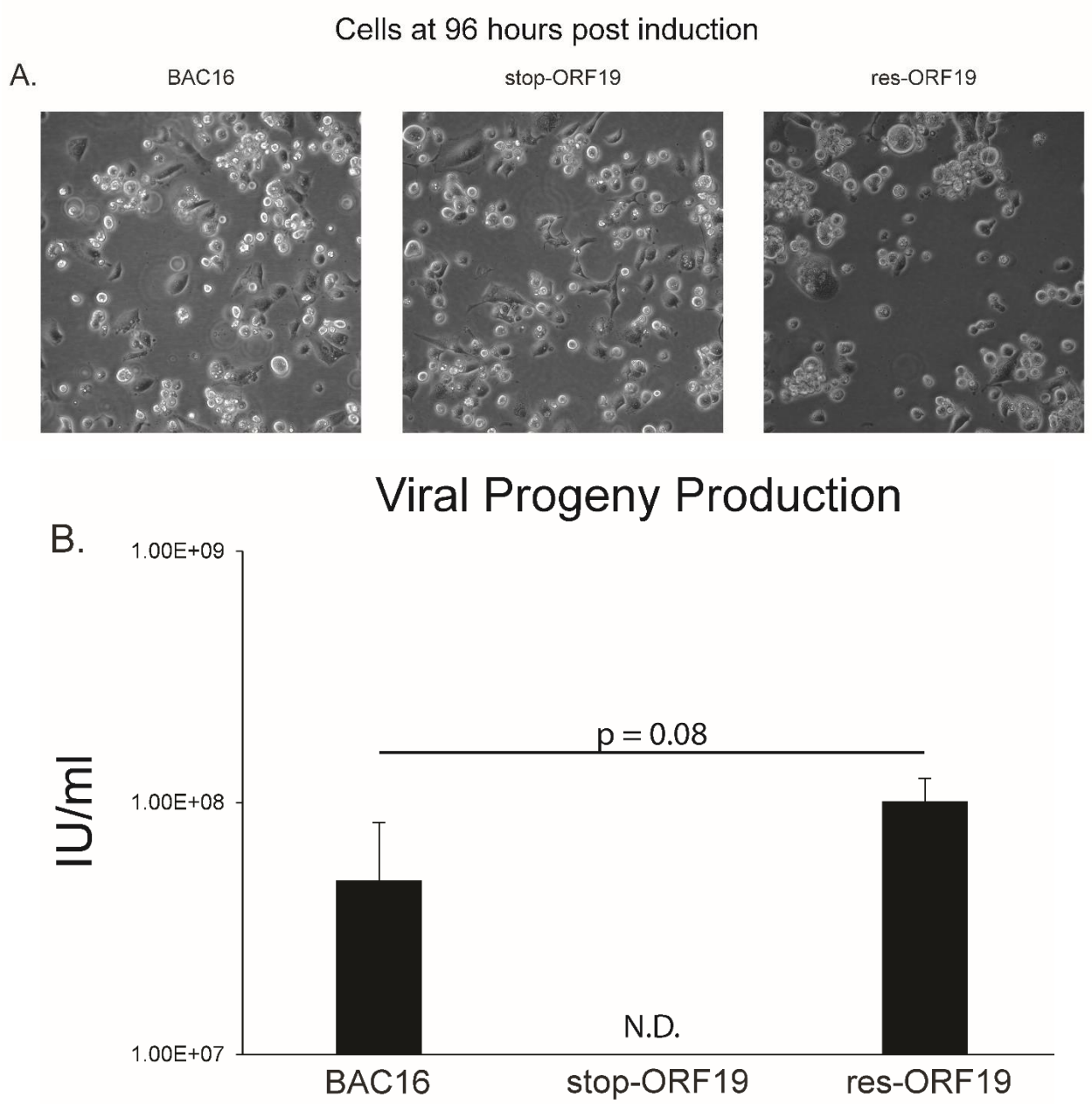

Figure 4: stop-ORF19 virus does not produce infectious progeny after extensive induction.

(A) Phase contrast photos of iSLK-BAC16, iSLK-stop-ORF19, and iSLK-res-ORF19 cells after induction with sodium butyrate and doxycycline for 96 hours. Total magnification 200X. (B) Quantification of viral progeny in cells and culture supernatant from iSLK-BAC16, iSLK-stop-ORF19, and iSLK-res-ORF19 cells after induction with sodium butyrate and doxycycline for 96 hours. Cells and supernatants were cleared via centrifugation and filtration, used to infected 293T cells, and infected cells were analyzed by fluorescent microscopy 48 hours post infection. All bars represent the average of four independent experiments, error bars represent 1 standard deviation, and p-values for Students 2-talied, unpaired T-test are reported.

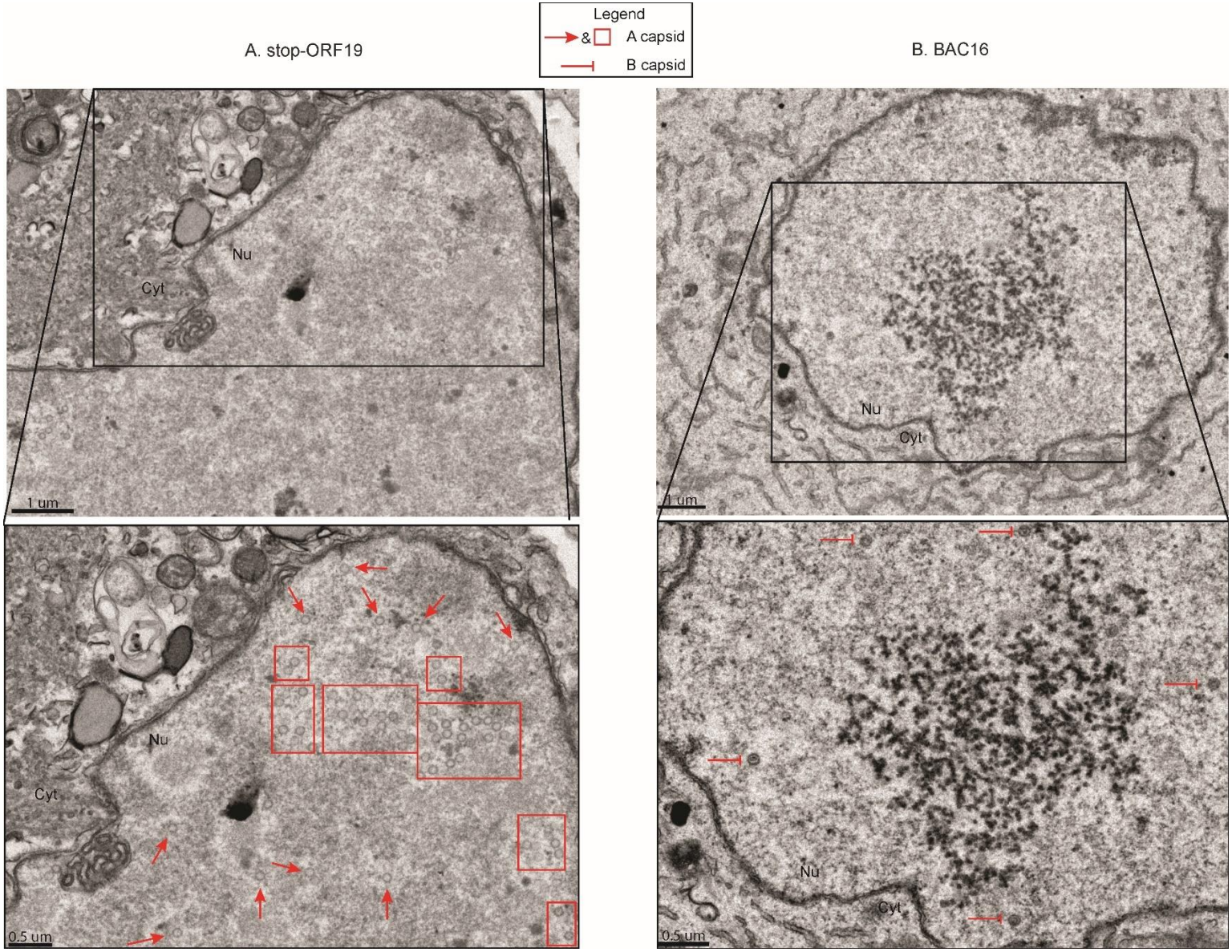

Figure 5: Induced stop-ORF19 virus infected cells accumulate A-type capsids in the nuclei after extensive induction.

(A) Electron micrograph of stop-ORF19 virus infected cells after induction with sodium butyrate and doxycycline for 4 days. Red boxes and pointed arrows mark the locations of A-capsids. (B) Electron micrograph of BAC16 virus infected cells after induction with sodium butyrate and doxycycline for 4 days. Flat-headed arrows mark the locations of B-capsids. All scale bars are in micrometers.

Table 1. Plasmid constructs used in the study

Plasmids	Description	Reference/source
KSHV BAC16	KSHV Bacterial Artificial Chromosome clone	[19]
stop-ORF19	KSHV Bacterial Artificial Chromosome clone with a stop codon insertion the 5' region of the ORF19 CDS (C-terminal truncation; 1-83)	This publication
res-ORF19	KSHV Bacterial Artificial Chromosome clone generated by removing the stop codon from the stop-ORF19 clone.	This publication
pEPkan-S	PCR template for en passant (two-step Red-mediated) mutagenesis	[21]

Table 2. Mutagenesis and sequencing primers used in the study

Name	Sequence
stop-ORF19 forward	GGACCGGCTTGTTCAGGTCCATGACTCACGCGTCCGCGTC**TAGGTAG ATAGG**ATTAACGCAGATATCGACGC*AGGATGACGACGATAAGTAGGG*
stop-ORF19 reverse	TGCCTATCATCTGTTTCACCGCGTCGATATCTGCGTTAAT**CCTATCTA CCTA**GACGCGGACGCGTGAGTCAT*AACCAATTAACCAATTCTGATTAG*
res-ORF19 forward	GGACCGGCTTGTTCAGGTCCATGACTCACGCGTCCGCGTCATTAACG CAGATATCGACGC*AGGATGACGACGATAAGTAGGG*
res-ORF19 reverse	TGCCTATCATCTGTTTCACCGCGTCGATATCTGCGTTAATGACGCGGA CGCGTGAGTCAT*AACCAATTAACCAATTCTGATTAG*
PCR forward	GATCCATTGGCGCGTAGTCTC
PCR reverse	AGCTCGGACGACGAATCAAG

Underlined sequences indicate homology to the BAC16. Single underline represents homology upstream of the insertion, and double underline represent homology downstream of the insertion. Bolded sequence represents the inserted stop codon. Italics represent homology to the pEP-KanS plasmid.

Table 3: Absolute and mean numbers of capsid types in stop-ORF19 and BAC16 virus infected cell nuclei

	stop-ORF19 (n=116)	BAC16 (n=10)
A-type	**1.52 ±0.70 (76%)**	**0.40 ±0.80 (20%)**
B-type	**0.19 ±0.51 (9%)**	**1.60 ±0.80 (80%)**
C-type	**0.29 ±0.49 (14%)**	**0.00 ±0.00 (0%)**
Total capsids observed	**257**	**15**

Means, standard deviations, and totals for capsid counts in stop-ORF19 and BAC16 cell lines. For capsid means and standard deviations, nuclear areas of $1um^2$ containing 2 capsids were counted. The numbers next to each virus (stop-ORF19 and BAC16) represent the number of capsids counted for capsid species analysis, and the percentages represent the number counted for each species. Total capsids observed is the number of capsids identified regardless of area constraints.

References:

1 Blossom A. Damania, E. C. *Fields Virology Sixth Edition, Chapter 65*. 2080-2128 (Lippincott Williams & Wilkins, 2013).

2 Ballestas, M. E., Chatis, P. A. & Kaye, K. M. Efficient persistence of extrachromosomal KSHV DNA mediated by latency-associated nuclear antigen. *Science* **284**, 641-644, doi:10.1126/science.284.5414.641 (1999).

3 Cotter, M. A., 2nd & Robertson, E. S. The latency-associated nuclear antigen tethers the Kaposi's sarcoma-associated herpesvirus genome to host chromosomes in body cavity-based lymphoma cells. *Virology* **264**, 254-264, doi:10.1006/viro.1999.9999 (1999).

4 Dittmer, D. *et al.* A cluster of latently expressed genes in Kaposi's sarcoma-associated herpesvirus. *J Virol* **72**, 8309-8315, doi:10.1128/JVI.72.10.8309-8315.1998 (1998).

5 Samols, M. A., Hu, J., Skalsky, R. L. & Renne, R. Cloning and identification of a microRNA cluster within the latency-associated region of Kaposi's sarcoma-associated herpesvirus. *J Virol* **79**, 9301-9305, doi:10.1128/JVI.79.14.9301-9305.2005 (2005).

6 Stedman, W. *et al.* Cohesins localize with CTCF at the KSHV latency control region and at cellular c-myc and H19/Igf2 insulators. *EMBO J* **27**, 654-666, doi:10.1038/emboj.2008.1 (2008).

7 Stedman, W., Deng, Z., Lu, F. & Lieberman, P. M. ORC, MCM, and histone hyperacetylation at the Kaposi's sarcoma-associated herpesvirus latent replication origin. *J Virol* **78**, 12566-12575, doi:10.1128/JVI.78.22.12566-12575.2004 (2004).

8 Ye, F. C. *et al.* Disruption of Kaposi's sarcoma-associated herpesvirus latent nuclear antigen leads to abortive episome persistence. *J Virol* **78**, 11121-11129, doi:10.1128/JVI.78.20.11121-11129.2004 (2004).

9 Stackpole, C. W. Herpes-type virus of the frog renal adenocarcinoma. I. Virus development in tumor transplants maintained at low temperature. *J Virol* **4**, 75-93, doi:10.1128/JVI.4.1.75-93.1969 (1969).

10 Newcomb, W. W. *et al.* Assembly of the herpes simplex virus capsid: characterization of intermediates observed during cell-free capsid formation. *J Mol Biol* **263**, 432-446, doi:10.1006/jmbi.1996.0587 (1996).

11 Newcomb, W. W. *et al.* Assembly of the herpes simplex virus procapsid from purified components and identification of small complexes containing the major capsid and scaffolding proteins. *J Virol* **73**, 4239-4250, doi:10.1128/JVI.73.5.4239-4250.1999 (1999).

12 Newcomb, W. W. *et al.* Isolation of herpes simplex virus procapsids from cells infected with a protease-deficient mutant virus. *J Virol* **74**, 1663-1673, doi:10.1128/jvi.74.4.1663-1673.2000 (2000).

13 Nealon, K. *et al.* Lytic replication of Kaposi's sarcoma-associated herpesvirus results in the formation of multiple capsid species: isolation and molecular characterization of A, B, and C capsids from a gammaherpesvirus. *J Virol* **75**, 2866-2878, doi:10.1128/JVI.75.6.2866-2878.2001 (2001).

14 Deng, B., O'Connor, C. M., Kedes, D. H. & Zhou, Z. H. Cryo-electron tomography of Kaposi's sarcoma-associated herpesvirus capsids reveals dynamic scaffolding structures essential to capsid assembly and maturation. *J Struct Biol* **161**, 419-427, doi:10.1016/j.jsb.2007.10.016 (2008).

15 Heming, J. D., Conway, J. F. & Homa, F. L. Herpesvirus Capsid Assembly and DNA Packaging. *Adv Anat Embryol Cell Biol* **223**, 119-142, doi:10.1007/978-3-319-53168-7_6 (2017).
16 Dai, X., Gong, D., Wu, T. T., Sun, R. & Zhou, Z. H. Organization of capsid-associated tegument components in Kaposi's sarcoma-associated herpesvirus. *J Virol* **88**, 12694-12702, doi:10.1128/JVI.01509-14 (2014).
17 Grzesik, P. *et al.* Incorporation of the Kaposi's sarcoma-associated herpesvirus capsid vertex-specific component (CVSC) into self-assembled capsids. *Virus Res* **236**, 9-13, doi:10.1016/j.virusres.2017.04.016 (2017).
18 Gong, D. *et al.* DNA-Packing Portal and Capsid-Associated Tegument Complexes in the Tumor Herpesvirus KSHV. *Cell* **178**, 1329-1343 e1312, doi:10.1016/j.cell.2019.07.035 (2019).
19 Brulois, K. F. *et al.* Construction and manipulation of a new Kaposi's sarcoma-associated herpesvirus bacterial artificial chromosome clone. *J Virol* **86**, 9708-9720, doi:10.1128/JVI.01019-12 (2012).
20 Myoung, J. & Ganem, D. Generation of a doxycycline-inducible KSHV producer cell line of endothelial origin: maintenance of tight latency with efficient reactivation upon induction. *J Virol Methods* **174**, 12-21, doi:10.1016/j.jviromet.2011.03.012 (2011).
21 Tischer, B. K., von Einem, J., Kaufer, B. & Osterrieder, N. Two-step red-mediated recombination for versatile high-efficiency markerless DNA manipulation in Escherichia coli. *Biotechniques* **40**, 191-197, doi:10.2144/000112096 (2006).
22 Chomczynski, P. & Sacchi, N. The single-step method of RNA isolation by acid guanidinium thiocyanate-phenol-chloroform extraction: twenty-something years on. *Nat Protoc* **1**, 581-585, doi:10.1038/nprot.2006.83 (2006).
23 Livak, K. J. & Schmittgen, T. D. Analysis of relative gene expression data using real-time quantitative PCR and the 2(-Delta Delta C(T)) Method. *Methods* **25**, 402-408, doi:10.1006/meth.2001.1262 (2001).
24 Tischer, B. K., Smith, G. A. & Osterrieder, N. En passant mutagenesis: a two step markerless red recombination system. *Methods Mol Biol* **634**, 421-430, doi:10.1007/978-1-60761-652-8_30 (2010).
25 Sun, R. *et al.* A viral gene that activates lytic cycle expression of Kaposi's sarcoma-associated herpesvirus. *Proc Natl Acad Sci U S A* **95**, 10866-10871, doi:10.1073/pnas.95.18.10866 (1998).
26 Xu, Y. *et al.* A Kaposi's sarcoma-associated herpesvirus/human herpesvirus 8 ORF50 deletion mutant is defective for reactivation of latent virus and DNA replication. *J Virol* **79**, 3479-3487, doi:10.1128/JVI.79.6.3479-3487.2005 (2005).
27 Toth, Z. *et al.* Biphasic euchromatin-to-heterochromatin transition on the KSHV genome following de novo infection. *PLoS Pathog* **9**, e1003813, doi:10.1371/journal.ppat.1003813 (2013).
28 Krishnan, H. H. *et al.* Concurrent expression of latent and a limited number of lytic genes with immune modulation and antiapoptotic function by Kaposi's sarcoma-associated herpesvirus early during infection of primary endothelial and fibroblast cells and subsequent decline of lytic gene expression. *J Virol* **78**, 3601-3620, doi:10.1128/jvi.78.7.3601-3620.2004 (2004).

29 Purushothaman, P., Dabral, P., Gupta, N., Sarkar, R. & Verma, S. C. KSHV Genome Replication and Maintenance. *Front Microbiol* **7**, 54, doi:10.3389/fmicb.2016.00054 (2016).
30 Ballestas, M. E. & Kaye, K. M. Kaposi's sarcoma-associated herpesvirus latency-associated nuclear antigen 1 mediates episome persistence through cis-acting terminal repeat (TR) sequence and specifically binds TR DNA. *J Virol* **75**, 3250-3258, doi:10.1128/JVI.75.7.3250-3258.2001 (2001).
31 Grundhoff, A. & Ganem, D. The latency-associated nuclear antigen of Kaposi's sarcoma-associated herpesvirus permits replication of terminal repeat-containing plasmids. *J Virol* **77**, 2779-2783, doi:10.1128/jvi.77.4.2779-2783.2003 (2003).
32 Broussard, G. & Damania, B. Regulation of KSHV Latency and Lytic Reactivation. *Viruses* **12**, doi:10.3390/v12091034 (2020).
33 Strahan, R. C., McDowell-Sargent, M., Uppal, T., Purushothaman, P. & Verma, S. C. KSHV encoded ORF59 modulates histone arginine methylation of the viral genome to promote viral reactivation. *PLoS Pathog* **13**, e1006482, doi:10.1371/journal.ppat.1006482 (2017).
34 Chang, P. C. *et al.* Kruppel-associated box domain-associated protein-1 as a latency regulator for Kaposi's sarcoma-associated herpesvirus and its modulation by the viral protein kinase. *Cancer Res* **69**, 5681-5689, doi:10.1158/0008-5472.CAN-08-4570 (2009).
35 Martinez, F. P. & Tang, Q. Leucine zipper domain is required for Kaposi sarcoma-associated herpesvirus (KSHV) K-bZIP protein to interact with histone deacetylase and is important for KSHV replication. *J Biol Chem* **287**, 15622-15634, doi:10.1074/jbc.M111.315861 (2012).
36 Wu, F. Y. *et al.* Origin-independent assembly of Kaposi's sarcoma-associated herpesvirus DNA replication compartments in transient cotransfection assays and association with the ORF-K8 protein and cellular PML. *J Virol* **75**, 1487-1506, doi:10.1128/JVI.75.3.1487-1506.2001 (2001).
37 Purushothaman, P., Uppal, T. & Verma, S. C. Molecular biology of KSHV lytic reactivation. *Viruses* **7**, 116-153, doi:10.3390/v7010116 (2015).
38 Deng, H., Young, A. & Sun, R. Auto-activation of the rta gene of human herpesvirus-8/Kaposi's sarcoma-associated herpesvirus. *J Gen Virol* **81**, 3043-3048, doi:10.1099/0022-1317-81-12-3043 (2000).
39 Cockrell, S. K., Huffman, J. B., Toropova, K., Conway, J. F. & Homa, F. L. Residues of the UL25 protein of herpes simplex virus that are required for its stable interaction with capsids. *J Virol* **85**, 4875-4887, doi:10.1128/JVI.00242-11 (2011).
40 Conway, J. F. *et al.* Labeling and localization of the herpes simplex virus capsid protein UL25 and its interaction with the two triplexes closest to the penton. *J Mol Biol* **397**, 575-586, doi:10.1016/j.jmb.2010.01.043 (2010).
41 Toropova, K., Huffman, J. B., Homa, F. L. & Conway, J. F. The herpes simplex virus 1 UL17 protein is the second constituent of the capsid vertex-specific component required for DNA packaging and retention. *J Virol* **85**, 7513-7522, doi:10.1128/JVI.00837-11 (2011).
42 Dai, X. & Zhou, Z. H. Structure of the herpes simplex virus 1 capsid with associated tegument protein complexes. *Science* **360**, doi:10.1126/science.aao7298 (2018).
43 Wang, J. *et al.* Structure of the herpes simplex virus type 2 C-capsid with capsid-vertex-specific component. *Nat Commun* **9**, 3668, doi:10.1038/s41467-018-06078-4 (2018).

44 Homa, F. L. *et al.* Structure of the pseudorabies virus capsid: comparison with herpes simplex virus type 1 and differential binding of essential minor proteins. *J Mol Biol* **425**, 3415-3428, doi:10.1016/j.jmb.2013.06.034 (2013).
45 Wang, W. *et al.* Near-atomic cryo-electron microscopy structures of varicella-zoster virus capsids. *Nat Microbiol* **5**, 1542-1552, doi:10.1038/s41564-020-0785-y (2020).
46 Bauer, D. W., Huffman, J. B., Homa, F. L. & Evilevitch, A. Herpes virus genome, the pressure is on. *J Am Chem Soc* **135**, 11216-11221, doi:10.1021/ja404008r (2013).
47 Snijder, J. *et al.* Vertex-Specific Proteins pUL17 and pUL25 Mechanically Reinforce Herpes Simplex Virus Capsids. *J Virol* **91**, doi:10.1128/JVI.00123-17 (2017).
48 Li, Z., Pang, J., Dong, L. & Yu, X. Structural basis for genome packaging, retention, and ejection in human cytomegalovirus. *Nat Commun* **12**, 4538, doi:10.1038/s41467-021-24820-3 (2021).
49 Zhang, Y. *et al.* Atomic structure of the human herpesvirus 6B capsid and capsid-associated tegument complexes. *Nat Commun* **10**, 5346, doi:10.1038/s41467-019-13064-x (2019).
50 Liu, W. *et al.* Structures of capsid and capsid-associated tegument complex inside the Epstein-Barr virus. *Nat Microbiol* **5**, 1285-1298, doi:10.1038/s41564-020-0758-1 (2020).
51 Yu, X., Jih, J., Jiang, J. & Zhou, Z. H. Atomic structure of the human cytomegalovirus capsid with its securing tegument layer of pp150. *Science* **356**, doi:10.1126/science.aam6892 (2017).
52 Dai, X. *et al.* The smallest capsid protein mediates binding of the essential tegument protein pp150 to stabilize DNA-containing capsids in human cytomegalovirus. *PLoS Pathog* **9**, e1003525, doi:10.1371/journal.ppat.1003525 (2013).
53 Dai, X. *et al.* Structure and mutagenesis reveal essential capsid protein interactions for KSHV replication. *Nature* **553**, 521-525, doi:10.1038/nature25438 (2018).
54 Zhou, Z. H. *et al.* Four levels of hierarchical organization, including noncovalent chainmail, brace the mature tumor herpesvirus capsid against pressurization. *Structure* **22**, 1385-1398, doi:10.1016/j.str.2014.05.019 (2014).
55 Dai, X. *et al.* CryoEM and mutagenesis reveal that the smallest capsid protein cements and stabilizes Kaposi's sarcoma-associated herpesvirus capsid. *Proc Natl Acad Sci U S A* **112**, E649-656, doi:10.1073/pnas.1420317112 (2015).
56 McElwee, M., Vijayakrishnan, S., Rixon, F. & Bhella, D. Structure of the herpes simplex virus portal-vertex. *PLoS Biol* **16**, e2006191, doi:10.1371/journal.pbio.2006191 (2018).
57 Mettenleiter, T. C., Muller, F., Granzow, H. & Klupp, B. G. The way out: what we know and do not know about herpesvirus nuclear egress. *Cell Microbiol* **15**, 170-178, doi:10.1111/cmi.12044 (2013).
58 Klupp, B. G., Granzow, H., Keil, G. M. & Mettenleiter, T. C. The capsid-associated UL25 protein of the alphaherpesvirus pseudorabies virus is nonessential for cleavage and encapsidation of genomic DNA but is required for nuclear egress of capsids. *J Virol* **80**, 6235-6246, doi:10.1128/JVI.02662-05 (2006).
59 Yang, K. & Baines, J. D. Selection of HSV capsids for envelopment involves interaction between capsid surface components pUL31, pUL17, and pUL25. *Proc Natl Acad Sci U S A* **108**, 14276-14281, doi:10.1073/pnas.1108564108 (2011).
60 Newcomb, W. W. *et al.* The Primary Enveloped Virion of Herpes Simplex Virus 1: Its Role in Nuclear Egress. *mBio* **8**, doi:10.1128/mBio.00825-17 (2017).

61 Leelawong, M., Guo, D. & Smith, G. A. A physical link between the pseudorabies virus capsid and the nuclear egress complex. *J Virol* **85**, 11675-11684, doi:10.1128/JVI.05614-11 (2011).
62 Bigalke, J. M., Heuser, T., Nicastro, D. & Heldwein, E. E. Membrane deformation and scission by the HSV-1 nuclear egress complex. *Nat Commun* **5**, 4131, doi:10.1038/ncomms5131 (2014).
63 Bigalke, J. M. & Heldwein, E. E. Structural basis of membrane budding by the nuclear egress complex of herpesviruses. *EMBO J* **34**, 2921-2936, doi:10.15252/embj.201592359 (2015).
64 Liang, Q. *et al.* Identification of the Essential Role of Viral Bcl-2 for Kaposi's Sarcoma-Associated Herpesvirus Lytic Replication. *J Virol* **89**, 5308-5317, doi:10.1128/JVI.00102-15 (2015).
65 Yu, H. R., Kim, Y. J. & Lee, H. R. KSHV vIRF4 enhances BCL6 transcription via downregulation of IRF4 expression. *Biochem Biophys Res Commun* **496**, 1128-1133, doi:10.1016/j.bbrc.2018.01.154 (2018).
66 Toth, Z. *et al.* Negative elongation factor-mediated suppression of RNA polymerase II elongation of Kaposi's sarcoma-associated herpesvirus lytic gene expression. *J Virol* **86**, 9696-9707, doi:10.1128/JVI.01012-12 (2012).

SUPPORTING INFORMATION

SUPPORTING FIGURES

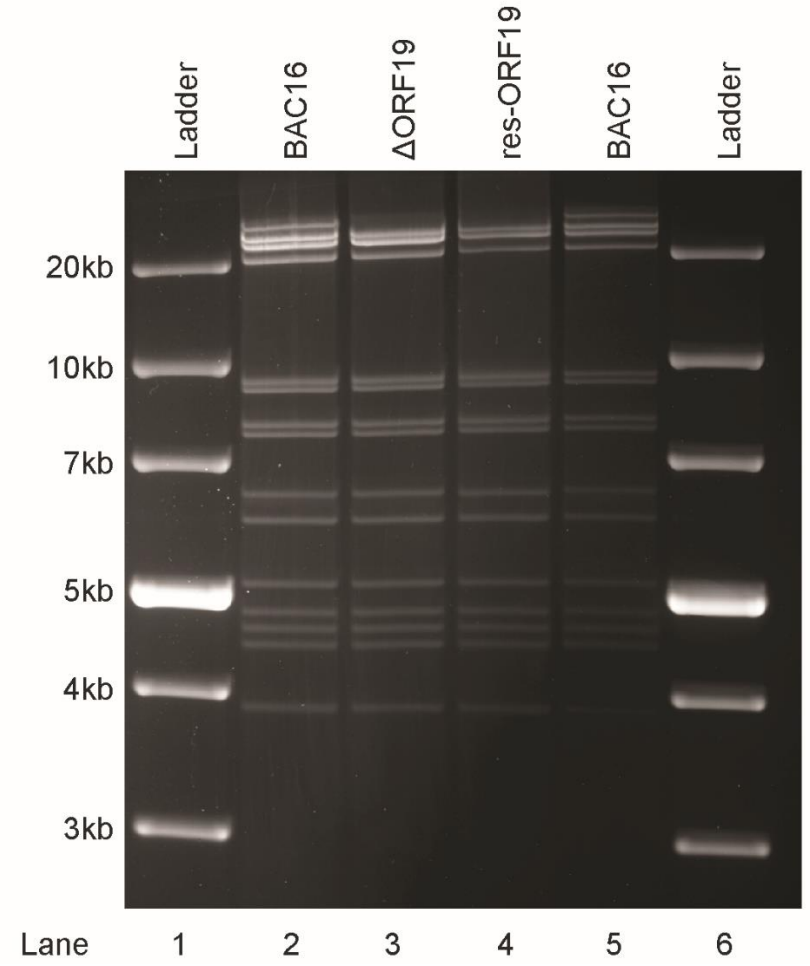

Figure S1. NheI digest of BAC16, stop-ORF19, and res-ORF19 genomes

Lane 1 represents the gene-ruler 1kb plus ladder, lane 2 is NheI digestion of BAC16 DNA, lane 3 is NheI digestion of stop-ORF19 DNA, lane 4 is NheI digestion of res-ORF19 DNA, lane 5 is NheI digestion of BAC16 DNA, Lane 6 represents the gene-ruler 1kb plus ladder.

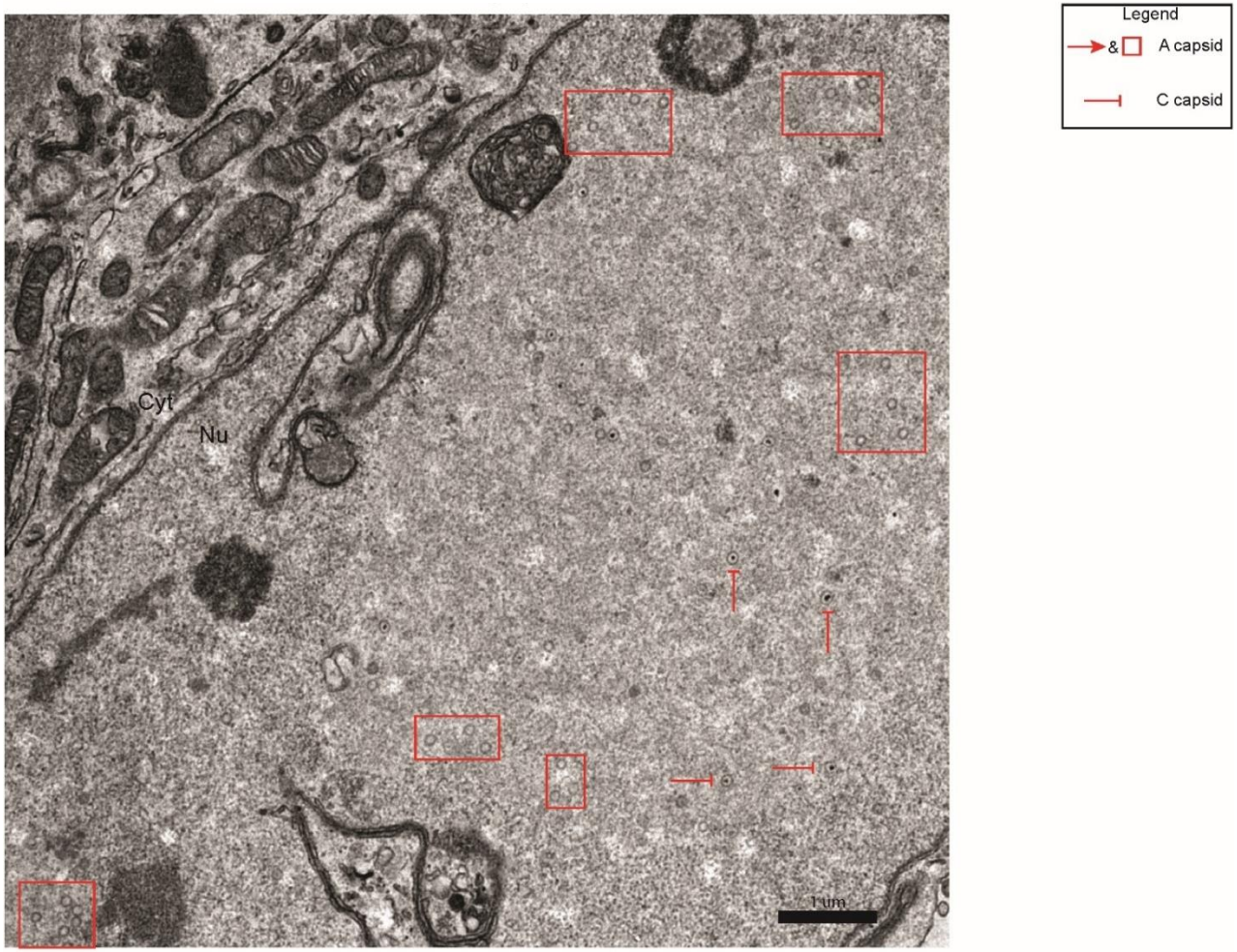

Figure S2. Nucleus of induced stop-ORF19 cell at 2-days post induction

Pointed arrows and boxes represent the location of “A-capsid”-like structures, and flat-headed arrows represent the location of “B-capsid”-like structures. The nucleus (Nu) and cytoplasm (Cyt) are labeled, and the scale bar is in micrometers.

SUPPORTING TABLES:

Table S1. RT-qPCR and qPCR primers

Name	Sequence	Source
LANA forward	GAGTCTGGTGACGACTTGGAG	64,65 66
LANA reverse	AGGAAGGCCAGACTCTTCAAC	64,6566
ORF50 forward	TTGCCAAGTTTGTACAACTGCT	64,6566
ORF50 reverse	ACCTTGCAAAGACCATTCAGAT	64,65
ORF45 forward	CCATACAGCGACCCTGATGA	65
ORF45 reverse	CCGATTCTCTGACTCAATACT	65
ORF25 forward	ACAGTTTATGGCACGCATAGTG	64,65
ORF25 reverse	GGTTCTCTGAATCTCGTCGTGT	64,65
18S forward	TTCGAACGTCTGCCCTATCAA	64
18S reverse	GATGTGGTAGCCGTTTCTCAGG	64

Appendix

Results:

Creation of the stop-ORF19 mutant

Using the 2-step red-mediated recombineering method (chapter 2) we inserted a 12bp sequence at nt. 34413 of the KSHV BAC16. This insertion corresponds to a stop-codon in every reading frame (5'-**TAG**G**TAG**A**TAG**G-3') (see chapter 2). Alkaline lysis miniprep combined with NheI restriction digest was used to screen stop-ORF19 mutants (figure 1A). We noticed no significant band shifts in the 7575 bp band, which contains a small direct repeat region (DR: 92495-92842), in the 6376 bp band, which contains two large direct repeat regions (DR1: 117942-118548 and DR2: 118549-119041) and an inverted repeat region (IR1: 119142-120320), or in the 4378 bp band, which contains a large direct repeat region (DR: 124979- 126633). The terminal repeats are found attached to the 9463bp band and adding 30 copies of them to the length of the band gives a final band size of 28-29kb, which is obscured by a genuine 28,862 bp band (chapter 2). No shifts are witnessed in the 21 kb and up band region compared to BAC16, indicating no large deletion or duplication events. ORF19 is found in the genuine 28,862 bp band and the insertion of a 12bp sequence cannot be resolved on this gel when compared to the BAC16.

We performed PCR on miniprep DNA to check for the 12 bp insert sequence (figure 1B). The expected band size of the BAC16 product is 563 bp and the expected size of the stop-ORF19 mutant product is 575 bp. The effect of an additional 12 bp in the stop-ORF19 amplicon length can be observed by an upward shift of PCR products compared to BAC16 PCR product (figure 1B lanes 2 and 4 compared to lanes 5). The bands were cut from the gel, purified using at Qiagen gel extraction kit and sequenced (figure 1C). The insertion of the 12bp sequence **TAGGTAGATAGG** is found inserted at nt 34413 as expected.

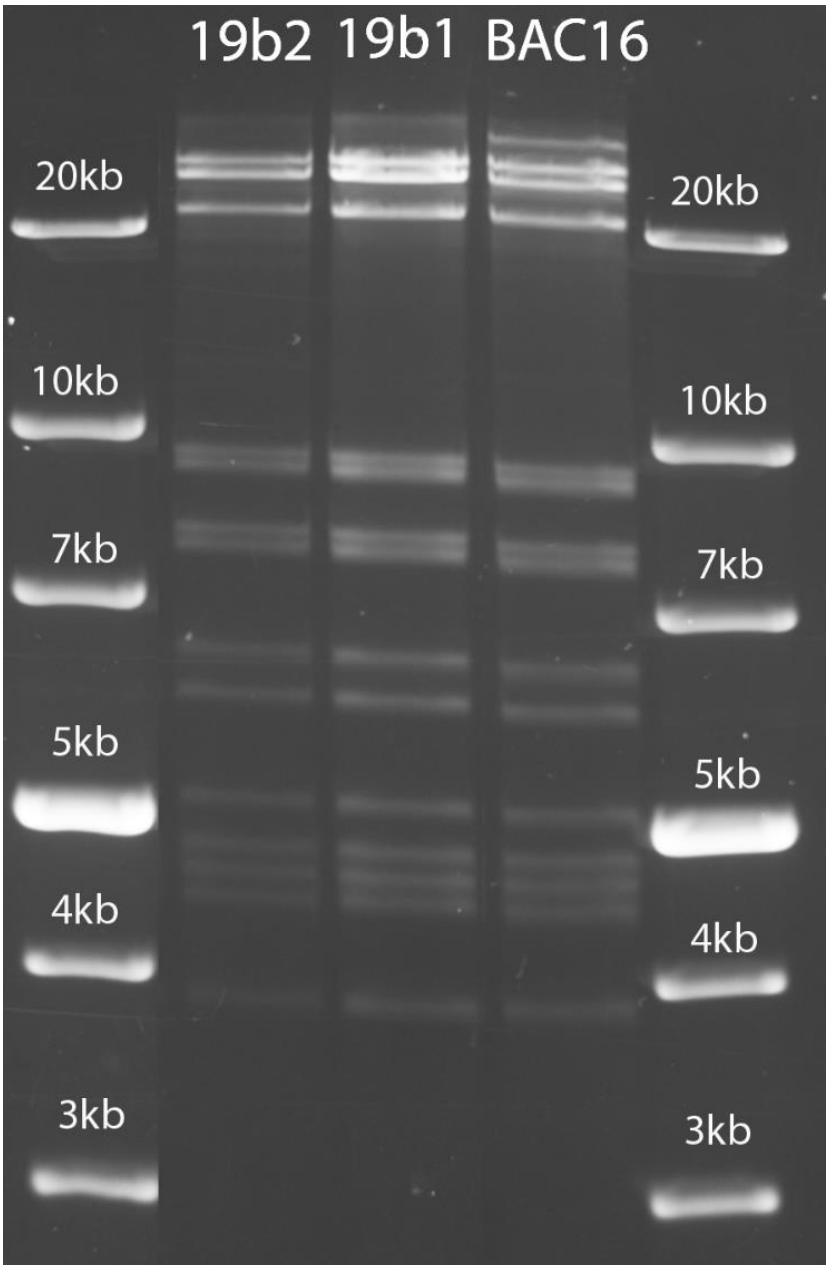

Figure 1A: NheI digest of stop-ORF19 mutants 19b2 and 19b1 and the BAC16.

Lane 1 is the 1kb plus gene ruler. Lane 2-3 are samples 19b2 and 19b1 respectively (stop mutants). Lane 4 is the BAC16. Lane 5 is the 1kb plus gene ruler.

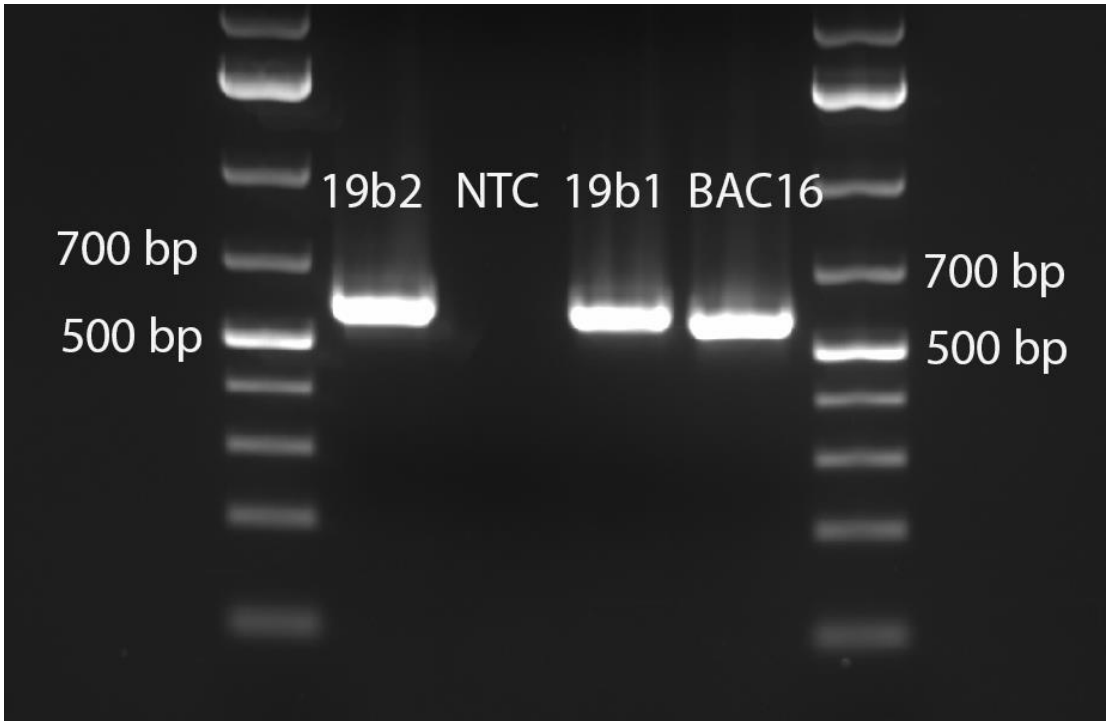

Figure 1B: PCR of stop-ORF19 mutants 19b2 and 19b1 and BAC16.

Lane 1 is the 1kb plus gene ruler. Lane 2 is the 19b2 mutant. Lane 3 is the no template control. Lane 4 is the 19b1 mutant. Lane 5 is the BAC16. Lane 6 is the 1kb plus gene ruler. NTC is no template control.



Figure 1C: Sequencing of stop-ORF19 mutant aligned to BAC16 Genebank Accession number: GQ994935.1 sequence.

The BAC16 sequence is the top row and the stop-ORF19 sample sequence is the bottom row. The vertical hyphens indicate sequence homology between the BAC16 and stop-ORF19 mutant sequences. The stars are placed after 10 nucleotides in each row. The numbers at the ends of the top row are the numbering of the first and last nucleotides in the row in the GQ994935.1 sequence. The horizontal hyphens in the top row indicate nucleotides that are missing from the BAC16 sequence and the nucleotides in the bottom row beneath the hyphens are the 12 bp insert sequence in the stop-ORF19 mutant. The alignment shows all strands oriented in the sense direction of the BAC16 reference genome, while the ORF19 coding strand is located in the opposite orientation.

Creation res-ORF19 from stop-ORF19: 1st and 2nd HR

From the stop-ORF19 mutant we created the revertant virus by removing the short 12bp insertion at nt. 34413 using the same general methodology (chapter 2). Both stop-ORF19 mutants 19b1 and 19b2 were used to make res-ORF19 BAC16s. stop-ORF19 mutant BACs were maintained in GS1783 E. coli, which were electroporated with a PCR product containing the kanamycin cassette that was flanked by sequence homology designed to remove the 12bp insert (table 2 and chapter 2). The PCR product corresponded to a single band of the expected size of approximately 1100 bp (data not shown). The product was electroporated in GS1783 E. coli containing stop-ORF19 BAC16 DNA and colonies were recovered in Kan-LB broth and screened via alkaline lysis, PCR, and NheI digest.

We observed an increase in the PCR product size of approximately 1100bp using the ORF19 PCR F/R primers on the 1st HR samples when compared to BAC16 (figure 4, lanes 2-6 and lane 12 compared to lane 9). This extra 1100bp in the PCR product represents the insertion of the kanamycin selection cassette and the necessary recombination sequences into stop-ORF19 BAC16 genomes at the ORF19 locus. We observed a PCR amplicon of approximately 1000bp using the 19 PCR F/KanR primers and no amplification in BAC16 (figure 4, lanes 10, 13-19 compared to lane 20). These products (figure 4, lanes 2-6 and lane 12, lanes 10, 13-19) confirm the correct location and orientation of the kanamycin selection cassette in the 1st HR samples. The BAC16 does not contain a kanamycin selection cassette and therefore there is no amplification in this reaction, as expected.

The results of the 1st HR NheI digest showed no signs of large-scale deletions or duplications and confirmed the integrity of the genome in all samples (data not shown). We selected 3 clones from each stop-ORF19 mutant 1st HR for the 2nd homologous recombination reaction: 19b1-b, 19b1-c, 19b1-d and 19b2-a, 19b2-c, 19b2-d. After induction with arabinose and negative selection on LB-Kan plates, we screed by alkaline lysis and NheI digest. The results of the 2nd second homologous recombination NheI digests can be found in Figure 5. Figure 5A represents the NheI digest results of the 2nd HR revertant candidates arising from the 19b1 stop-ORF19 mutant. Figure 5B represents the NheI digest results of the 2nd HR revertant candidates arising from the 19b2 stop-ORF19 mutant. The first homologous recombination removes the inserted 12bp stop sequence and replaces it with a 1100bp sequence in the 29kb band. The second recombination removes the 1100bp sequence and results in the scarless deletion of the inserted 12bp stop sequence. The gel does not have the resolution to visualize removal of the 12bp insertion in the 2nd homologous recombination samples when the digest is compared to the BAC16 digest (figure 5A-B). However, it is important to note that we did not observe any major deletions or duplications in the repeat regions of the genome for any of the 19b1 and 19b2 2nd HR samples, and their digest patterns matched the BAC16 digest (figure 5A-B).

Figure 6 shows the results of PCR using second homologous recombination miniprep DNA and the ORF19 PCR F/R primers. All 2nd HR samples gave amplification products that matched the size of the BAC16 amplicon (figure 6, lanes 6-8 and 10-12 compared to lanes 5 and 13). This indicates that the kanamycin selection cassette has been removed from the ORF19

locus and it implies the scarless deletion of the 12bp stop insertion. To confirm the scarless deletion of the 12bp stop insertion, these PCR bands were cut from the gel and sequenced. A representative sequencing sample is shown in Figure 7. The insertion of the 12bp sequence at nt 34413 of the BAC16 genome has been removed (compare figure 3 and figure 7) and the entire sample sequence is complementary to the BAC16 reference genome with no gaps or mismatches. These data confirm the scarless deletion of the of the inserted stop codon in our res-ORF19 mutants.

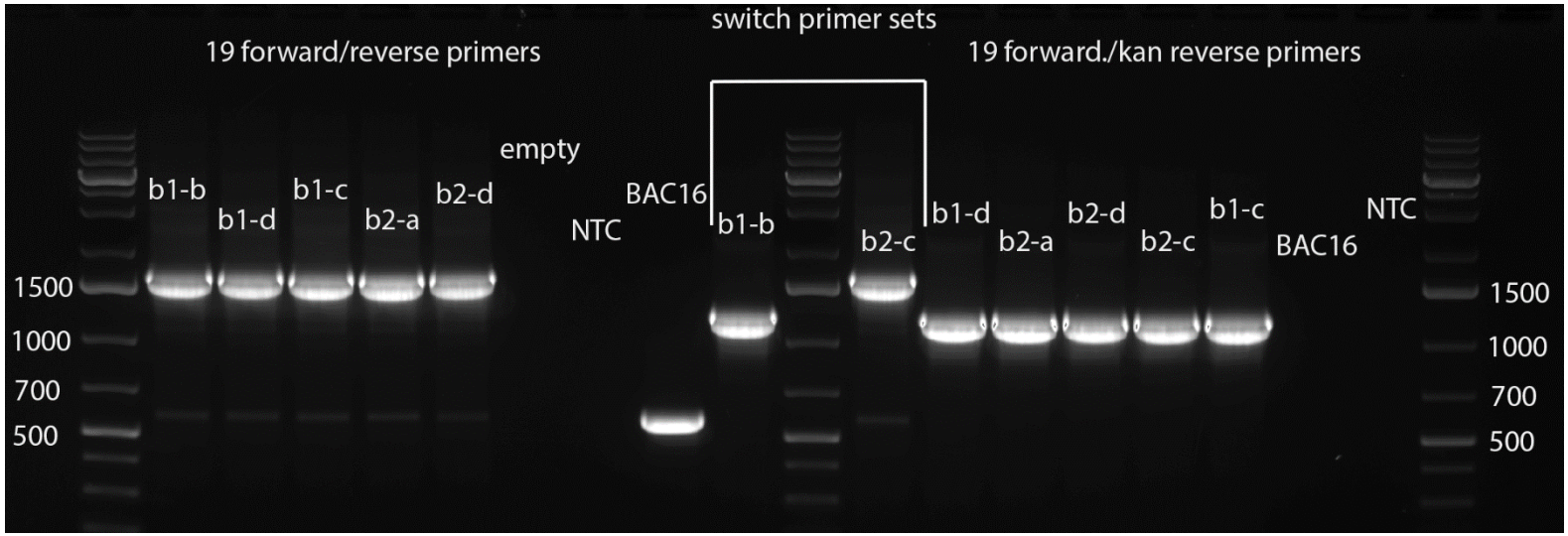

Figure 4: PCR results of the res-ORF19 1st HR.

Lane 1 is the 1kb plus ruler. Lanes 2-9 and lane 12 represent the PCR products with ORF19 PCR F/R primers on the rescue 1st HR samples from 19b1 (lanes2-4) and 19b2 (lanes 5-6 and 12), the no template control (lane 8), and BAC16 DNA (lane 9). Lane 11 is the 1kb plus gene ruler. Lanes 10 and 13-19 represent the PCR products with ORF19 PCR F/KanR primers on rescue 1st HR 19b1 samples (lanes 10, 13, and 17) and19b2 samples (lanes 14-16), the BAC16 DNA (lane 18), and the no template control (lane 19) Lane 20 is the 1kb plus gene ruler. Lanes 10 and 12 are switched with respect to their location in the gel and the primer sets used.

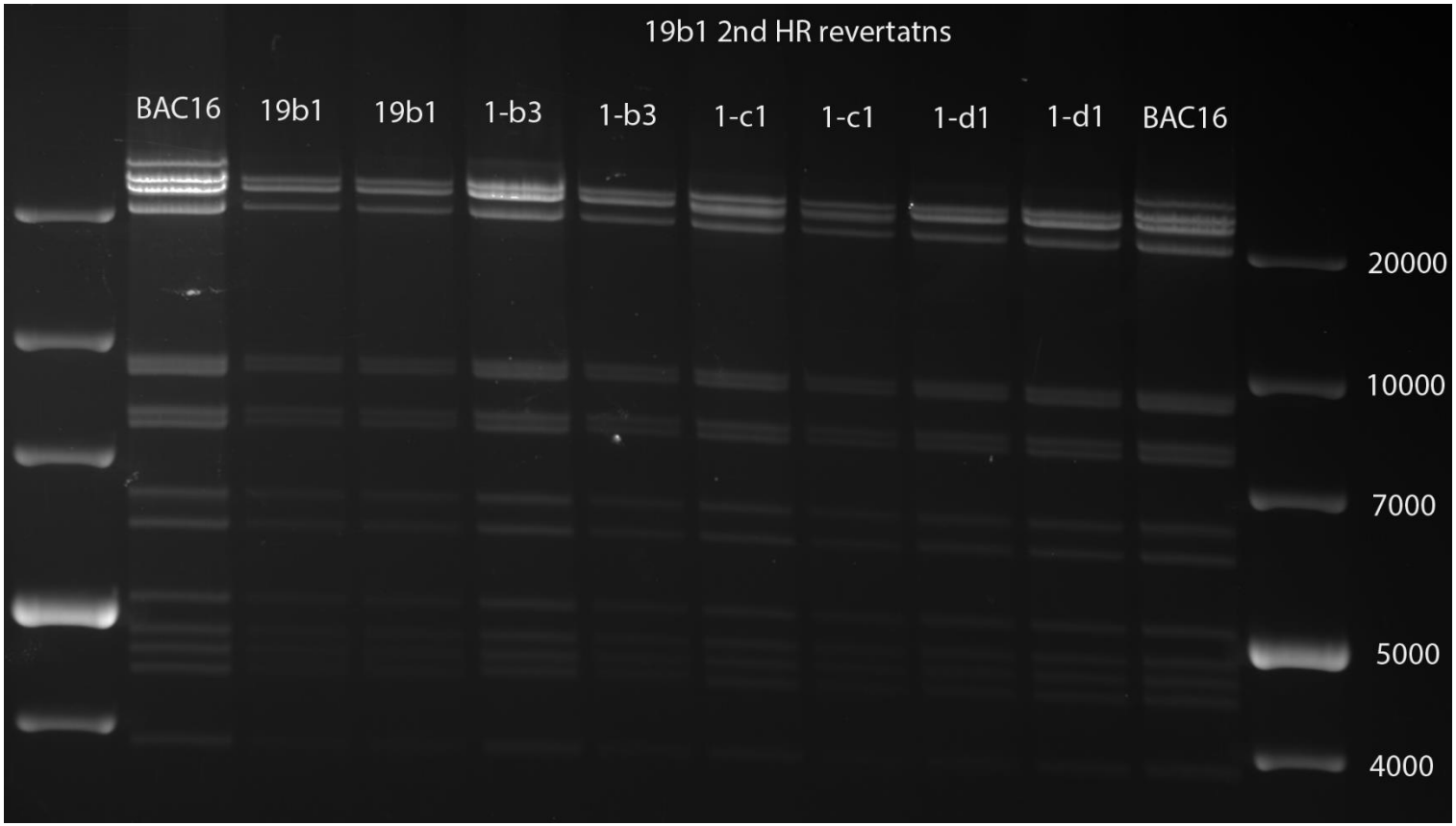

Figure 5A: NheI digest of the rescue-19b1 2nd HR clones.

Lane 1 represents the 1kb plus ladder. Lane 2 represents the BAC16. Lanes 3-4 represent the stop-ORF19 mutant 19b1. This is the stop-ORF19 mutant that the rescue candidates in lanes 5-6, lanes 7-8 and lanes 9-10 arose from. Lanes 5-6 represents rescue 2nd HR candidate 1-b3. Lanes 7-8 represents rescue 2nd HR candidate 1-c1. Lanes 9-10 represents rescue 2nd HR candidate 1-d1. Lane 11 represents the BAC16. Lane 12 represents the 1kb plus ruler.

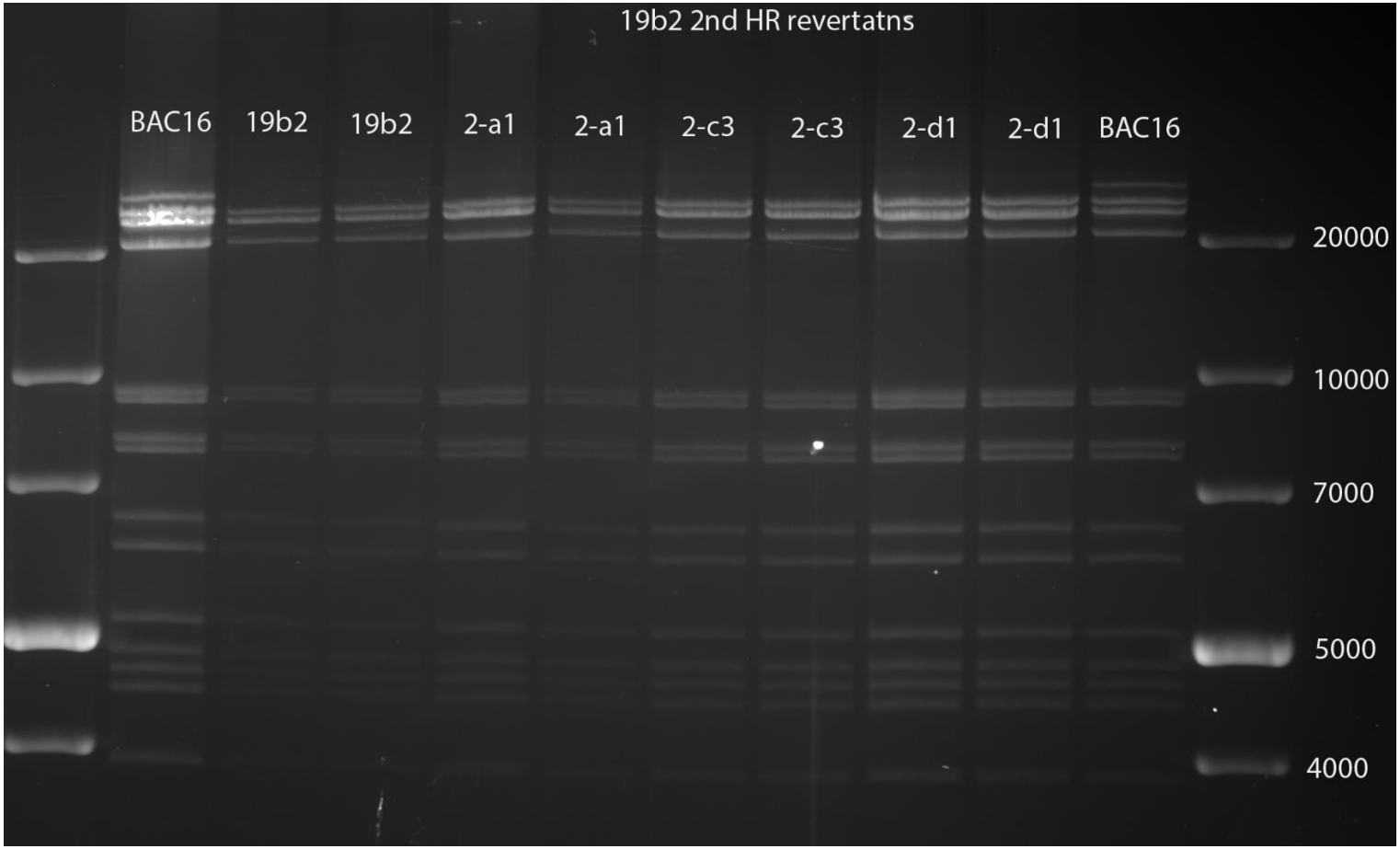

Figure 5B: NheI digest of the rescue-19b2 2nd HR clones.

Lane 1 is the 1kb plus gene ruler. Lane 2 is the BAC16. Lane 3-4 is the stop-ORF19 mutant 19b2. This is the stop-ORF19 mutant that the rescue candidates in lanes 5-6, lanes 7-8 and lanes 9-10 arose from. Lane 5-6 represents the rescue 2nd HR candidate 2-a1. Lanes 7-8 represents the rescue 2nd HR candidate 2-c3. Lanes 9-10 represents the rescue 2nd HR candidate 2-d1. Lane 11 represents the BAC16. Lane 12 represents the 1 kb plus gene ruler.

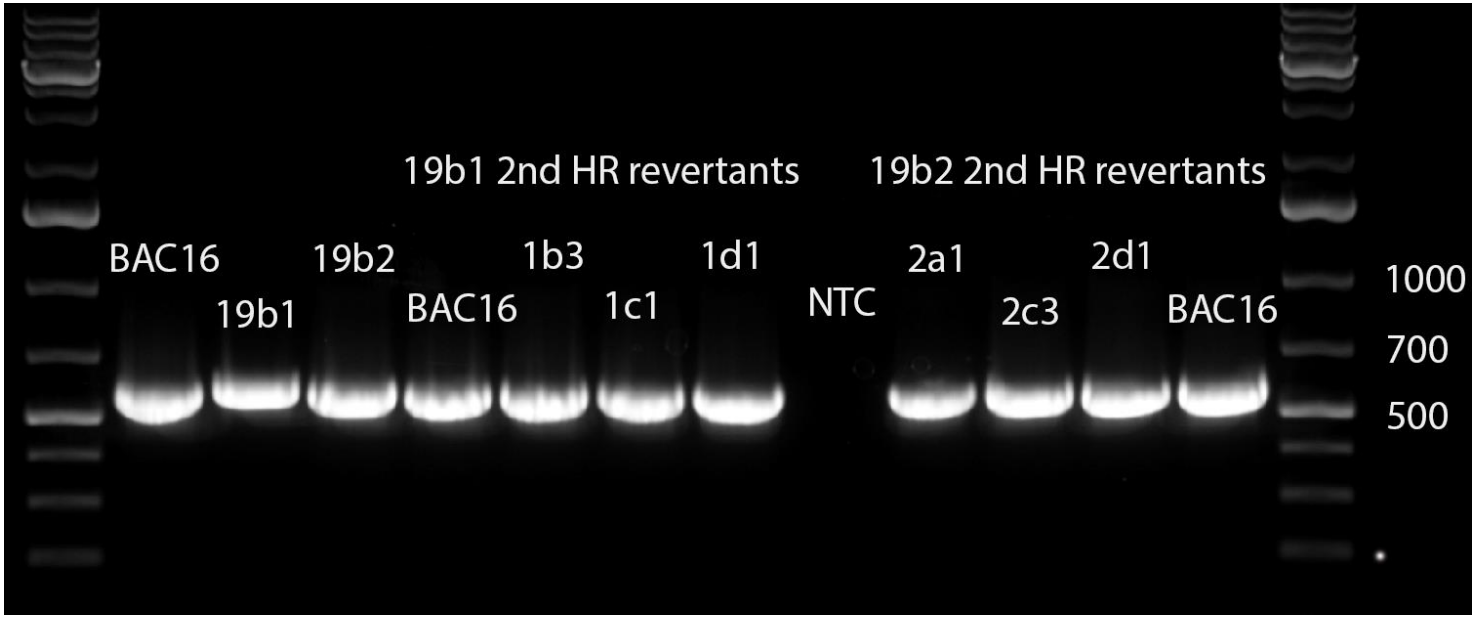

Figure 6: PCR of res-19b1 and res-19b2 2nd HR clones.

Lane 1 is the 1kb plus gene ruler. Lane 2-12 represent the PCR products using the 19 PCR F/R primers. Lane 2 is the BAC16. Lane 3 is the stop-ORF19 mutant 19b1. Lane 4 is the stop-ORF19 mutant 19b2. Lane 5 is the BAC16. Lane 6-8 represent the rescue 2nd HR candidates arising from the stop-ORF19 mutant 19b1. Lane 6 is the rescue 2nd HR candidate 1b3. Lane 7 is the rescue 2nd HR candidate 1c1. Lane 8 is the rescue 2nd HR candidate 1b3. Lane 9 is the no template control. Lane 10-12 represent the rescue 2nd HR candidates arising out of the stop-ORF19 mutant 19b2. Lane 10 is the rescue 2nd HR candidate 2a1. Lane 11 is the rescue 2nd HR candidate 2c3. Lane 12 is the rescue 2nd HR candidate 2d1. Lane 13 is the BAC16. Lane 14 is the 1kb plus gene ruler.

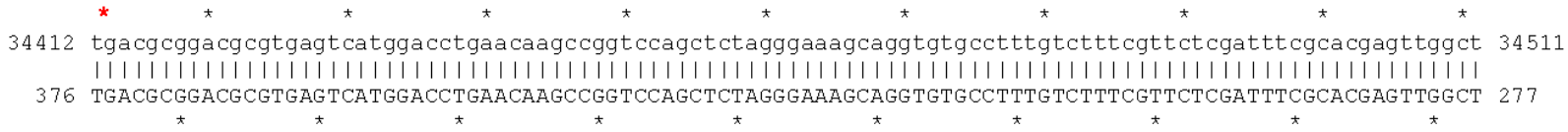

Figure 7: Sequencing of res-ORF19 clone 19b2-2a1 aligned to BAC16 Genebank Accession number: GQ994935.1 sequence.

The BAC16 sequence is the top row and the res-ORF19 clone 19b2 sequence is the bottom row. The vertical hyphens indicate sequence homology between the BAC16 and res-ORF19 clone 19b2. The red star indicates the location of 12bp insert in the stop-ORF19 mutant; between nt 34413 and nt 34414 in the BAC16. The 12bp sequence is now absent from the res-ORF19 clone 19b2 and the two sequences align perfectly with no gaps. The black stars are placed after 10 nucleotides in each row. The numbers at the ends of the top row are the numbering of the first and last nucleotides in the row in the GQ994935.1 sequence.

Creation of the stop-ORF19, res-ORF19 mutant and BAC16 cell lines

We extracted stop-ORF19, res-ORF19, and BAC16 DNA from E. coli using the nucleobond BAC100 kit and transfected it into iSLK cells using lipofectamine 200 (chapter 2). The stop-ORF19 and res-ORF19 and BAC16 DNA all induced large amounts of cell death in transfection culture several hours after the addition of the transfection complexes (chapter 3). This cytopathic effect was characterized by the rounding and lysis of cells and significant clearance of the monolayer. This effect was observed before culture selection began. During selection we observed the rounding and detachment of cells indicating the removal of; iSLK cells that did not receive the transfection complexes, cells that received the complexes but did not transport or express the hygromycin resistance products successfully, or cells did not receive enough DNA to become resistant to the high concentration of hygromycin we added to the media (data not shown). Approximately 1 month after transfection we observed the appearance of 1 to 10 independent colonies of attached GFP+ cells that exhibited a similar, although distorted, phenotype when compared to naïve iSLKs. These colonies were 2-8 cells in size (data not shown). These cells appear to have established a latent infection state that mimics in-vivo viral latency.

Induction of the stop-ORF19, res-ORF19 mutant and BAC16 cell lines

We cultured and expanded these transfectants under selection pressure and then induced approximately 6 million cells with induction media (chapter 2). We observed high levels of induction phenotype in the stop-ORF19 mutant cell lines compared to res-ORF19 and BAC16 cells. The induction phenotype was characterized by the rounding and swelling of cells as well as detachment and lysis of cells from a significant portion of the monolayer (figure 8). There were also cells that remained attached to the monolayer, however their morphology was elongated by induction, mimicking the general features of spindle cell morphology in KSHV infected endothelial cells (figure 8). The induction phenotype in the stop-ORF19 mutant cells was significantly more pronounced than the induction phenotype in the res-ORF19 and BAC16 cells in terms of numbers of rounding and detached cells, and the extent of elongation and morphological distortion of adherent cells (Figure 8).

Tittering of the stop-ORF19, res-ORF19 mutant and BAC16 cell lines

4 days post induction we collected the cells and supernatants from stop-ORF19, res-ORF19 and BAC16 samples, cleared and concentrated them, and tittered them on 293T cells using fluorescence microscopy and FACS (chapter 2). We did not observe any GFP signal from 293T cells infected with supernatant from induced stop-ORF19 cell lines. Low titer growth analysis confirmed the lack of any infectious progeny in the stop-ORF19 mutant (chapter 2). However, we observed significant numbers of GFP+ cells in the res-ORF19 and BAC16 cell line supernatants (main text, figure 4B). This indicates that while res-ORF19 and BAC16 cell lines produce cell-free viral progeny in significant and comparable quantities, stop-ORF19 cell line was unable to produce viable progeny. We interpreted these results as the stop-ORF19 mutant is deficient in one of the following viral lifecycle steps; lytic DNA replication, capsid assembly,

genome packaging, primary envelopment, secondary envelopment/egress, attachment/fusion, or the trafficking/uncoating steps.

There were several mutants in our deletion library that did not produce viable progeny as measured by GFP+ 293T cells (chapter 3 part I-figure 2 and part II-figure 9). However, some essential mutants did result in significant morphological changes when their supernatants were tittered on 293T cells, especially at more concentrated inoculums (data not shown). We hypothesized that mutants causing significant morphological changes in infected 293T cells with no GFP expression were defective in the trafficking/uncoating steps of the viral lifecycle. We did not observe these morphological changes in 293T cells when tittering the stop-ORF19 mutant. Several cell lines in our library mutated for genes encoding for putative *Gammaherpesvirus* specific transcription factors did not produce any significant induction phenotype (chapter 3 part II-subsection IV). Thus, we hypothesized this step of the viral lifecycle was not impaired in the stop-ORF19 mutant (figure 8). Cell lines that were mutated in gene putatively responsible for capsid maturation produced strong induction phenotypes and no infectious cell free viral progeny (chapter 3 part II-subsection I). Thus, we decided to examine stop-ORF19 mutant for the accumulation of capsids in the nucleus and cytoplasm of induced cells.

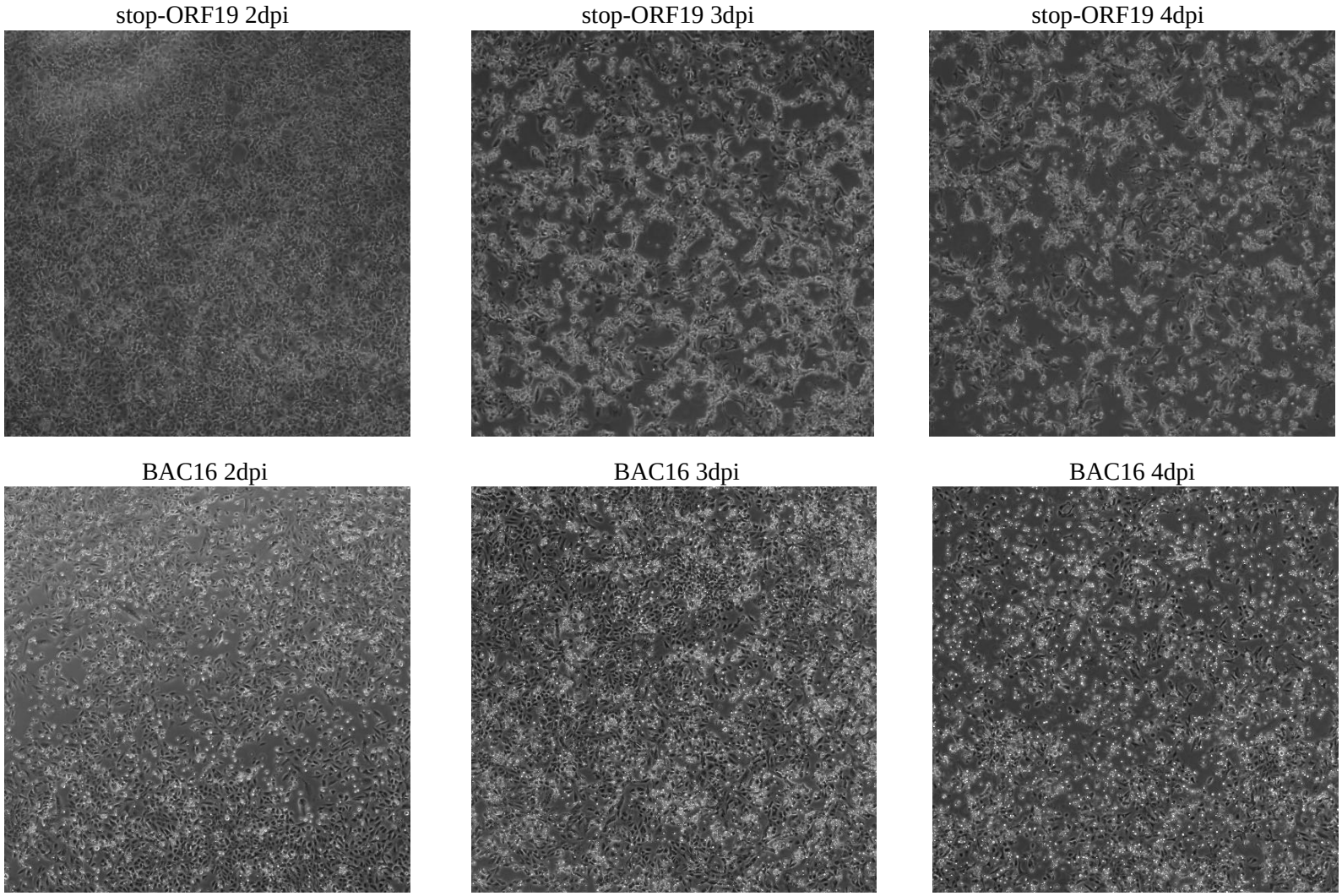

Figure 8: Induction phenotype of stop-ORF19 and BAC16 cell lines.

The top row is phase micrscopy the stop-ORF19 cell line under induction conditons at 2, 3, and 4 days post induction. The bottom row is phase microscopy of BAC16 cell line under induction conditons at 2, 3, and 4 days post induction. All photos have a total maginfication of 40X.

Transmission electron microscopy of induced stop-ORF19 cell line

Herpesviruses undergo DNA replication, capsid assembly, and genome packaging in the nucleus of cells. To examine these steps in the viral lifecycle in more granular detail, we decided to run transmission electron microscopy (TEM) on the induced stop-ORF19 cell line, with a focus on nuclear anomalies. We induced, fixed, embedded, and imaged cells at 2, 3, and 4 days post induction (chapter 2). The stop-ORF19 mutant cell lines exhibited several different nuclear anomalies that were absent in induced naïve iSLK cell lines. We observed significant amounts of internuclear membranous structures that varied in size, shape, number of layers, and density. These internuclear membrane structures were present in the stop-ORF19 and BAC16 cell lines (data not shown). We observed patterns of speckled nuclear densities composed of many individual spherical units, each unit ranging from 50nm to 150nm in diameter. Our analysis of induced naïve cells lines led us to believe that these areas are sites of capsid assembly (figure 9). They appear to represent a very early stage in capsid maturation where the core capsid components are agglomerated, and before they become assembled into ordered structures. We do not believe that these structures correspond to heterochromatin for several reasons. First, these structures are not observed in the negative control (induced and uninduced iSLK's). Second, treatment with n-butyrate would be expected to abrogate heterochromatin structures and create a randomly dispersed pattern of heterochromatin throughout the nucleus due to its broad-spectrum activity on several distinct HDAC enzymes. Third, we have regularly observed heterochromatin under our experimental conditions, and it does not appear as a dense and clustered object composed of regularly repeating units in such a concentrated space (data not shown). The spatial arrangement and concurrence in size of these densities indicates a targeted and tightly regulated process.

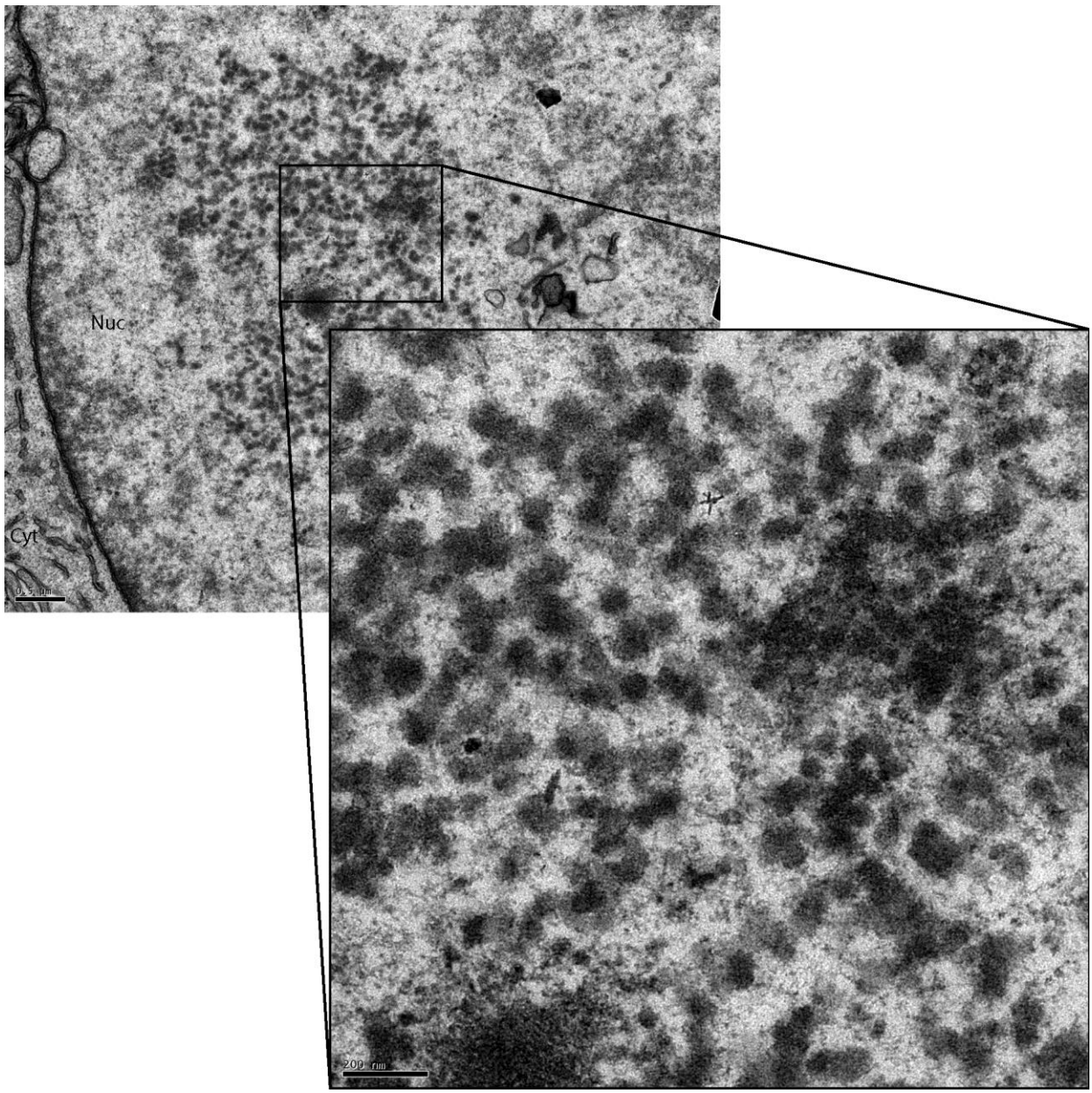

Figure 9: TEM of capsid assembly sites in induced stop-ORF19 cell lines.

Capsid assembly sites.

Chapter 5

The role of KSHV ORF74 in spontaneous reactivation

“That was moment I saw beyond myself. My pain was selfish. There will always be someone who has less.” – *redacted*

Overview and acknowledgements

This chapter outlines the examination of KSHV ORF74 in reactivation. This chapter has been submitted with the help of Nicholas Carry. The work presented here was included in his undergraduate thesis, and he produced most of the data. I am in indebted to him for his help.

Introduction:

KSHV ORF74 encodes a viral G-protein coupled receptor (vGPCR) which is constitutively active[1]. There is strong evidence supporting a role for vGPCR in several physiological features of KS including cellular transformation and angiogenesis mediated by VEGF. Transfection of vGPCR into NIH3T3 cells induces the focus formation, results in the upregulation and secretion of VEGF into the culture medium which is sufficient to induce proliferation of primary endothelial cells, and the injection of these treated cells into nude mice results in vascularized tumor formation[2]. Transgenic mice engineered to express the vGPCR in hematopoietic cells also develop lesions high reminiscent of KS[3]. vGPCR-mediated upregulation of VEGF expression has been shown to occur through MAPK/p38 signaling and HIFa activation[4,5].vGPCR has also been observed to activate of NFKB signaling which results in the production of the proinflammatory chemokines IL6, TNF-alpha and IL8[5]. These data support an indirect, paracrine induced transformation mechanism by ORF74.

Spontaneous reactivation is biological significant phenomena in KSHV infection and pathogenesis[6]. Reactivation from latency is an essential step in the development, progression and prognosis of KS, and correlates strongly with symptomatic episodes of MCD[7,8]. Spontaneous reactivation is thought to serve at least two significant roles in-vivo. The first is to replenish and maintain an infected cell population from being depleted by dying cells or dividing cells that fail to segregate and maintain the latent viral episome faithfully[9]. The second is spontaneous reactivation provides an alternative pathway to KSHV-mediated transformation via the expression of lytic transcripts from a small subset of infected cells[10,11]. These lytic transcripts drive oncogenic signaling pathways and help promote an inflammatory and cytokine rich environment characteristics of MCD and KS[12]. The latter is especially relevant considering that infection of primary cells in-vitro with KSHV is non-immortalizing[13].

Results:

Creation of the pUC19_ORF74 vector

ORF74 was PCR amplified from the BAC16 with pUC19_ORF74 primers (primer table 1). The amplification resulted in the addition of an EcoRI and HindIII site to either end of the PCR product for directional cloning. Double digestion of the ORF74 PCR product resulted in the expected band size of 1170bp (figure 1, lanes 2-5). Double digestion of pUC19 by HindIII and EcoR1 causes linearization of the plasmid and removes a small (approximately 20bp) fragment. The digested pUC19 plasmid produced the expected size of approximately 2700bp (figure 1 lanes 6-9). The double digested PCR product (figure 1, lanes 2-5) was ligated to double digested pUC19 (figure 1 lanes 6-9) and the reaction was transformed into NEB5 alpha E. coli. Ampicillin resistant colonies were recovered in Amp-LB broth and were screening via restriction digest with MIu1. There is a single MIu1 site inside the ORF74 reading frame and no MIu1 sites in pUC19. Digestion with MIu1 results in the linearization of the candidate pUC19_ORF74 plasmids and confirms the insertion of the ORF74 PCR product. Digestion of plasmid candidates produced the expected band size of approximately 3900bp, which corresponds to the natural size of pUC19 plus the size of the ORF74 PCR insert (2700bp plus 1170bp). MIu1 digested pUC19. runs slightly below 2000bp, which is expected as MIu1 does not cleave pUC19 and the band in the 2000bp range matches uncut plasmid (compare figure 2, lane 3 with figure 4, lane 2).

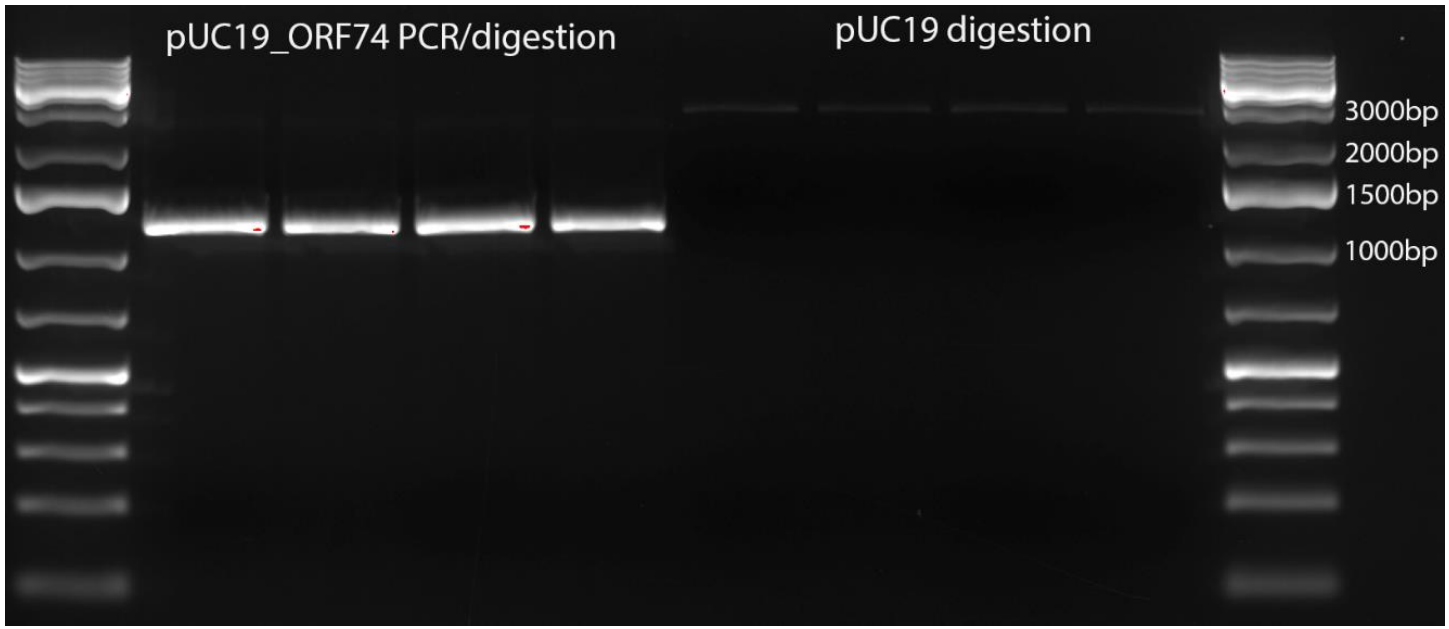

Figure 1: Double digestion of the ORF74 PCR product and pUC19 using EcoRI and HindIII.

Lane 1 is the 1kb plus gene ruler. Lanes 2-5 are the HindIII and EcoR1 double digested PCR products from the pUC19_ORF74 primer amplification. Lanes 6-9 represent the double digested pUC19 plasmid. Lane 10 is the 1kb plus gene ruler.

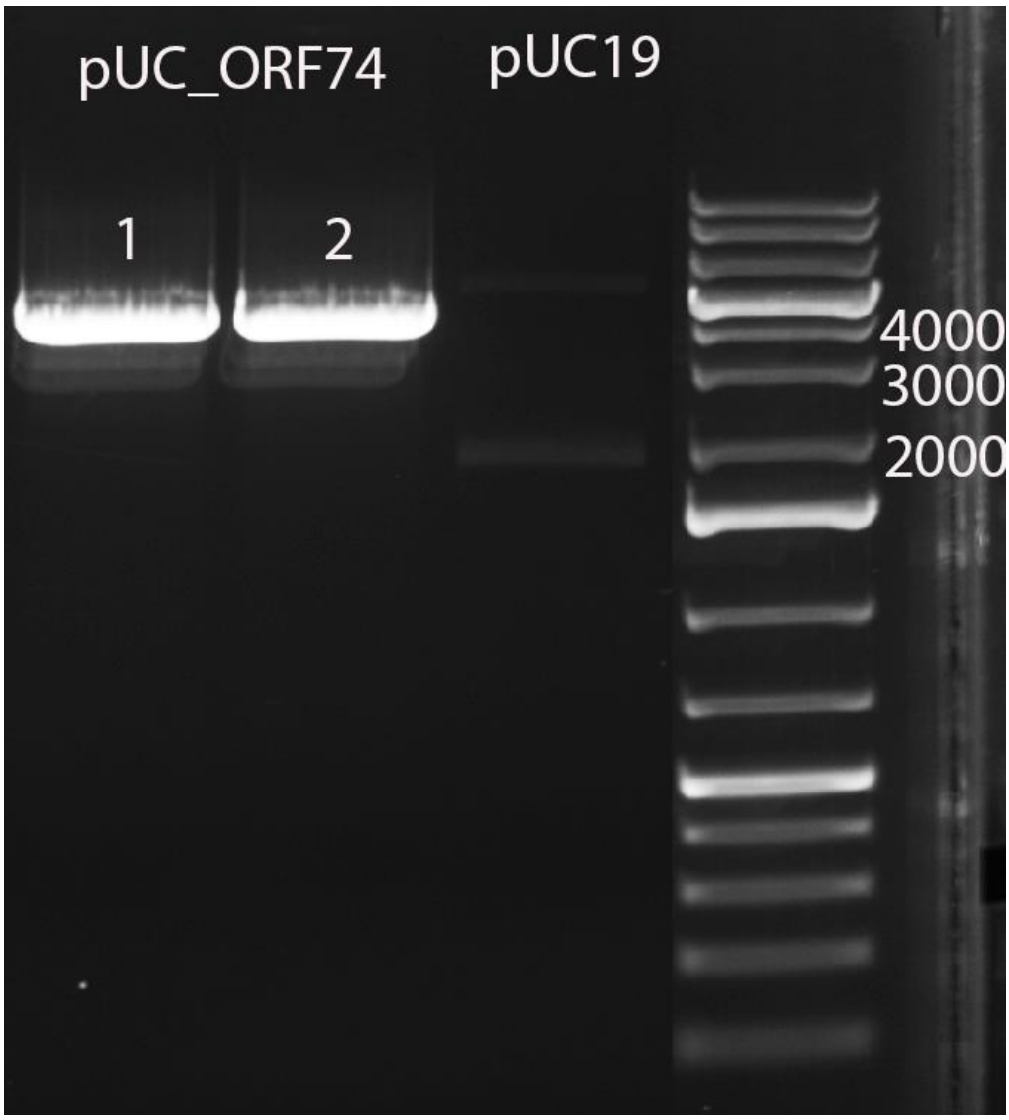

Figure 2: Results of the MIu1 screen of two potential pUC19_ORF74 constructs.

Lane 1-2 represent possible pUC19_ORF74 vectors. Lane 3 represents pUC19 digested with MIu1. Lane 4 is the 1kb plus gene ruler.

Creation of the ORF74_UTC vector

KSHV ORF74 contains a unique MIu1 site in the middle of its reading frame and MIu1 sites are absent from pUC19 and the kanamycin selection cassette. Thus, this unique restriction site allows the insertion of the kanamycin cassette into pUC19_ORF74 via PCR and cloning. The forward and reverse ORF74_UTC primers included MIu1 sites on their 5' ends. The forward primer also duplicated 50bp of sequence downstream of the MIu1 site in ORF74 and added a SceI meganuclease site to the PCR product (chapter 2, primer table 1). The kanamycin cassette was amplified from the pEPKanS plasmid with the ORF74_UTC primers and reaction was digested with MIu1. This resulted in the expected band length of 1017bp (figure 3, lanes 2-7). This product was ligated to MIu1 digested pUC19_ORF74. The ligation reaction was transformed into NEB5-alpha E. coli, kanamycin resistant colonies were recovered in Kan-LB broth and screened via restriction digest with MIu1. Ligation of the kanamycin cassette into the pUC19_ORF74 plasmid results in the duplication of the MIu1 site, and thus digestion with MIu1 is expected to result in the removal of kan-cassette (1017bp). The digest screen of the ORF74_UTC vector resulted in the expected band size of approximately 1000bp (kanamycin cassette) and another band of about 3800bp (the backbone pUC19_ORF74 plasmid) (figure 4, lane 4). MIu1 digestion of the parental plasmid pUC19_ORF74 produced the expected band size of 3800bp (figure 4, lane 3) and confirmed the 3800bp band in figure 4, lane 4 represents the parent plasmid backbone, pUC19-ORF74. The correct orientation of the inserted kanamycin cassette was confirmed by sequencing (data not shown).

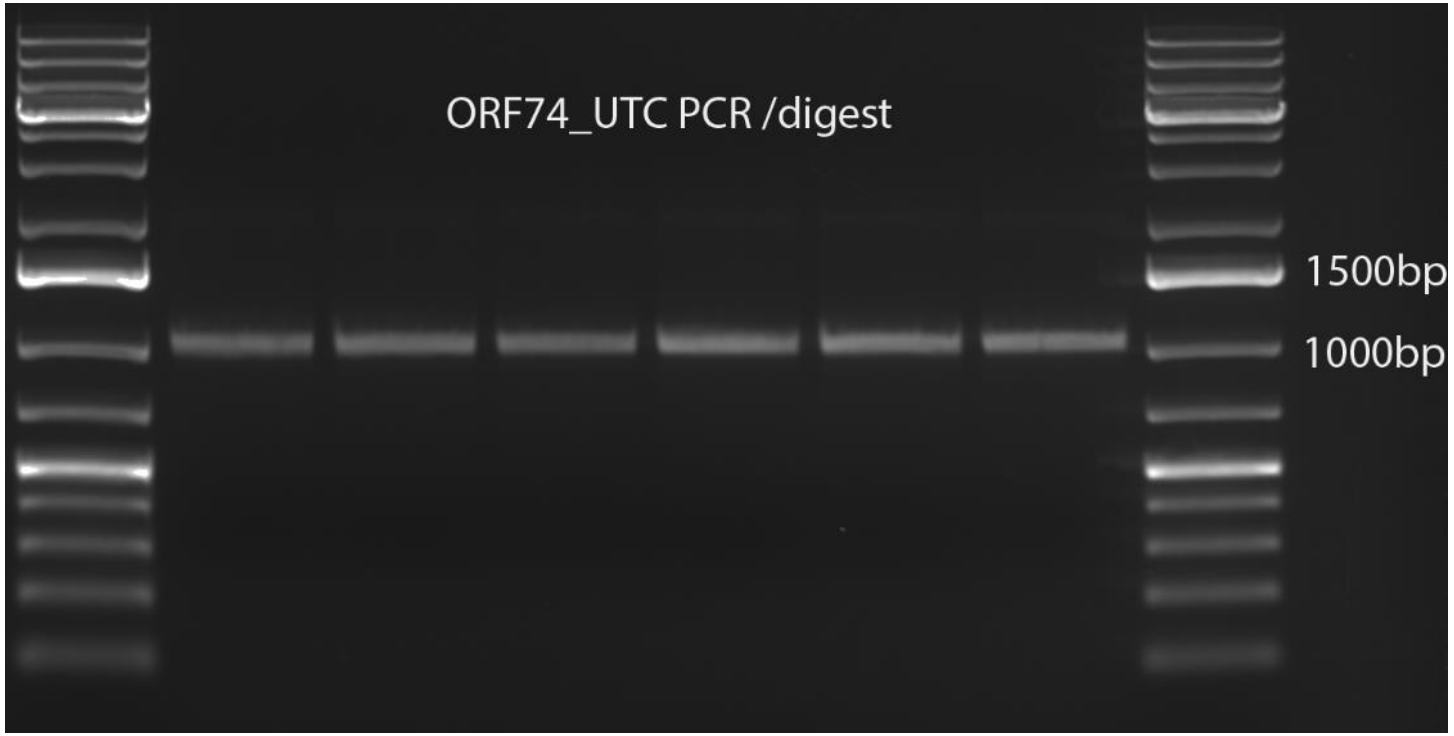

Figure 3: Results of the ORF74_UTC PCR product digestion with MIu1.

Lane 1 is the 1kb plus gene ruler. Lanes 2-7 are the results of the pEPKanS DNA and ORF74_UTC primer PCR reaction. Lane 8 is the 1kb plus gene ruler.

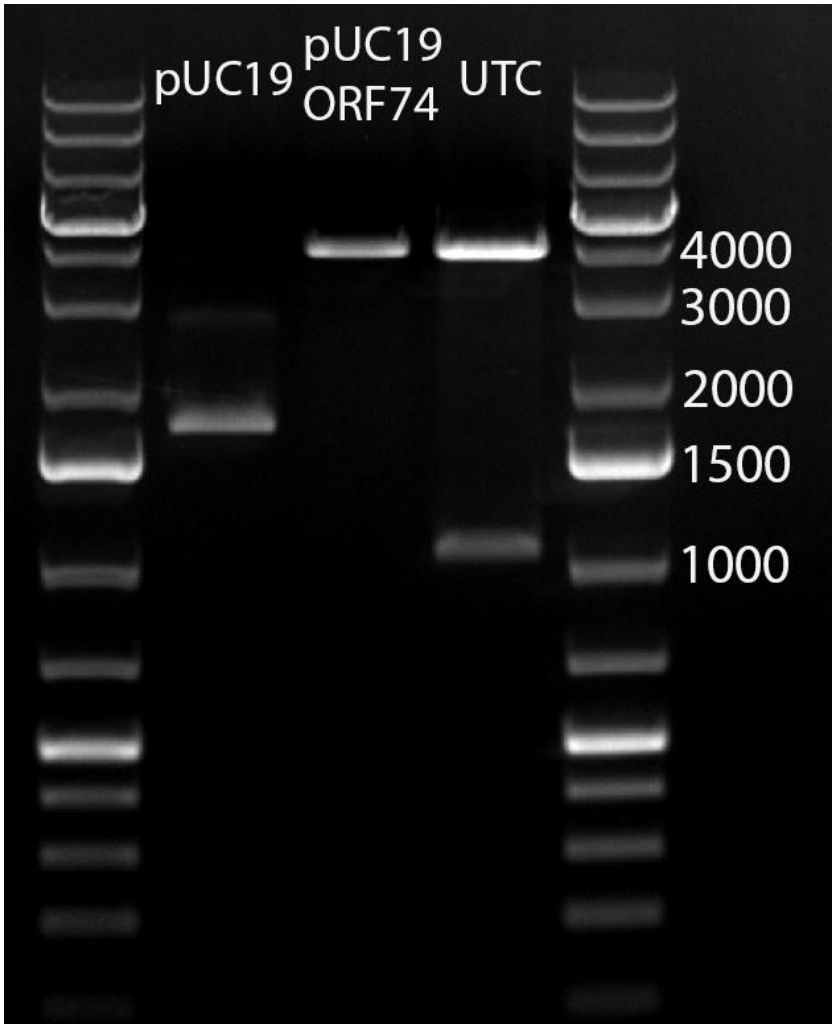

Figure 4: MIU1 screen of vectors.

Lanes 1 is the 1kb plus gene ruler. Lane 2 is MIu1 digested pUC19. Lane3 is the Miu1 digested pUC19_ORF74 vector. Lane 4 is Miu1 digested ORF74_UTC vector. Lane 5 is the 1kb plus gene ruler.

Insertion of the ORF74_UTC into BAC16-ΔORF74: 1st Homologous Recombination

PCR using Phusion enzyme and ORF74_UTC plasmid DNA was conducted with HR1 primers (primer table 1) to create a linear UTC for electroporation in BAC16-ΔORF74 containing E.coli. The HR1 forward primer added 50bp of homology directly upstream of ORF74 to the PCR product, and the HR1 reverse primer added 50bp of homology directly downstream of ORF74 to the PCR product (chapter 2). These regions of homology are used to direct its insertion into the correct genomic region of BAV16-ΔORF74. The PCR resulted in the expected band size of approximately 2300bp (1170bp-ORF74, 1017bp-Kan-cassette, 50bp-sequence duplication, 18bp-SceI meganuclease site = 2255bp) (figure 5, lanes 1-6) This product was electroporated in E.coli containing BAC16-ΔORF74 and kanamycin resistant colonies were recovered in LB-kan broth and screened via restriction digest and PCR.

The BAC16-ΔORF74 has the entire 1029bp ORF74 removed from the genome (accession number GQ994935.1 nt 129679- 130725) and ORF74 is expected to be found in the 5011bp band. NheI digest resulted in the expected band shift of the 5011bp band to approximately 6200bp (figure 6, lanes 1-4 compared to figure 6, lane 5). The red box highlights the 5100bp band in the BAC16 and its absence in the 1st HR ORF74 mutants. The green box highlights the presence of the 6100bp band in the 1st HR ORF74 mutants and its absence in the BAC16. Digestion of the BAC16 DNA also confirmed that no other off target insertions, deletions, or duplications occurred in the 7600bp, 6400bp, and 4400 bp bands of the 1st HR samples when compared to the BAC16 digest (figure 6, lane 5). These regions contain various repeat sequences which are prone to large scale deletion and duplication events during homologous recombination (Chapter 2 and unpublished data)

The PCR reaction with forward and reverse HR1 primer pair (primer table 1) on 1st HR BAC16-ΔORF74 candidates results in the expected band size of 2200bp (figure 7, lanes 2-5) and the expected band size of approximately 1100bp for the BA16 genome (figure 7, lane 6). The extra 1100bp in the BAC16-ΔORF74 1st HR amplicons represent the insertion of the approximately 1000bp kanamycin selection cassette and the 50bp sequence duplication inside of ORF74. The approximately 1100bp band in the BAC16 represents the native ORF74 sequence with the additional base-pairs added by the primers. PCR with the forward HR1 primer and the kanamycin reverse primer pair (primer table 1) on BAC16-ΔORF74 1st HR results in the expected band size of approximately 1300bp (figure 7, lanes 8-11) and no amplification in the BAC16, as BAC16 does not contain the kan-cassette (figure 7, lane 12). These results confirm the insertion, location, and orientation of the UTC in the BAC16-ΔORF74 candidates.

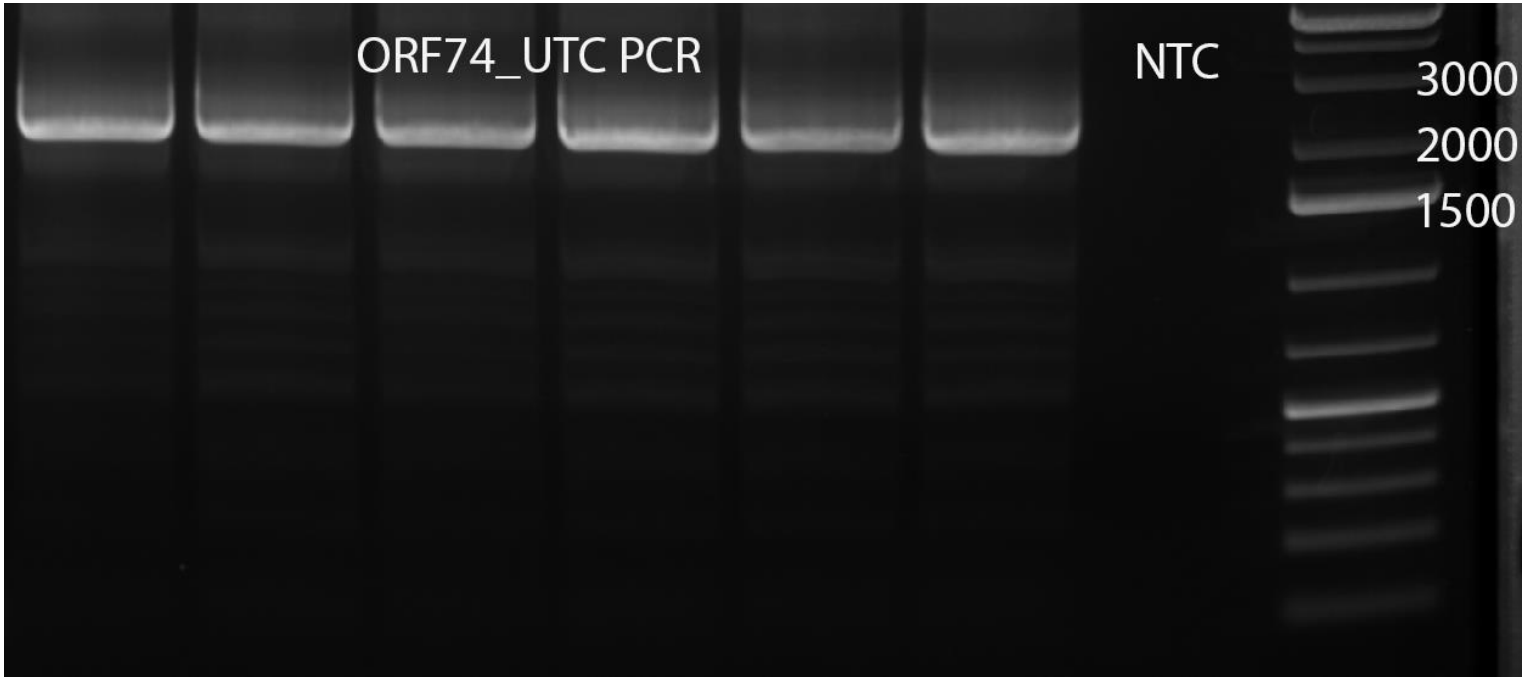

Figure 5: Linear ORF74 UTC PCR results.

Lane 1-6 represent the PCR product from the ORF74_UTC construct and HR1 F/R primer PCR. Lane 7 is a no template control. Lane 8 is the 1kb plus gene ruler.

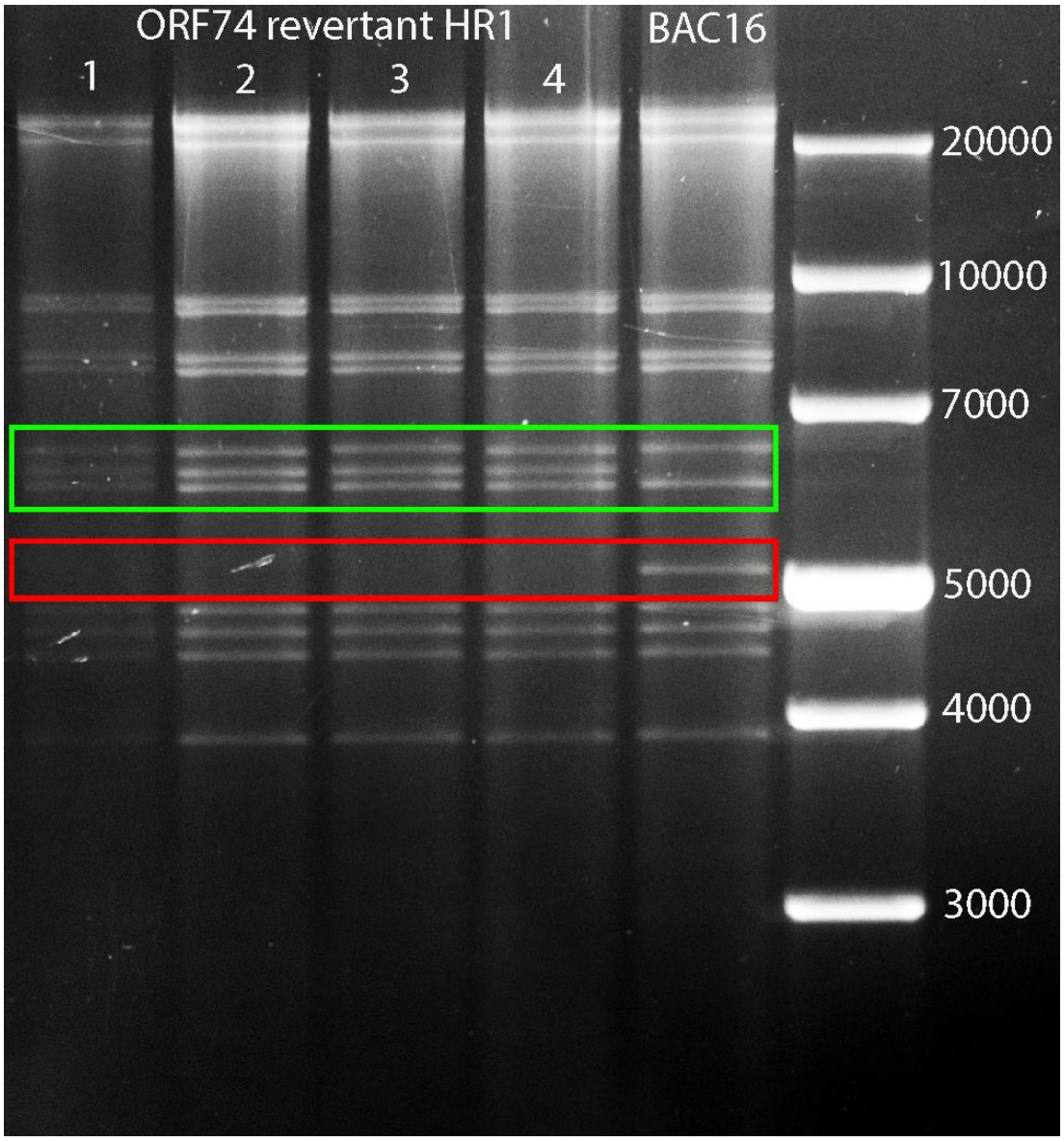

Figure 6: NheI digest of BAC16-ΔORF74 1st HR candidates 1-4.

Lanes 1-4 contain BAC16-ΔORF74 1st HR candidates, lane 5 represents the BAC16, and lane 6 is the 1kb plus gene ruler. The red bar indicates the absence of the 5011bp band from the BAC16-ΔORF74 1st HR candidates and its presence in the BAC16. The green box represents the new location of the 5011bp after insertion of UTC containing ORF74, kan cassette, and 50bp sequence duplication in the BAC16-ΔORF74 1st HR candidates and its absence in the BAC16.

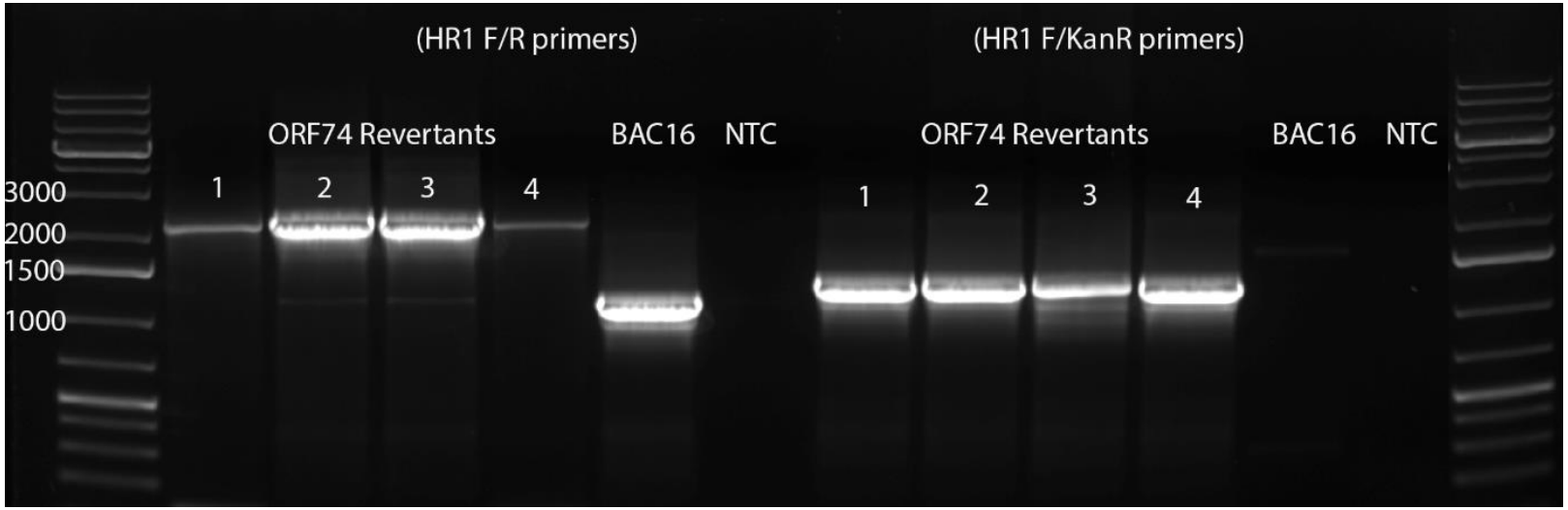

Figure 7: PCR screening of the BAC16-ΔORF74 revertant 1st HR candidates 1-4.

Lane 1 contains the 1kb plus gene ruler. Lanes 2-7 are the results of the PCR reaction with the HR F/R primers on BAC16-ΔORF74 1st HR candidates 1-4 (lanes2-5), BAC16 (lane 6) and a no template control reaction (lane 7). Lanes 8-13 contain the results of the PCR reaction with the HR F/KanR primers on BAC16-ΔORF74 1st HR candidates 1-4 (lanes 8-11), BAC16 (lane 12) and a no template control reaction (lane 13) Lane 14 is the 1kb plus gene ruler.

Removal of the kan-cassette from BAC16-ΔORF74: 2nd Homologous recombination

The kanamycin selection cassette was removed from the ORF74 reading frame via Sce-I mediated cleavage and a second homologous recombination event mediated by the 50bp sequence duplication inside of ORF74. Colonies arising from BAC16-ΔORF74 1st HR sample #3 (figure 6, lane 3 and Figure 7, lanes 4 and 10) that were negative for growth on kanamycin plates and positive for growth on chloramphenicol plates after the 2nd HR were recovered in Cm-LB broth. They were screened via alkaline lysis, PCR and sequencing.

PCR using the 1st HR primers (primer table 1) on BAC16-ΔORF74 2nd HR colonies yielded the expected band size of 1100bp, corresponding to ORF74 and 50bp of sequence upstream and downstream of ORF74 (figure 8, lanes 1-3). PCR using the 1st HR primers on BAC16 resulted in a product that also runs at the expected band size of 1100bp (figure 8, lane 5). These results indicate that the kanamycin selection cassette has been removed from the interior of ORF74 in the 2nd HR colonies, and that the PCR product is the same size in the revertant colonies and the BAC16. PCR reactions using the HR1 forward and kanamycin reverse primers on 2nd HR samples shows no amplification, confirming the kanamycin selection cassette was removed from the interior of ORF74 (figure 8, lanes 7-9). This primer set also shows no amplification in BAC16 (figure 8, lane 11), as BAC16 contains no Kan-cassette. Importantly, the BAC16-ΔORF74 #3 sample that gave rise to the 2nd HR mutants results in the expected band size of 1300bp and serves as a positive control for the PCR reaction using this primer set (figure 8, lane 12).

NheI digest on BAC16-ΔORF74 2nd HR sample 3k (figure 8, lanes 2 and 8) and the BAC16 produced identical banding patterns (figure 9, lanes 2 and 3). The extra approximately 6200bp band has been removed and the 5011bp band has reappeared (figure 9, lanes 2 and 3). There are also no major duplications or deletions observed in BAC16-ΔORF74 2nd HR sample 3k's 7600bp, 6400bp, and 4400bp bands when comparing it the BAC16 digest (figure 9, lane 2 compared to lane 3). These data are consistent with the hypothesis that ORF74 has been successfully re-inserted into the BAC16-ΔORF74 with no additional sequences and confirms the integrity of the BAC16-ΔORF74 2nd HR sample 3k genome. The results of sequencing the BAC16-ΔORF74 2nd HR sample 3k show it aligns perfectly with the BAC16 sequence (figure 10), indicating that ORF74 has been reinserted in the correct orientation and location. Importantly, the two sequences align with no gaps and/or inserts in the yellow highlighted MIu1 site (figure 10), indicating that the 2nd HR and removal of the sequence duplication has occurred. Thus, we rename BAC16-ΔORF74 2nd HR sample 3k as ORF74-rvt.

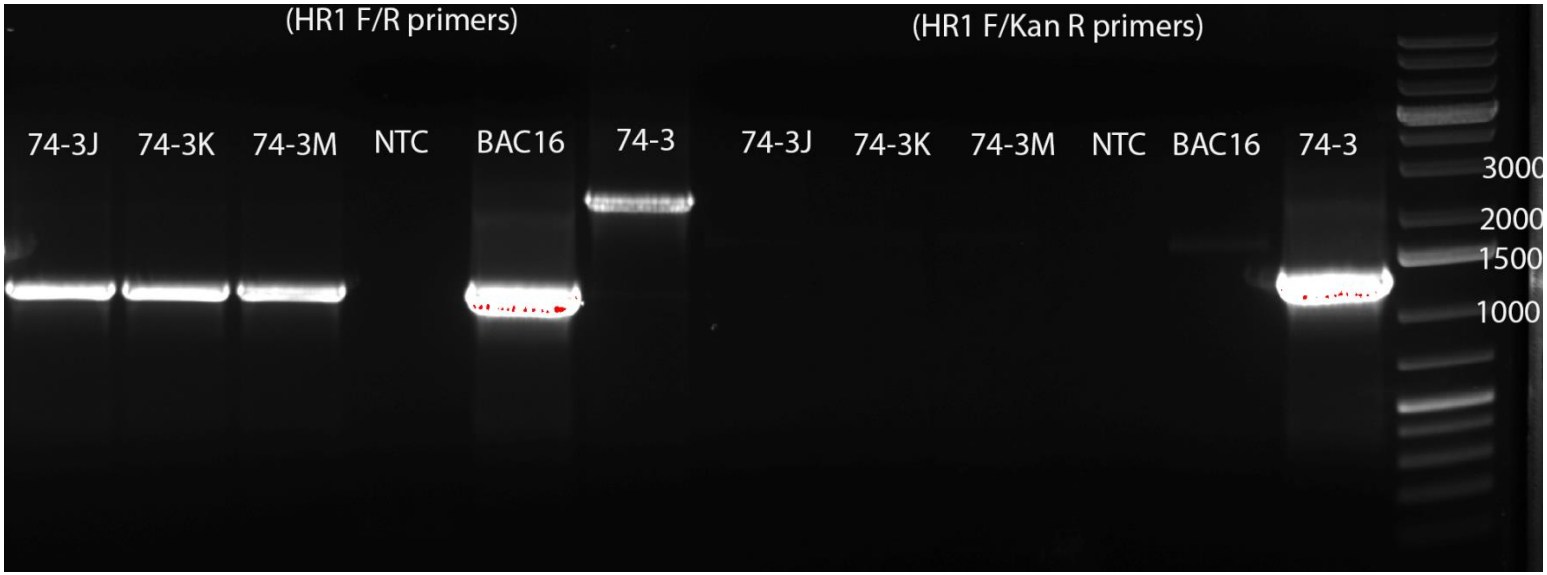

Figure 8: PCR of 2nd HR clones arising from BAC16-ΔORF74 1st HR sample 3:

Lanes 1-6 represent the PCR products with HR F/R primers on the 2nd HR clones (lanes1-3), no template control (lane 4), BAC16 DNA (lane 5) and BAC16-ΔORF74 1st HR clone 3; the sample which clones in lanes 1-3 arose from (lane 6). Lanes 7-12 represent the PCR products with HR F/kanR primers on 2nd HR clones (lanes7-9), no template control (lane 10), BAC16 DNA (lane 11), and BAC16-ΔORF74 1st HR sample 3; the sample which clones in lanes 7-9 arose from (lane12). Lane 13 is the 1kb plus gene ruler.

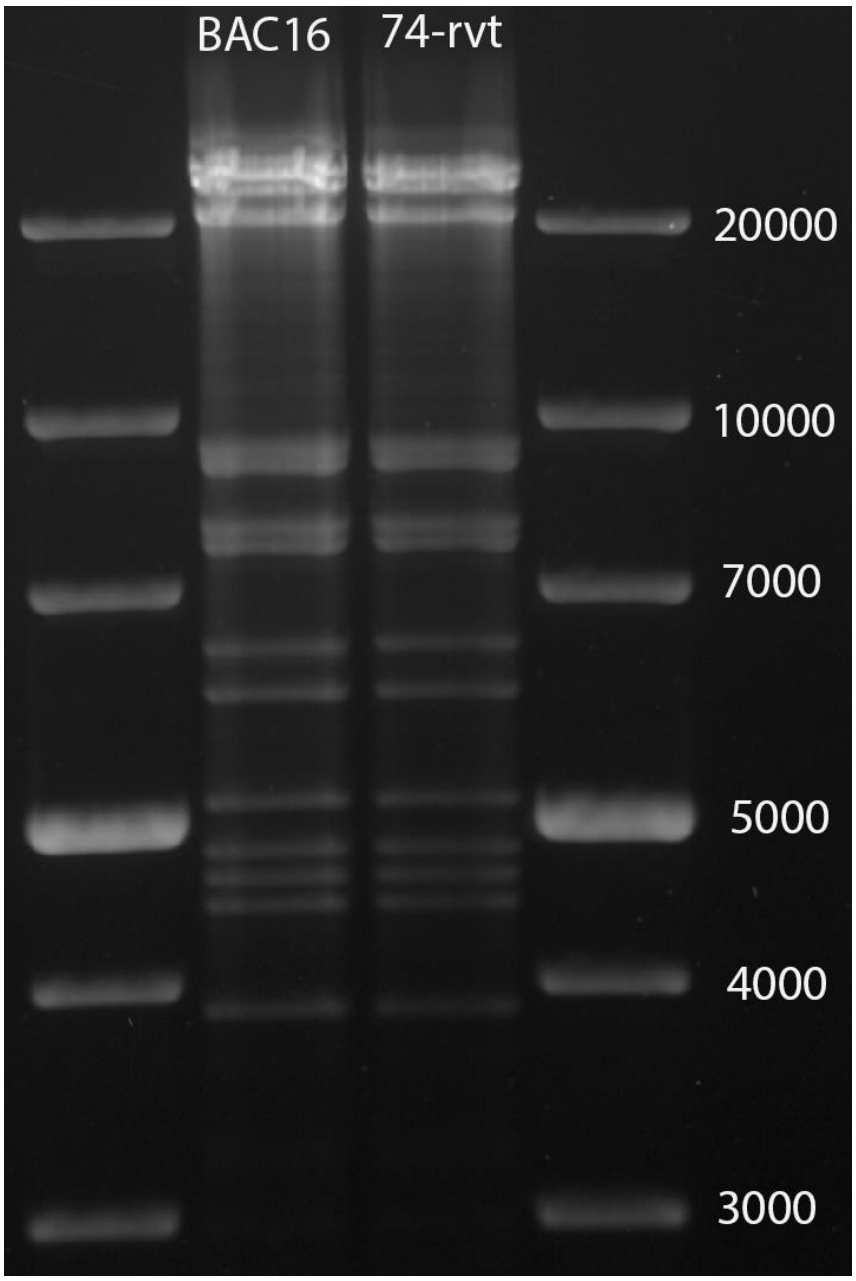

Figure 9: NheI digest of the BAC16-ΔORF74 2nd HR sample 3k and BAC16.

Lane 1 is the 1kb plus gene ruler. Lane 2 is BAC16 DNA. Lane 3 is BAC16-ΔORF74 2nd HR 3k DNA (renamed ORF74-rvt). Lane 4 is 1kb plus gene ruler.

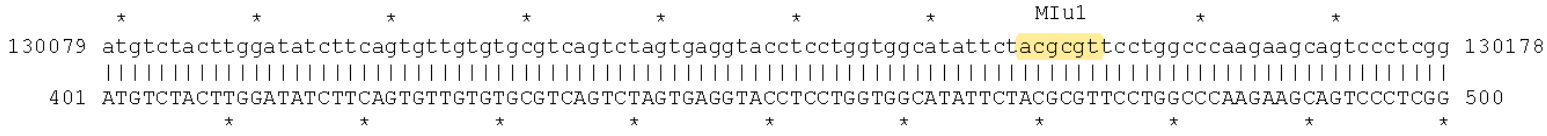

Figure 10: Sequence alignment of ORF74 revertant to BAC16 Genebank Accession number: GQ994935.1 sequence.

The BAC16 sequence is the top row and the ORF74 revertant sequence is the bottom row. The vertical hyphens indicate sequence homology between the BAC16 and ORF74 revertant sequence. The yellow highlighted sequence indicates the location of the internal MIu1 site. The black stars are placed after 10 nucleotides in each row. The numbers at the ends of the top row are the numbering of the first and last nucleotides in the row in the GQ994935.1 sequence.

Generation and induction of ORF74 revertant cell line

BAC16 ORF74 revertant DNA (figure 8 lane 2 and lane 10, figure 9 and figure 10) was extracted from E.coli using the nucleobond BAC100 kit and the DNA was transfected into naive iSLK cells (chapter 2). Selection of successful transfectants was done by the addition of hygromycin B to the growth media. The establishment of viral latency and the selection process took over two months to complete. Eventually, a pure population of latently infected BAC16 ORF74 revertant transfectants was established (data not shown)**.** Approximately 4 million transfectants (100ml of culture media) were induced by the addition of doxycycline and butyrate to the media. The cells were cultured under inducing conditions for 4 days and increasing levels of CPE were observed each day (data not shown). The supernatant was harvested, cleared by centrifugation and filtration, and concentrated by ultracentrifugation. Concentrated viral stocks were tittered on 293T cells via fluorescence microscopy and FACS.

Immediate early, early, and late gene expression under non-inducing conditions

A temporal cascade of gene expression is a hallmark of herpesviruses' lifecycles. The temporal cascade proceeds from immediate early genes to early genes and finally to late genes. KSHV ORF50 is an immediate early gene that is necessary to drive the entire lytic cascade of gene expression. ORF45 is a surrogate for other immediate early and early gene products. ORF25 is the major capsid protein and serves as a surrogate for late gene products.

To evaluate spontaneous reactivation potential of BAC16-ΔORF74, we infected iSLK cells at an MOI=1 with virus harvested from BAC16, ORF74 revertant, and BAC16-ΔORF74 cell lines. We observed clusters of GFP+ cells 24-48 hours post infection for all samples (data not shown). This indicated that each virus was able to enter cells, transport to the nucleus, uncoated successfully and undergo transcription. We harvest total RNA from cells using Qiagen columns and homemade buffers (chapter 2). DNase I treatment was done on column to remove contaminating DNA from the nucleic acid preparations. We assessed efficiency of DNase I treatment and RNA quality by gel electrophoresis (Figure 10). DNase treatment removed the major top band, which represents DNA contamination in our RNA preparation, from both mock and BAC16 infected cell RNA preparations (figure 10, lanes 2 and 3 compared to lanes 4 and 5). DNase I treatment also caused no noticeable decrease in RNA quality as assessed by 28S and 18S rRNA bands. Both bands are sharply present with no smearing, and the 28S band is 2-3 times brighter than the 18S band (figure 10, the band at approximately 1800bp is 28S and the band at approximately 800bp is 18S).

We conducted RT-qPCR for KSHV ORF50, ORF45, and ORF25 transcripts at 0,12,24,48,72, and 96 hours post infection. Figures 11-13 show the results of the RT-qPCR reaction on two biological replicates for the BAC16-ΔORF74 and ORF74 revertant mutants under non-inducing conditions. Expression levels of ORF50, ORF45, and ORF25 is relative to BAC16 expression levels. In each graph the horizontal axis is set 1. A value of 1 means that the expression level of the mutant was equal to the expression level in the BAC16 as determined by ΔCq values. We observed a strong reduction in ORF50, ORF45 and ORF25 expression levels relative to the

BAC16 in the BAC16-ΔORF74. The reduction in expression levels was also strongly dependent on sample time, with longer incubations resulting in stronger decreases in relative expression levels. The ORF74 revertant abrogated these effects on expression levels to near BAC16 levels for all transcripts at all time points. These results indicate that KSHV ORF74 plays a critical role in spontaneous reactivation of de-novo infected iSLK cells.

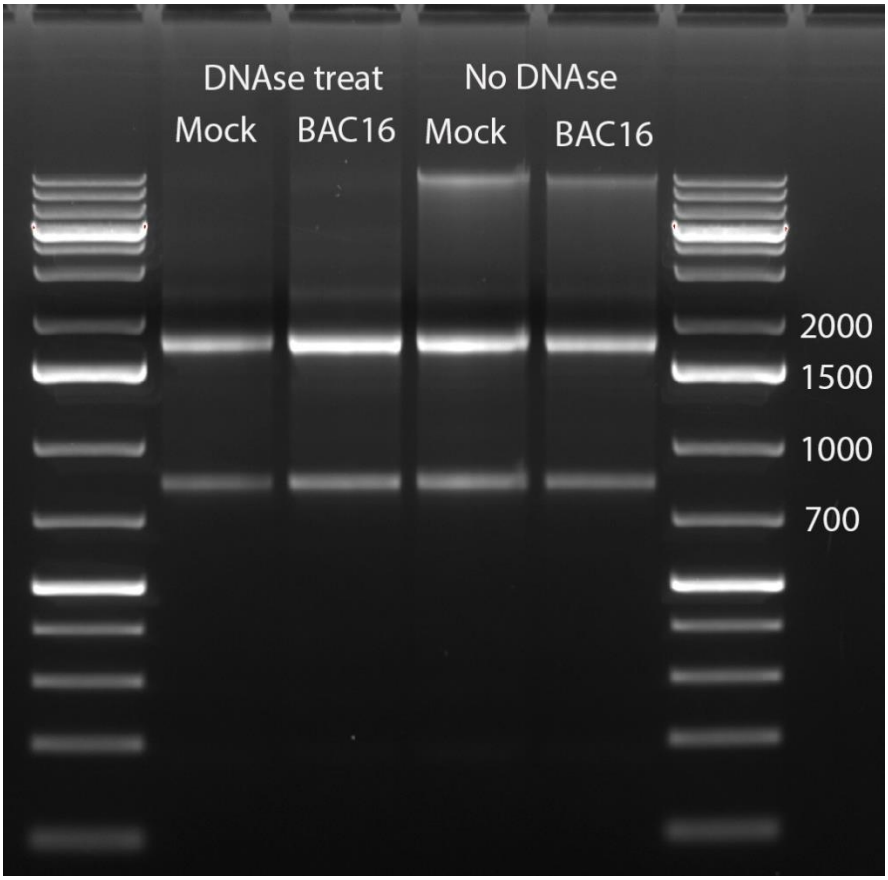

Figure 10: Representative photo DNase I treatment and RNA quality control:

Lane1 is the 1kb plus ladder from gene ruler. Lane 2 is RNA harvest from mock infected cells with DNase treatment. Lane 3 is RNA harvested from BAC16 infected cells with DNase treatment. Lane 4 is RNA harvest from mock infected wells with no DNase treatment. Lane 5 is RNA harvested from BAC16 infected cells with no DNase treatment. Lane 6 is the 1bk plus gene ruler.

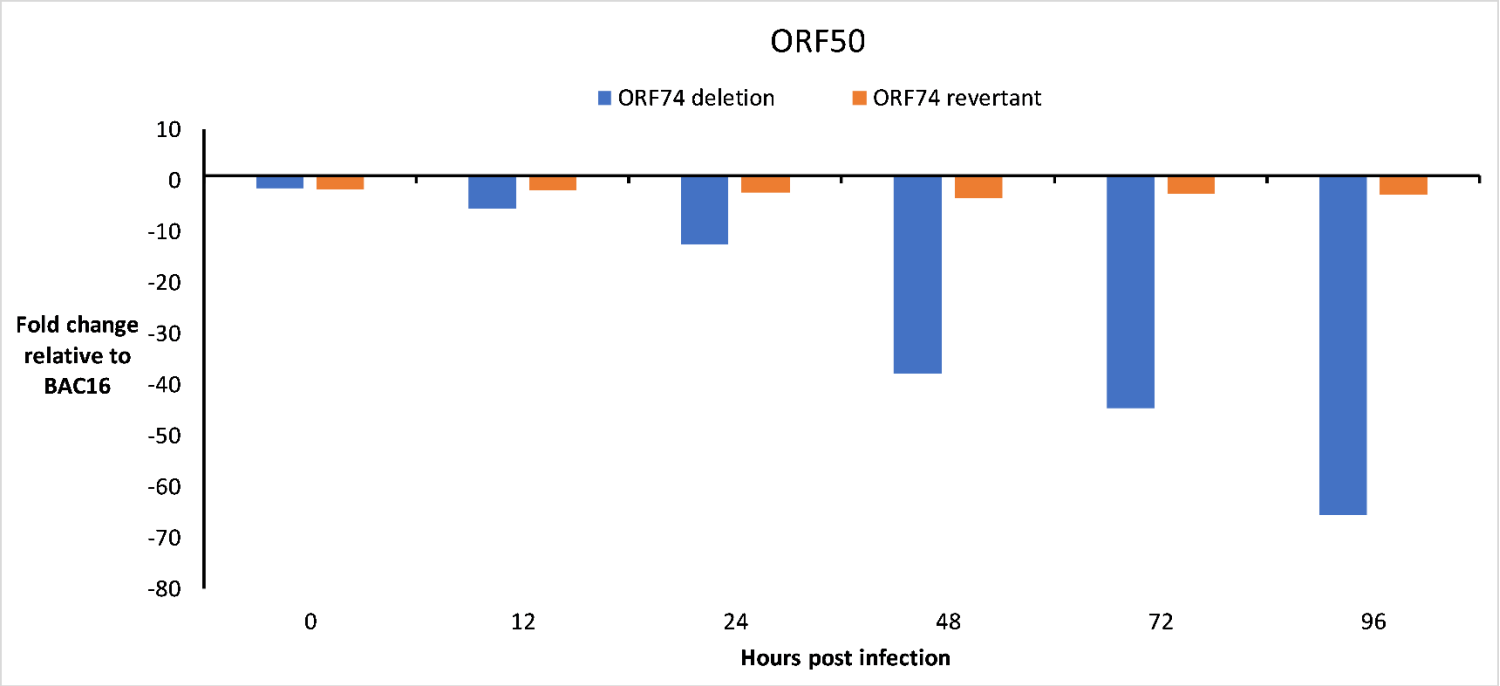

Figure 11: RT-qPCR results of ORF50 expression in BAC16-ΔORF74 and ORF74 revertant mutants relative to BAC16 under non-inducing conditions

Blue bars represent the fold change in expression levels relative to BAC16 for ORF50 in the BAC16-ΔORF74 virus infected iSLK cells at various hours post infection. Orange bars represent the fold change in the expression levels relative to BAC16 for ORF50 in the ORF74 revertant virus infected iSLK cells at various hours post infection.

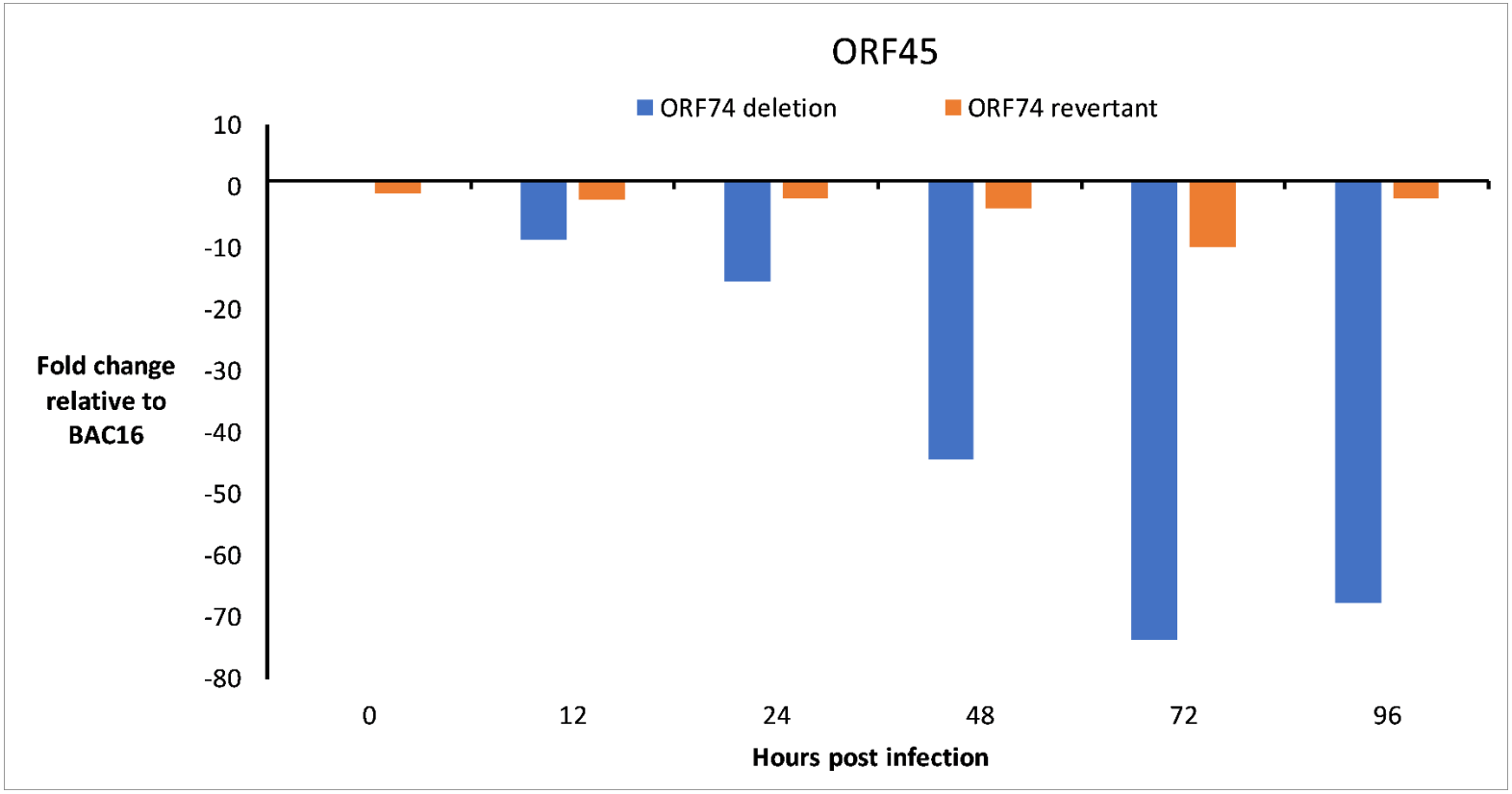

Figure 12: RT-qPCR results of ORF45 expression in BAC16-ΔORF74 and ORF74 revertant mutants relative to BAC16 under non inducing conditions:

Blue bars represent the fold change in expression levels relative to BAC16 for ORF45 in the BAC16-ΔORF74 virus infected iSLK cells at various hours post infection. Orange bars represent the fold change in the expression levels relative to BAC16 for OR45 in the ORF74 revertant virus infected iSLK cells at various hours post infection.

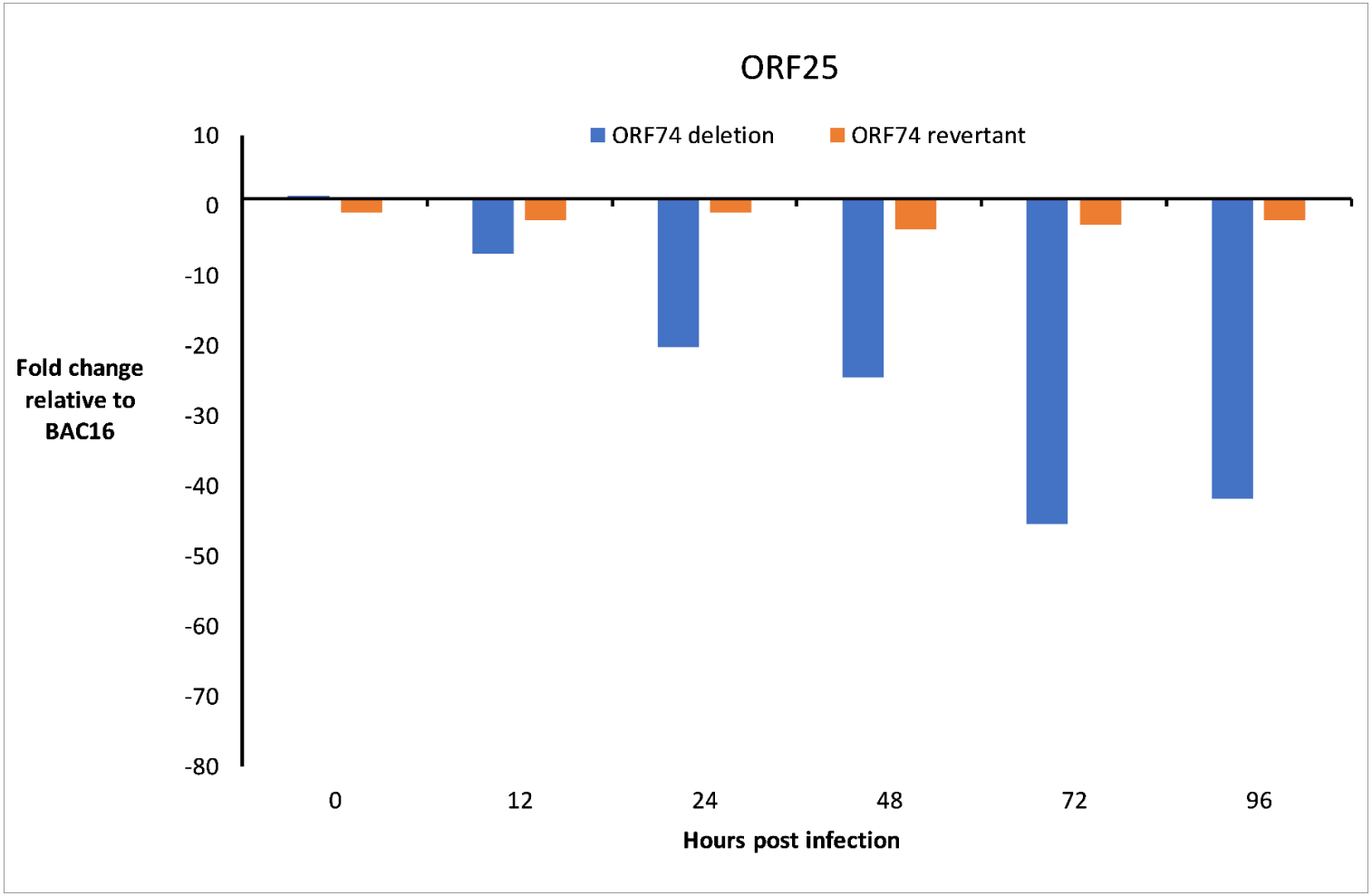

Figure 13: RT-qPCR results of ORF25 expression in BAC16-ΔORF74 and ORF74 revertant mutants relative to BAC16 under non-inducing conditions:

Blue bars represent the fold change in expression levels relative to BAC16 for ORF25 in the BAC16-ΔORF74 virus infected iSLK cells at various hours post infection. Orange bars represent the fold change in the expression levels relative to BAC16 for ORF25 in the ORF74 revertant virus infected iSLK cells at various hours post infection.

Discussion:

KSHV ORF74 is a viral G-protein coupled receptor that constitutively activates MAPK and AKT signaling[4]. Moreover, activation of MAPK pathways is necessary and sufficient to induce ORF50 expression and reactivate KSHV from latency[14]. Spontaneous reactivation from latency is a salient feature of KSHV infection in-vivo. The pathogenic effects of this process are mediated through paracrine signaling, the oncogenic effects of certain lytic cycle proteins, and infection of naïve cells[12]. Despite its significance, little is known about the viral proteins governing the control of spontaneous reactivation. Here we report that KSHV ORF74 is an important viral factor that regulates spontaneous reactivation at the gene expression level. These results also support our findings in chapter 3 part I (figure 3C).

Primer Table: Primers used in this study

Mutagenesis primers	
Name	**Sequence**
Forward pUC19_ORF 74	GATAG**GAATTC**AAGGCGTGGCTAAACAACAC
Reverse pUC19_ORF 74	GCATAA**AAGCTT**GATTCGCCTCTCTGCATCAT
Forward ORF74_UTC	GATCC**ACGCGT**TCCTGGCCCAAGAAGCAGTCCCTCGGATGGGTACTGACATCCGCTGCACT*TAGGGATAACAGGGTAATCGATTT*ATTCAACAAAGC
Reverse ORF74_UTC	CTGGC**ACGCGT**CCCCGCGCCGCCGATTAACCAATTCTGATTA
Forward HR	GGGTAAAAGGCGTGGCTAAAC
Reverse HR	ACGGGAGGCTAGATTAAATTAAGGG
Kan reverse	CCATGAGTGACGACTGAATCCG
RT-qPCR primers	
Name	**Sequence**
ORF50 forward	TTGCCAAGTTTGTACAACTGCT
ORF50 reverse	ACCTTGCAAAGACCATTCAGAT
ORF45 forward	CCATACAGCGACCCTGATGA
ORF45 reverse	CCGATTCTCTGACTCAATACT
ORF25 forward	ACAGGTTATGGCACGCATAGTG
ORF25 reverse	GGTTCTCTGAATCTCGTCGTGT
GAPDH forward	GAAGGTGAAGGTCGGAGTCAAC
GAPDH reverse	CAGAGTTAAAAGCAGCCCTGGT

Primer Table: **Bolded** sequences represent the addition of restriction sites. As they appear from top to bottom in rows; EcoRI, HindIII, and MIu1. Underlined sequence represents the duplication of 50bp downstream of the internal ORF74 MIu1 site. *Italics* represent the addition of the SceI meganuclease site. All primers are written in the 5'→3' orientation.

Plasmid table: Plasmids used and created in this study

Plasmids	**Description**	**Reference/source**
KSHV BAC16	KSHV Bacterial Artificial Chromosome clone	[15]
BAC16-ΔORF74	KSHV Bacterial Artificial Chromosome clone deleted for ORF74	This publication
BAC16-ORF74 revertant	KSHV Bacterial Artificial Chromosome clone generated by inserting ORF74 into the BAC16-ΔORF74	This publication
pEPkan-S	PCR template for en passant (two-step Red-mediated) mutagenesis	[16]
pUC19_ORF74	pUC19 with ORF74 inserted in between the EcoRI and HindIII sites	This publication
ORF74_UTC	pUC19_ORF74 with the kanamycin cassette inserted into pUC19_ORF74 at the ORF74 MIu1 site.	This publication

References:

1 Arvanitakis, L., Geras-Raaka, E., Varma, A., Gershengorn, M. C. & Cesarman, E. Human herpesvirus KSHV encodes a constitutively active G-protein-coupled receptor linked to cell proliferation. *Nature* **385**, 347-350, doi:10.1038/385347a0 (1997).

2 Bais, C. *et al.* G-protein-coupled receptor of Kaposi's sarcoma-associated herpesvirus is a viral oncogene and angiogenesis activator. *Nature* **391**, 86-89, doi:10.1038/34193 (1998).

3 Yang, T. Y. *et al.* Transgenic expression of the chemokine receptor encoded by human herpesvirus 8 induces an angioproliferative disease resembling Kaposi's sarcoma. *J Exp Med* **191**, 445-454, doi:10.1084/jem.191.3.445 (2000).

4 Smit, M. J. *et al.* Kaposi's sarcoma-associated herpesvirus-encoded G protein-coupled receptor ORF74 constitutively activates p44/p42 MAPK and Akt via G(i) and phospholipase C-dependent signaling pathways. *J Virol* **76**, 1744-1752, doi:10.1128/jvi.76.4.1744-1752.2002 (2002).

5 Sodhi, A. *et al.* The Kaposi's sarcoma-associated herpes virus G protein-coupled receptor up-regulates vascular endothelial growth factor expression and secretion through mitogen-activated protein kinase and p38 pathways acting on hypoxia-inducible factor 1alpha. *Cancer Res* **60**, 4873-4880 (2000).

6 Aneja, K. K. & Yuan, Y. Reactivation and Lytic Replication of Kaposi's Sarcoma-Associated Herpesvirus: An Update. *Front Microbiol* **8**, 613, doi:10.3389/fmicb.2017.00613 (2017).

7 Martin, D. F. *et al.* Oral ganciclovir for patients with cytomegalovirus retinitis treated with a ganciclovir implant. Roche Ganciclovir Study Group. *N Engl J Med* **340**, 1063-1070, doi:10.1056/NEJM199904083401402 (1999).

8 Oksenhendler, E. *et al.* High levels of human herpesvirus 8 viral load, human interleukin-6, interleukin-10, and C reactive protein correlate with exacerbation of multicentric castleman disease in HIV-infected patients. *Blood* **96**, 2069-2073 (2000).

9 Grundhoff, A. & Ganem, D. Inefficient establishment of KSHV latency suggests an additional role for continued lytic replication in Kaposi sarcoma pathogenesis. *The Journal of Clinical Investigation* **113**, 124-136, doi:10.1172/JCI17803 (2004).

10 Staskus, K. A. *et al.* Kaposi's sarcoma-associated herpesvirus gene expression in endothelial (spindle) tumor cells. *J Virol* **71**, 715-719, doi:10.1128/JVI.71.1.715-719.1997 (1997).

11 Zhong, W., Wang, H., Herndier, B. & Ganem, D. Restricted expression of Kaposi sarcoma-associated herpesvirus (human herpesvirus 8) genes in Kaposi sarcoma. *Proc Natl Acad Sci U S A* **93**, 6641-6646, doi:10.1073/pnas.93.13.6641 (1996).

12 Blossom A. Damania, E. C. in *Fields Virology 6th edtion* Ch. Kaposi's Sarcoma–Associated Herpesvirus, 2080-2128 (Philadelphia, PA: Lippincott Williams & Wilkins, 2013).

13 Lebbe, C. *et al.* Characterization of in vitro culture of HIV-negative Kaposi's sarcoma-derived cells. In vitro responses to alfa interferon. *Arch Dermatol Res* **289**, 421-428, doi:10.1007/s004030050215 (1997).

14 Xie, J., Ajibade, A. O., Ye, F., Kuhne, K. & Gao, S. J. Reactivation of Kaposi's sarcoma-associated herpesvirus from latency requires MEK/ERK, JNK and p38 multiple mitogen-activated protein kinase pathways. *Virology* **371**, 139-154, doi:10.1016/j.virol.2007.09.040 (2008).

15 Brulois, K. F. *et al.* Construction and manipulation of a new Kaposi's sarcoma-associated herpesvirus bacterial artificial chromosome clone. *J Virol* **86**, 9708-9720, doi:10.1128/JVI.01019-12 (2012).
16 Tischer, B. K., von Einem, J., Kaufer, B. & Osterrieder, N. Two-step red-mediated recombination for versatile high-efficiency markerless DNA manipulation in Escherichia coli. *Biotechniques* **40**, 191-197, doi:10.2144/000112096 (2006).